# Patterns within centimeter-scale bedding in carbonate rocks in the Archean Transvaal Supergroup, South Africa

A Thesis Presented for the
Master of Science
Degree
The University of Tennessee, Knoxville

James Harvey Alexander
August 2020

# DEDICATION

Mr. George “Larry” Ganley
TMSCA/UIL Science Coach
Flour Bluff Junior High School
*12/17/1941 – 2/27/2009*

*Thank you*

# ACKNOWLEDGEMENTS

This project was supported by funding from the Geological Society of America (GSA), the Society for Sedimentary Geology (SEPM), the University of Tennessee (Graduate Teaching Assistantship), and the Kenneth R. Walker faculty endowment (to Linda Kah).

Many individuals and groups contributed to this work including:
Dr. Linda Kah for the opportunity to work, grow, and travel with unbridled support;
Dr. Wladyslaw Altermann for his guidance and friendship in South Africa;
Dr. Robert Riding, Dr. Chris Fedo, and Dr. Edmund Perfect for critical review;
Agustin Kriscautzky for field assistance in South Africa;
Jordan Romero for preparation of petrographic slides and geochemical work;
Gert, Marti, Handre, and Archie for accommodations at Riverview Lodge Prieska;

My family for their unconditional love.

ABSTRACT

The interpretation of Archean marine depositional environments relies on precise evaluation of facies that reflect shifts in sediment distribution and accumulation, which in turn are driven by changes in accommodation, *in situ* carbonate precipitation and detrital deposition, and hydrodynamic energy conditions. In the Griqualand West sub-basin of the Transvaal Supergroup, the Ghaap Plateau Facies (Reivilo Formation) and Prieska Facies (Upper Nauga Formation) represent distinct facies belts (250 km apart) that both consist of cm-scale bedding alternations within primarily carbonate strata. In this study, facies descriptions and stratigraphic analyses are combined with limited petrographic and geochemical investigation to compare bedding style and environments of deposition.

Centimeter-scale bedding couplets are composed of a lower interval consisting of coarsely recrystallized calcite (A-type laminae) and an upper interval consisting of finely crystalline dolomite that can contain detrital sediment (B-type laminae). Couplets are inferred to represent changes in depositional conditions that potentially reflect eustatic sea level changes that resulted in variation in both detrital input and energy conditions of carbonate environments.

Petrographic and geochemical analysis of facies within the Reivilo and Upper Nauga Formations reveal pervasive diagenesis that limits interpretation of microscale fabrics. However, the degree of diagenesis is similar in A- and B-type components in both of the two localities.

Stratigraphic analysis of cm-scale couplets suggests similarity in response to oscillating parameters but with differing magnitudes. Modified Fischer plots, which

examine both the overall change in stacked couplet thickness through time, as well as changes in contributions from A- and B-components to couplet thickness, indicate that carbonate deposition was consistent within and between both facies belts, and that changes in detrital input played a primary role impacting couplet thickness.

Strata of the Campbellrand Subgroup has previously been interpreted as a carbonate platform (Ghaap Plateau Facies) with a discrete, tectonically enhanced margin—reaching a penultimate relief of ~900 m—adjacent to deep slope and basinal (Prieska Facies) environments. This study, however, suggests that the Ghaap Plateau and Prieska facies accumulated carbonate in much more similar environments, which requires rethinking the current basin model.

# TABLE OF CONTENTS

LIST OF FIGURES

# 1 INTRODUCTION

Sedimentary carbonate systems first appear in the geologic record in the Meso- to Neo-archean and persist as an integral component of basins to the present (Beukes, 1987; Altermann and Wotherspoon, 1995; Riding et al., 2014). Although biological and chemical conditions of marine carbonate production have changed through earth history, an uniformitarian approach suggests that key parameters of sedimentation that result from geological processes should remain consistent in both scale and scope (Cecil, 2003; Miall, 2005), and that perturbations of these parameters would result in variation in the style of bedding within depositional environments (Miall, 2005; 2014). Patterns of sedimentation in marine systems are dependent on three primary parameters: availability of accommodation space, sediment deposition, and energy conditions (hydrodynamics) within the environment (Posamentier et al., 1988; Cecil, 2003).

Accommodation space is the vertical zone between the seafloor and sea level in which sediment can accumulate (Jervey, 1988). Changes in accommodation space can result from internal forces such as erosion, compaction, sediment loading, and local thermal subsidence, and from external forces such as tectonic subsidence and eustatic sea level change (Drummond and Wilkinson, 1993; Eriksson et al., 2005; Tucker and Wright, 2009). Within carbonate systems, small changes in accommodation space can also be associated with chemical changes, such as evaporation and redox, which may affect sediment formation.

The transport of siliciclastic sediment and the authigenic precipitation of carbonate sediment, when combined with the effects of compaction and cementation, results in the accumulation and lithification of rocks in marine sedimentary systems. In marine sedimentary systems that are dominantly composed of carbonate rocks (i.e. carbonate platforms, ramps, and build-ups), the hydrodynamic processes that control the transport and distribution of siliciclastic sediment play a similar role in the transport of detrital carbonate in allochthonous carbonate deposits (Scholle, 1971; Cook et al., 1972; Read, 1985; Matyszkiewicz, 1996; Playton et al., 2010). Influx of non-carbonate materials (e.g. siliciclastic or volcaniclastic sediment) as well as periods of erosion or non-deposition cannot be ignored, as they provide regional setting and global context, when categorizing depositional environments (Read, 1985; Osleger, 1991; 1994; Burchette and Wright, 1992; Osleger and Montañez, 1996; Kietzmann et al., 2014). Analytical evaluation of changes in lithology combined with the principle of Waltherian stratigraphic relationships facilitate the development of system models.

Geological processes in shallow marine environments (subaerial exposure, tides, and waves) result in physical sedimentary structures preserved in strata such as mudcracks, cross-stratification, hummocks, and swales (Demicco and Hardie, 1994). Although more commonly identified within siliciclastic sedimentary systems, a similar record of hydrodynamic conditions can also be preserved in carbonate strata (Demicco and Hardie, 1994). The hydrodynamics of a marine environment are in turn, directly correlated to water depth, with sediment in shallow environments frequently experiencing agitation from tides, waves, and currents. High-energy hydrodynamic events then decrease in frequency and magnitude in deeper water, resulting in a decrease and eventual loss of storm-reworked sedimentary deposits such as graded, distal tempestites (Burchette and Wright, 1992). In the most basinal deposits, slope breaks zone are often recognized from evidence of slumping and aprons of debris, depending on the geometry of shelf-slope-basin transitions (Burchette and Wright, 1992). The observation of physical sedimentary structures and the interpretation of water-depth are thus strongly linked to substrate morphology and the overall evolution of the basin. An uniformitarian approach that integrates a broad combination of parameters facilitates the interpretation of depositional environments within marine sedimentary systems.

In Precambrian basins, the absence of macroscopic fauna does not permit straightforward identification of depositional environments (Read, 1985; James et al., 2010). However, overall sediment accumulation rates were likely similar across geologic time (Altermann and Nelson, 1998). Sediment accumulation in peritidal environments often exceeds the maximum generation of accommodation space, resulting from combined eustatic changes and tectonic subsidence in these environments. By contrast, sediment accumulation in subtidal shelf, slope, and basin environments is typically limited by sediment input. Generation of accommodation space, however, is generally consistent through time, although variable between different basin types (Maynard and Klein, 1995; Eriksson et al., 1998; Eriksson et al., 2005). In the Precambrian we must therefore rely on detailed evaluations and interpretations of changing facies to both recognize shifts in environmental parameters and to constrain depositional environments. In addition to physical parameters (accommodation, sediment deposition, and water-energy), biological signatures from microbial induced and/or mediated precipitation of carbonate rocks can be used to aid in the classification of Precambrian depositional environments (Eriksson et al., 1998).

The preservation of biologically-mediated carbonate from cyanobacterial activity at or near the sediment-water interface (e.g. microbialites and stromatolites) provides an additional mechanism to constrain depositional environments (Grotzinger and Knoll, 1995; Grotzinger and Rothman, 1996; Sumner and Grotzinger, 1996; Grotzinger, 2000). This is achieved through the evaluation and interpretation of morphological changes in laminae shape, such as synoptic relief and inheritance of morphology from translation of surfaces, as a response to changes in water depth and energy conditions. Even when pervasively recrystallized, many carbonate rocks still preserve meso-scale fabrics such as physical sedimentary structures and mat structures that can help diagnose depositional environment (Demicco and Hardie, 1994; Eriksson et al., 1998).

In order to evaluate depositional environments of the Archean Transvaal Supergroup, South Africa, this study uses observations from the field, microscopic observations, geochemical evaluations, and qualitative and quantitative stratigraphic analyses to describe and compare two discrete facies that represent distinct, yet interrelated environments. The Ghaap Plateau and Prieska facies of the Transvaal Supergroup have been interpreted to represent rimmed carbonate platform-edge sedimentation and slope to basinal sedimentation, respectively (Beukes, 1987). Although the age of the Prieska Facies is well bounded through Pb-Pb and U-Pb radiometric dating of zircons derived from tuffaceous deposits (Barton et al., 1994; Altermann, 1996; Altermann and Nelson, 1998), the paucity of volcaniclastic strata in the Ghaap Plateau Facies reduces the chronological certainty of correlations between the plateau and basin (Fig. 1). However, these two facies have been accepted as broadly time-equivalent deposits of the same platform (Fig. 1; Beukes, 1987; Altermann and Siegfried, 1997; Eriksson et al., 2006; Sumner and Beukes, 2006). Despite potential differences in exact age, field observations show astounding similarity in bedding thickness and bedding style in these two facies (Fig. 2).

This study uses a combination of: (1) detailed measurement and description of facies in the field to define bedding components and to make initial interpretation of depositional environments; (2) limited petrographic and geochemical analyses to expand our understanding of facies, their depositional environments, and their diagenesis; (3) modified Fischer plots to evaluate controls on observed bedding patterns; and (4) statistical analyses to examine similarities in bedding style between these distinct facies. Ultimately, these analyses permit a detailed evaluation of depositional environments for these two, broadly time-equivalent facies.

## 1.1 Geologic Setting

### 1.1.1 The Transvaal Supergroup

The 2.5 Ga Transvaal Supergroup is exposed in northeastern South Africa and southern Botswana, and is composed of three lithologically similar sub-basins: the Transvaal sub-basin and the Griqualand West sub-basin in South Africa, and the Kanye sub-basin in Botswana (Fig. 3, Kanye sub-basin omitted). Each of these sub-basins preserves a thickness of ~2000 m of strata consisting of carbonate, siliciclastic, and volcaniclastic strata, overlain by banded iron formation (Beukes, 1987; Klein and Beukes, 1992; Altermann, 1996; Sumner and Beukes, 2006). Although the current extent of carbonate rock exposed at the surface today is only 200,000 $km^2$, the initial basin likely exceeded 600,000 $km^2$ and was deposited upon mafic to intermediate igneous bedrock of the Kaapvaal Craton (Beukes, 1987; Altermann and Wotherspoon, 1995; Eriksson et al., 2006; Humbert et al., 2018; Humbert et al., 2019).

In South Africa, strata of the Transvaal Supergroup were deposited in a thermally subsiding basin and are exposed in the Transvaal sub-basin to the northeast and the Griqualand West sub-basin to the southwest (Eriksson et al., 2005). In the Griqualand West sub-basin, the focus of this study, strata has experienced sub-greenschist metamorphism, with the highest degrees of metamorphism associated with Proterozoic compressional tectonic activity along the southernmost margins of preserved outcrop (Miyano and Beukes, 1984; Altermann and Hälbich, 1991). In the Griqualand West sub-basin, the Transvaal

Supergroup overlies the 2.7 Ga Ventersdorp Supergroup, which is composed of mafic volcanic strata of the basal Klipriviersberg Group, intermixed siliciclastic sedimentary and volcanic rocks of the Platberg Group, and relatively mature siliciclastic strata of the Pniel Sequence. Together, the Ventersdorp Supergroup represents a transition from dominantly volcanic to sedimentary deposition and an overall decrease in tectonic activity within the Kaapvaal Craton prior to deposition of the Transvaal Supergroup (Beukes, 1979; Armstrong et al., 1991; Van der Westhuizen et al., 1991; Walraven and Martini, 1995; Eriksson et al., 2006).

In the Griqualand West sub-basin, the Transvaal Supergroup consists of three subgroups; the Schmidstdrif Subgroup, the Campbellrand Subgroup, and the Asbestos Hill Subgroup (Altermann and Nelson, 1998; Sumner and Beukes, 2006). Strata have been partitioned into two discrete facies belts: the Ghaap Plateau Facies and the Prieska Facies, which are spatially separated by the Griqualand fault-zone (GFZ; Figs. 1 and 3). The GFZ has been interpreted as a syndepositional hinge fault, active throughout deposition of the Transvaal Supergroup, that resulted in a steep-sided carbonate platform (Beukes, 1980). This study focuses on two discrete facies within the Campbellrand Subgroup: the Revilio Formation of the Ghaap Plateau Facies belt and the Nauga Formation in the Prieska Facies belt.

### 1.1.2 The Campbellrand Subgroup

The Campbellrand Subgroup of the Griqualand West sub-basin (Fig. 1) consists of ~2000 m carbonate strata, with minor contribution from siliciclastic and volcanic lithologies. Strata have been interpreted to represent progressive evolution of a platform-basin margin (*cf*. Truswell and Eriksson, 1973; Clenedin, 1989; with Beukes, 1987; Grotzinger, 1989), influenced by tectonic activity along the GFZ (Beukes, 1987; Altermann and Nelson, 1998), and resulting in distinct platform (Ghaap Plateau) and basinal (Prieska) facies belts. Directly underlying the Campbellrand Subgroup, the 2.7 Ga Schmidstdrif Subgroup consists of 200 m of sedimentary strata which consist of quartzite, calcarenite, and shale. The Schmidstdrif Subgroup has been interpreted to represent initial progradational siliciclastic sedimentation of fluvial to shallow marine sedimentary strata from the emergent Kaapvaal Craton (Beukes, 1987; Altermann and Siegfried, 1997; Sumner and Beukes, 2006). The age of the Schmidstdrif Subgroup is constrained by Pb-Pb single zircon dating of tuff deposits at 2642 +/-3 Ma (Walraven and Martini, 1995; Altermann and Nelson, 1998) in the upper Vryburg Formation, the oldest formation in the Schmidstdrif Subgroup. The upper age of the Campbellrand Subgroup is constrained by U-Pb single zircon dating of tuffaceous mudrocks in the 2.43 Ga Kuruman banded iron formation of the Asbestos Hill Subgroup (Trendall et al., 1990; Pickard, 2003).

Ghaap Plateau strata of the Campbellrand Subgroup are subdivided into eight formations: the Monteville, Reivilo, Fairfield, Heuwel, Klipfontein, Papkuil, Kogelbeen, and Gamohaan formations. Ghaap Plateau facies are dominantly microbial carbonate strata with rare shale and marly intercalations which together are interpreted to represent aggradation during the development and maintenance of the platform (Sumner and Bowring, 1996). Within this sequence, the Monteville Formation represents a low-relief, ramp depositional environment, the Reivilo Formation marks initial aggradational activity along the GFZ and development of a discrete platform edge of ~250 m relief, and the Gamohaan Formation marks the maximum relief (>500 meters) of the platform margin (Sumner and Beukes, 2006). Ultimately, carbonate production ceased in the Griqualand West sub-basin as carbonate facies are overlain by banded iron formation of the Kuruman Formation, which are associated with flooding and drowning of the carbonate platform (Beukes, 1987; Trendall et al., 1990; Pickard, 2003).

Prieska Facies of the Campbellrand Subgroup consists of ~600 m of strata divided between two formations: the Nauga, and Naute Shale formations. The facies within the Nauga Formation are dominantly carbonate strata with intercalated volcanic strata. The Nauga Formation is loosely defined into two units, wherein the Lower Nauga represent initial growth and aggradation of a carbonate ramp, and the Upper Nauga represents slope to basinal deposits. The Naute Shale represents the continued deepening of environment, until drowning of the Prieska Facies by banded iron formation (Altermann and Nelson, 1998; Sumner and Beukes, 2006; Schröder et al., 2006; 2009).

Within the Campbellrand Subgroup, broad lithostratigraphic correlations between platform and basinal facies have been made (Beukes, 1987), yet sequence stratigraphic models do not attempt to correlate between the Ghaap Plateau and Prieska facies (cf. Fig. 2 in Sumner and Beukes, 2006). Although the

Campbellrand Subgroup overlies the Schmidstdrif Subgroup and is conformably overlain by BIF in both the Ghaap Plateau and Prieska facies, the most discrete correlation at present is constructed via geochronological evidence from volcanic tuff deposits. Volcanic deposits are rare and thin in the Ghaap Plateau, and radiometric age dates constrain only the uppermost Monteville Fm (2555 +/-19 Ma, $U\text{-}Pb_{zircon}$; Altermann and Nelson, 1998) and the upper Gamohaan Fm (2521 +/-3 Ma, $Pb\text{-}Pb_{carbonate}$; Sumner and Bowring, 1996; 2516 +/-4 Ma, $U\text{-}Pb_{zircon}$; Altermann and Nelson, 1998). Radiometric dates of zircons in tuff deposits using SHRIMP II U-Th-Pb have been determined for the Nauga Formation at 2588 +/-6 Ma and for the, specifically for Upper Nauga Formation, at 2549 +/-7 Ma (Altermann and Nelson, 1998).

Within the present chronological framework, these dates suggest deposition of the Nauga Formation was broadly penecontemperaneous with the deposition of the Monteville and overlying Reivilo formations of the Ghaap Plateau Facies (Altermann and Nelson, 1998; Eriksson and Altermann, 1998).

### 1.1.3 Locations of Study

This study focuses on measured sections of the upper Reivilo Formation and Upper Nauga Formation in the Ghaap Plateau and Prieska facies, respectively (Fig. 1).

The Reivilo Formation consists of cycles of stromatolitic bioherms and associated facies, including giant stromatolitic domes with smooth to tufted laminae, domal and columnar stromatolites, stratiform laminae with rare shale and marl intercalations, and substrate-nucleated carbonate fans (Beukes, 1987; Altermann and Wotherspoon, 1995; Altermann and Siegfried, 1997; Altermann and Nelson, 1998; Sumner and Grotzinger, 2000; 2004; Altermann, 2008). This study focuses on 13 m of the upper Reivilo Formation, which is dominated by giant stromatolitic domes with rhythmic bedding of smooth to tufted laminae. The Reivilo Formation is typically considered to have been deposited in a subtidal shelf environment (Beukes, 1987; Altermann and Wotherspoon, 1995; Altermann and Nelson, 1998; Sumner and Grotzinger, 2004; Sumner and Beukes, 2006; Altermann, 2008).

The Upper Nauga Formation consists primarily of microbial lamination, laterally-continuous laminae of silty to muddy detrital carbonate, and interbedded volcaniclastic materials. Strata of the Upper Nauga Formation have been variously interpreted to represent detrital carbonate and siliciclastic materials transported to deep shelf to slope environments by turbidity currents, interbedded with microbialites that grew within slope environments (Beukes, 1987; Altermann and Nelson, 1998; Schröder et al., 2006; Schröder et al, 2008; Knoll and Beukes, 2009). Conversely, the Upper Nauga Formation has also been described as consisting of predominantly peritidal microbialites and detrital facies, and interbedded tuffs from a local, subaerial source (Altermann and Herbig, 1991; Altermann and Wotherspoon, 1995; Altermann and Siegfried, 1997).

# 2 METHODS

## 2.1 Field Methods

### 2.1.1 Site Selection

Two primary field sites were chosen for investigative study; the first is near Boetsap, South Africa in the North West Province, and the second is near Prieska, South Africa in the Northern Cape Province (Fig. 3). These two sites represent well-exposed portions of two distinct depositional environments within the Griqualand West sub-basin (platform and basin), that are readily accessible, and have been the source of a variety of previous study (Beukes, 1980; Beukes, 1987; Altermann and Herbig, 1991; Altermann, 1996; Altermann and Nelson, 1998; Sumner and Grotzinger, 2004; Sumner and Beukes, 2006). Both of these field sites also show an intriguing similarity in cm-scale bedding patterns (Fig. 2).

### 2.1.2 Data Collection

Prior to measurement of strata thicknesses, outcrop was examined to describe facies to explore how variable weathering affects identification of facies and to identify specific sections for measurement.

Sections were measured using a combination of cm- to m-scale measuring sticks and tapes. Measurements were conducted in tandem with a field assistant. The observer moved laterally along the outcrop in order to identify bed components and confirm the continuity of beds in outcrop. The partner then measured the thickness of defined intervals to the mm-scale and reported back to the observer for recording. In the Ghaap Plateau Facies, one complete section of exposed strata and two, overlapping subset sections separated by 23 m of lateral offset were measured with the goals of providing both a single composite succession and measuring multiple parallel sections to investigate lateral consistency of bedding measurements. In the Prieska Facies, six independent sections were measured resulting in a composite section of 53.18 m. Additionally, laterally adjacent sections, separated by 2 m of offset, were measured within a single section to explore lateral continuity of cm-scale bedding features.

During measurement, markers were placed on outcrop to aid in accurately correlating photo documentation. Photographs were acquired at a distance of approximately 1 m to capture cm- to dm-scale resolution of bedding and at ~1 dm to capture the structure of mm-scale laminae within individual cm-scale beds. Digital models of outcrops were constructed using Agisoft Metashape software from images collected with a GoPro Hero 3+ camera. Details on sections (stratigraphic and location) are provided in Appendix B, and charts of measurement data are provided in Appendix C.

# 3 DATA

## 3.1 Generalized Stratigraphy

### 3.1.2 Platform: Ghaap Plateau Facies

The Revilio Formation is exposed in outcrop (Figs. 4 and 5) in a drainage of the Harts River north of Boetsap Township, North West Province, South Africa

(-27.964179, 24.454329). The total thickness of the formation, determined from previous work on drill core, consists of over 900 m of variously stromatolitic carbonate with rare shale and marl intercalations (Altermann and Wotherspoon, 1995). The composite section measured here (Fig. 6) covers an interval of 13.26 m and consists of stromatolitic carbonate characterized by cm-scale beds of alternating stratiform and tufted laminae that feature variable detrital sediment (Boetsap-style lamination of Sumner and Grotzinger, 2004). Individual, overlapping measured sections with accompanying descriptions are provided in Appendix B.

### 3.1.2 Basin: Prieska Facies

The Upper Nauga Formation is well exposed along drainages of the Orange River (Fig. 7) north of the town of Prieska, Northern Cape Province, South Africa (-29.665228, 22.749342). The total exposed section at this site has previously been described as consisting of ~100 m of the Upper Nauga Formation, overlain by ~50 m of Naute Shale and by ~200 m of the Kuruman Iron Formation (Altermann and Nelson, 1998; Pickard, 2003). The area traversed during the field work of this study stretched from the northeastern shore of the Orange River up to the base of the Naute Shale. The identification of the upper chert member below the Naute Shale places strata firmly in the Upper Nauga Formation from the most recent published stratigraphic descriptions (Schröder et al. 2006; 2009). Here, the Prieska Facies consists of interbedded limestone, dolostone, and volcanic tuffs, with strata measured in six discrete sections compromising a total thickness of 53 m (Fig. 8).

Individual stratigraphic columns for each of the six sections measured are presented in Appendix B.

### 3.2 Facies Descriptions

#### 3.2.1 Ghaap Plateau Facies

The primary facies of the Reivilo Formation exposed at Boetsap consists of laterally connected, giant, elongate stromatolite domes composed of cm-scale beds of mm-scale microbial laminae (Figs. 4 and 5). The synoptic relief of domes ranges from 10-60 cm (Figs. 5, 9); microbial laminae are generally uniform in thickness across the top of a dome, but thin dramatically at the margins between adjacent domes and occasionally show evidence of up to 1 cm scouring of underlying beds at margins of these stromatolites. In some cases, adjacent domes show growth of much smaller domes at margins.

Lamination within giant stromatolites at Boetsap are characterized by what has been referred to as Boetsap-style laminae (Fig. 10; Sumner and Grotzinger, 2004). Previously, Boetsap-style laminae have been described as consisting of a lower interval of *in situ* precipitated microbial carbonate and an upper interval that includes detrital sediment (Sumner and Grotzinger, 2004). In this study, we retain the primary divisions of Boetsap lamination, but focus explicitly on lower and upper components of couplets that preserve distinct differences in weathering (A-type laminae and B-type laminae) that are observable in outcrop.

In this subdivision, both A- and B-type laminae consist of stratiform, wavy, and tufted laminae (Fig. 11). Laminae are typically sub-mm to mm-scale in thickness, and show irregularities in thickness on length-scales of millimeters, which is indicative of microbial lamination. Although subtle in cross-section, the tufted character of these microbial mats is readily visible on exposed surfaces. In outcrop, exposed bedding surfaces show wrinkle marks (Hagadorn and Bottjer, 1997) with a dimpled texture (Fig. 12A) that can show modification to a linear arrangement of tufts that lies perpendicular to the elongation of stromatolites near their crests (Fig. 12B), and parallel to dome elongation between adjacent domes.

A-type laminae are also identified by a more massive weathering profile and less distinct lamination; by contrast, B-type laminae show more distinct laminae, represented by the interlamination of microbial carbonate with more highly recessive laminae. The upper surfaces of B-type laminae are commonly marked by a distinct crack in the outcrop that is occasionally filled with modern calcrete. Finally, these components frequently differ in color, with A-type laminae being grey to light-brown in color, and B-type laminae more commonly showing a brown to red color (cf. Fig. 11A).

*Facies variation in the upper Reivilo Formation*

Variation in facies in the upper Reivilo Formation result primarily from differences in the distribution of A- and B-type lamination, as well as from minor facies that occur either within A-type lamination, or which appear to overprint both A- and B-type lamination. In all observed cases, variations are representative of distinct horizons and are traceable, with little change, across the exposed outcrop.

Minor facies that occur within A-type intervals are represented most commonly by the small columnar to domal stromatolites (Fig. 13). Columnar stromatolites are typically 1-2 cm in diameter, are unwalled, and show a synoptic relief typically <2 mm (Fig. 13A). Morphology of individual laminae range from domal to slightly peaked. The low synoptic relief and unwalled character of columnar stromatolites indicates that microbial growth within the columns occurred simultaneously with growth of flat-lying microbial laminae between columns. Typically, relief on columns within A-type intervals disappears with the appearance of B-type laminae; more rarely (cf. Fig. 13A), B-type laminae irregularly drape relief of underlying columns.

Small domal stromatolites also occur within A-type intervals. These domal features are characterized by lamination that expands increasingly outward from a single point source to form a low synoptic relief (1-3 cm) with unwalled domes (Fig. 13B, C, D). As with columnar forms, laminae from within the domes can be traced to adjacent flat-lying lamination, showing synchronous accretion of domes and intervening flat-lying microbial mats, with the angle of the contact between domal and flat-lying laminae providing an indicator of potential differences in carbonate accumulation between adjacent domes and flat-laminated mats. Domes also typically show a reduction in synoptic relief upward, and disappearance of relief prior to deposition of B-type laminae.

Locally domal stromatolites preserve a thin, typically <1 cm thick, encrustation of crystalline carbonate (Figs. 13C, D). In these cases, features interpreted as acicular to bladed crystals occur oriented perpendicularly to the uppermost laminae of small domes, but are not observed to continue onto intervening microbial laminae. In a single case, much larger (10-30 cm long) acicular features, identified primarily via a radial weathering pattern, penetrate through A-type laminae, and even through multiple couplets composed of both A- and B-type lamination (Figs. 13E, F). In the former case, acicular structures are associated with low relief (<5 cm) doming of the bedding, which is reduced during deposition of B-type layers. In the latter case, competitive growth between the largest acicular structures results in laterally-linked, low-relief domes that retain traceable A- and B-type bedding couplets within the structures. Pseudomorph crystal fans have been previously described from the Reivilo section and are inferred to represent penecontemperaneous growth of aragonite within microbial laminae (Sumner, 2002; Sumner and Grotzinger, 2000; 2004).

The most prominent shift in facies within the upper Reivilo section is represented by a ~50 cm thick, laterally-continuous argillaceous unit (Fig. 9B) and an approximately 50-cm thick columnar stromatolite (Fig. 14) unit that caps the outcrop at Boetsap. The argillaceous unit consists of stacked couplets of A- and B-type lamination, similar to the rest of the Boetsap section, but shows consistently more recessive weathering and a larger number of breaks in sedimentation marked by cracks filled with modern diagenetic calcrete.

The columnar stromatolite interval was excluded from stratigraphic measurement of the section because of laterally discontinuous, and often difficult to reach outcrop, and instead its base represents the top of the upper measured sections. Stromatolites consist of laterally-linked columns that show irregular inheritance (Fig. 14A), often expanding or contracting in width, and circular to irregularly elongate cross sections (Fig. 14B). Interestingly, weathering patterns and color differences associated with A-type and B-type lamination remain visible within these columnar stromatolites.

*Problems of differential weathering*

As stated above, A- and B-type lamination intervals are derived from a combination of the intensity of lamination in weathered outcrop and associated differences in color. Visual tracing of laminae along the outcrop is therefore critical to defining bedding couplets, as the extent of time that the outcrop is exposed can greatly affect interpretation of lamination and bedding. Figure 15, for example shows an approximately 10 cm thick interval exposed over approximately 2 lateral meters of outcrop. Freshly exposed surfaces typically show little or no evidence of lamination (Fig. 15A), whereas continued exposure enhances the topographic relief along laminae (Fig. 15B, C, and D). Differences in topographic relief then permit differentiation of A-type intervals, in which successive laminae are similar in weathering relief, and B-type intervals, in which successive laminae show differential relief. Cracks at the top of B-type intervals can also show expansion from precipitation of modern calcrete and, in places, small springs result in travertine coatings that obscure lamination.

### 3.2.2 Prieska Facies

The primary carbonate facies in the Upper Nauga Formation exposed near Prieska, South Africa consists of cm-scale couplets of alternating, A-type and B-type intervals that were identified based on field observation of fabric, texture, and color (Fig. 16). Multiple sequences of couplets are referred to stratigraphically as units. Individually measured stratigraphic descriptions are provided in Appendix B.

A-type intervals are composed predominantly of grey- to brown-weathering, mm-scale stratiform to tufted laminae. As in the Reivilo Formation, A-type laminae are generally sub-mm to mm-thick, and show irregularities on length-scales of millimeters, which is indicative of microbial lamination. On exposed bedding planes, A-type intervals can show a variety of textures that include tufts, interconnected ridges, and raised polygonal structures with chert-filled cracks (Fig. 17A, B).

By contrast, B-type intervals in the Upper Nauga Formation consist of brown-weathering, fine-grained intervals that can be finely laminated to unlaminated, and commonly drape topography of the underlying A-type laminae. Although well-laminated B-type intervals are rare, they can preserve details of bedforms when bedding planes are exposed (Fig. 17C).

*Facies variation in the Upper Nauga Formation*

Variation in facies in the upper Nauga Formation result primarily from differences in the texture of either the A- or B-type intervals. Here we describe three endmember variations observed within Upper Nauga Formation couplets. One endmember consists of A-type intervals that consist of flat-laminated to slightly tufted microbial laminae with relatively uniform weathering profile separated by more recessively weathered lamination forming B-type intervals or B-type cracks (Fig. 16A, B). This end member is most closely analogous to microbial couplets observed in the upper Reivilo Formation. The most commonly observed couplet type in the Upper Nauga Formation consists of nearly identical flat-laminated to tufted A-type interval followed by a fine-grained drape of brown dolomite comprising the B-type interval (Fig. 16C, D). Although B-type intervals are largely unlaminated, they can preserve lamination associated with small-sale bedforms. A final endmember consists of A-type intervals that preserve irregular lamination, tufted microbialites with up to 1 cm of synoptic relief, and abundant void space within microbial elements—now marked by infilling late diagenetic quartz. In these forms, B-type intervals are represented by unlaminated to laminated drapes, that pinch and swell over the contact with A-type laminae and preserve planar upper surfaces, to B-type cracks with laterally inconsistent evidence for draping laminae (Fig. 16E, F).

*Additional facies within the Upper Nauga Formation*

In the Upper Nauga Formation, mafic to intermediate tuffs are intercalated within the carbonate beds (Fig. 18). Tuffs vary in thickness from 1.5-30 cm, and display a range of sedimentological features. Thick tuffs (>10 cm) are commonly composed of multiple amalgamated events that show abrupt changes in texture and color (Fig. 18A). Color changes are typically associated with differences in grain size within individual tuffs and the presence or absence of carbonate cement. Multiple tuffs show accretionary lapilli (<1 mm to 5 mm diameter) that grade normally into finer-grained material (Fig. 18C). Several tuffs also show a baked zone of altered carbonate strata at their base (Figs. 18A and 18C) and density inversion structures in the few centimeters of carbonate that underlie the baked zone. Several tuffs also preserve a <1 cm thick red-purple lamina at the contact with overlying carbonate strata, which may also represent a baked zone (Fig. 18B). The thickest tuffaceous deposit (cumulatively 70 cm) is composed of multiple amalgamated tuffs. At least one tuff in this deposits contains a series of bedforms with an amplitude of a few centimeters and a wavelength of up to 20 centimeters, and the upper 10 centimeters of the amalgamated deposit consists of a mixed carbonate-volcanic interval showing asymmetrical climbing ripples with well-preserved internal, ripple cross lamination (Fig. 18D). Thin tuffs (<10 cm) are uniformly dark grey with microcrystalline texture. Detailed measurement and location data of Prieska Facies tuffs are compiled in Appendix B.

The majority of sedimentary structures and bedforms occur in association with volcanic input (Figs. 19, 20, 21). The stratigraphically lowest sections measured at the Prieska locality contain a number of anomalous beds, always associated with the occurrence of volcanic tuffs within the section. These include hummocky cross-stratification interbedded with predominantly planar beds (Fig.

21A); individual beds that show stratal disruption, such as convolute bedding and delamination of beds (Fig. 21B); presumed soft-sediment deformation wherein B-type intervals intrude into underlying sedimentary couplets, forming inverted conical structures (Figs. 20, 21C); and the disruption and mixing of welded tuff beds with underlying carbonate beds (Figs. 20, 22A, 22B). Although most of these features are associated with more common volcaniclastic contribution in the lower portions of the measured section, inverted conical structures occur throughout the measured section of the Upper Nauga Formation, although not in such abundance. All occurrences of inverted conical structures occur in carbonate beds directly beneath tuff horizons.

*Evidence for structural repetition*

Although the Upper Nauga Formation has experienced sub-greenschist metamorphism (Miyano and Beukes, 1984; Altermann and Hälbich, 1991), the carbonate strata are inferred to be structurally intact, although the section contains a variety of small folds and faults (Fig. 23). The presence of structural repetition, however, was confirmed by the observation and correlation of tuff deposits in different regions of the stratigraphic section. Specifically, the 70-cm thick amalgamated tuff capped with climbing ripples was identified multiple times within the measured section (Fig. 22). A remarkable consistency in the stratigraphy of the tuff, its associated carbonate deposits, and overlying strata indicate structural repetition by faulting not observed at the surface.

*Questions of differential weathering*

Carbonate strata composed of cm-scale A-B couplets in the Upper Nauga Formation also preserve a meter-scale rhythmicity of grey- and brown-weathering (Fig. 24). Within this rhythmic alternation in color, there is no clear alternation in the type of couplet that occurs. In both grey- and brown-weathered units, B-type intervals are consistently brown; by contrast, A-type intervals show distinct differences in weathering color, appearing either grey or brown. Brown-weathered A-type intervals, however, are identical in color and texture to grey-weathered A-type intervals when a fresh surface is exposed.

## 3.3 Interpretation

### 3.3.1 Lithofacies and Depositional Environment of Ghaap Plateau Facies

The Reivilo Formation consists of up to 900 m of carbonate strata. The Reivilo Formation exposed at Boetsap has previously been described as large-scale elongate stromatolites containing heterogeneous combinations of fine microbial laminae intercalated with columnar stromatolites and rare marl (Beukes, 1980; Beukes, 1987; Altermann and Wotherspoon, 1995; Altermann and Siegfried, 1997; Sumner and Grotzinger, 2004; Sumner and Beukes, 2006). A deep intertidal to shallow subtidal interpretation of this lithofacies is based on shore-perpendicular elongation of stromatolitic domes with symmetrically rippled surfaces (Altermann, 2008), microbial laminae that trap and bind clastic carbonate (Sumner and Grotzinger, 2004), and direct precipitation of seafloor carbonate fans (Sumner and Grotzinger, 2004). Together, these observations imply relatively stable, quiescent open marine environmental conditions occurred within, or close to the base of the tidal zone.

In this study, we examine a <20 m thick section of upper Reivilo Formation. This section is dominated by large, elongate stromatolites that preserve minimal change in morphology throughout the section, supporting the interpretation of aggradational deposition in a generally stable environment. The primary facies that comprises these stromatolites is represented by cm-scale smooth to tufted microbial laminae that alternate between grey laminae that weather to smooth, polished surfaces (A-type) and brown-red-weathered laminae that show recessive intervals (B-type). The browner color and more recessive weathering of B-type intervals suggest potential for a fine-grained detrital component to these intervals. Interpretation of environment of deposition, however, is ambiguous. In the observed section, there is no clear evidence of subaerial exposure surfaces, and there is little evidence of energetic hydrodynamic events other than some potentially subtle (<1 cm) scouring that occurs in low-points between domes, and an associated differential orientation of tufts along the tops and some edges of larger stromatolites. The presence of acicular fan-shaped crystal fans (Fig. 13) suggests *in situ* carbonate precipitation contemporaneous with microbial growth and implies low-energy conditions. These observations suggest quiescent environments, but do not directly provide evidence of whether quiescence is related to deep water or shallow water environments.

Specific observations, however, may provide additional constrains on depositional environment. For example, large elongate domes that make up the upper Reivilo Formation show synoptic relief of 10-60 cm, which implies the minimum accommodation depth.  As noted by  Sumner and Grotzinger (2004), elongation of giant stromatolitic domes and laterally-linked, minor columnar stromatolites provide evidence of hydrodynamic conditions inherent to specific environments, wherein elongation of large-scale microbial build-ups is inferred to represent the effect of incoming and outgoing tides during the growth of microbial mats, and irregularly elongate forms (cf. Fig. 14) likely reflect the combination of tides, and variable currents (e.g. wave-driven currents) in intertidal to shallow subtidal environments (Hoffman, 1976; Grotzinger and Knoll, 1999; Grotzinger et al., 2000). The observation of linear-aligned tufts on exposed dome surfaces that are perpendicular to elongation at the crests of domes, and more irregular in regions between domes further suggests deposition within a tidal regime, where low regions between domes may indicate funneling of tides and higher velocity flows between domes, which is consistent with tidal energies in marine environments.

In the modern, tidal ranges on Earth range from microtidal (<2 m) to macrotidal regimes (>4 m) and are affected by the complex interactions of astronomically controlled tides, the rotation of the Earth and position of amphidromic points relative to shorelines (Houbolt, 1986; Kvale, 2006), and local effects from submarine bathymetry (Archer and Hubbard, 2003; Dalrymple, 2010).

Contributions to tidal range also include latitudinal differentials associated with lunar tidal cycles and shoreline morphology. The most extreme tidal range at present occur in the Bay of Fundy, Canada, where these contributions to tidal range combine in a process termed resonant amplification and result in tides >13 m (Garret, 1972). Early models of Archean tidal ranges suggested an equivalent range of tides to that observed in the modern (0-13 m; Klein, 1971). Other work, however, has suggested that tidal range may have been amplified into the macrotidal regime if we consider increased gravitational effects from a more proximal Earth-Moon relationship (Hobday and Van Brunn, 1976; Eriksson et al., 2006). Interpretations of wide, shallow, and broad shelves along the Kaapvaal Craton have, in fact, been used to suggest amplified tides (Eriksson and Donaldson, 1986; Eriksson et al., 1998).

Another primary measure for estimating water depth is the relationship between fair-weather wave base and storm wave base. Fair-weather wave-base is defined as the depth at which daily wind-driven waves and associated currents (e.g. offshore rip-currents, longshore currents) mobilize very fine sand-sized grains, generally down to a depth of approximately 7-10 m (Plint, 2010; *after* Snedden and Nummedal, 1991). Storm wave base is defined as the depth to which storms can cause bedload transport (Plint, 2010; *after* Snedden and Nummedal, 1991), and reflects the maximum depth at which hydrodynamic energy from storm-generated waves disrupt the sediment-water interface. Typically storm wave base can reach depths ~50 m (Cacchione et al., 1999); extreme events such as hurricanes, however, have been measured to depths ~115 m on broad, shallow shelves (Snedden and Nummedal, 1991). Ultimately, the depth at which storms can interact with the sediment-water interface is limited by regional substrate topographies, with steeper geometries and deeper water resulting in deepening storm wave base, and shallow geometries or expansive shallow-water environments diminishing storm wave base (Cacchione et al., 1999). Stromatolites within the Reivilo Formation show evidence that suggest potential interaction with both tides and nearshore wind-driven currents; it is unlikely that the absence of high-energy events is related to deposition below storm wave base. By inference, deposition therefore likely represents intertidal to shallow subtidal conditions, where fair-weather and storm energy were potentially dampened by frictional interaction with the substrate.

This study's inference of intertidal to relatively shallow subtidal environments is consistent with the presence of cm-scale beds containing mm-scale tufted microbial laminae. Tufted mats require motile filamentous bacteria (Horodyski, 1975; 1977; Horodyski et al., 1977) that migrate to form peaked geometries as a tactic response. Although such motility has been ascribed to both photosynthesis (Horodyski, 1975) and chemosynthesis, if below the photic zone (Simonson et al., 1993; Sumner, 1997a; Cavalazzi et al., 2007; Bartley et al., 2015). Most observations of mm- to cm-scale tufted mats, however, occur in upper intertidal to supratidal environments (Horodyski, 1977; Kah and Knoll, 1996; Knoll et al., 2013; Homann et al., 2015) where they are associated with reduced microbial diversity driven by exposure and evaporation (Horodyski, 1977; Horodyski et al., 1977).

### 3.3.2 Lithofacies and Depositional Environment of Prieska Facies

The interpretation of depositional environments of the Upper Nauga Formation is controversial. The traditional interpretation infers the Upper Nauga Formation to represent deep basinal environments that are both subtidal and below storm wave base (Beukes, 1987; Grotzinger, 1989; Sumner and Beukes, 2006; Schröder et al., 2006; 2009). This interpretation is based on the appearance of cm-scale rhythmic bedding of carbonate that have been interpreted as deposition of detrital carbonate by turbidity currents (Beukes, 1987) and the presence of tufted to peaked microbialites that have been inferred to be deposited below storm wave base (Sumner and Beukes, 2006; Schröder et al., 2006; 2009). By contrast, strata of the Upper Nauga Formation have also been interpreted to have been deposited in supratidal to intertidal environments (Altermann and Herbig, 1991; Altermann and Nelson, 1998; Eriksson et al., 2006), based on polygonal structures on bedding surfaces that are inferred to reflect mudcrack formation during subaerial exposure (Altermann and Herbig, 1991), the tufted morphology of microbial mats (Altermann and Nelson, 1998), and rare tidal channel carbonate sand bodies (Altermann and Nelson, 1998).

In this study, we examine a <60 m thick section of Upper Nauga Formation. Although faults have been identified in previous field-based stratigraphic studies of the Prieska Facies (Beukes, 1987; Altermann and Nelson, 1998), this study's identification of duplicated section suggests that careful reanalysis is required to determine the true cumulative thickness of the Nauga Formation. Consistency in the stratigraphy of thick, interbedded tuff and carbonate deposits suggests that numerous unexposed faulting may exist in the Nauga Formation, with strikes oriented generally NNW along the Diamond Mine Access Road (cf. Fig. 7). These observations suggest that the thickness of exposed outcrop at Prieska between the Orange River and the Naute Shale has been over reported by a factor of 2.

Primary facies within the Upper Nauga Formation are cm-scale bedding couplets of microbial carbonate laminae overlain by a detrital component. The similarity in A-type/B-type couplets throughout the section suggests broadly aggradational deposition in a generally stable environment. The interpretation of potential water depth, however, is ambiguous. Polygonal features interpreted as evidence of subaerial exposure (Altermann and Herbig, 1991) has alternatively been interpreted as deep-water, fenestral microbialites (Sumner and Grotzinger, 2004), leaving no clear indication of subaerial exposure. With the exception of high-energy events and bedding disruption associated with volcanic events, there is little evidence for high-energy hydrodynamic conditions. These observations and interpretations suggest a generally quiescent environment of deposition but do not explicitly determine whether quiescence is a result of deeper subtidal or shallower-water environments in which high-energy events would be infrequent or suppressed, respectively.

Specific observations may reduce ambiguity with respect to depositional environments. Tuff beds provide evidence of depositional environment that may aid in this analysis. Tuffaceous beds range in thickness from several cm to 70 cm (cumulative, multi-episode beds), providing a minimum amount of accommodation for the environment. The presence of normally-graded accretionary lapilli at the base of tuffaceous horizons suggests settling in a generally quiescent environment (Reedman et al., 1987; Chough, 1990). The presence of baked zones in the upper centimeter of underlying carbonate may provide additional constraints on water depth. Baked zones, although not universal to all observed tuff beds, suggest that hot volcanic ash settled to the seafloor prior to becoming completely quenched. Other ambiguous observations of tuff beds, such as rippled tuffaceous and carbonate beds and potentially seismically-induced breccia with soft-sediment deformation, may represent variable input of hydrodynamic energy conditions associated with regional volcanism and not inherent within the marine environment (Ross, 1986; Sohn and Park, 2005; Berra and Felletti, 2011). Occurrences of hummocky cross-stratification, however, that are associated with several volcanic events indicate a combination of unidirectional (wave) and oscillatory (tidal) flows which implies that the environment of deposition was within active tidal environments (Dumas et al. 2005; Dumas and Arnott, 2006).

As noted previously, intertidal zones typically span <15 meters of depth (Dalrymple, 2010), and can overlap with hydrodynamic regimes defined by both fair-weather and storm wave base, which are directly affected by local, regional, and global controls on tidal processes (Houbolt, 1986; Archer and Hubbard, 2003; Kvale, 2006; Dalrymple, 2010). Given apparent tidal influence inferred from hummocky cross-stratification and associated high-energy events that are process-linked with volcanic activity, it is unlikely that deposition occurred below storm wave base. In the relatively thin sections measured for this study, the absence of frequent storm-related sedimentary structures suggests either deposition above fair-weather wave base where energy was dampened by friction with the substrate, or below fair-weather wave base in similarly depth-restricted environments.

As previously described, tufted mats are consistent with intertidal environments of deposition, although the interpretation of polygonal structures is still ambiguous (either as exposure surfaces and mudcracks; Altermann and Herbig, 1991; or as deep subtidal microbial structures; Sumner and Grotzinger, 2004). Variable surface texture of mats are consistent with growth differences in small changes of environmental conditions within upper intertidal depositional realms (cf. Kendall and Skipwith, 1969; Horodyski, 1977). Lastly, B-type intervals occasionally preserve irregularly crested ripples consistent with deposition in quiescent deeper intertidal to shallow subtidal environmental regimes.

# 4 ANALYSIS

## 4.1 Petrographic and Geochemical Analysis

In order to more thoroughly understand the make-up of A-B couplets, a limited number of samples were collected for petrographic and geochemical analysis. Samples from the Reivilo Formation, Ghaap Plateau Facies were collected to examine petrographic differences between A-type bed and B-type bed materials. Samples from the Upper Nauga Formation, Prieska Facies were collected from stratigraphically adjacent brown and grey weathering cycles (Fig. 24) to examine A-type and B-type couplet materials and to determine potential geochemical drivers of distinct brown and grey weathering. NOTE: This project was largely completed by an undergraduate student, Jordan Romero, as an independent study project that was directed and supervised by J.H. Alexander.

### 4.1.1 Methods

*Petrographic Methods*

A suite of hand samples representing the most common facies were collected from both Ghaap Plateau and Prieska facies. Samples were cut into approximately 2x3x1 cm billets that were used to make paired thin and thick sections. Thin sections were prepared to standard 30 μ thickness, with 600 grit finish. Thick sections were cut off to ~1.5 mm thickness and polished to 1 μ finish.

Standard petrographic analyses were performed using an Olympus BX60 Optical Microscope in plane and cross-polarized light with multiple objective magnification. Photomicrographs were acquired using a Q-Imaging Micropublisher camera and Q-Capture Software Suite. Cathodoluminescence analysis was performed using a CL8200 Mk5-2 Optical Cathodoluminescence system at 0.003 torr, ~14.8 kV, and ~280 μA. Photomicrographs were taken with a dedicated CCD camera and MagnaFire Software Suite.

*Geochemical Methods*

A limited subset of samples collected in the field were analyzed geochemically by Isotope Ratio Mass Spectrometry (IRMS) and Inductively Coupled Plasma Optical Emission Spectrometry (ICP-OES) for isotopic and elemental analyses, respectively. Discrete carbonate phases identified during petrographic and cathodoluminescence examinations, were drilled from thick sections using a Servo tabletop drill press equipped with 0.3 mm diameter drill bits. Approximately 2 mg of carbonate powder was collected from drill tailings. Geochemical analyses were completed at the University of Tennessee in the Department of Earth and Planetary Sciences and Department of Chemistry, respectively.

For isotopic analysis approximately 200 µg of carbonate powder was placed into a glass vial, and flushed with ultra-high purity He gas for 5 minutes. Samples were then acidified with 100 µl of phosphoric acid at 72˚C for a minimum of 1 hour using a Thermo-Finnegan Gas Bench II. The resultant $CO_2$ gas was transferred to a Thermo-Finnegan DeltaPlus XL mass spectrometer for measurement of isotope ratios. The isotope ratios of both carbon and oxygen are reported in delta notation as per mil relative to the Vienna Pee Dee Belemnite (VPDB) standard. Precision and calibration of data were monitored through routine analysis of internal laboratory standards and the IAEA LSVEC (d13C = −46.6‰; d18O = −26.41‰) and NBS 19 (d13C = +1.95‰; d18O = −2.2‰) international standards. Analyses were reproducible to better than ± 0.1‰ for carbon and ± 0.2‰ for oxygen, based on analysis of replicates and internal laboratory standards.

Carbonate powders were analyzed for major and minor trace elemental concentrations (Ca, Mg; Sr, Mn, Fe) using an Agilent Technologies 5110 ICP-OES. Approximately 1 mg of powdered carbonate samples was placed in 15 mL Falcon tubes and digested in 2 mL of 2% trace-metal grade $HNO_3$. Solutions were agitated and centrifuged to pelletize insoluble residue, and solutions were decanted into clean 15 mL Falcon tubes prior to analysis. Solutions were then diluted with an additional 8 mL of 2% trace-metal grade $HNO_3$. Spectral measurements were calibrated using a series of gravitational standards and reproducibility was >95% on replicate data and standards. Geochemical data are provided in Appendix C.

### 4.1.2 Results

*Ghaap Plateau Facies*

Boetsap-style laminae consisting of A-type and B-type beds show differences in grain-size, texture, and carbonate species (Fig. 25). A transition from a B-type lamina to an A-type lamina (Fig. 25A) reveals that B-type laminae consist of undulose to tufted bands of intermixed micrite and dolomite microspar, while A-type laminae consist of coarsely recrystallized calc-dolospar with minimal micrite. Another view B-type lamina is displayed in Figs. 25B and 25C which emphasizes that recrystallization of B-type laminae was destructive to primary fabric.

*Prieska Facies – Petrographic Results*

Samples collected from Upper Nauga Formation showcase differential weathering of A-type beds within m-scale alternations of grey- and brown-weathered units (cf. Fig. 24). On fresh surfaces, A-type beds of both colors have similar macroscopic texture. In microscopic analysis, A-type beds consist of undulose to tufted laminae within a heterogeneous matrix of calc-dolospar and micrite (Fig. 26). B-type beds are consistently brown, finely-laminated beds of carbonate with a strong detrital clay component, and microscopically consist of planar-s dolospar and substantial quantities of opaque minerals.

Investigation into facies with strongly tufted microbial laminae (A-type) and draping detrital clay-rich laminae (B-type) that have surficial character of polygonal structures indicate similar relationships of A-type and B-type beds as noted above. Vugs within A-type beds (Figs. 27A and 27B) consist of hexagonal quartz crystals with FeO minerals occurring interstitially between quartz and calcite. Dolomite rhombs with disaggregated debris of calc-dolospar surround vugs (Figs. 27A and 27B), however overall fabric of couplets has high similarity to primary facies throughout Upper Nauga Formation carbonates (cf. Figs. 26 with Figs. 27C and 27D).

*Prieska Facies – Isotope Results*

Values of δ13C across the full suite of A-type and B-type intervals range from -3.55‰ to -0.79‰, and values are relatively stable with an average value of

-1.48‰. Values of δ18O, however, vary between A-type and B-type intervals with A-type laminae ranging from -11.2‰ to -6.84‰ (avg. δ18O = -9.27‰) and B-type laminae from -4.32‰ to -0.75‰ (avg. δ18O = -7.02‰). Fluctuations between more negative isotopic compositions in A-type intervals and less negative isotopic compositions in B-type intervals is consistent in the stratigraphy across both grey- and brown-weathered cycles (Fig. 28).

*Prieska Facies – Elemental Results*

Across all beds in both weathering colors, [Ca] ranges from 198,856 ppm to 362,400 ppm with an average concentration of 256,408 ppm. In A-type intervals, [Mg] is higher in brown-weathered beds (avg. [Mg] = 80,311 ppm) than in grey-weathered beds (avg. [Mg] = 51,646 ppm). In B-type intervals, [Mg] ranges from 22,015 ppm to 83,238 ppm, although most samples are similar to the average concentration (avg. [Mg] = 67,885 ppm). Mg/Ca ratios are therefore lower in grey A-type intervals (avg. Mg/Ca = 0.21) than that measured in other components (avg. Mg/Ca = 0.30). Comparatively, Mg/Ca ratio in A-type intervals is lower in grey-weathered cycles, than in brown-weathered cycles (Fig. 29).

The [Fe] in the full suite of samples, with the exclusion of two Fe-rich veins (samples J3 and J18) identified in petrographic analysis, ranges from 24,259 ppm to 57,761 ppm (avg. [Fe] = 41,174 ppm). The average [Fe] for A-type intervals is 35,463 ppm, and for B-type beds is 49,170 ppm (Fig. 30). Manganese concentrations follow a similar trend in enrichment as [Fe] (Fig. 31). The average concentration of [Mn] is 7800 ppm and 11,403 ppm in A- and B-type intervals, respectively.

### 4.1.3 Interpretation

*Petrographic*

A-type and B-type beds in both the Ghaap Plateau and Prieska facies show similar petrographic character with A-type beds consisting of coarser-grained calc-dolospar, and B-type beds contain dominantly planar-s dolospar, micrite, and more FeO incorporation. Both facies are coarsely recrystallized, often to an extent where subtle primary fabric features observed in outcrop (e.g. tufted mat features) are not visible. This is consistent with previous analysis that showed recrystallization obfuscating original textures in carbonate rocks (Sumner and Grotzinger, 2004). Microscopic analysis of Prieska Facies components indicated a more clear differentiation of A- and B-type components with significantly higher concentrations of opaque Fe-oxide in B-type intervals.

*Geochemical*

Oxygen and carbon isotopic signatures measured by IRMS and plotted by stratigraphic position within a m-scale alternation of grey- and brown-weathered Prieska Facies carbonate strata (Fig. 28) show δ13C values that are similar throughout, but with δ18O values that vary between A- and B-type intervals. Oxygen isotopes are commonly interpreted as an indicator of water-rock interaction, with more negative values representing isotopic exchange with meteoric waters (Banner and Hanson, 1990). More negative δ18O values in A-type intervals suggest ongoing recrystallization during burial diagenesis, and, comparatively, less negative δ18O values in B-type intervals suggest potential for early diagenesis via dolomitization of a more porous phase. Evidence of relict dolomite crystals (Fig. 27) supports this interpretation.

Dolomitization of predecessor carbonate fabric in B-type intervals during burial suggests potentially differential diagenesis during post-depositional fluid flow. Ratios of Mg/Ca are lower in grey-weathered A-type intervals which implies a dominant low-Mg calcite carbonate phase. Higher concentrations of Mg in brown-weathered A-type intervals and all analyzed B-type intervals implies higher amounts of dolomite and/or high-Mg calcite (Fig. 29) which suggests that color differential (grey-brown cycles) is associated with dolomitization. Moreover, [Fe] and [Mn] values are, overall, lower in A-type intervals when compared to B-type intervals (Figs. 30 and 31), which indicates that stabilization of minor trace elements in these components are a result of different diagenetic responses to water-rock interaction across couplet components (Brand and Veizer, 1980; 1981). Extreme [Fe] values of two samples (J3 and J18) coupled with petrographic observations of late diagenetic veins that cross-cut both components suggest a different, potentially more recent diagenetic phase, possibly associated with faulting.

## 4.2 Analysis of Stratigraphic Architecture

### 4.2.1 Fischer Plot Analysis of Bedding Alternations

Fischer plots provide a graphical visualization of changes in net accommodation space interpreted from increasing and decreasing thickness of stratigraphic cycles relative to the mean cycle thickness. These plots were first developed to describe relative sea level changes (e.g. sum of subsidence and eustasy) recorded in m-scale cycles of peritidal facies in a carbonate ramp by Fischer (1964), and later were adapted for the use of interpreting the role of orbital forcing (i.e. Milankovitch cycles) in the formation of cyclic successions (Fischer and Bottjer, 1991). Typically, Fischer plots will rise quickly and fall slowly as a reflection of rapid transgressions creating accommodation space and more gradual accommodation response to decreases in sea level. Additional analyses determined Fischer plots to be effective in exploring details of changing accommodation space resulting from small scale changes in sea level (i.e. 3$^{rd}$ to 5$^{th}$ order sequences) on carbonate platforms (Goldhammer, 1987; Goldhammer et al., 1990), including in peritidal carbonate successions that can rapidly change from sub- to supratidal (Koerschner and Read, 1989; Montanez and Read, 1992; Goldhammer et al., 1993). Despite the rich history of investigation using Fischer plots, using fewer than 50 cycles (Sadler et al., 1993) or directly interpreting sea level curves from Fischer plots (Boss and Rasmussen, 1995) are both strongly discouraged; a Fischer plot displaying <50 cycles can result in random noise affecting the interpretation of signal in the curve, and direct interpretations of sea level from curves assumes a complete stratigraphic record, which, in reality, is rare.

### 4.2.2 Methods

In this study we use modified a Fischer plot similar in design and utility to those developed to evaluate changes in cycle thickness of two-component (i.e. siliciclastic and carbonate), m-scale parasequences in the Mesoproterozoic Belt Supergroup (Welch, 2005). By comparing a Fischer plot constructed for the overall cycle thickness to ones constructed independently for the carbonate-dominated and silt-dominated components of the cycles, Welch (2005) was able to evaluate both spatial variation in accommodation across the basin (i.e. by assuming a linear background thermal subsidence) and the extent to which different sediment sources (i.e. allochthonous siliciclastic input or autochthonous carbonate production) contributed to cycle thickness.

In this study, we are interested in exploring the astounding similarity in cm-scale bedding couplets in distinct facies belts within Archean-aged strata of the Transvaal Supergroup, South Africa. Traditional views of the Transvaal Supergroup place the Ghaap Plateau and Prieska facies belts in shallow subtidal platform and deep basin environments, respectively, separated by a high-relief platform margin marked by an active fault zone (Beukes, 1987; Sumner and Beukes, 2004; Schröder, 2006; 2009). Such environments would be expected to experience very different subsidence regimes. Additionally, such deeper water environments would not be as susceptible to limits of accommodation as potentially peritidal environments, particularly when examining cm-scale bedding couplets (Wilkinson et al., 1991).

To avoid uncertainties with potential subsidence rates in different regions of the basin, we utilized a Microsoft Excel spreadsheet macro for Fischer plots developed to not require an input for subsidence (Husinec et al., 2007). Husinec and others (2007) proposed the application of this model to estimate variation in accumulation rates in subtidal successions. Addition of modifications proposed by Welch (2005) then permits additional exploration of the variability in A- and B-type components of bedding cycles (here, bedding couplets).

The Husinec and others (2007) model creates Fischer plots that note the cumulative departure from mean cycle thickness as a proxy for sediment accumulation (i.e. accommodation in traditional parlance) versus couplet number as a proxy for time (Fig. 32). Although this program assumes measurements be input as meters, measurements here were input as centimeters and axes were scaled and labelled appropriately. Cumulative thickness is expressed on the vertical axis with changes in the slope of the curve reflecting relative changes to previous couplet thickness (Fig. 32B). Finally, the macro generates a Fischer plot that shows departures from mean thickness which are displayed as positive slopes (i.e. positive residuals; when accumulation is greater than cumulative mean of couplet thicknesses) which indicate an increasing rate of accumulation relative to older beds, and as negative slopes (i.e. negative residuals; when accumulation is less than cumulative mean of couplet thicknesses) which indicate a decreasing rate of accumulation (Fig. 32C).

The fundamental interpretation of positive and negative residuals reflects the component (A- or B-type) or couplet (A+B) thickness against the mean of all components or couplets of the same type in that sequence. Therefore, if the first thickness is less than the cumulative mean, a negative residual will occur with a steep slope. Even when sequential cycles are increasing in thickness, but remain below the cumulative mean thickness, negative residuals will occur. As cycles thicken relative to previous departures from cumulative mean, positive residuals will occur, although these cycles may still represent a negative cumulative departure from mean thickness. If and when a component/couplet thickness exceeds the cumulative mean, the curve will cross zero.

**4.2.3 Results**

In this study, modified Fischer plots were generated for couplet (i.e. bedding) thickness, thickness of component A, and thickness of component B, and compiled into a single graph per measured section. Plots generated for each measured section within both Facies were evaluated to identify contributions of components to total couplet thickness. For all couplets measured in sections of the Ghaap Plateau and the Prieska facies, average couplet thickness (A+B) was 4.14 cm in the Reivilo Formation, and 5.92 cm in the Upper Nauga Formation. Results for measured sections in the Reivilo Formation, Ghaap Plateau Facies are presented in Figs. 33 and 34. Results for measured sections in the Upper Nauga Formation, Prieska Facies are presented in Figs. 35 and 36.

### 4.2.4 Interpretation

If the couplet curve is lays above individual component curves, then the sum of the two components are contributing to relative accumulation increases in couplet thickness. If the couplet curve lays below individual component curves, then the sum of the two components contribute to decreasing accumulation in couplet thickness. If the couplet curve lies between the two component curves, then the thinner component (A or B) is offset by an increase in thickness of the other component. Another qualitative analysis that can be performed is to identify which component trends more similarly to couplet thickness; this is an indication of greater contribution of that component (i.e. deposition of that component is the dominant process controlling couplet thickness), although brief changes in a non-dominant component can have short-lived effects on couplet thickness.

*Ghaap Plateau*

Four stratigraphic sections of strata from the Reivilo Formation, Ghaap Plateau Facies (Fig. 33) were measured and combined into a single composite stratigraphic column (Fig. 34). Sections GP1 and GP2 (Figs. 33B and 33C) were measured 23 meters apart and overlap between couplets 192-276 within the composite section (Fig. 34). Section GP3 is a longer section of 189 couplets, but has traceable connectivity to GP1 and GP2 at cycles 184 and 192, respectively, within the composite section. Section GP4 is stratigraphically lower than all other sections, but correlated via GP4 couplet 91 and the base of GP3.

GP sections 1, 2, 3 (upper portion of strata) and 4 (lower portion of strata) were measured approximately 25 m apart from each other, and distinct intervals within the outcrop (e.g. beds of pseudomorphic fans, recessive-interval) permitted direct correlation (Figs. 33 and 34). Across these sections, Fischer plots show similar relationships with respect to overlapping couplets of the recessive-interval (GP1, 24-35; GP2, 28-40; GP3, 124-135), and overlapping intervals in the upper fan beds (GP1, 74-82; GP3, 180-188). There are also differences between these sections with respect to short-term changes as a result of dominant component inversion, as well as the result of challenges in the field in identifying weathered outcrop (Fig. 15). Overall similarities, however, suggest B-type components are the dominant component of couplet thickness.

Comparison of GP1 and GP2 (the two most overlapping sections) suggests that lateral continuity of individual couplets is limited. GP1 was the first section to be measured in the field, and challenges of identifying components most likely led to errors in classifying A- and B-type components (GP1, 55-73). A major challenge of interpreting Fischer plots of overlapping sections, however, also results from different starting couplet and associated effects on the cumulative mean. A major difference of overlapping sections GP1 and GP2 is the lack of exposure of seven couplets with thicker than average B-type beds at the base of GP1, that appear in both GP2 and GP3 (GP2, 1-7; GP3, 96-103; cf. Figs. 33B, 33C, and 33D).

The recessive-interval identified in the field (i.e. Figs. 5 and 10B) was laterally continuous, although the thickness of attributed to this feature varied in the field (GP1, 38 cm; GP2, 36 cm; GP3, 53 cm). Within Fischer plots, this interval shows couplets with thicker than average B-type components and extremely thin A-type counterparts in the recessive-interval which suggests that thinner intervals, such as GP2 (38-55), may result from a similar geological process (such as increased terrigenous/detrital input), but which might not be exposed in outcrop that has not weathered to the extent of GP3 (cf. Fig. 33C). Conversely, immediately after the recessive-interval (GP1, 36; GP2, 56(?); GP3, 136) A-type beds dominant signal for ~15 couplets, which suggests a shift in geologic process, such as *in situ* microbial-dominated precipitation of carbonate.

Interpretation of the Ghaap Plateau composite section (GPC, Fig. 34) shows variable control on couplet thickness with individual components contributing to different magnitudes through the section. Observations from the field provide geologic implications of these qualitative interpretations. The lower portion (GP4) of the composite section has two beds of small, domal stromatolites that contain evidence for precipitation of crystal fans. In both of these occurrences, A-type components contribute short-term influence on couplet thickness in GPC (Fig. 34), while B-type components more closely mirror changes in couplet thickness with consideration to major excursions of negative-residuals (GPC, 120-150) and positive-residuals (GPC, 12-55, 170-226).

The patterns described here, as well as the discrepancy in ranges of cumulative departure for component thickness (A-type, +7 to -48 cm; B-type, +27 to -68 cm), suggest that variable influx of detrital sediment encouraged deposition of B-type intervals and discouraged *in situ* precipitation of microbial laminae associated with A-type intervals. Conversely, when influx of allochthonous sediment was low, environmental conditions favored precipitation of *in situ* carbonate with occasional precipitation of pseudomorphic fans.

*Prieska*

Six stratigraphic sections of strata from the Upper Nauga Formation, Prieska Facies (Figs. 7 and 35) were measured for couplet thickness. Sections of the Prieska Facies had no exposed lateral connection (Figs. 35B, 35C, 35D, 35E, 35F, and 35G), however, the correlation of sections was achieved by identifying patterns of sedimentary structures and careful measurement of tuff beds (Appendix B). Section LP1 contains 181 couplets and lies stratigraphically below section RELP, although outcrop connecting the two is not exposed. Section RELP, a shorter section of only 54 couplets, is correlated with section UP1 (193 couplets) by stratigraphic measurement and comparison (Fig. 22). These two sections overlap (RELP, 24-54; UP1, 1-30) although the presence of fabric-destructive inverted conical structures (e.g. Fig. 21C) results in some dissimilarity in number of couplets. Correlation of sections UP1 (193 couplets) and LP2 (507 couplets) was achieved by observation and measurement of a 26 cm tuff that featured a remarkably well-preserved baking zone at its base (Appendix B). Likewise, LP2 was correlated with LP3 (125 couplets) via a 15.5 cm multi-horizon tuff bed. Lastly, section UP2 was highly weathered, featured many fabric destructive and volcanic beds, and thus is not correlated with any other strata in this study.

Across these sections, Fischer plots show similar relationships, although definitively overlapping intervals are not apparent. A duplicate set of 1.5 m measurements offset by 2 m in section LP2 (Fig. 36) demonstrates similarity in the thickness of A-type intervals, while B-type intervals show variable thickness. This supports our interpretation that B-type intervals consist of allochthonous input of sedimentary drapes that can vary in thickness with respect to underlying topography.

In all sections, the presence of beds with inverted conical structures results in steep positive residuals that represent artificial inflation of the cumulative mean for B-type bed thickness as a result of measuring process. This results in short-lived perturbations to couplet curve slopes, in which couplet thicknesses diverge from the dominant A-type component. This can be observed to dramatic effect in sections RELP (at bedding couplets 5, 8, and 16) and in UP2 (at bedding couplets 21, 55, 58, 59, 89, and 111), where the couplet curve (A+B) diverges rapidly away from the symmetrical relationship with A-type components (Fig. 35).

Broad similarities in sections LP1, UP1, LP2, LP3, and, to a lesser extent, UP2 (Figs. 35B, 35D, 35E, 35F, and 35G) indicate a dominant contribution of A-type beds to overall couplet thickness, and overall a decreasing rate of accumulation. Sections display rapid positive-residuals in thickness of cm-scale beds that correlate with identified sedimentary structures. In A-type beds, positive residual trends coincide with hummocky cross-stratification (LP1, 130-176), climbing/asymmetrical ripples of carbonate intercalated with tuffaceous sediment (RELP, 42-54; UP1, 18-30), and highly-tufted microbial laminae marked by chert filled vugs (UP1, 175-193; LP2, 193-252, 346-361, 481-504).

The patterns described here in which thin cycles co-occur with evidence of high energy environments (e.g. hummocky cross-stratification, asymmetrical ripple marks) and thick cycles co-occur with strongly tufted microbial laminae are consistent with changes in water-depth in a broadly intertidal environment that are reflected in accumulation. Hummocky cross-stratification and asymmetrical ripple marks show brief increases in relative thickness section LP1, but they are not on the same magnitude as the rapid positive residuals occurring with strongly tufted laminae in sections UP1 and LP2. The symmetric positive residual trends of A-type and couplet thickness in LP3 (18-57) and in UP2 (75-106) could be indicative of a similar relationship, however, these occurred in carbonate facies that were altered by diagenesis. The evidence points toward microbial-dominated A-type beds controlling couplet thickness throughout all sections, with consistently low rates of accumulation in B-type beds suggesting a steady, but not overwhelming, influx of detrital sediment.

*Comparison of Ghaap Plateau and Prieska*

Ghaap Plateau and Prieska facies show opposite relationships in regard to which component (B-type, Ghaap Plateau; A-type, Prieska) shows greater rates of accumulation and a greater contribution to cm-scale couplet thickness. However, B-type beds in the Reivilo Formation are interpreted to represent a combination of allochthonous input and thin, tufted microbial laminae (*this study*; Sumner and Grotzinger, 2004). A-type beds in Prieska are here interpreted as microbial carbonate deposited in broadly peritidal environments (cf. Altermann and Herbig, 1991; Altermann and Nelson, 1998; Eriksson et al., 2006).

Interestingly, Fischer plot analysis here may provide a means of testing the interpretation of Beukes (1987), wherein Prieska Facies couplets are interpreted as distal deep basin turbidites. To evaluate contributions of A- and B-type beds to overall couplet thickness, a series of hypothetical modified Fischer plots are presented (Fig. 37). When both components (A- and B-type) are equal in thickness throughout a sequence, they will plot synchronously and the couplet (A+B) curve will follow the same wavelength at a greater magnitude (Fig. 37A). This type of Fischer plot relationship would be expected in idealized distal D and E components of classic turbidites (Bouma, 1962). Conversely, if one component of a couplet contributes more to overall couplet thickness, the resulting curve would appear as a variation on Fig. 37B, wherein a hypothetical succession with greater magnitude of changes in both positive and negative residuals of A-type bed thicknesses when compared to more subtle changes in B-type bed thicknesses. Here, the couplet curve closely follows the same path of the A-type, with less contributory impact from changes in B-type thicknesses. It is possible, however, that switching of dominant component could occur in which the couplet curve would be preferentially affected by both components at different points in a succession (Fig. 37C). Here, asynchronous thinning and thickening of components (A, B) contributes to a suppression of changes to couplet thickness (A+B). For the Fischer plots for the composite section in Ghaap Plateau, we interpret asynchronous behavior of thinner on average A-type components and dominant B-type contribution to couplet thickness as a depositional response to environmental changes in allochthonous influx.

Fischer plots from Prieska Facies sections clearly show (with the exception of sections with frequent evidence of soft-sediment deformation) that A-type components contribute more to couplet thickness. This is not what would be expected for distal deposition of allochthonous carbonate to the deep basin. Moreover, an overarching similarity of Fischer plots in both the Ghaap Plateau and Prieska facies is that one component typically mirrors, and thus dominates, couplet thickness changes. This also implies that, although A- and B-type components have different genetic interpretations between the two discrete Facies, the dynamics controlling differential accumulation rates of A- and B-type components in these depositional environments are not that different.

### 4.3.1 Statistical Analysis of Bedding Alternations

A second method of understanding behavior of couplet thickness of both Ghaap Plateau and Prieska facies, is to apply statistical analyses to measurements from the field. The application of statistics to aid in interpreting stratigraphic patterns is not new to stratigraphy, and previous work by (Maurer et al., 2004; *after* Hinnov and Goldhammer, 1991) has successfully applied components of Time-Series Analysis to interpret changes in accumulation rate and parse out cyclic signals of bedding rhythms in basinal carbonate rock using a comparative approach of cyclostratigraphic principles with geochronological data that incorporated facies study, sediment source determination, and transport mechanisms.

Radiometric dates of volcanic ash deposits for the Campbellrand Subgroup, especially in the Ghaap Plateau Facies, are limited (Barton et al., 1994; Walraven and Martini, 1995; Altermann, 1996; Sumner and Bowring, 1996; Altermann and Nelson, 1998). The paucity of geochronological data is compounded by the inherent statistical error associated with dating such ancient strata, and chronostratigraphic relationships between sections that are 250 km apart from each other is not assumed. Therefore, we proposed using stratigraphic relative time as a proxy for absolute time to compare the alternations from both Facies. This study applied common Time-Series Analysis techniques by modifying the time-component into a spatial sequence of beds, although we neglect to use the term cycles (here, couplets) to describe these components (Maurer et al., 2004).

We use autocorrelation and cross-correlation techniques to explore similarity in behavior of two successions traditionally inferred to represent very different depositional environments. Couplet thickness data is input for two sections that are similar in thickness and in total number of couplets. Results are displayed as correlation coefficients for successive couplets within sequences (autocorrelation) and between the two sections (cross-correlation). One challenge of interpreting similarity from statistical signals in geologic datasets is the potential for noise in the analysis to disrupt signals (i.e. frequency of cycles). Based on the absence of exposure surfaces and evidence for lower intertidal to shallow subtidal deposition in both the Ghaap Plateau and Prieska facies, we make the assumption that subtidal deposition was uninterrupted. Still, changes in sedimentation style, such as volcaniclastic material and high-energy events, can disrupt the signal from the primary alternation of carbonate beds, and obscure evaluations of potential periodic changes in the strata. The reduction of signal noise was accomplished by modifying outliers from stratigraphic measurements. Stochastic, non-carbonate strata that interrupted patterns of bedding couplets, such as volcanic tuff deposits and evidence of the destruction of primary bedding, were adjusted to conserve couplet integrity by replacing tuff thickness with a minimal, non-zero thickness boundary. Simplification of the stratigraphic section is in line with the approach used in the study of core by Maurer and others (2004).

### 4.3.2 Methods

Statistical Time-Series Analysis techniques were performed using Statistical Analysis System (SAS) version 9.4 software. The couplet dataset input in the previous Fischer plot analysis was used and autocorrelation and cross-correlation were performed using a group of SAS procedure statements (gplot, TIMESERIES, print) in a PROC step to produce statistics, analyses, and graphics. Statistical analyses include autocorrelation and cross-correlation of couplet thicknesses to evaluate data for variance of bedding patterns by considering random and non-random distribution of thicknesses through time.

*Autocorrelation*

Autocorrelation is applied here as a measure of offset similarity within a sequence of couplets which compares changes in thickness of successive beds within a section by offsetting couplets over increasing lag distances ($\tau$ = 0, 1, 2, 3, etc.; Fig. 38). Results provide the autocorrelation coefficient ($r_\tau$) of offset couplet thickness which expresses the degree of similarity between couplets within the section of measured strata. The autocorrelation ($r_\tau$) between pairs of beds in a spatial series $y_i$ & $y_{i+\tau}$ separated by a lag number of $\tau$ where *N* = total number of beds in the series:

$$r_\tau = \frac{\sum_{i=1}^{N-\tau}(y_i - \bar{y})\,(y_{i+\tau} - \bar{y})}{\sum_{i=1}^{N}(y_i - \bar{y})^2} \qquad (1)$$

Here, we determine offset similarity of sections by evaluating randomness, with increasing variance of thickness reflecting non-random data. If data are random, and do not show any relationship between variables, then autocorrelation $(r_\tau)$ = 0. If data are non-random, then autocorrelation $(r_\tau)$ ≠ 0. Thus as autocorrelation $(r_\tau)$ approaches $(r_\tau)$ = 1, the degree of offset similarity of cm-scale beds within sections increases.

*Cross-correlation*

Cross-correlation is a comparison of variation of couplet thickness between two stratigraphic sections that are relatively equal in both the number of stratal packages (i.e. cm-scale couplets) and in overall thickness of the section. Attempts have been made in the past to use this method to correlate strata (Sackin and Merriam, 1969; Nosal and Vrbik, 1982), but is frequently regarded as a poor way to provide true lithostratigraphic correlation due to gaps in the stratigraphic record (Smith and Waterman, 1980). Here we use cross-correlation only to estimate similarity of bedding couplets between sections, and only suggest that observations of facies in potentially repeating, fault-bounded sections are statistically supported. In this method, cross-correlation $r_\tau(x, y)$ reflects the fit of bed similarity between two series, $x$ & $y$, when displaced by a lag of $\tau$ where *N* = total number of beds in the series:

$$r_\tau(x,y) = \frac{\sum_{i=1}^{N-\tau}(x_i - \bar{x})\,(y_{i+\tau} - \bar{y})}{\sqrt{\sum_{i=1}^{N}(x_i - \bar{x})^2} \;\times \sqrt{\sum_{i=1}^{N}(y_{i+\tau} - \bar{y})^2}} \tag{2}$$

Truly random data results in a cross-correlation coefficient $r_\tau(x,y)$ = 0, and if data are non-random, then $r_\tau(x,y) \neq 0$. Values for autocorrelation between 0<1 indicate greater similarity of sections with values approaching 1 indicating a high degree of similarity.

**4.3.3 Results**

Here we separately explore auto- and cross-correlation analyses, although graphs for both analyses are presented together (Figs. 39, 40, 41, 41, and 43). The objective of autocorrelation analysis is to determine consistency of couplet (combined A-type and B-type bed) thickness in facies within the Reivilo Formation and Upper Nauga Formation by evaluating correlograms that plot $(r_\tau)$ versus $\tau$, wherein autocorrelation aims to identify potential periodicity of changes in bedding thickness. All input data is provided in Appendix D.

The cross-correlograms presented here fall into two categories: (1) short comparisons of offset similarity in duplicate and tectonically repeated sections that were measured in close proximity to each other, and (2) comparisons between disparate sections to estimate similarity in couplet thickness in different regions of the basin to evaluate similarity of deposition in different environments (not lithostratigraphic correlation). Cross-correlograms presented here plot covariance of bedding thickness $r_\tau(x, y)$ versus lag number $\tau$. By comparing strata in pairs, we attempt to identify statistically significant correlation coefficients to better understand the similarities and differences between and within the Ghaap Plateau and Prieska facies.

In Fig. 39, two duplicate, 1.5 m thick sections of 39 couplets each (interval shown in Fig. 24B), are compared with autocorrelation to evaluate internal similarities of each bed, and with cross-correlation to evaluate similarities between the two sequences to check for lateral continuity of bedding thickness. These laterally adjacent sub-sections within section LP2 (Figs. 39A and 39B) shows little statistically significant offset similarity (autocorrelation), yet a cross-correlation coefficient (Fig. 39C) of 0.6 at a lag of 0 couplets (p-value <0.05) was anticipated due to measurements beginning at the same surface for both of the 1.5 m sections.

In Fig. 40, two overlapping sections of strata (GP1, 88 couplets, 4.6 m; GP2, 92 couplets, 4.3 m) offset by ~23 m in the Ghaap Plateau Facies were analyzed for the same intent as described above, although these sections were known to be offset vertically by 7 couplets from observations in the field. Although there is no dramatic degree of offset similarity internal to bedding thickness patterns, the values of autocorrelation coefficient follow similar trends of decreasing correlation (GP1: $\tau$ = 1-2, $(r_\tau)$ = 0.397 to 0.245, p-values <0.05; GP2: $\tau$ = 1-2, $(r_\tau)$ = 0.410 to 0.301, p-values <0.05) suggesting similar variation in couplet thicknesses across the sections (Figs. 40A and 40B). Cross-correlation of GP1 and GP2 (Fig. 40C) correctly correlated these two columns of cm-scale beds, returning a non-random signal at a lag of -7 couplets (p-value <0.05). Results for comparison within and between GP2 (92 couplets, 4.3 m) and a full measure of GP3 (189 couplets, 8 m; Figs. 41A and 41C) showed similar results for offset similarity (autocorrelation; GP2: $\tau$ = 1-4, $(r_\tau)$ = 0.311, 0.219, 0.210, 0.195, p-values <0.05; GP3: $\tau$ = 1, 3-4, $(r_\tau)$ = 0.0.258, 0.220, 0.193, p-values <0.05), yet cross-correlation results returned statistically significant correlations of bedding thickness between couplets offset by a lag of 1 and 7 couplets (Fig. 41C; : $\tau$ = 1, 7, $r_\tau(x, y)$ = 0.278, 0.1943, p-values <0.05).

Over longer distances (Fig. 42), cross-correlation analysis returned a high coefficient in comparison of similar cm-scale beds from RELP and UP1 (~2 km distant) in the Prieska Facies at a lag of 3 couplets (Fig. 42C; $r_\tau(x, y)$ = 0.690, p-value = 0). By contrast, only a weak cross-correlation coefficient of -0.13 (p-value <0.05) over a lag of 20 couplets was determined between the Ghaap Plateau and Prieska Facies sections over the extreme distance of 250 km (Fig. 43C).

### 4.3.4 Interpretation

Statistical approaches indicate that elements of Time-Series Analysis can be used to evaluate similarity of couplet thickness within facies. Autocorrelation analysis results from duplicate sections in the Ghaap Plateau Facies (Figs. 40 and 41) agree with Fischer plot analyses that indicate lateral continuity of bedding thickness of these sections. Autocorrelation of sections GP1, GP2, and GP3 indicate slow changes in depositional thickness over lags of 3 couplets (p-values <0.05), suggesting potential for a periodic fluctuation in depositional conditions and accumulation potentially reflecting small changes in accommodation associated with shallowing-upward cycles in shallow marine environments.

Cross-correlograms for overlapping measured sections (Figs. 40 and 41; GP1 and GP2; GP2 and GP3), separated by ~25 m of lateral distance, in the Ghaap Plateau Facies confirm field observations of consistent bedding thickness across adjacent giant elongate domes, and confirm accurate identification of A-type and B-type beds in the field. In the Prieska Facies, cross-correlation analysis of 1.5 m sections offset by 2 m (Fig. 39) indicates nearly symmetrical lateral continuity at lags -1 and -2 couplets (p-value <0.05) and also confirms A-type and B-type bed identification despite variation in m-scale weathering patterns, which implies that deposition occurred in an environment with relatively stable rates of accumulation.

Cross-correlation within the Prieska Facies (Fig. 42) indicates a high correlation coefficient (0.7) at a lag of 3 couplets (p-value <<0.05). These sections were specifically examined because they were thought to represent structural duplication of section, and thus, strong correlation is consistent with field observations (Fig. 22) of duplicate section in the Upper Prieska 1 section and the River's Edge Lower Prieska section.

Attempts at cross-correlation between disparate Facies (Fig. 43C) via 280 couplets of compositely compiled strata in the Reivilo Formation and 280 couplets of Prieska Facies strata compiled from the UP1 and LP2 indicate only weak correlation (-0.13) at a lag of 20 couplets (p-value <0.05). This suggests that over intervals of 20 couplets (~0.5 m of cm-scale beds), there is a subtle, inverse relationship between these two disparate facies, whereas as Ghaap Plateau Facies couplets get thicker on an interval of 20 couplets, Prieska Facies couplets would decrease in the same period. This implies either that lower-order cyclicity ($4^{rd}$-$5^{th}$ order) had different effects in these two environments, or, given that we do not assume direct time-correlation of these that could be a subtle change in accommodation space as a response to differing levels of subsidence, or regional controls on eustatic sea level change.

# 5 DISCUSSION

Here we explored bedding-scale facies and depositional patterns in discrete facies belts of the Archean Transvaal Supergroup, South Africa. Specifically we examine bedding patterns in the upper Reivilo and Upper Nauga formations, which show strikingly similar style of cm-scale bedding couplets. These two formations represent sections of the Ghaap Plateau Facies (Beukes, 1987; Altermann and Wotherspoon, 1995; Altermann, 1996; Altermann and Siegfried, 1997; Altermann and Nelson, 1998; Eriksson et al., 1998; Sumner and Grotzinger, 2004; Eriksson et al., 2006; Schröder et al., 2006; Sumner and Beukes, 2006; Altermann, 2008; Knoll and Beukes, 2009; Schröder et al., 2009; Eroglu et al., 2015; Altermann, 2016; Eroglu et al., 2017) and the Prieska Facies (Beukes, 1987; Altermann and Hälbich, 1991; Altermann and Herbig, 1991; Altermann and Wotherspoon, 1995; Altermann, 1996; Altermann and Siegfried, 1997; Altermann and Nelson, 1998; Eriksson et al., 1998; Wright and Altermann, 2000; Sumner and Grotzinger, 2004;

Eriksson et al., 2006; Schröder et al., 2006; Sumner and Beukes, 2006; Altermann, 2008; Knoll and Beukes, 2009; Schröder et al., 2009; Eroglu et al., 2015; Altermann, 2016; Eroglu et al., 2017) of the Campbellrand Subgroup. Although sections cannot be directly correlated, current geochronology (Barton et al., 1994; Walraven and Martini, 1995; Sumner and Bowring, 1996; Altermann and Nelson, 1998) and basin models (Beukes, 1987; Grotzinger, 1989; Sumner and Beukes, 2006) suggest that the two sections are broadly coeval.

In traditional depositional models of the Griqualand West sub-basin (Sumner and Beukes, 2006; *after* Beukes, 1987 and Grotzinger, 1989), the Ghaap Plateau and Prieska facies are interpreted to reflect a growing disparity in depositional environments, wherein activation of syndepositional movement along the GFZ resulted in development of a steep margin separating distinct platform and basin environments. Prior to movement along the GFZ, the Transvaal Supergroup was inferred to be representative of a broad carbonate ramp (Lokammona and Monteville formations; Beukes, 1987; Grotzinger, 1989; Schröder et al., 2006; Sumner and Beukes, 2006). By the time of deposition in the upper Reivilo and Upper Nauga formations, which are the focus of this study, the platform margin is inferred to have reached >500 m of depositional relief (cf. Fig. 2 in Beukes, 1987; Fig. 13 in Grotzinger, 1989; Fig. 2 in Sumner and Beukes, 2006; Fig. 4 in Schröder et al., 2009). Ultimately, this margin is inferred to have reached >900 m during deposition of the Naute Shale and the Gamohaan formations in the latest Archean.

## 5.1 Implications for Basin Structure

In both upper Reivilo and Upper Nauga formations, sedimentation consists of cm-scale couplets that are dominated by planar to tufted microbial mat facies. In the Ghaap Plateau Facies (Reivilo Formation) B-type components consist of microbial growth with a much stronger relief in weathering, possibly associated with influx of a fine-grained detrital component (see also Sumner and Grotzinger, 2004). A-type components in the Ghaap Plateau Facies consist of similarly planar to tufted microbial facies. In the Prieska Facies (Upper Nauga Formation), non-dominant, B-type beds consist of a detrital component with evidence of deposition from suspension (draping, pinch and swell) or via traction (currents, waves).

In addition to the striking similarity of cm-scale bedding patterns, detailed comparison of the full range of facies provides evidence that depositional environments in these two localities are similar. The presence of hummocky cross-stratification in Prieska Facies and persistent elongation of stromatolites in Ghaap Plateau Facies suggest deposition largely within intertidal to shallow subtidal environments. The absence of unambiguous evidence for subaerial exposure in both facies belts, however, suggests the shallowest water environments may be limited to lower intertidal realms. The identification of baked zone contact surfaces of carbonate strata beneath volcanic tuffs (Fig. 18) in the Prieska Facies implies that water depths were likely not deeper than shallow subtidal. Generally, low-energy deposition argues for tide-dominated rather than storm-dominated deposition (Kvale, 2006; Dalrymple, 2010). Rare evidence of high-energy deposition—scours and convolute bedding—in Prieska Facies all occur in association with thick volcanic intervals, suggesting local energy input.

Analysis of modified Fischer plots (*after* Welch, 2005) and statistical evaluations of couplet thickness trends and similarities, respectively, further identify that patterns of sediment accumulation are similar in upper Reivilo and Upper Nauga formations. Specifically, Fischer plot analysis shows that, although different components control overall changes in couplet thickness, the behavior of these two component systems, combining a microbial-dominated carbonate component that dominates couplet thickness and a stable component of background sedimentation with short-lived, subtle influence on couplet thickness trends, are remarkably similar. Statistical evaluations of similarity between couplets within independent sections (autocorrelation) of the Ghaap Plateau Facies agree with Fischer plot analysis that beds are relatively uniform in thickness, which suggests a stable, quiescent environment, and implies that beds have a slightly periodic component that may reflect a depositional response to changes in accommodation. Cross-correlation analysis between couplets in overlapping sections in the Ghaap Plateau Facies support lateral continuity of couplet thickness and confirm positive identification of A- and B-type components during measurement. In the Prieska Facies, autocorrelation supports lateral consistency in thick, A-type components suggesting a stable environment of deposition in microbial facies, while irregularity in lateral thickness consistency of

B-type components indicates a higher degree of variation in accumulation, supporting a detrital origin.

Combined, these features are inconsistent with deposition in facies that span >500 m of water depth. Although the Ghaap Plateau and Prieska facies are not precisely chronostratigraphically correlative or identical in depositional style, analyses suggest deposition on a substrate with low regional slope. In this scenario, a broad carbonate ramp, with spatially extensive areas of the marine substrate would be subject to tidal influence, regardless of regional or temporal variations in tidal range. Small differences in substrate topography, as well as proximity to detrital sources, could result in subtle differences in environment that is recorded here in subtle variations in couplet components.

**5.2 Implications for Basin Polarity**

Detailed measurement and statistical analyses in Prieska facies also revealed unreported structural duplication, which potentially provides for Upper Nauga Formation to be thinner than the currently reported thickness, although published stratigraphic thickness of the Nauga Formation varies (~500 meters in Beukes, 1987; ~700 meters in Altermann and Nelson, 1998; 600-1000 meters in Schröder et al., 2006; 2009). Additionally, the similarity in cumulative average of all cm-scale couplets for each facies (4.14 cm for Reivilo Formation couplets and 5.92 cm for Upper Nauga Formation couplets) suggests that sedimentation rate is remarkably similar. In the traditional basin model (Beukes, 1987; Sumner and Beukes, 2006), differences in total strata thickness between the similarly-aged

Ghaap Plateau and Prieska facies are attributed to differential subsidence and generation of accommodation, combined with limited hydrodynamic transport of allochthonous carbonate to deep basin (Schröder et al., 2009). An alternative model was proposed (Altermann and Herbig, 1991) and later expanded (Altermann and Nelson, 1998) that shifted polarity of the basin. In this model, differential subsidence resulting from intracratonic sag (thermal subsidence) north of the GFZ generated greater accommodation in the Ghaap Plateau Facies, and the GFZ is reinterpreted as a post-depositional strike-slip fault. This was supported by potential subaerial exposure surfaces within the Upper Nauga Formation. Moreover, evidence suggesting sustained volcaniclastic input in Prieska Facies sections and structural interpretations of Neo-archean to Paleoproterozoic terrane accretion associated thrust-faulting along the SW margin of the Griqualand West sub-basin (Figs. 1 and 2 of Altermann and Hälbich, 1991; Altermann and Nelson, 1998; Eriksson et al., 2006) complicates assumptions of differential accommodation across a syndepositional GFZ. Our investigation supports a ramp structure during upper Reivilo and Upper Nauga time.

**5.3 Implications for Archean Environments**

One most profound change in early Earth history was the Great Oxygenation Event (GOE) which occurred between approximately 2.4 to 2.0 Ga, and marked a dramatic change in the atmosphere-ocean system (Bekker et al., 2004; Bekker and Holland, 2011). Prior to the GOE (>2.40 Ga), reducing conditions dominated Archean marine environments (Bekker et al., 2004). The disappearance of mass-independent fractionation of sulfur isotopes, which requires atmospheric oxygen concentrations of at least $10^{-5}$ present atmospheric level (PAL), mark the GOE (Farquhar et al., 2000; Bekker et al., 2004), and it is inferred that continued oxygenation of Earth surface environments was irreversible (Holland, 2002; 2006). Geological constraints on the Transvaal Supergroup places strata near the start of the GOE at ~2.5 Ga (Barton et al., 1994; Walraven and Martini, 1995; Sumner and Bowring, 1996; Altermann and Nelson, 1998). Therefore, the units within the Transvaal Supergroup are critical for defining chemistry of oceans just prior to the GOE (cf. Pavlov and Kasting, 2002; Partin et al., 2013; Liu et al., 2016).

An outstanding question of the GOE is how to determine the extent of oxygenation of surface environments and the influence of oxygenation on ocean chemistry. Even prior to the GOE, it is expected that low oxygen concentrations in surface environments, as a result of oxygenic photosynthesis, would result in oxygenated surface oceans (Riding and Fralick, 2014; Riding et al., 2014; Fralick and Riding, 2015; Kurucz and Fralick, 2018), even if the deep ocean remained anoxic (Aharon, 2005; Partin et al., 2013).

Recent studies of redox chemistry from cores through the Transvaal Supergroup reveal potentially ambiguous data (Schröder et al., 2006; Eroglu et al., 2015; Eroglu et al., 2017). Geochemical investigation of the Monteville and Nauga formations suggest switching of siliciclastic provenance early in the deposition of the Transvaal Supergroup progradation (Schröder et al., 2006). Similarly, isotopic analysis of molybdenum in carbonate strata shows potential for oxic environments in both shallow-water and basinal environments (Eroglu et al., 2015). Such ambiguous data for oxygenation of both shallow and deep-water environments was therefore interpreted as indicating preservation of primarily diagenetic signals. These investigations utilize drill cores recovered from south of the GFZ, and base interpretations on the traditional model where Prieska Facies are interpreted as having been deposited in deep subtidal to basinal environments. If we consider this data within the context of a more ramp-like geometry proposed here, in addition to potential for a shift in basin polarity (cf. Schröder et al., 2006), Mo-isotope records could be reinterpreted to reflect a broader spatial occurrence of oxygenated conditions across a broadly shallow ramp environment.

# 6 CONCLUSIONS

1) Detailed stratigraphic analysis of lithofacies suggest that both Ghaap Plateau and Prieska facies represent dominantly microbial deposition in intertidal to shallow subtidal environments.
2) Stratigraphic investigations of cm-scale bedding patterns via modified Fischer plots and Time-Series Analysis (autocorrelation) indicate similar patterns of sediment accumulation, supporting interpretations of similar depositional setting.
3) Statistical comparison (cross-correlation) of Prieska Facies sections RELP and UP1 support field observations of stratigraphic repetition resulting from tectonic activity with strike oriented roughly NW to SE.

4) Combination of detailed analyses of Ghaap Plateau and Prieska Facies, previously described as representing platform and basin separated by the GFZ, suggests a need for further study and a reexamination of traditional Griqualand West sub-basin model.

# LIST OF REFERENCES

Aharon, P., 2005. Redox stratification and anoxia of the early Precambrian oceans: implications for carbon isotope excursions and oxidation events. Precambrian Research 137, 207-222.

Altermann, W., 1996. Sedimentology, geochemistry and palaeogeographic implications of volcanic rocks in the Upper Archaean Campbell Group, western Kaapvaal craton, South Africa. Precambrian Research 79, p. 73-100.

Altermann, W., 2008. Accretion, trapping and binding of sediment in Archean stromatolites – morphological expression of the antiquity of life. Space Science Reviews 135, p. 55-79.

Altermann, W., 2016. Archean stromatolites and their depositional environments. 35th International Geological Congress Field Trip Guide, International Union of Geological Sciences, Pretoria, RSA, pp. 1-64.

Altermann, W., Hälbich, I.W., 1991. Structural history of the south western corner of the Kaapvaal Craton and the adjacent Namaqua Realm: New observations and reappraisal. Precambrian Research 52, 133-166.

Altermann, W., Herbig, H.G., 1991. Tidal flat deposits of the Lower Proterozoic Campbell Group along the southwestern margin of the Kaapvaal Craton, Northern Cape Province, South Africa. Journal of African Earth Sciences 13, 415– 435.

Altermann, W., Nelson, D.R., 1998. Sedimentation rates, basin analysis and regional correlations of three Neoarchaean and Palaeoproterozoic sub-basins of the Kaapvaal craton as inferred from precise U – Pb zircon ages from volcaniclastic sediments. Sedimentary Geology 120, 225–256.

Altermann, W., Siegfried, H.P., 1997. Sedimentology and facies development of an Archaean shelf: carbonate platform transition in the Kaapvaal Craton, as deduced from a deep borehole at Kathu, South Africa. Journal of African Earth Sciences 24, 391–410,

Altermann, W., Wotherspoon, J.M., 1995. The carbonates of the Transvaal and Griqualand West Sequences of the Kaapvaal craton, with special reference to the Lime Acres limestone deposit. Mineralium Deposita 134, 124–134.

Archer, A.W., Hubbard, M.S., 2003. Highest tides of the world. In: Chan, M.A., Archer, A.W. (Eds.), Extreme Depositional Environments: Mega End Members in Geologic Time. Geological Society of America, Special Paper 370, 151-173.

Armstrong, R.A., Compston, W., Retief, E.A., Williams, I.S., Welke, H.J., 1991. Zircon ion microprobe studies bearing on the age and evolution of the Witwatersrand triad. Precambrian Research 53, p. 243-266.

Banner, J.L., Hanson, G.N., 1990. Calculation of simultaneous isotopic and trace element variations during water-rock interaction with applications to carbonate diagenesis. Geochemica et Cosochimica Acta 54, 3123-3137.

Bartley, J.K., Kah, L.C., Frank, T.D., Lyons, T.W., 2015. Deep-water microbialites of the Mesoproterozoic Dismal Lakes Group: microbial growth, lithification, and implications for coniform stromatolites. Geobiology 13, 15-32.

Bekker, A., Holland, H.D., 2011. Oxygen overshoot and recovery during the early Paleoproterozoic: Earth and Planetary Science Letters 317–318, 295–304.

Bekker, A., Holland, H.D., Wang, P., III, D.R., Stein, H.J., Hannah, J.L., Coetzee, L.L., Beukes, N.J., 2004. Dating the rise of atmospheric oxygen: Nature 427, 117–120.

Berra, F., Felletti, F., 2011. Syndepositional tectonics recorded by soft-sediment deformation and liquefaction structures (continental Lower Permian sediments, Southern Alps, Northern Italy): Stratigraphic significance. Sedimentary Geology 235, 249-263.

Beukes, N.J., 1979. Litostratigrafiese onderverdeling van die Schmidstdrif-subgroep van die Ghaap-groep in noord-Kaapland Trans. Geol. Soc. S. Afr. 82, 313-328.

Beukes, N.J., 1980. Lithofacies and stratigraphy of the Kuruman and Griquatown iron-formations, northern Cape Province, South Africa. Trans. Geol. Soc. S. Afr. 83, 69-86.

Beukes, N.J., 1987. Facies relations, depositional environments and diagenesis in a major early Proterozoic stromatolitic carbonate platform to basinal sequence, Campbellrand Subgroup, Transvaal Supergroup, Southern Africa. Sedimentary Geology 54, 1–46.

Boss, S.K., Rasmussen, K.A., 1995. Misuse of Fischer plots as sea-level curves. Geology 23, 221–224.

Bouma, A.H., 1962. Sedimentology of some flysch deposits: A graphic approach to facies interpretation. Elsevier, Amsterdam.

Brand, U., Veizer, J., 1980. Chemical diagenesis of a multicomponent carbonate system – 1: Trace elements. Journal of Sedimentary Petrology 50, 1219-1236.

Brand, U., Veizer, J., 1981. Chemical diagenesis of a multicomponent carbonate system – 1: Stable isotopes. Journal of Sedimentary Petrology 51, 987-997.

Burchette, T.P., Wright, V.P., 1992. Carbonate ramp depositional systems. Sedimentary Geology 79, 3-57.

Cacchione, D.A., Wilberg, P.L., Lynch, J., Irish, J., Traykovski, P., 1999. Estimates of suspended-sediment flux and bedform activity on the inner portion of the Eel continental shelf. Marine Geology 154, 83-97.

Cavalazzi, B., Barbieri, R., Ori, G.G., 2007. Chemosynthetic microbialites in the Devonian carbonate mounds of Hamar Laghdad (Anti-Atlas, Morocco). Sedimentary Geology 200, 73-88.

Cecil, C.B, 2003. The concept of autocyclic and allocyclic controls on sedimentation and stratigraphy, emphasizing the climatic variable. In: Cecil, C.B., Edgar, N.T. (Eds.), Climate Controls on Stratigraphy. SEPM Special Publication 44, Tulsa, OK, pp. 13-20.

Chough, S.K., Sohn, Y.K., 1990. Depositional mechanics and sequences of base surges, Songaksan tuff ring, Cheju Island, Korea. Sedimentology 37, 1115-1135.

Clenedin, C.W., 1989. Tectonic influence on the evolution of the early Proterozoic Transvaal Sea, southern Africa. Ph.D. Dissertation, Witwatersrand University, Johannesburg, 376 pp.

Cook, H.E., McDaniel, P.N., Mountjoy, E.W., Pray, L.C., 1972. Allochthonous carbonate debris flows at Devonian bank (‘reef’) margins Alberta, Canada. Bulletin of Canadian Petroleum Geology 20, 439-497.

Dalrymple, R.W., 2010. Tidal depositional systems. In: James, N.P., Dalrymple, R.W. (Eds.), Facies Models 4. Geological Association of Canada, Newfoundland, 201-231.

Demicco, R.V., Hardie, L.A., 1994. An inventory of common sedimentary structures and early diagenetic features of shallow marine carbonate deposits. SEPM Atlas Series No. 1, Tulsa, Oklahoma.

Drummond, C. N., Wilkinson, B. H., 1993, Aperiodic accumulation of cyclic peritidal carbonate. Geology 21, 1023-1026.

Dumas, S., Arnott, R.W.C., 2006. Origin of hummocky and swaley cross-stratification – The controlling influence of unidirectional current strength and aggradation rate. Geology 34, 1073-1076.

Dumas, D., Arnott, R.W.C., Southard, J.B., 2005. Experiments on oscillatory-flow and combined-flow bed forms: Implications for interpreting parts of the shallow-marine sedimentary record. Journal of Sedimentary Research 75, 501-513.

Eriksson, K.A., Donaldson, J.A., 1986. Basinal and shelf sedimentation in relation to the Archaean-Proterozoic boundary. Precambrian Research 33, 103-121.

Eriksson, K.A., Simpson, E.L., Mueller, W., 2006. An unusual fluvial to tidal transition in the Mesoarchean Moodies Group, South Africa: A response to high tidal range and active tectonics. Sedimentary Geology 190, 13-24.

Eriksson, P.G., Altermann, W., 1998. An overview of the Transvaal Supergroup dolomites (South Africa). Environmental Geology 36, 179-188.

Eriksson, P.G., Catuneanu, O., Nelson, D.R., Popa, M., 2005, Controls on Precambrian sea level change and sedimentary cyclicity. Sedimentary Geology 176, 43-65.

Eriksson, P.G., Condie, K.C., Tirsgaard, H., Mueller, W.U., Altermann, W., Miall, A.D., Aspler, L.B., Catuneanu, O., Chiarenzelli, J.R., 1998. Precambrian clastic sedimentation systems. Sedimentary Geology 120, 5-53.

Eriksson, P.G., Altermann, W., Hartzer, F.J., 2006. The Transvaal Supergroup and its precursors. In: Johnson, M.R., Anhaeusser, C.R., Thomas, R.J. (Eds.), The Geology of South Africa. Geological Society of South Africa, Johannesburg, RSA, pp. 237-260.

Eroglu, S., Schoenberg, R., Wille, M., Beukes, N., 2015. Geochemical stratigraphy, sedimentology, and Mo isotope carbonate platform, South Africa. Precambrian Research 266, 27–46.

Eroglu, S., Zuilen, M.A., Taubald, H., Drost, K., Wille, M., Swanner, E.D., Beukes, N.J., Schoenberg, R., 2017. Depth-dependent δ13C trends in platform to slope settings of the Campbellrand-Malmani carbonate platform and possible implications for Early Earth oxygenation. Precambrian Research 302, 122-139.

Farquhar, J., Bao, H., Thiemens, M., 2000. Atmospheric influence of earth’s earliest sulfur cycle. Science 289, 756–759.

Fralick, P., Riding, R., 2015. Steep Rock Lake: Sedimentology and geochemistry of an Archean carbonate platform. Earth-Science Reviews 151, 132-175.

Fischer, A.G., 1964. The Lofer cyclothems of the Alpine Triassic. Geological Survey of Kansas Bulletin 169, 107-149.

Fischer, A.G., Bottjer, D.J., 1991. Orbital forcing and sedimentary sequences. Journal of Sedimentary Petrology 61, 1063-1069.

Garrett, C., 1972. Tidal resonance in the Bay of Fundy and Gulf of Maine. Nature 238, 441-443.

Goldhammer, R.K., 1987. Platform carbonate cycles, Middle Triassic of northern Italy: The interplay of local tectonics and global eustasy. Ph.D. Dissertation, Johns Hopkins University, Baltimore, MD, 468 pp.

Goldhammer, R.K., Dunn, P.A., Hardie, L.A., 1990. Depositional cycles, composite sea-level changes, cycle stacking patterns, and the hierarchy of stratigraphic forcing: Examples from the Alpine Triassic platform carbonates. Geological Society of America Bulletin 102, 535-562.

Goldhammer, R.K., Lehmann, P.J., Dunn, P.A., 1993. The origin of high-frequency platform carbonate cycle and third-order sequences (Lower Ordovician El Paso Gp, West Texas): Constraints from outcrop data and stratigraphic modeling. Journal of Sedimentary Petrology 63, 318-359.

Grotzinger, J.P., 1989. Facies and evolution of Precambrian carbonate depositional systems: Emergence of the modern platform archetype. SEPM Special Publication 44, 79-106.

Grotzinger, J.P., 2000. Facies and paleoenvironmental setting of Thrombolite-Stromatolite Reefs, Terminal Proterozoic Nama Group (ca. 550-543 Ma), central and southern Namibia. Communs geol. Surv. Namibia 12, 251-264.

Grotzinger, J.P., Knoll, A.H., 1995. Anomalous carbonate precipitates: Is the Precambrian the key to the Permian?. Palaios 10, 578-596.

Grotzinger, J.P., Knoll, A.H., 1999. Stromatolites in Precambrian carbonates: Evolutionary mileposts of environmental dipsticks?. Annual Review of Earth and Planetary Sciences 27, 313-358

Grotzinger, J.P., Rothman, D.H., 1996. An abiotic model for stromatolite morphogenesis. Nature 383, 423-425.

Hagadorn, J.W., Bottjer, D.J., 1997. Wrinkle structures: Microbially mediated sedimentary structures common in subtidal siliciclastic settings at the Proterozoic-Phanerozoic transition. Geology 25, 1047-1050.

Hinnov, L.A., Goldhammer, R. K., 1991. Spectral analysis of Middle Triassic Latemar Limestone. Journal of Sedimentary Research 61, 1173-1193.

Holland, H.D., 2002. Volcanic gases, black smokers, and the great oxidation event. Geochimica et Cosmochimica Acta 66, 3811–3826.

Holland, H.D., 2006. The oxygenation of the atmosphere and oceans: Philosophical Transactions of the Royal Society B: Biological Sciences 361, 903–915.

Hobday, D.K., Von Brunn, V., 1976. Evidence of anomalously large tidal ranges in the Early Precambrian Pongola Supergroup. South African Journal of Science 72, 182.

Hoffman, P.F., 1976. Environmental diversity of Middle Precambrian stromatolites. In: Walter, M.R. (Ed.), Stromatolites. Developments in Sedimentology 20, Elsevier, Amsterdam, pp. 599-611.

Homann, M., Heubeck, C., Airo, A., Tice, M.M., 2015. Morphological adaptations of 3.22 Ga-old tufted microbial mats to Archean coastal habitats (Moodies Group, Barberton Greenstone Belt, South Africa). Precambrian Research 266, 47-64.

Horodyski, R.J., 1975. Stromatolites of the lower Missoula group (middle Proterozoic), belt Supergroup, Glacier National Park, Montana. Precambrian Research 2, 215-254.

Horodyski, R.J., 1977. *Lyngbya* mats at Laguna Mormona, Baja California, Mexico: Comparison with Proterozoic stromatolites. Journal of Sedimentary Petrology 47, 1305-1320.

Horodyski, R.J., Bloeser, B., Vonder Haar, S., 1977. Laminated algal mats from a coastal lagoon, Laguna Mormona, Baja California, Mexico. Journal of Sedimentary Petrology 47, 680-696.

Houbolt, J.H.C., 1968. Recent sediment in the Southern Bight of the North Sea. Geologie en Mijnbouw 47, 245-273.

Humbert, F., de Kock, M., Lenhardt, N., Altermann, W., 2019. Neoarchean to Early Palaeoproterozoic within-plate volcanism of the Kaapvaal Craton: Comparing the Ventersdorp Supergroup and the Ongeluk and Hekpoort Formations (Transvaal Supergroup). In: Kroner, A., Hofmann, A. (Eds.), The Archaean Geology of the Kaapvaal Craton, Southern Africa. Regional Geology Reviews. Springer, Cham, pp. 277-302.

Husinec, A., Basch, D., Rose, B., Read, J.F., 2008. FISCHERPLOTS: An Excel spreadsheet for computing Fischer plots of accommodation change in cyclic carbonate successions in both the time and depth domains. Computers & Geosciences 34, 269-277.

James, N.P., Kendall, A.C., Pufahl, P.K., 2010. Introduction to biological and chemical sedimentary facies models. In: James, N.P., Dalrymple, R.W. (Eds.), Facies Models 4. Geological Association of Canada, Newfoundland, 323-339.

Jervey, M.T., 1988. Quantitative geological modeling of siliciclastic rock sequences and their seismic expression. In: Wilgus, C.K., Hastings, B.S., Kendall, C.G.St.C., Posamentier, H.W., Ross, C.A., Van Wagoner, J.C. (Eds.), Sea Level Change – An Integrated Approach. SEPM Special Publication 42, Tulsa, OK, pp. 47-69.

Kah, L.C., Knoll, A.H., 1996. Microbenthic distribution of Proterozoic tidal flats: Environmental and taphonomic considerations. Geology 24, 79-82.

Kendall, C.G.St.C., Skipwith, P.A.d'E., 1969. Holocene shallow-water carbonate and evaporite sediments of Khor al Bazam, Abu Dhabi, southwest Persian Gulf. American Association of Petroleum Geologists Bulletin 53, 841-869.

Kietzmann, D.A., Palma, R.M., Riccardi, A.C., Martín-Chivelet, J., López-Gómez, J., 2014. Sedimentology and sequence stratigraphy of a Tithonian-Valanginian carbonate ramp (Vaca Muerta Formation): A misunderstood exceptional source rock in the Southern Mendoza area of the Neuquén Basin, Argentina. Sedimentary Geology 302, 64-86.

Klein, G.deV., 1971. A sedimentary model for determining paleotidal range. Geological Society of America Bulletin 82, 2585-2592.

Klein, C., Beukes, N.J., 1992. Proterozoic iron-formations. Developments in Precambrian Geology 10, 383-418.

Knoll, A.H., Beukes, N.J., 2009. Introduction: Initial investigations of a Neoarchean shelf margin-basin transition (Transvaal Supergroup, South Africa). Precambrian Research 169, 1-14.

Koerschner III, W.F., Read, J.F., 1989. Field and modeling studies of Cambrian carbonate cycles, Virginia Appalachians. Journal of Sedimentary Petrology 59, 654-687.

Kurucz, S., Fralick, P., 2018. Internal fabric of giant domes in the Mesoarchean Steep Rock carbonate platform, Superior Province, Canada. Canadian Journal of Earth Sciences 55, 343-355.

Kvale, E.P., 2006. The origin of neap-spring tidal cycles. Marine Geology 235, 5-18.

Liu, X.-M., Kah, L.C., Knoll, A.H., Cui, H., Kaufman, A.J., Shahar, A., Hazen, R.M., 2016. Tracing Earth's O2 evolution using Zn/Fe ratios in marine carbonates. Geochemical Perspectives Letters 2, 24–34.

Matyszkiewicz, J., 1996. The significance of Saccocoma-calciturbidites for the analysis of the Polish epicontinental late Jurassic Basin: An example from the Southern Cracow-Wielun Upland (Poland): Facies 34, 23-40.

Maurer, F., Hinnov, L., Schlager, W., 2004. Statistical time-series analysis and sedimentological tuning of bedding rhythms in a Triassic basinal succession (Southern Alps, Italy). In: d'Argenio, B. (Ed.), Cyclostratigraphy: Approaches and Case Histories. SEPM Special Publication 81, Tulsa, OK, pp. 83-99.

Maynard, J.B., Klein, G.D, 1995. Tectonic subsidence analysis in the characterization of sedimentary ore deposits: Examples form the Witwatersrand (Au), White Pine (Cu), and Molango (Mn). Economic Geology 90, 37-50.

Miall, A.D., 2005. Testing for eustatic sea-level control in the Precambrian sedimentary record. Sedimentary Geology 176, 9-16.

Miall, A.D., 2014. Updating uniformitarianism: stratigraphy as just a set of ‘frozen accidents’. In: Smith, D.G., Bailey, R.J., Burgess, P.M., Fraser, A.J. (Eds.), Strata and Time: Probing the gaps in our understanding. Geological Society of London, Special Publications 404, pp. 11-36.

Miyano, T., Beukes, N.J., 1984. Phase relations of stilpnomelane, ferri-annite, and riebeckite in very low-grade metamorphosed iron-formations. South African Journal of Geology 87, 111-124.

Montañez, I.P., Read, J.F., 1992. Eustatic control on early dolomitization of cyclic peritidal carbonates: Evidence from the Early Ordovician Upper Knox Group, Appalachians. Geological Society of America Bulletin 104, 872-886.

Nosal, M., Vrbik, J., 1982. Stratigraphic analysis and the asymptotic distribution of the coefficient of cross-association. Mathematical Geology 14, 11-36.

Osleger, D., 1991. Subtidal carbonate cycles: Implications for allocyclic vs. autocyclic controls. Geology 19, 917–920.

Osleger, D., 1994. Aperiodic accumulation of cyclic peritidal carbonate. Geology 22, 79-80.

Osleger, D.A., Montañez, I.P., 1996. Cross-platform architecture of a sequence boundary in mixed siliciclastic-carbonate lithofacies, Middle Cambrian, southern Great Basin, USA. Sedimentology 43, 197-217.

Partin, C.A., Bekker, A., Planavsky, N.J., Scott, C.T., Gill, B.C., Li, C., Podkovyrov, V., Maslov, A., Konhauser, K.O., Lalonde, S.V., Love, G.D., Poulton, S.W., Lyons, T.W., 2013, Large-scale fluctuations in Precambrian atmospheric and oceanic oxygen levels from the record of U in shales: Earth and Planetary Science Letters 369–370, 284–293.

Pavlov, A.A., Kasting, J.F., 2002. Mass-Independent Fractionation of Sulfur Isotopes in Archean Sediments: Strong evidence for an anoxic Archean atmosphere. Astrobiology 2, 27–41.

Pickard, A.L., 2003. SHRIMP U-Pb zircon ages for the Palaeoproterozoic Kuruman Iron Formation, Northern Cape Province, South Africa: Evidence for simultaneous BIF deposition on Kaapvaal and Pilbara Cratons. Precambrian Research 125, 275-315.

Playton, T.E., Janson, X., Kerans, C., 2010. Carbonate slopes. In: James, N.P., Dalrymple, R.W. (Eds.), Facies Models 4. Geological Association of Canada, Newfoundland, pp. 449-476.

Plint, A.G., 2010. Wave- and storm-dominated shoreline and shallow-marine systems. In: James, N.P., Dalrymple, R.W. (Eds.), Facies Models 4. Geological Association of Canada, Newfoundland, 167-199.

Posamentier, H.W., Jervey, M.T., Vail, P.R., 1988. Eustatic controls on clastic deposition, I. Conceptual framework. In: Wilgus, C.K., Hastings, B.S., Kendall, C.G.St.C., Posamentier, H.W., Ross, C.A., Van Wagoner, J.C. (Eds.), Sea Level Change – An Integrated Approach. SEPM Special Publication 42, Tulsa, OK, pp. 110-124.

Read, J.F., 1985, Carbonate platform facies models. American Association of Petroleum Geologists Bulletin 69, 1-21.

Reedman, A.J., Howells, M.F., Orton, G., Campbell, S.D.G., 1987. The Pitts Head Tuff Formation: a subaerial to submarine welded ash-flow tuff of Ordovician age, North Wales. Geological Magazine 124, 427-439.

Riding, R., Fralick, P., Liang, L., 2014. Identification of an Archean marine oxygen oasis. Precambrian Research 251, 232-237.

Ross, G.M., 1986. Eruptive style and construction of shallow marine mafic tuff cones in the Narakay volcanic complex (Proterozoic, Hornby Bay Group, Northwest Territories, Canada). Journal of Volcanology and Geothermal Research 27, 265-297.

Sackin, M.J., Merriam, D.F., 1969. Autoassociation, a new geological tool. Mathematical Geology 1, 7-16.

Sadler, P.M., Osleger, D.A., Montanez, I.P., 1993. On the Labeling, Length, and Objective Basis of Fischer Plots. Journal of Sedimentary Petrology 63, 360–368.

Scholle, P.A., 1971. Sedimentology of fine-grained deep-water carbonate turbidites, Monte Antola Flysch (Upper Cretaceous), Northern Apennines, Italy. Geological Society of America Bulletin 83, 629-658.

Schröder, S., Lacassie, J.P., Beukes, N.J., 2006. Stratigraphic and  geochemical framework of the Agouron drill cores, Transvaal Supergroup (Neoarchean-Paleoproterozoic, South Africa). South African Journal of Geology 109, 23–54.

Schröder, S., Beukes, N.J., Sumner, D.Y., 2009. Microbialite-sediment interactions on the slope of the Campbellrand carbonate platform (Neoarchean, South Africa). Precambrian Research 169, 68–79.

Simonson, B.M., Schubel, K.A., Hassler, S.W., 1993. Carbonate sedimentology of the early Precambrian Hamersley Group of Western Australia. Precambrian Research 60, 287-335.

Smith, T.F., Waterman, M.S., 1980. New stratigraphic correlation techniques. Journal of Geology 88, 451-457.

Snedden, J.W., Nummedal, D., 1991. Origin and geometry of storm-deposited sand beds in modern sediments of the Texas continental shelf. In: Swift, D.J.P, Oertel, G.F., Tillman, R.W., Thorne, J.A. (Eds.), Shelf Sand and Sandstone, Geometry, Facies, and Sequence Stratigraphy. Special Publication 14, International Association of Sedimentologists, pp. 283-308.

Sohn, Y.K., Park, K.H., 2005. Composite tuff ring/cone complexes in Jeju Island, Korea: possible consequences of substrate collapse and vent migration. Journal of Volcanology and Geothermal Research 141, 157-175.

Sumner, D.Y., 1997a. Carbonate precipitation and oxygen stratification in Late Archean seawater as deduced from facies and stratigraphy of the Gamohaan and Frisco Formations, Transvaal Supergroup, South Africa. American Journal of Science 297, 455-487.

Sumner, D.Y., 2002. Decimetre-thick encrustations of calcite and aragonite on the sea-floor and implications for Neoarchaean and Neoproterozoic ocean chemistry. In: Altermann, W., Corcoran, P.L. (Eds.), Precambrian Sedimentary Environments: A Modern Approach to Ancient Depositional Systems. Special Publication 33, International Association of Sedimentologists, pp. 107-120.

Sumner, D.Y., Bowring, S.A., 1996. U-Pb geochronologic constraints on deposition of the Campbellrand Subgroup, Transvaal Supergroup, South Africa. Precambrian Research 79, 25-35.

Sumner, D.Y., Beukes, N.J., 2006. Sequence Stratigraphic Development of the Neoarchean Transvaal carbonate platform, Kaapvaal Craton, South Africa. South African Journal of Geology 109, 11–22.

Sumner, D.Y., and Grotzinger, J.P., 1996. Were kinetics of Archean calcium carbonate precipitation related to oxygen concentration?. Geology 24, 119-122.

Sumner, D.Y., Grotzinger, J.P., 2000. Late Archean aragonite precipitation: Petrography, facies associations, and environmental significance: In: Grotzinger, J.P., and James, N.P. (Eds.), Carbonate Sedimentation and Diagenesis in the Evolving Precambrian World. SEPM Special Publications 67, Tulsa, OK, pp. 124-144.

Sumner, D.Y., Grotzinger, J.P., 2004. Implications for Neoarchaean ocean chemistry from primary carbonate mineralogy of the Campbellrand-Malmani Platform, South Africa. Sedimentology 51, 1273-1299.

Trendall, A.F., Compston, W., Williams, I.S., Armstrong, R.A., Arndt, N.T., McNaughton, N.J., Nelson, D.R., Barley, M.E., Beukes, N.J., de Laeter, J.R., Retief, E.A., Thorne, A.M., 1990. Precise zircon U-Pb chronological comparison of the volcano-sedimentary sequences of the Kaapvaal and Pilbara Cratons between about 3.1 and 2.4 Ga. In: Glover, J.E., Ho, S.E. (Eds.), 3rd Int. Archean Symp., Perth. Geoconferences (W.A.) Inc., Perth ed. Vol. Extended Abstracts, pp. 81-83.

Truswell, J.F., Eriksson, K.A., 1973. Stromatolitic associations and their palaeoenvironmental significance: A reprisal of a lower Proterozoic locality from the northern Cape Province, South Africa. Sedimentary Geology 10, 1-23.

Tucker, M. E. Wright, V. P., 2009. Carbonate Sedimentology. Blackwell, Oxford.

Van der Westhuizen, W.A., De Bruiyn, H., Meintjes, P.G., 1991. The Ventersdorp Supergroup: an overview. Journal of African Earth Sciences 13, 83-105.

Walraven, F., Martini, J., 1995. Zircon Pb-evaporation age determinations of the Oak Tree Formation, Chuniespoort Group, Transvaal Sequence: Implications for Transvaal-Griqualand West basin correlations. South African Journal of Geology 98, 58-67.

Welch, S.A., 2005. Deciphering eustatic and tectonic influences during parasequence development in the Mesoproterozoic Helena/Wallace Formation, Belt Supergroup, Montana and Idaho. M.S. Thesis, University of Tennessee, Knoxville, 141 pp.

Wilkinson, B.H., Opdyke, B.N., Algeo, T.J., 1991. Time partitioning in cratonic carbonate rocks. Geology 19, 1093-1096.

# APPENDICES

## Appendix A: Figures

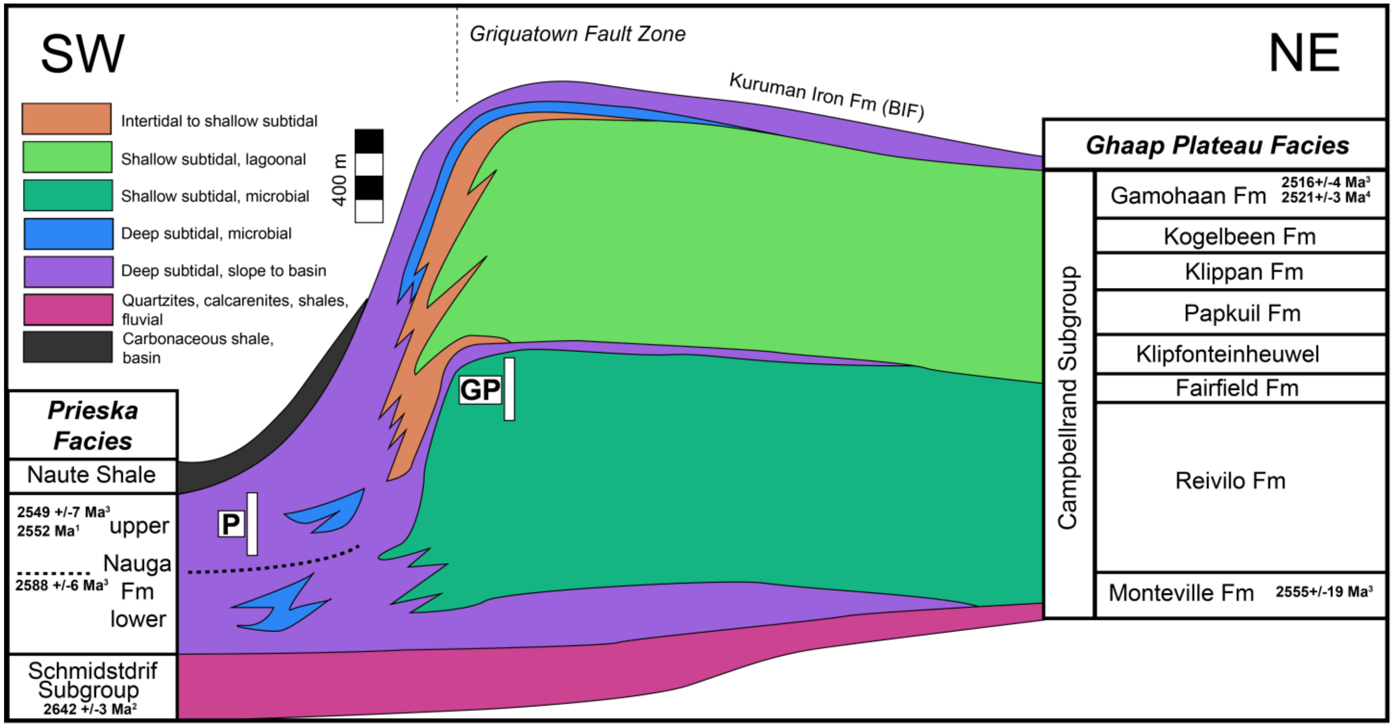


Figure 1 Campbellrand Platform Architecture

Paleoenvironments of the Campbellrand Subgroup, Transvaal Supergroup, South Africa (modified from Schröder et al., 2009; *after* Beukes, 1987 and Sumner and Beukes, 2006). The Campbellrand Subgroup of the Griqualand West sub-basin includes two discrete facies that are divided by the Griquatown Fault Zone; the Ghaap Plateau [GP] Facies to the northeast and the Prieska [P] Facies to the southwest with the Kuruman banded iron formation overlying the entire platform. Scale is 400 m and overall relief in the platform is >900 m (Grotzinger, 1989). Ages for formations: Upper Nauga Formation (Barton et al., 1994)[1]; Vryburg Formation [Schmidstrdif Subgroup] (Walraven and Martini, 1995)[2]; Nauga, Upper Nauga, Monteville, and Gamohaan formations (Altermann and Nelson, 1998)[3]; Gamohaan Formation (Sumner and Bowring, 1996)[4]

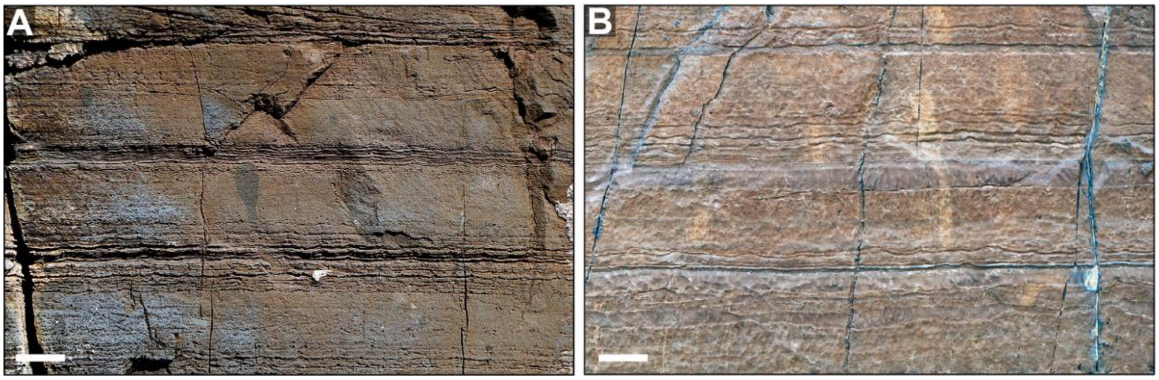

Figure 2 Centimeter-scale Bedding of Ghaap Plateau and Prieska facies

Similarity of bedding in dolomite strata (A) microbial laminae at Ghaap Plateau Facies and (B) microbial laminae at Prieska Facies. Note: the internal laminae have similar undulose texture with closely spaced laminae featuring recessive weathering. Scale is 1 cm.

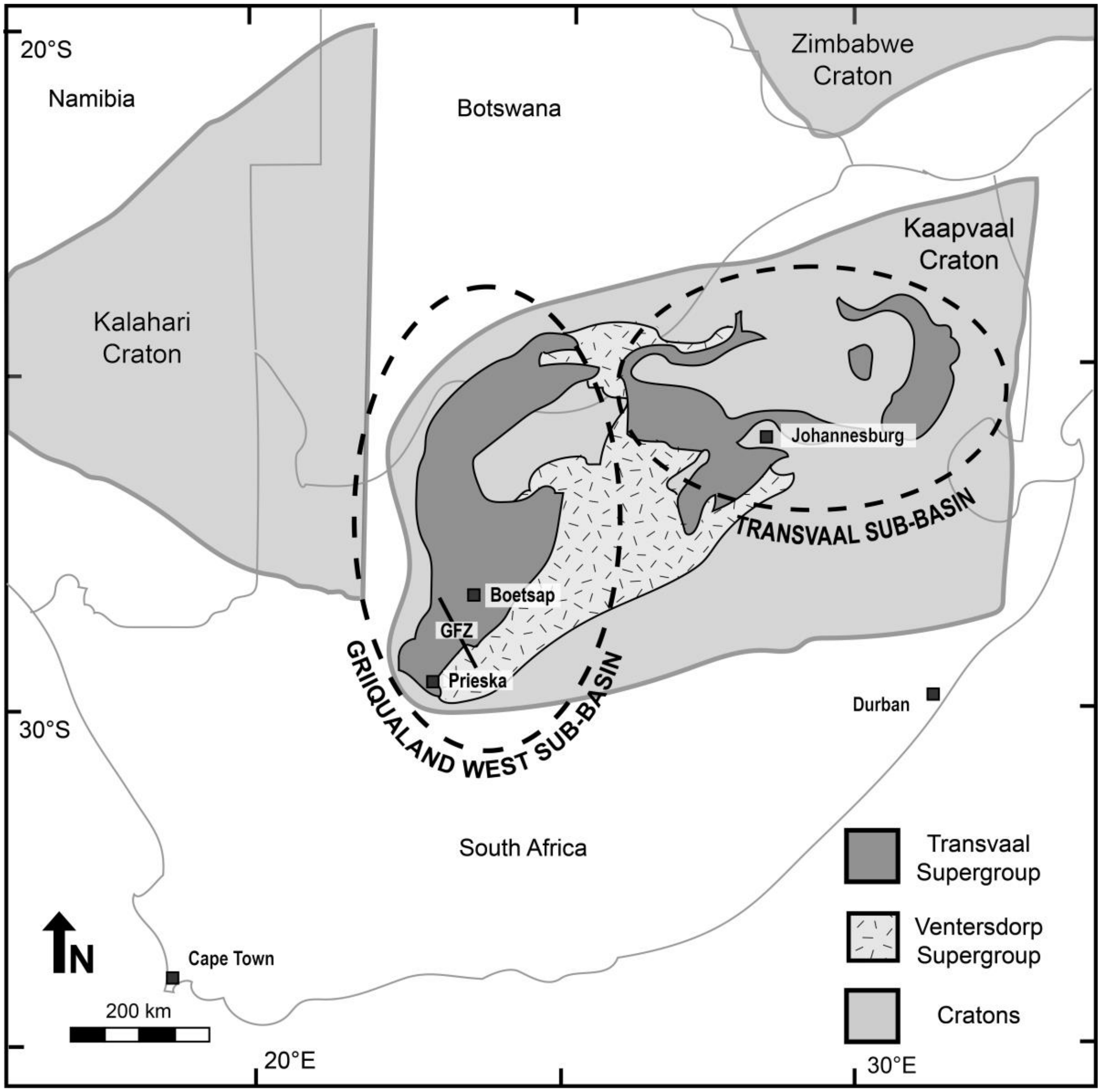


Figure 3 Transvaal Basin Map

Map of South Africa and neighboring countries displaying Precambrian cratons (modified from Schröder et al., 2006). Note: exposures of the Campbellrand Subgroup, Transvaal Supergroup described herein are located near Boetsap (Ghaap Plateau Facies) and Prieska (Prieska Facies) with the two Facies being subdivided along the GFZ (Griqualand Fault Zone) in the Griqualand West sub-basin (Beukes, 1987).

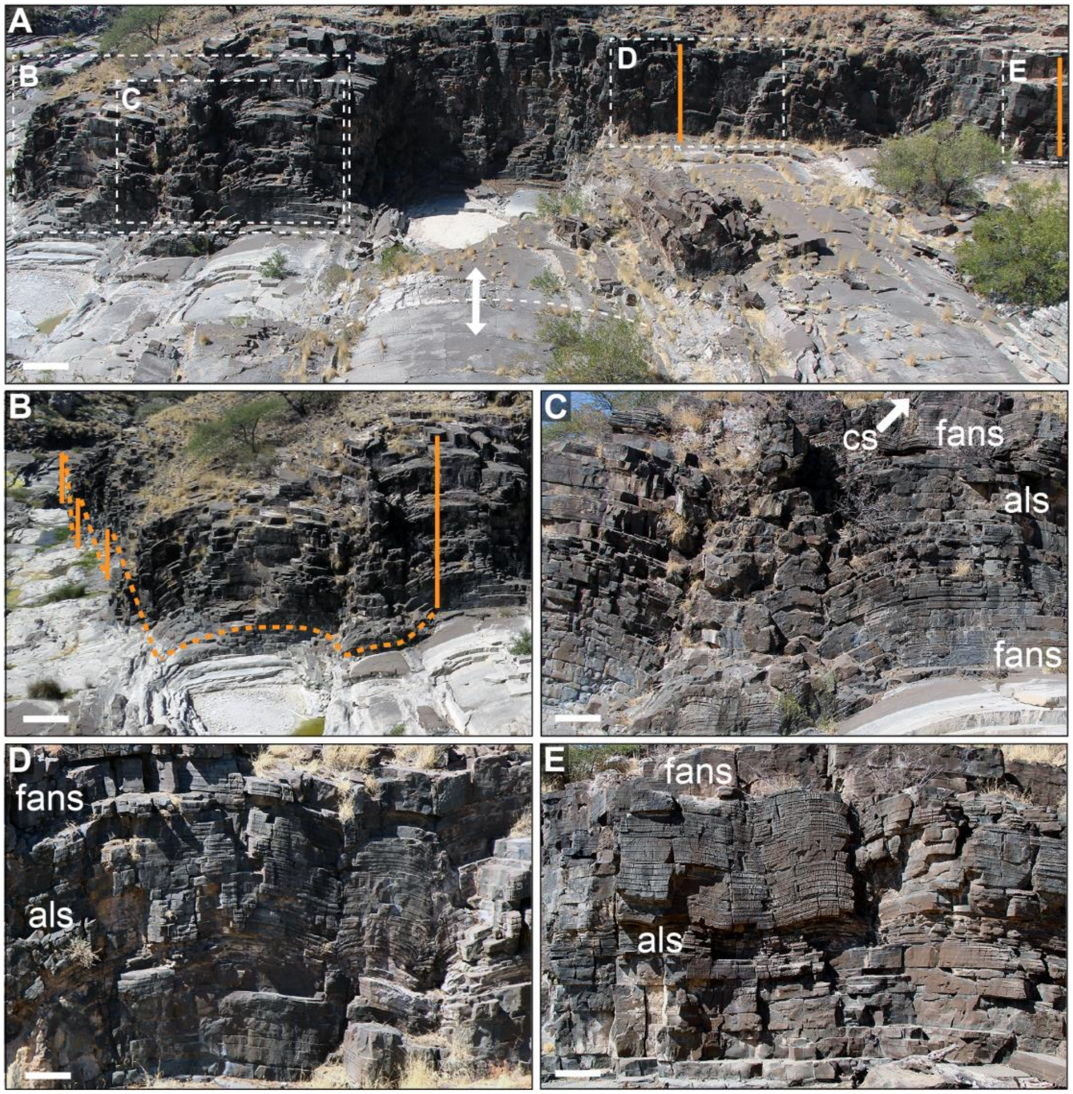


Figure 4 Boetsap Field Site

Outcrop images at Ghaap Plateau Facies near Boetsap, South Africa. (A) Outcrop-scale photo of exposure with inset frames of dashed white lines for (B), (C), (D), and (E). Vertical orange lines indicate locations of measured stratigraphic sections. Arcuate dashed white line shows convex geometry of elongate stromatolite domes and double-sided arrow shows symmetric current direction from ripple marks on upper surfaces. (B) Inset photo of synthetic stratigraphic section. Dashed orange-lines indicate lateral connection of segments. (C) Inset photo of two elongate domes. (D, E) Inset photos of congruent, duplicate measured section offset laterally by 23 m. Note: cs = columnar stromatolites, fans = pseudomorphic crystal fans, als = argillaceous carbonate. Scale in (A) is 2 m, (B) is 1.5 m, and (C, D, and E) are 1 m.

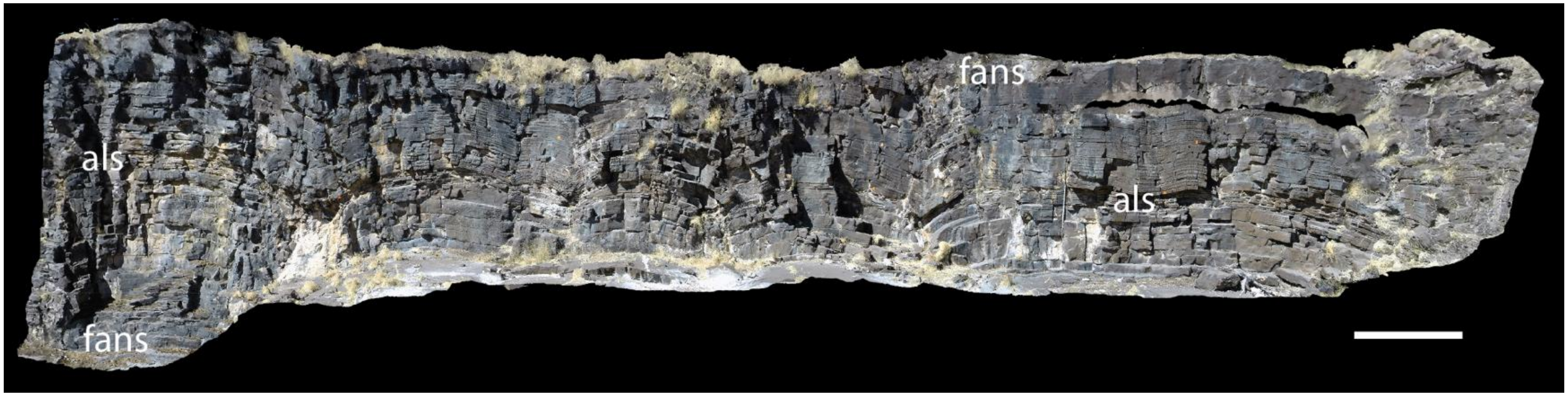


Figure 5 Digital Model of Ghaap Plateau Facies

Digital model of Ghaap Plateau Facies outcrop composed of 137 photos using Agisoft Metashape software. Note: fans = pseudomorphic crystal fans, als = argillaceous carbonate. Scale is 2 m.

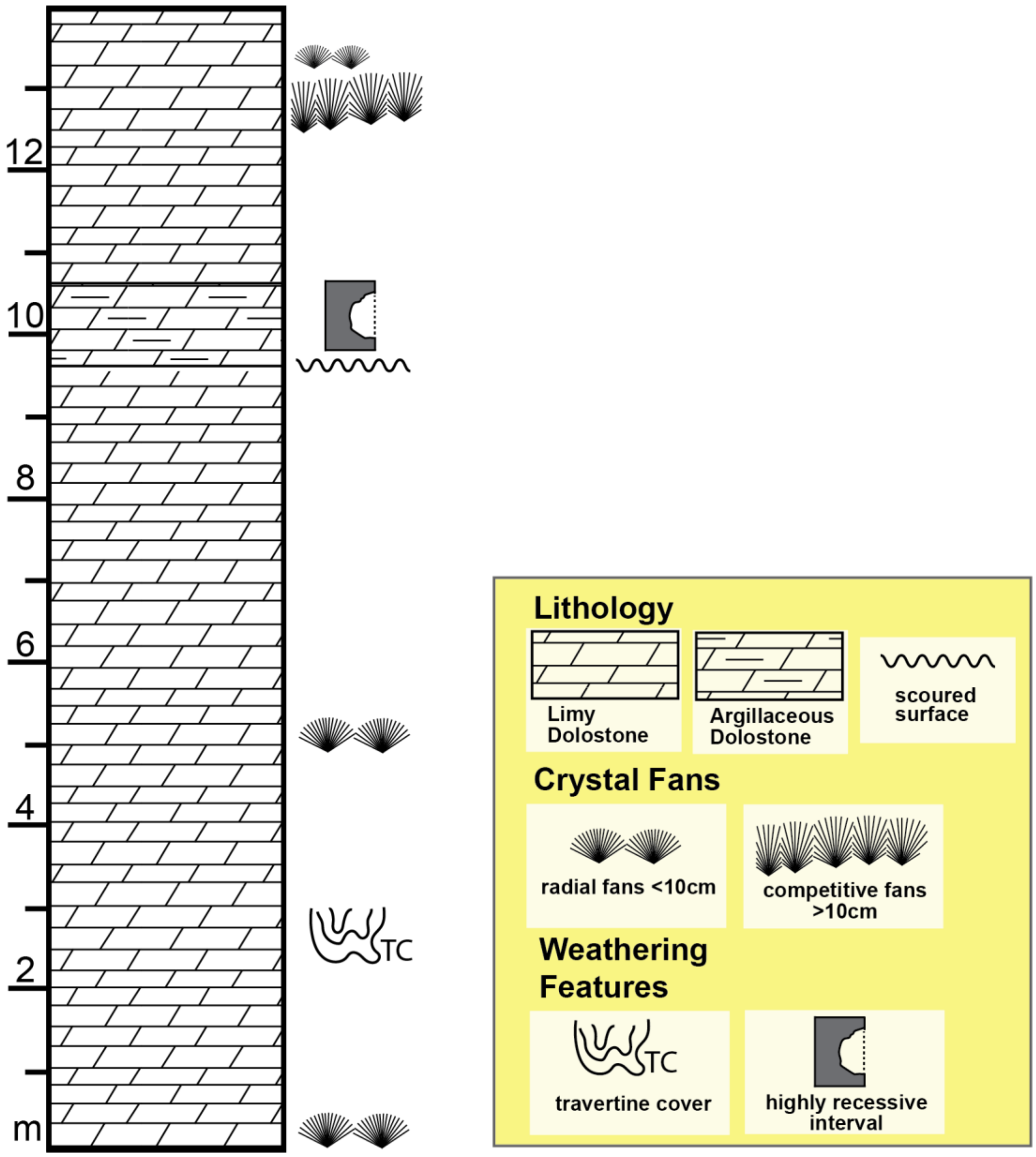


Figure 6 Composite Stratigraphic Column Reivilo Formation

Composite stratigraphic column of 13.26 m of measured strata in the Reivilo Formation, Ghaap Plateau Facies near Boetsap, South Africa. Limy dolostone consists of Boetsap-style laminae with stratiform to tufted laminae. Highly recessive, laterally continuous interval coincides with a significant increase in argillaceous dolostone and minor erosion of thinning laminae at elongate dome connections.

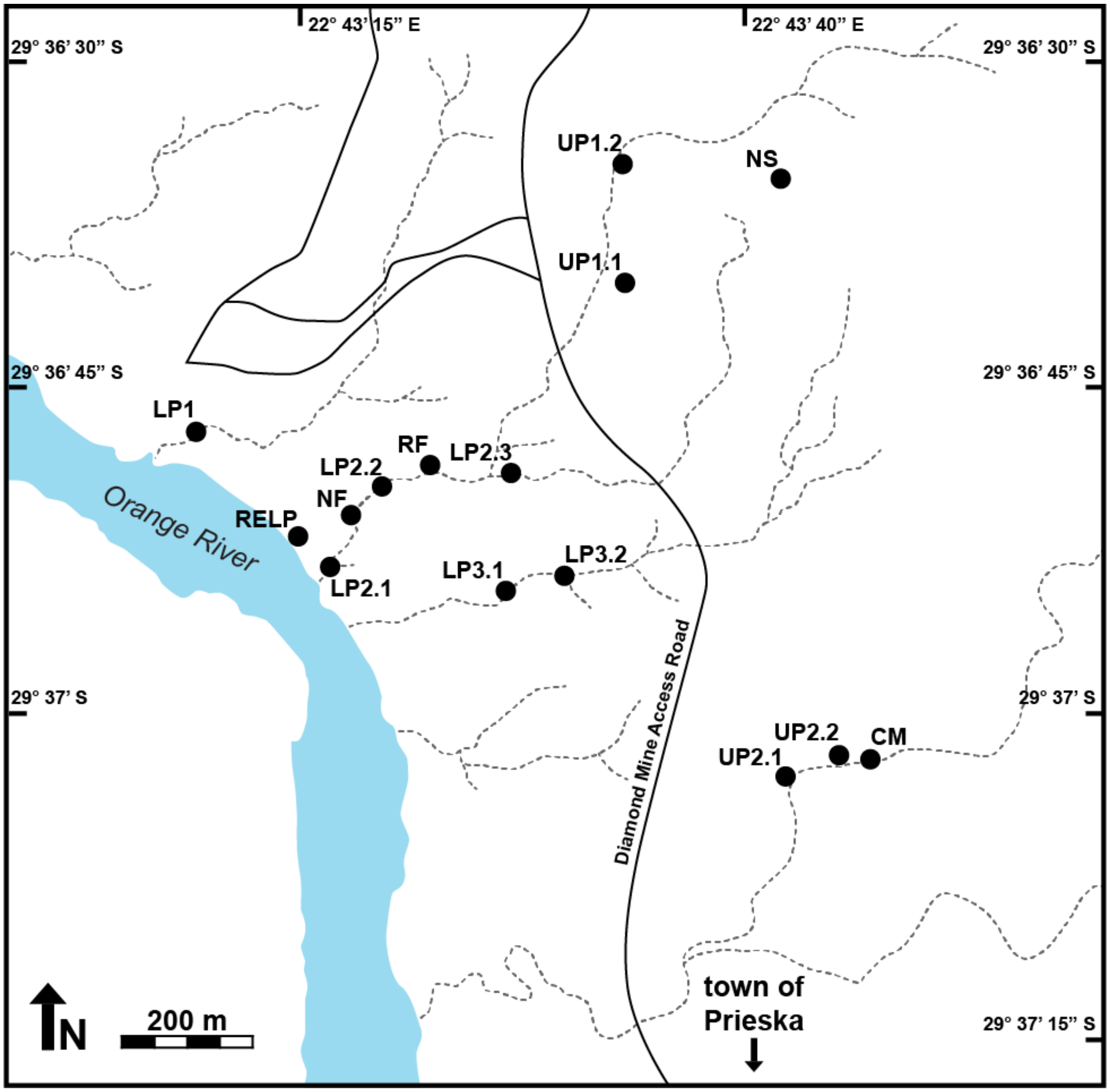


Figure 7 Prieska Field Site Map

Location map of carbonate strata of the Prieska Facies exposed along drainages [dashed grey lines] of the Orange River near Prieska, South Africa. Note: LP1 = Lower Prieska 1; RELP = River's Edge Lower Prieska; LP2.1, 2.2, 2.3 = Lower Prieska 2; LP3.1 = Lower Prieska 3; UP1.1, 1.2 = Upper Prieska 1; UP2.1, 2.2 = Upper Prieska 2; NF = normal fault; RF= reverse fault; NS = Naute Shale; CM = upper Chert Member of Nauga Fm. Scale is 200 m.

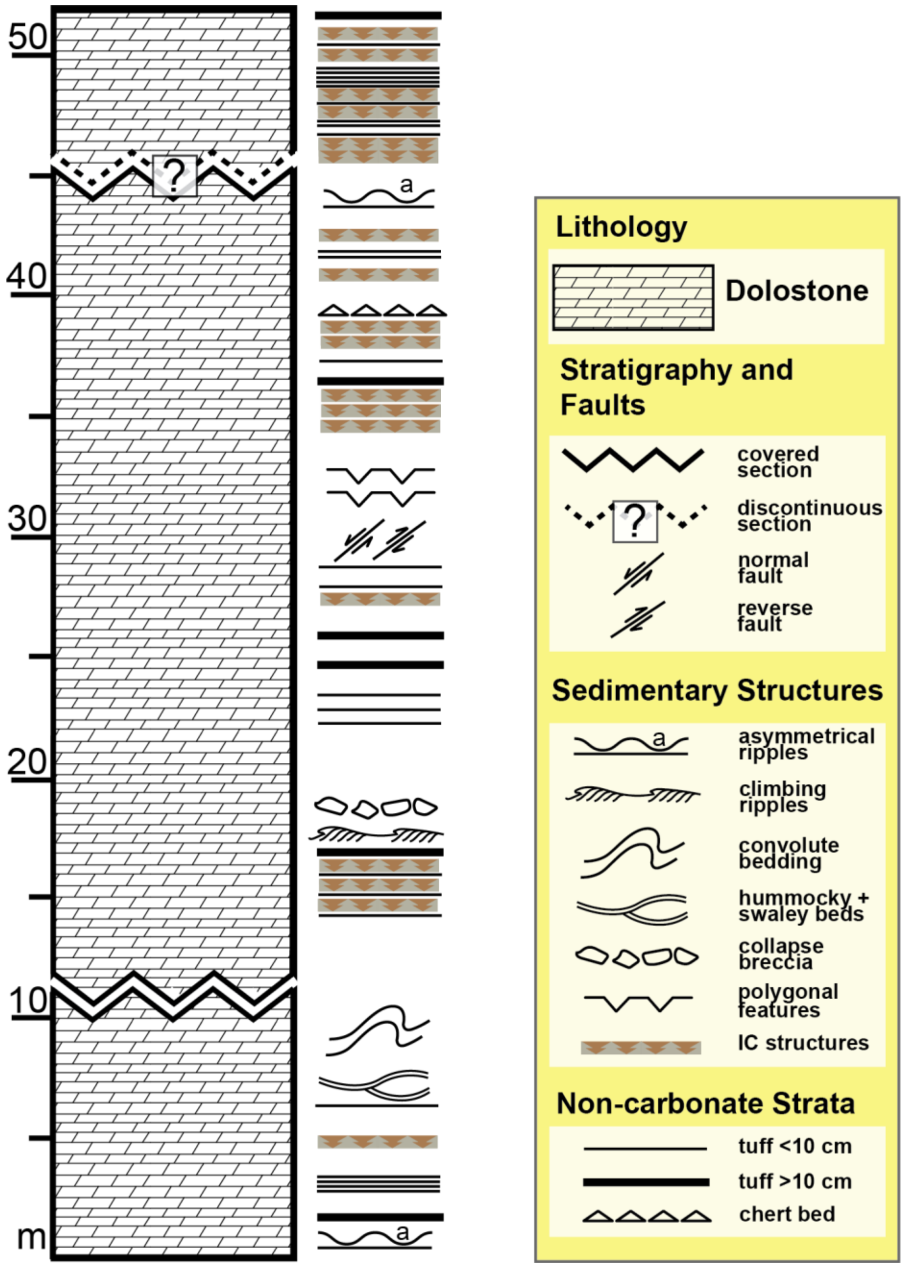


Figure 8 Composite Stratigraphic Column Upper Nauga Formation

Composite stratigraphic column of 53 m of measured strata in the Nauga Formation, Prieska Facies near Prieska, South Africa. Composite measured section of cumulative sections (LP1) Lower Prieska 1, (RELP) River's Edge Lower Prieska, (UP1) Upper Prieska 1, (LP2) Lower Prieska 2, (LP3) Lower Prieska 3, and (UP2) Upper Prieska 2. Dolostone strata consist of stratiform and tufted mm-scale laminae with minor fine-grained detrital sediment in fine-grained, dark-brown laminae that that pinch and swell.

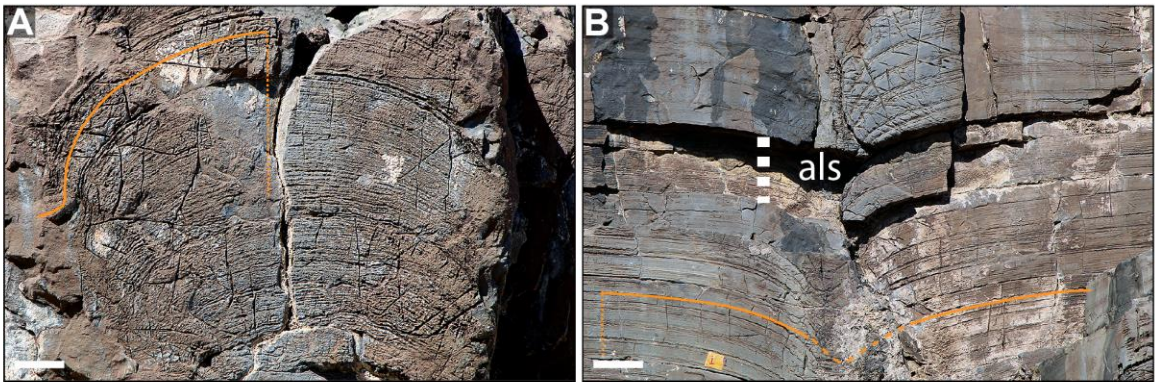


Figure 9 Synoptic Relief of Stromatolites at Ghaap Plateau Facies

Photos showing synoptic relief of (A) small and (B) large domal elongate stromatolites of the Ghaap Plateau Facies. (A) Domal stromatolite in between the margins of two large elongate domal stromatolites. Orange line traces a convex, draping lamina from crest to valley. Dashed orange line indicates minimum water depth at time of upper dome surface lamina formation. (B) Convergence of two large elongate stromatolites below the argillaceous carbonate interval [thick white dashed line, als]. Arcuate orange dashed line indicates approximate link between adjacent domes, and dashed vertical orange line indicates minimum water depth at time of deposition. Scale in (A) is 5 cm and (B) is 10 cm.


Figure 10 Boetsap-style Laminae

Photos of major and minor facies of the Boetsap-style laminae in dolomite strata in the Ghaap Plateau Facies near Boetsap, South Africa. (A) Strongly tufted microbial laminae [arrow]. Scale in (A) is 1 cm.

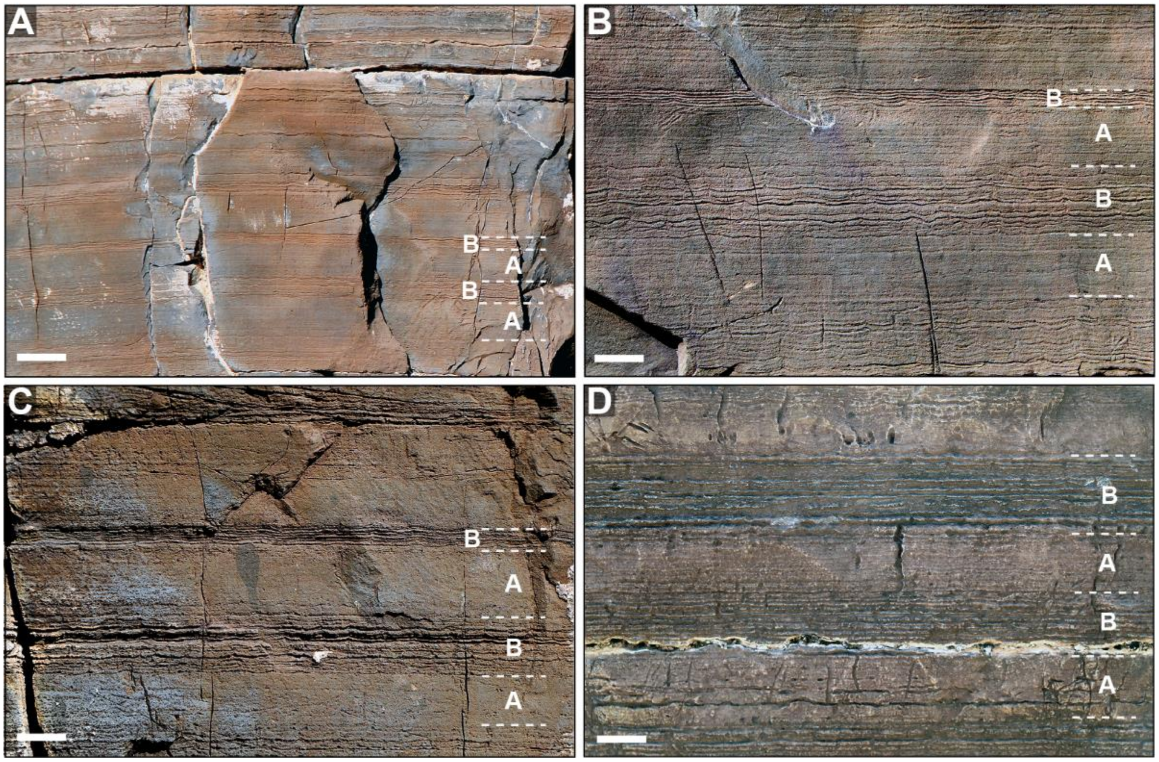


Figure 11 Ghaap Plateau Facies Centimeter-scale Beds

Centimeter-scale facies of dolomite strata in the Ghaap Plateau Facies near Boetsap, South Africa. Alternations of A-type beds of wavy to tufted microbial carbonate and B-type beds of tufted microbial carbonate with a strong detrital component. Laminae in A-type beds are lighter grey in color and composed of mm-scale layers that are subtly undulose. Laminae in B-type beds are darker grey, weather to brown, and composed of mm-scale layers that are strongly tufted. Scale in (A) is 3 cm; (B, C, and D) are 1 cm.

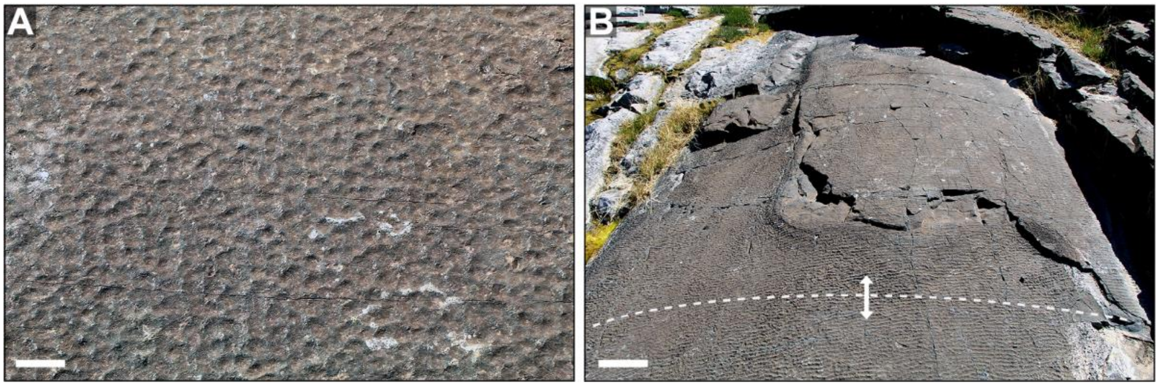


Figure 12 Ghaap Plateau Facies Bedding Surface

Photos of bedding surfaces of dolomite strata in the Ghaap Plateau Facies near Boetsap, South Africa. (A) Surface view of tufted microbial laminae. (B) Aerial view of elongate stromatolite dome with ripple marks perpendicular to axis of elongation. Scale in (A) is 2 cm and (B) is 30 cm.

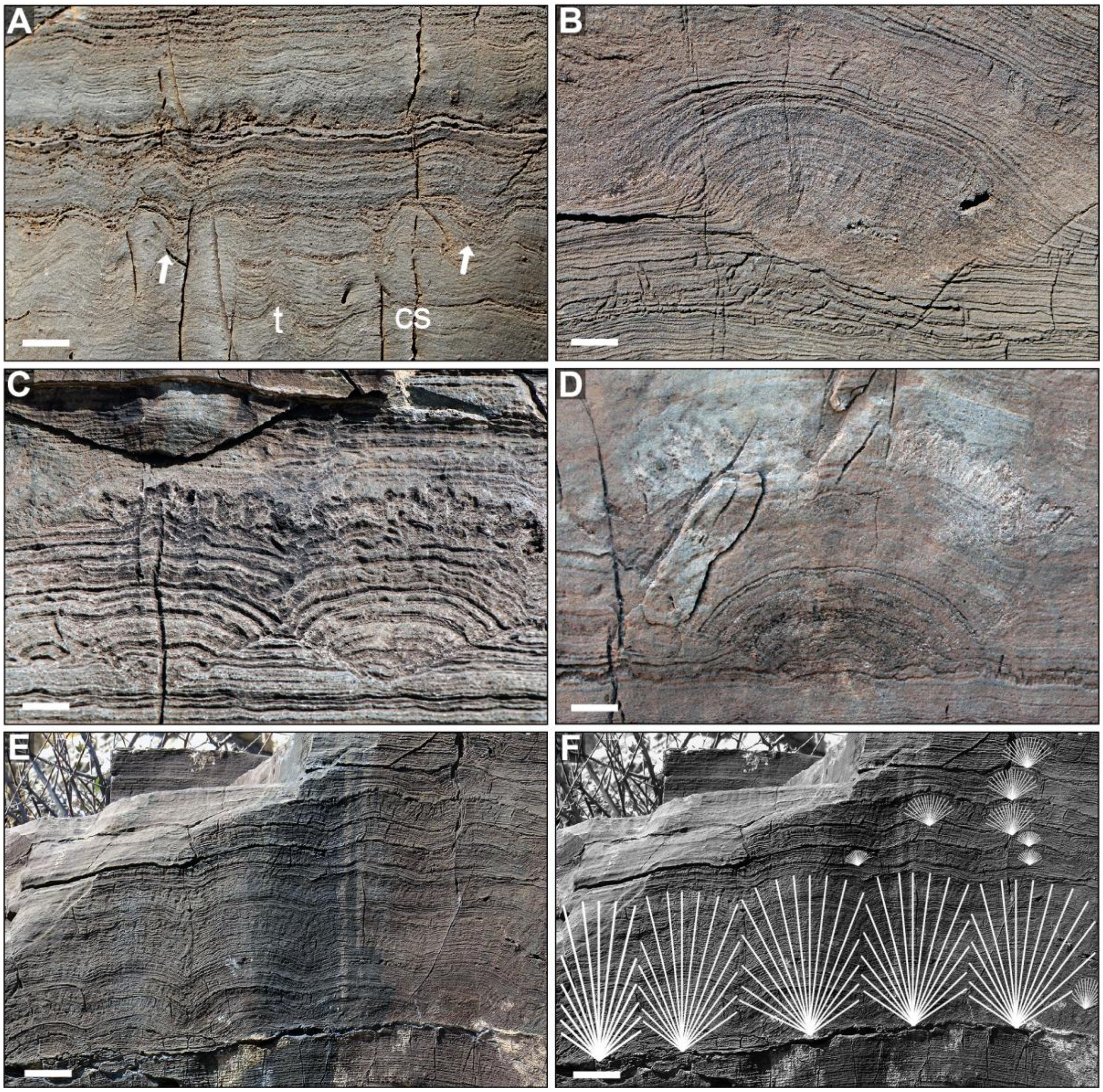


Figure 13 Variation on Bedding Style

Photos of variation of Boetsap-style laminae in dolomite strata in the Ghaap Plateau Facies. (A) Subtle columnar stromatolites [cs] with trapped detrital sediment [arrows] and a small tented stromatolite. (B) Small domal stromatolite with laterally continuous laminae, increasing synoptic relief, and gently folding exterior laminae. (C) Radial pseudomorph crystal fans with abrupt transition to exterior, non-fan microbial laminae. Upper surface of fan is strongly acicular. (D) Isolated radial pseudomorph aragonite fan with strongly acicular upper termination and an additional interior <1 cm fan below termination. (E and F) Meter-scale photo of domal stromatolites that appear coated by bladed precipitates. Scale in (A) is 2 cm, (B, C, D) is 1cm, and scale in (E, F) is 10 cm.

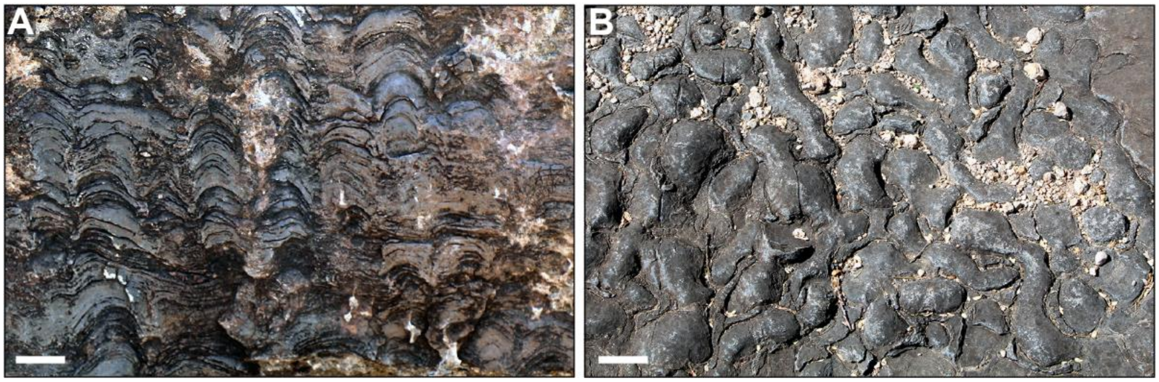


Figure 14 Columnar Stromatolites

Photos of laterally-linked columnar stromatolites identified above measured section. (A) Columnar stromatolites consist of grey micrite with detrital material trapped in between convex laminae and interstitially between columns that featuring ~5cm of synoptic relief. (B) Surface view of laterally-linked columnar stromatolites suggesting elongation from current processes. Scale is 5cm.

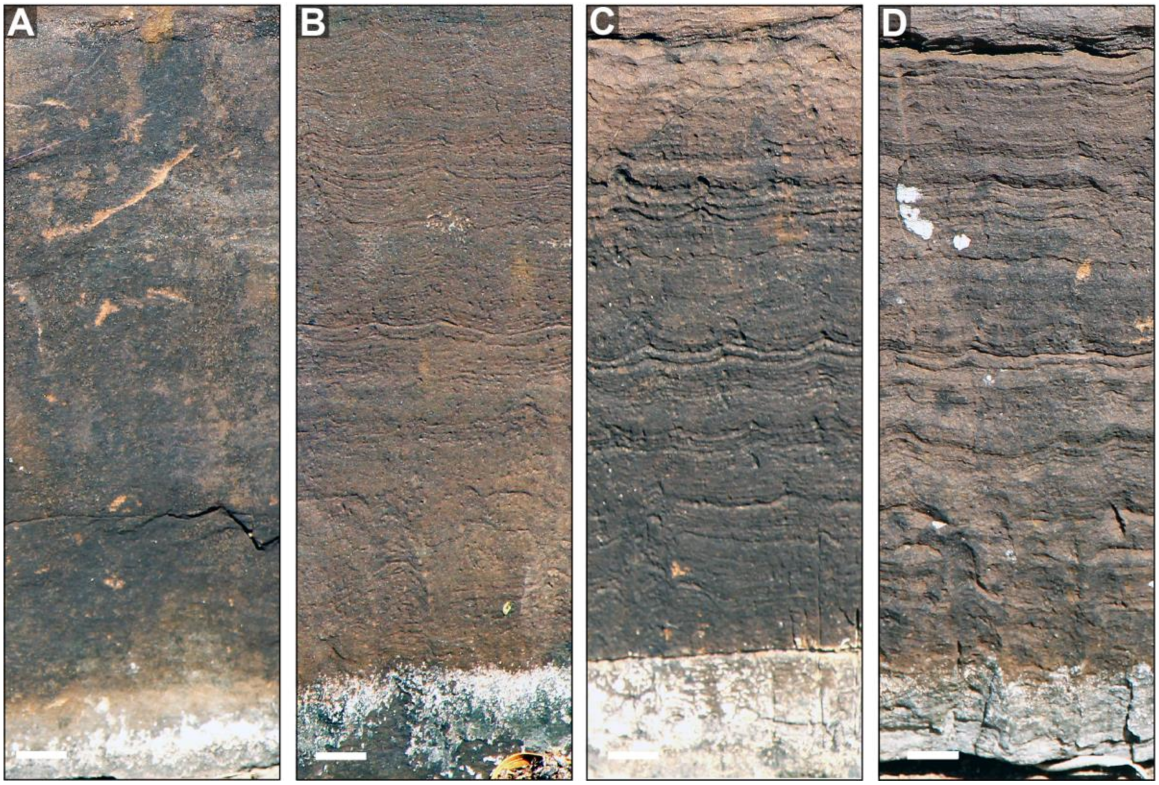

Figure 15 Boetsap Weathering Variation

Photos of a weathering profile along one bed of dolomite strata in the Ghaap Plateau Facies near Boetsap, South Africa. (A) to (D) shows progressive weathering of couplets containing A-type and B-type beds. Weathering of couplets results in B-type laminae with increased relief and rusty brown staining of subjacent layers. A-type stratiform laminae progressively weather away to a polished surface. Weathering patterns result in loss of recognizable smoother laminae, but increase appearance of tufted, detrital-rich laminae. Scale is 1 cm.

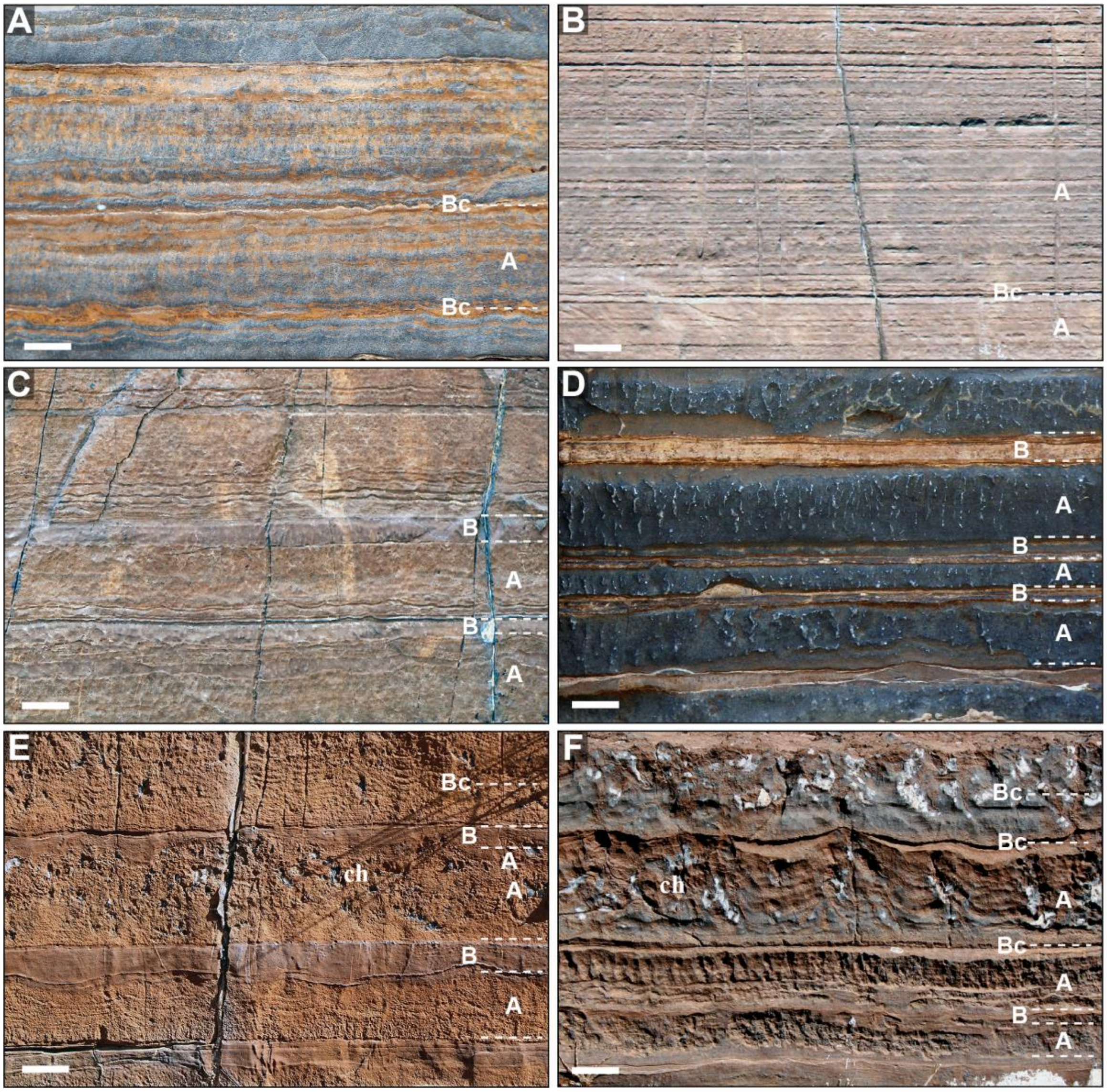


Figure 16 Prieska Facies Centimeter-scale Beds

Centimeter scale facies variable weathering in the Prieska Facies near Prieska, South Africa. Alternations of A-type beds with lighter grey to brown, stratiform to tufted microbial beds and B-type beds with dark-brown to orange color composed of fine-grained laminae. Thin “B” beds often result in cracks notated “Bc”. (A, B) Couplets composed of thin mm-scale laminae with tufts “A” separated by weathered cracks “Bc”. (C, D) Couplets composed of tufted laminae “A” separated by thinly-bedded, fine-grained brown laminae “B”. (E, F) Couplets composed of tufted and tented fenestral mm-scale laminae with chert-filled vugs “A” draped by fine-grained, dark brown laminae with pinch and swell geometry and planar upper boundary “B” or draped by thin, recessive laminae “Bc”. Scale is 1 cm.

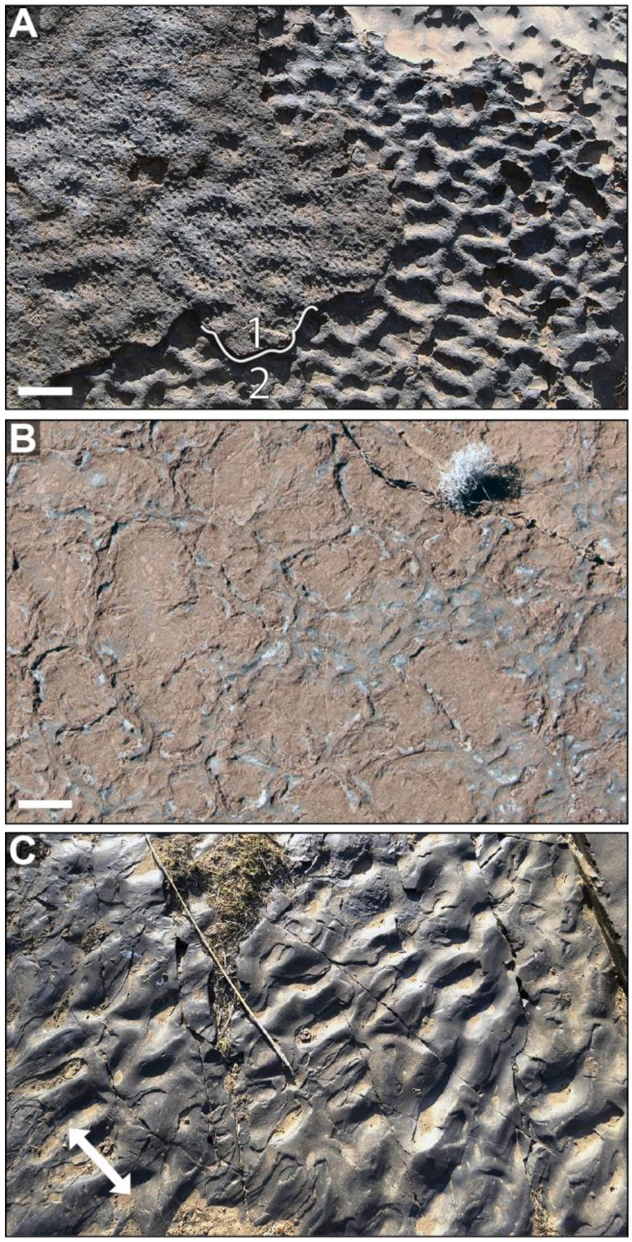


Figure 17 Prieska Facies Bedding Surfaces

Photos of bedding surfaces in the Prieska Facies near Prieska, South Africa. (A) Tufted microbial beds with ridge-like connections [2] overlain by fine-grained carbonate bedding [1]. (B) Polygonal features in tufted microbial beds with chert interstitial to polygons. (C) Symmetrical ripples of grey carbonate beneath a cm-scale tuff [upper right of image]. Current direction indicated by arrow. Scale in (A) is 6 cm, (B) is 3 cm, and (C) is 15 cm

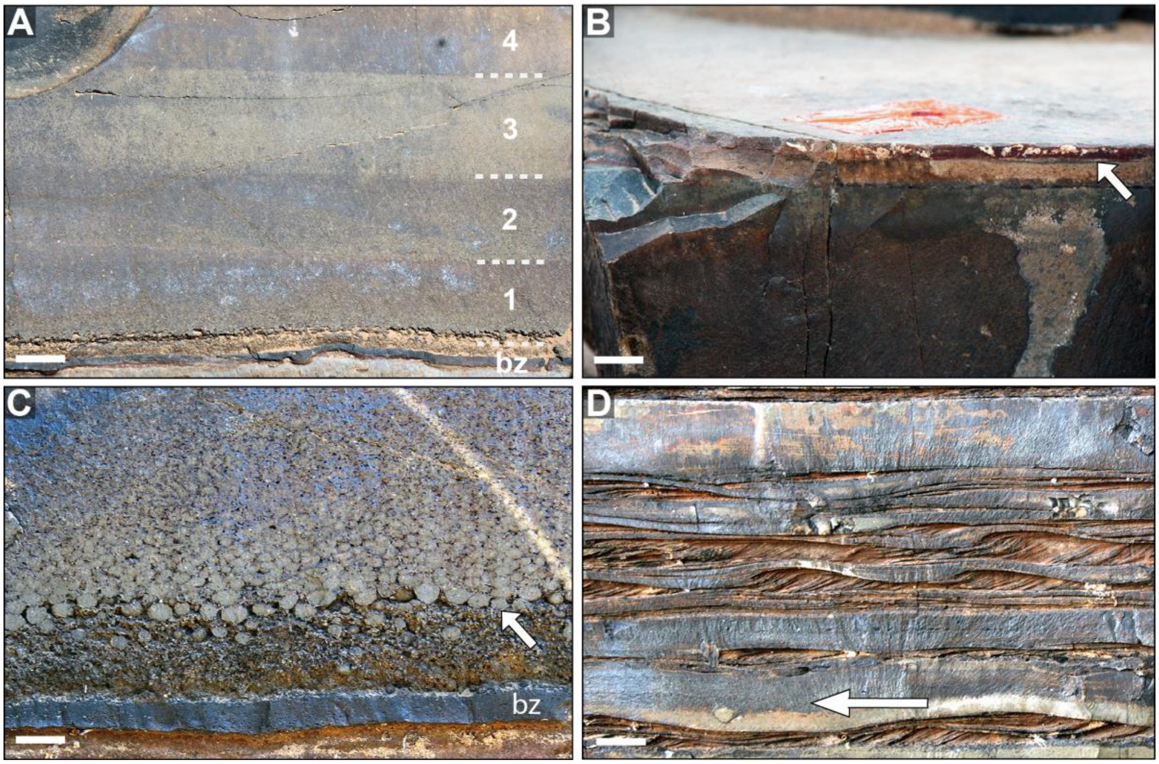


Figure 18 Volcaniclastic Beds in the Upper Nauga Formation

Photos of various volcanosedimentary deposits in the Upper Nauga Formation, Prieska Facies near Prieska, South Africa. (A) Multi-stage tuff featuring a welded baking zone above preexisting carbonate strata [bz], a layer of normally graded accretionary lapilli [1], a second event with another, smaller layer of normally graded accretionary lapilli [2], a light grey layer with minor <5 mm accretionary lapilli [3], and a fourth horizon of tuff at the top. This sequence indicates successive volcanic events. (B) Enigmatic purple layer (potentially a baked zone) superjacent to a light-colored tuff. (C) Tuff lapilli from volcanic ashfall with diameters ranging from 1-5 mm above a baked zone [bz]. The lapilli bed exhibits normal grading from gravity-driven settling. (D) Rippled cross-lamination of coarse-grained carbonate grains and tuffaceous sediment within cm-scale tuff beds. Ripples are composed of low-angle climbing ripples and are intercalated with dark, tuffaceous beds that are thicker between clinoforms. Current direction is SSW [white arrow]. Scale in (A) is 2 cm, (B) is 1 cm, (C) is 7.5 mm, (D) is 1.5 cm.

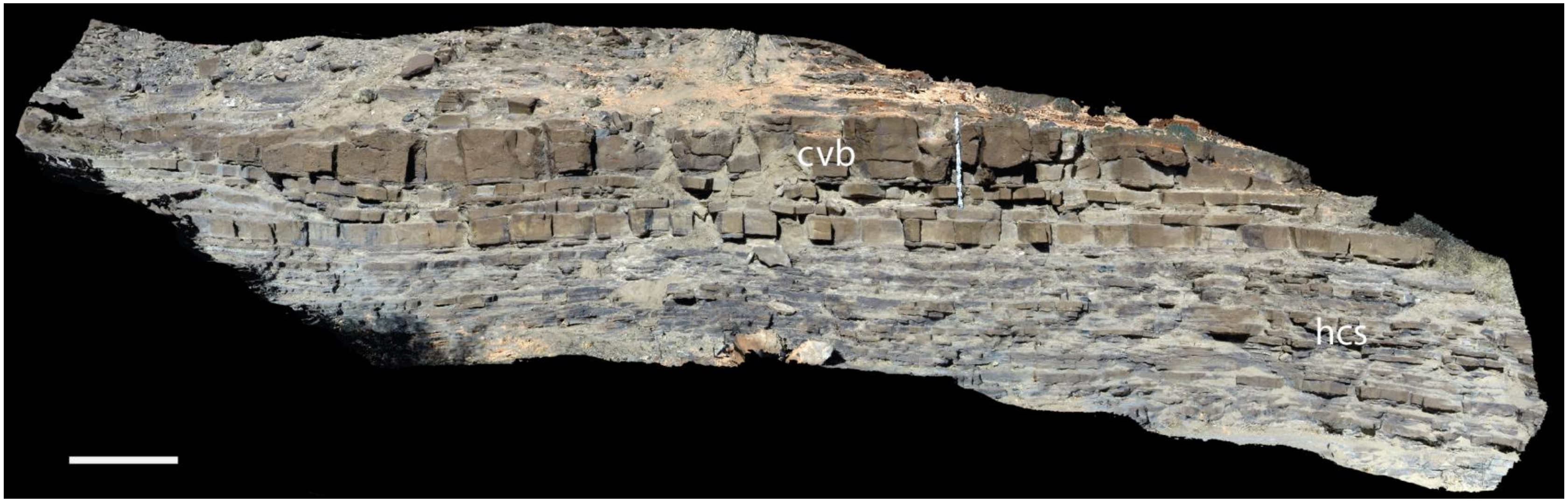


Figure 19 Digital Model of Lower Prieska 1 Section

Digital model of Lower Prieska 1 (LP1) uppermost outcrop composed of 187 photos using Agisoft Metashape software. Note: convolute bedding [cvb] and hummocky cross-stratification [hcs]. Scale is 1.5 m.

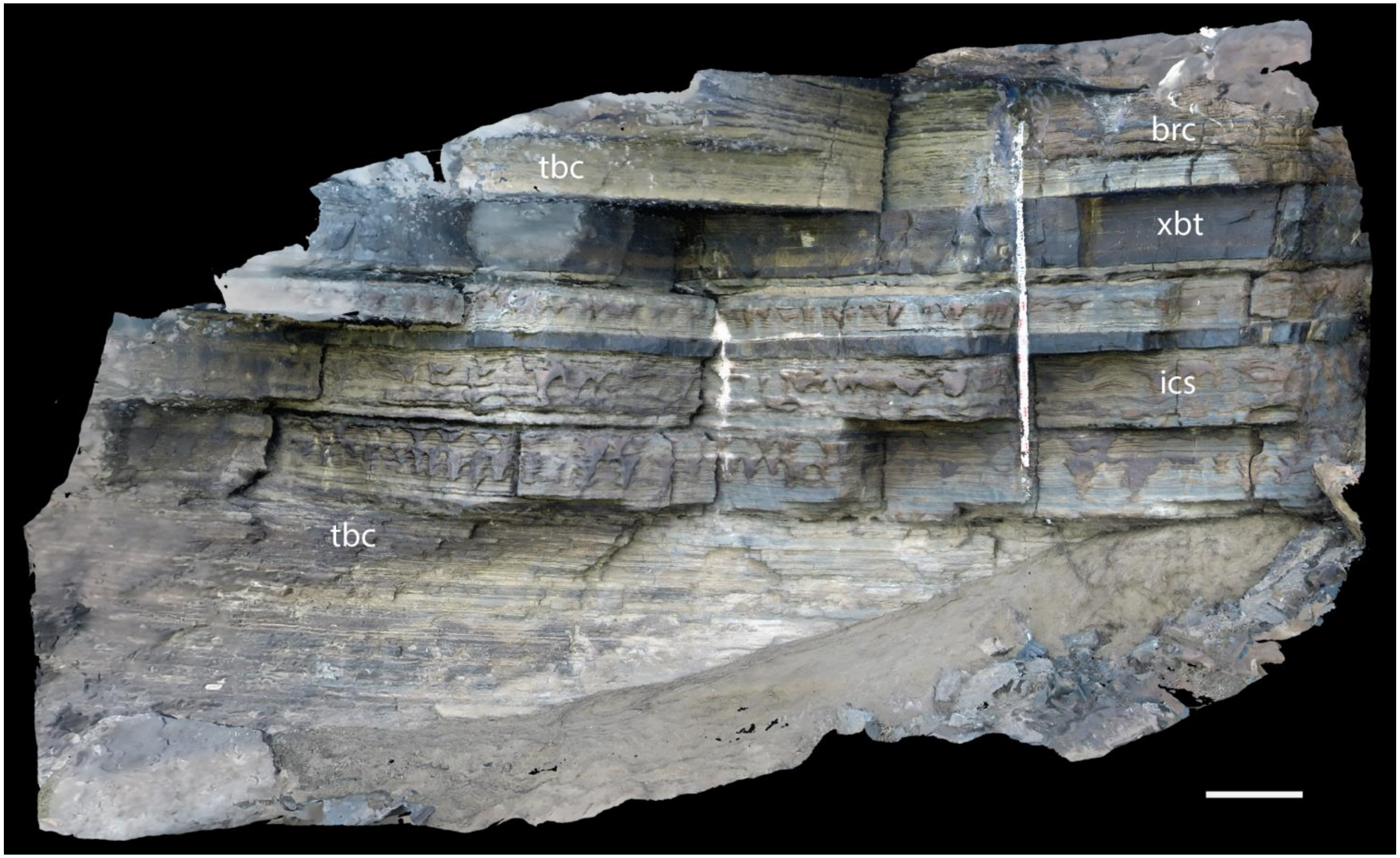


Figure 20 Digital Model of RELP Section

Digital model of River's Edge Lower Prieska Facies (RELP) outcrop composed of 160 photos using Agisoft Metashape software. Note: thinly-bedded carbonate [tbc], brecciated tuff in a brown carbonate matrix [brc], cross-bedded, intercalated tuff and carbonate sand [xbt], and inverted conical structures [ics]. Scale is 50 cm.

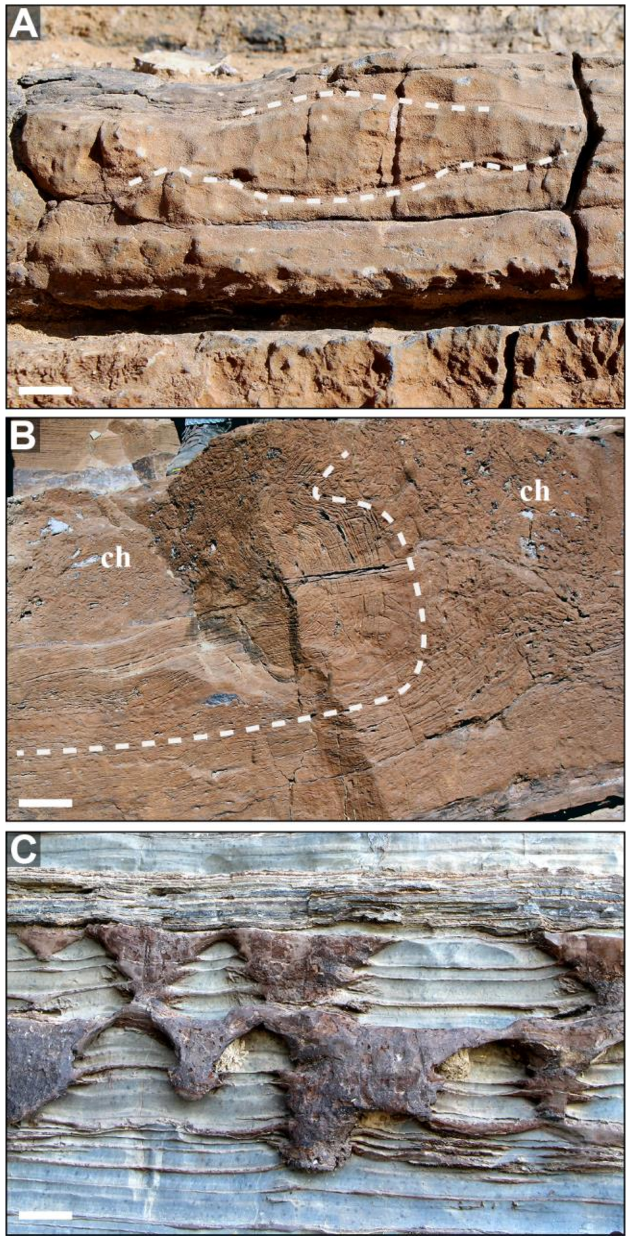


Figure 21 Disrupted Bedding in Prieska Facies

Photos of sedimentary structures in dolomite strata of the Upper Nauga Formation near Prieska, South Africa. (A) Hummocky and swaley cross stratified coarse-grained carbonate indicating above fair-weather wave base conditions. Dashed white lines indicate scour and fill surfaces. (B) Convolute bedding of carbonate strata indicating above storm-wave base conditions [dashed white line] with chert-filled vugs [ch]. (C) Enigmatic “inverted conical” structures with coarser-grained, grey carbonate and finer-grained, brown carbonate. Brown carbonate structures are often laterally linked by thin laminae. Scale in (A) is 1 cm, and (B, C) is 3 cm.

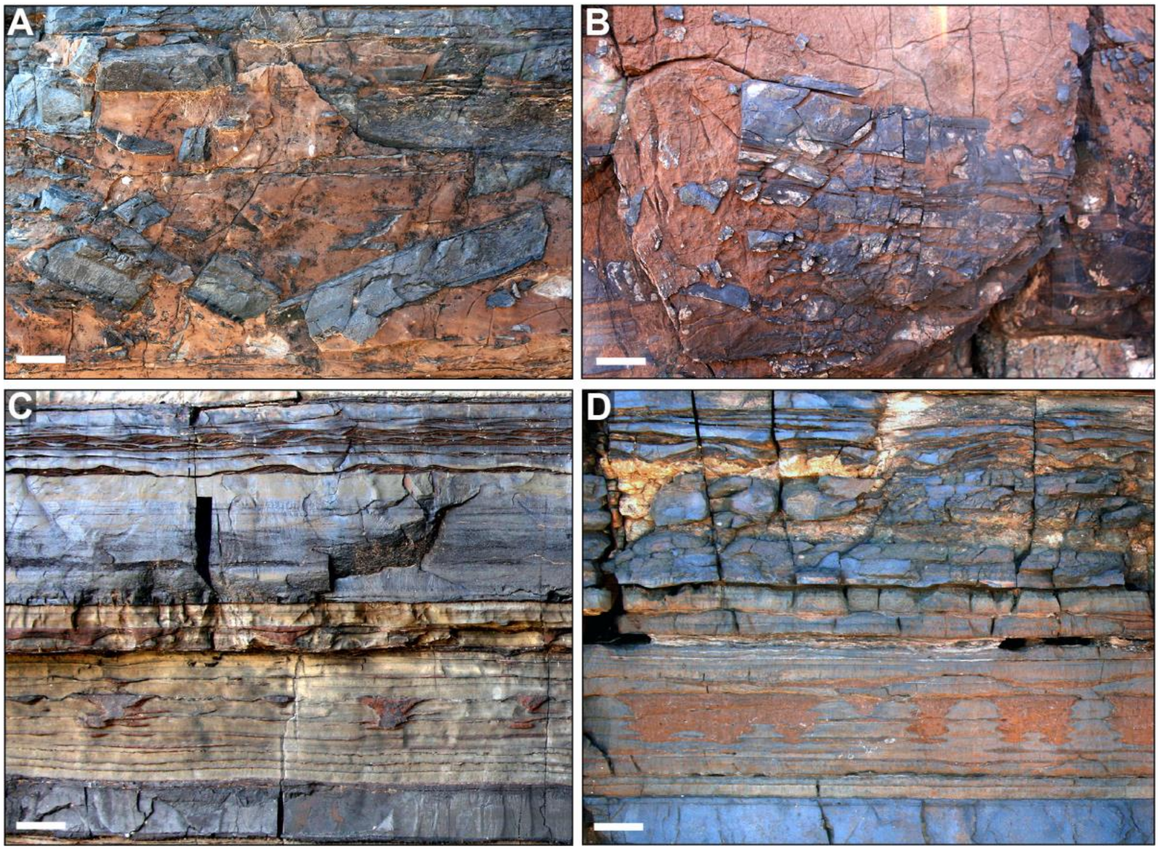


Figure 22 RELP vs UP1 Stratigraphic Comparison

Photos of brecciated tuff and cross-bedded tuff with subjacent “inverted conical” structures from (A, C) River’s Edge Lower Prieska section and (B, D) Upper Prieska 1 section. These two exposures are >500 m distant yet show similar thicknesses of units with an identical sequence of sedimentary structures. This indicates the presence of structural normal faulting not exposed at the surface, potentially underlying the Diamond Access Road (Fig. 7) which results in repetition of strata within the Upper Nauga Formation. Scale in (A) is 4 cm, (B) is 3 cm, (C) is 10 cm, and (D) is 8 cm.

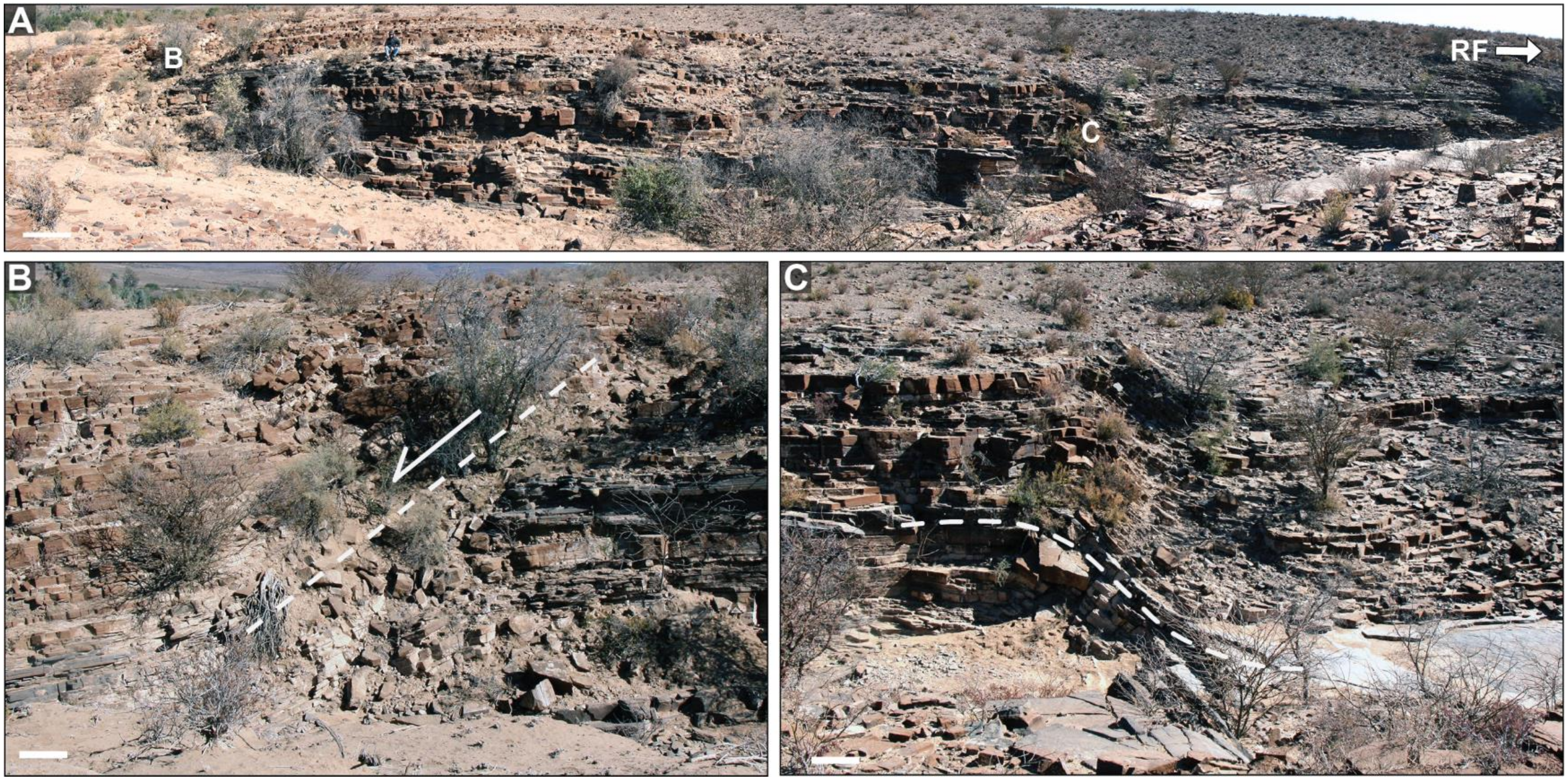


Figure 23 Faults in Lower Prieska 2 Section

Outcrop photos of Upper Nauga Formation, Prieska Facies along the Lower Prieska 2 drainage (see Fig. 7). (A) Panorama of LP2 facing north showcasing a normal fault (B) and subsequent back fold (C). A conjugate reverse fault [RF] is outside of the field of view to the east. Dry creek bed in (C) is a repetition of tuff deposit at the base of LP1, with white dashed line following this tuff. Scale in (A) is 2 m, and (B, C) is 50 cm.

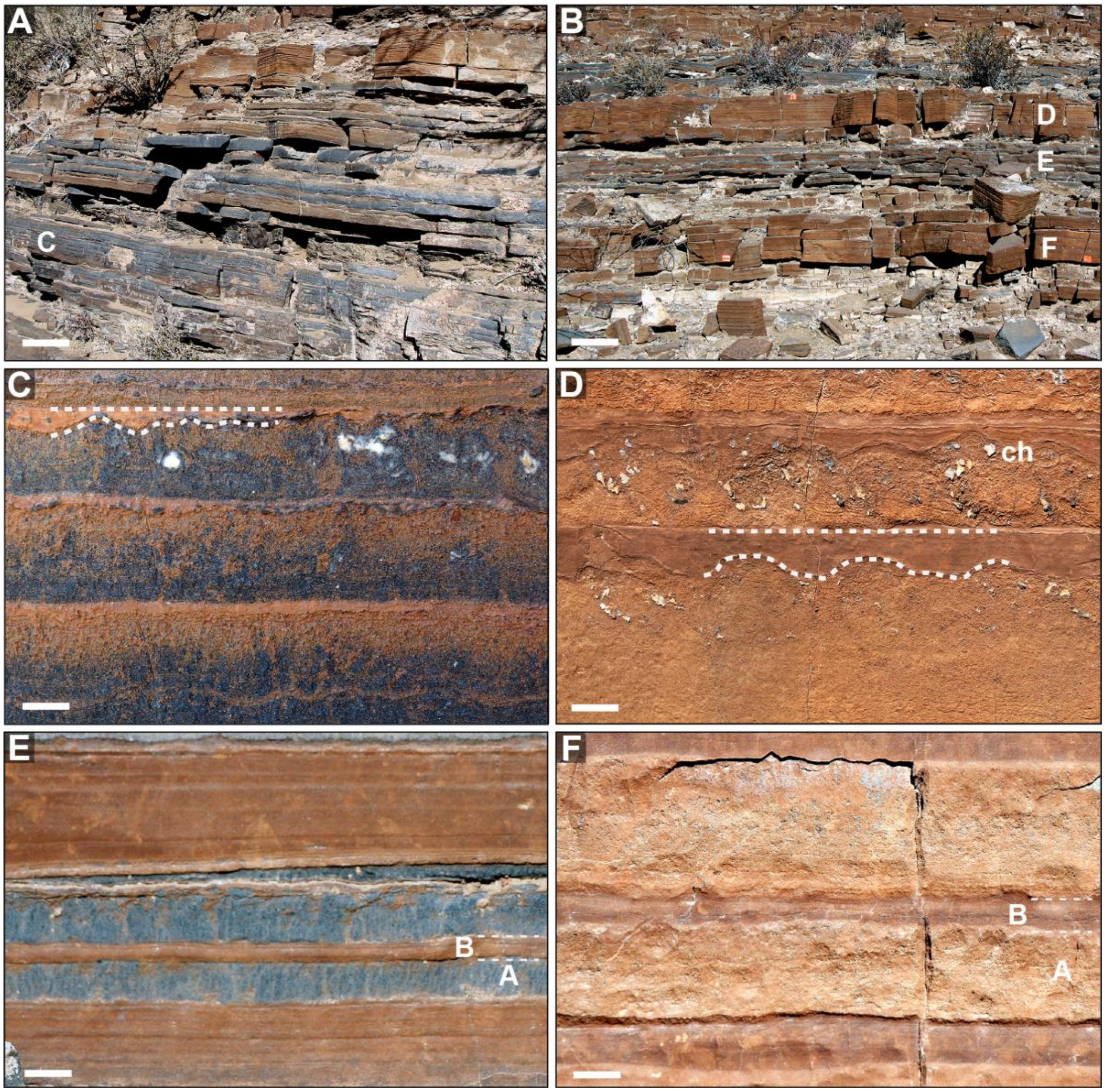


Figure 24 Alternating Grey- and Brown-weathering Units

Photos of two outcrops (A, B) and inset photos of bedding (C, D, E, F) that compare weathering variations of carbonate strata in the Prieska Facies, near Prieska, South Africa. (A, B) Alternating m-scale weathering variations from grey units to brown units. Compare (C) mm-scale, dark grey, tufted laminae with chert-filled vugs and fine-grained, brown laminae that drape tufts with (D) in which tufted laminae weather brown. Compare (E) coarsely recrystallized grey beds “A” with thin, fine-grained, brown laminae “B” with (F) in which recrystallized beds “A” weather brown. Note: overall similarity in texture and components, yet different weathering profiles. Scale in (A) is 30 cm, (B) is 40 cm, and (C, D, E, F) is 1 cm.

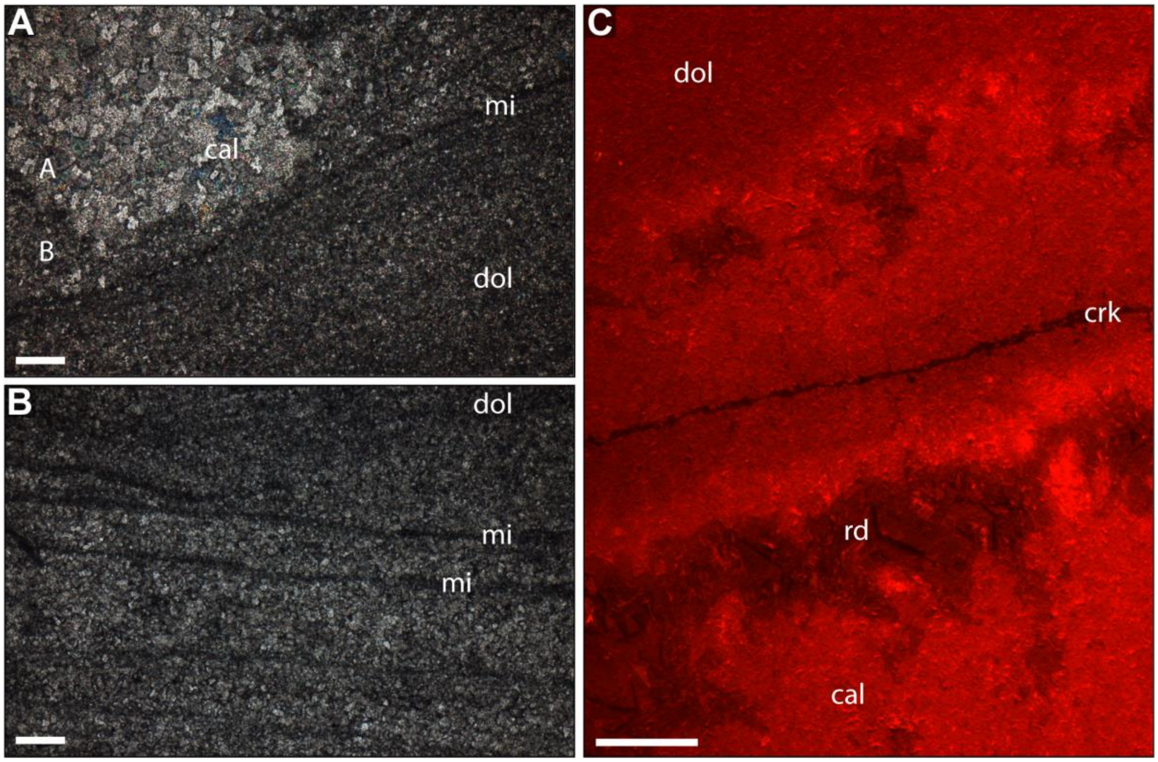


Figure 25 Photomicrographs of Ghaap Plateau Facies

Photomicrographs showing the relationship of A- and B-type microbial strata from Ghaap Plateau Facies near Boetsap, South Africa. (A) Tufted layer B-type transitioning to A-type lamina. A-type lamina consists of coarsely recrystallized calc-dolospar. B-type lamina consists of recrystallized dolomite microspar with strongly linear micritic fabric cement. (B) Interior view of B-type lamina containing banded micrite and finely recrystallized dolospar with dark micritic cement. (C) Cathodoluminescence image of dully luminescent dolospar and brightly luminescent calcite microspar. Relict dolomite visible in zones recrystallized calcite spar. A late diagenetic crack with FeO cuts sub-horizontally through calcite. Scale is 100 μm. Notes: A = A-type lamina, B = B-type lamina, cal = calcite, mi = micrite, dol = dolomite, crk = crack, rd = relict dolomite.

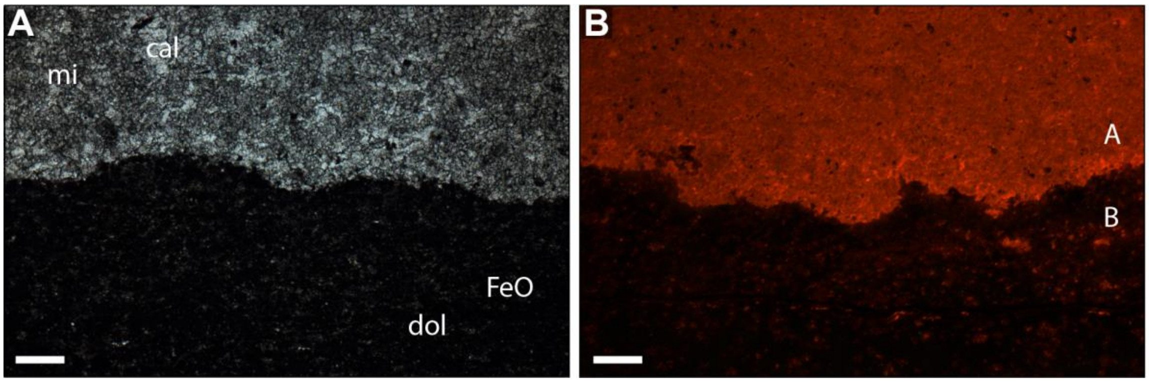


Figure 26 Photomicrographs of Prieska Facies

Photomicrographs showing the relationship of A- and B-type laminae of carbonate strata from the Prieska Facies. (A, B) Paired micrographs showing the boundary between A-type bed and B-type bed. A-type laminae are coarsely recrystallized calcite (white in PPL and bright orange in CL) with fine grained carbonate in a micritic cement (gray in PPL and dark orange in CL). B-type bed is dully luminescent in CL and black in PPL with disaggregated dolomite rhombs. Scale is 100 μm. Notes: mi = micrite, cal = calcite, dol = dolomite, FeO = Fe-oxide cement.

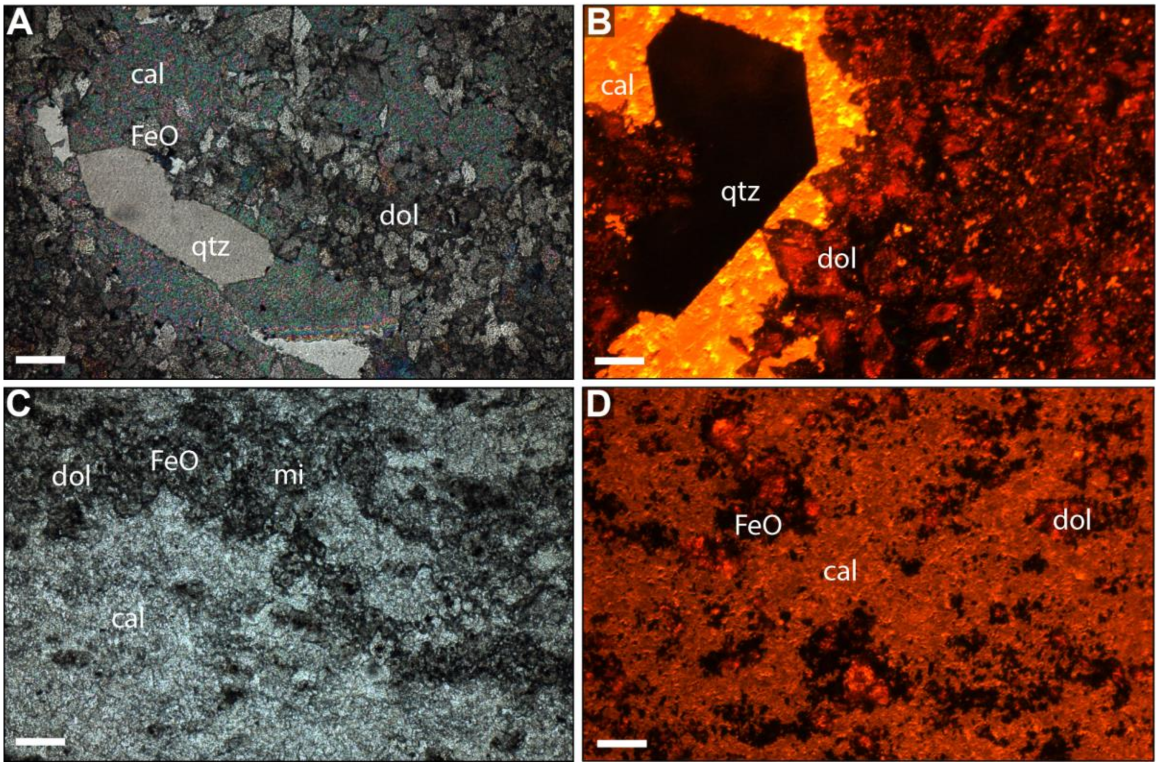


Figure 27 Photomicrographs of Prieska Facies 2

Photomicrographs of rare fabric and mineralogy in the Prieska Facies associated with chert/calcite vugs and polygonal cracks on bedding surface. (A, B) Carbonate strata consists of void-filling calcite cements influencing quartz crystal preservation with fringing FeO cements interstitial to calcite-quartz grain boundaries. Anhedral dolomite spar also feature FeO cements. Cathodoluminescence shows disaggregated dolomite rhombs with dull cores and anhedral fragments of previous dolomite rhombs (orange-red in CL). (C, D) Strata consist of coarsely recrystallized calcite (white in PPL and bright orange in CL) with blebs of recrystallized dolomite rhombs, FeO cements, and micrite within a linear fabric. Scale is 75 µm. Notes: cal = calcite, FeO = Fe-oxide cement, qtz = quartz, mi = micrite.

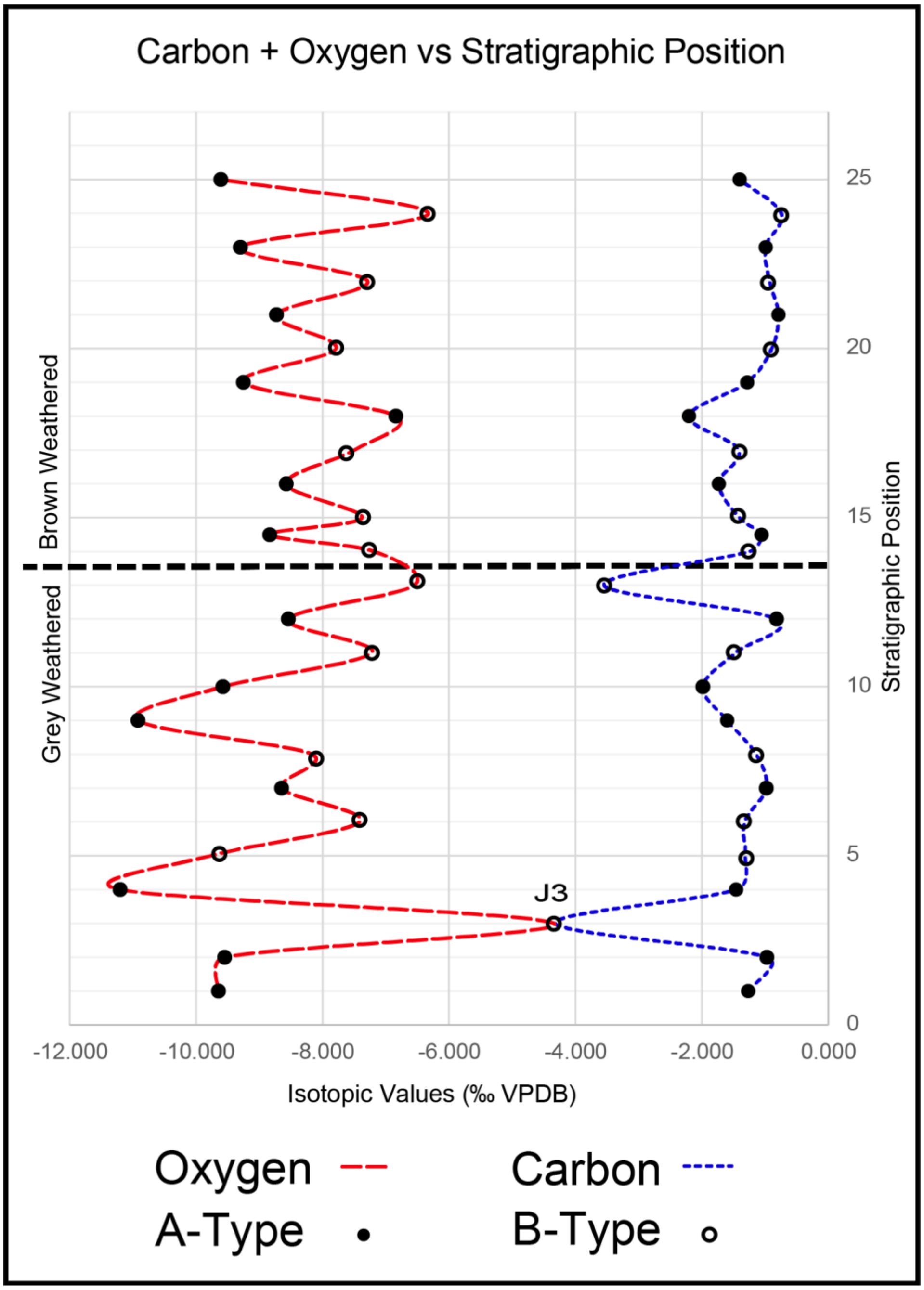


Figure 28 Carbon and Oxygen Isotope Trends in Weathering Color

Carbon and oxygen isotopic composition of carbonate from alternating grey- and brown-weathering profiles in m-scale strata. C-isotopes are similar throughout. O-isotopes vary between A-type and B-type laminae which suggests the potential for differential diagenesis during post-depositional fluid migration. Note: Sample J3 was identified as a late diagenetic Fe-rich vein.

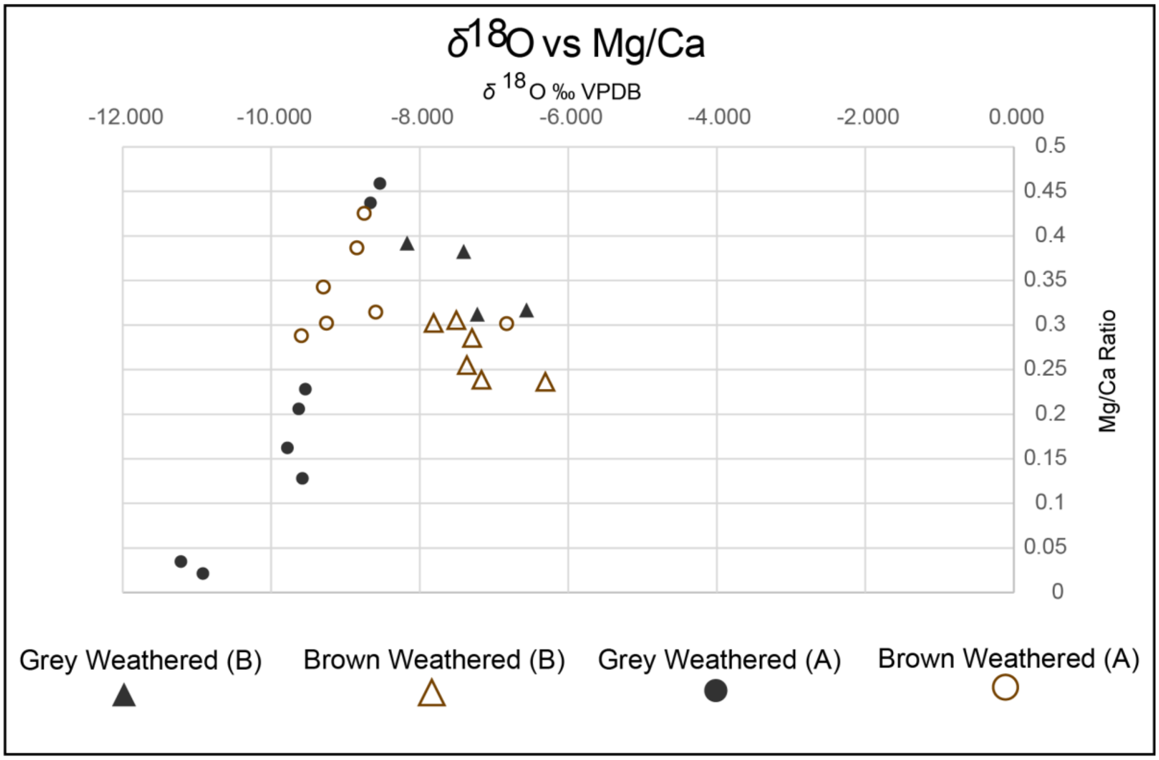


Figure 29 Mg/Ca v O

Mg/Ca molar ratio *vs* oxygen isotopes in B-type layers show similar compositions which suggests that both grey- and brown-weathered B-type layers have little to no difference in dolomite/calcite ratio. However, A-type layers show variation with brown-weathered A-type layers having a higher amount of dolomite then brown-weathered A-type layers. This suggests that the brown-weathering color is a product of post-depositional diagenesis that resulted in preferentially higher degrees of dolomitization.

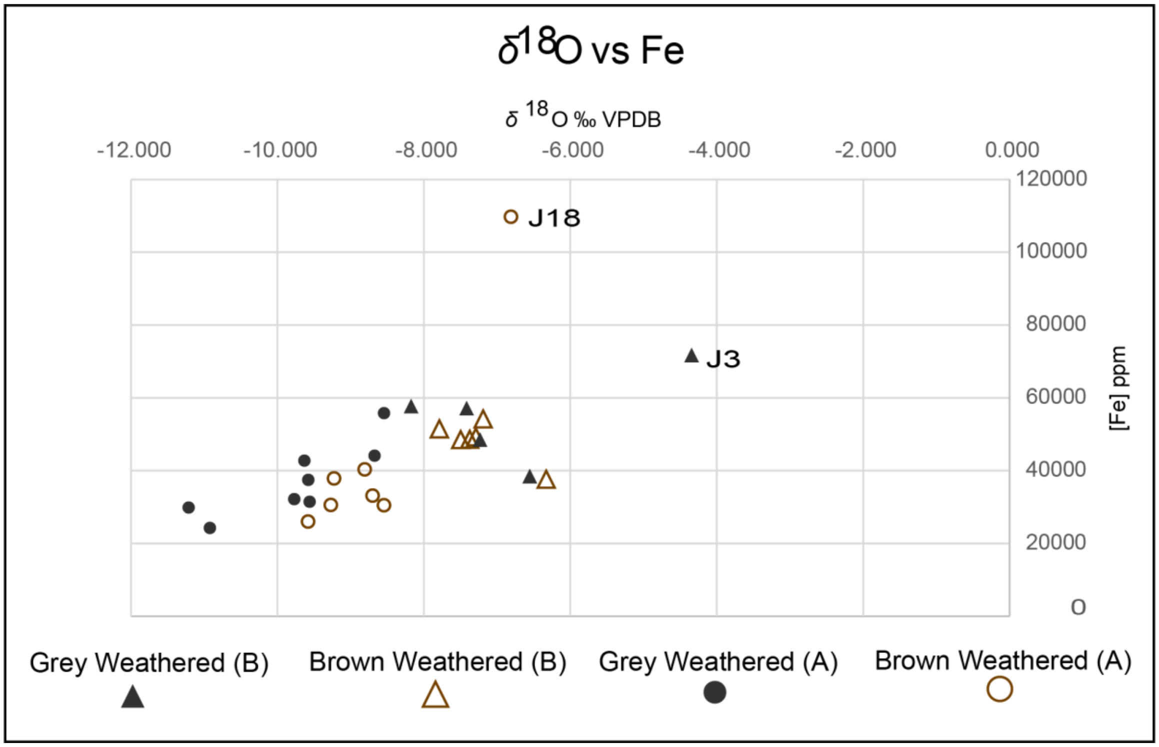


Figure 30 Fe v O

Fe concentration [ppm] *vs* oxygen isotopes have a similar range between A-type and B-type laminae of both grey- and brown-weathering profiles in m-scale strata, although B-type layers have higher [Fe]. Outliers (J3, J18) reflect Fe-rich veins.

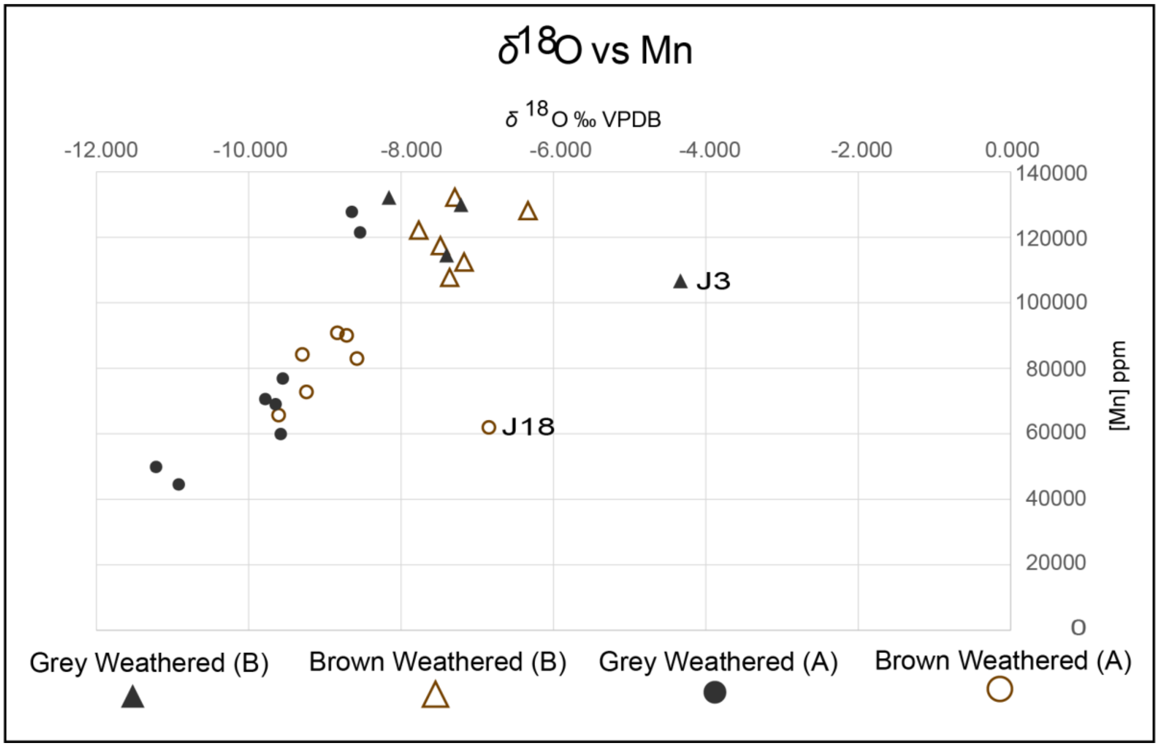


Figure 31 Mn v O

Mn concentration [ppm] *vs* oxygen isotopes trend from lower to higher concentrations between all A-type beds to all B-type beds, with grey-weathered A-type beds having the lowest Mn values. This suggests that grey weathering may be related to a different diagenetic phase during post-depositional fluid flow. Outliers (J3, J18) reflect Fe-rich veins.

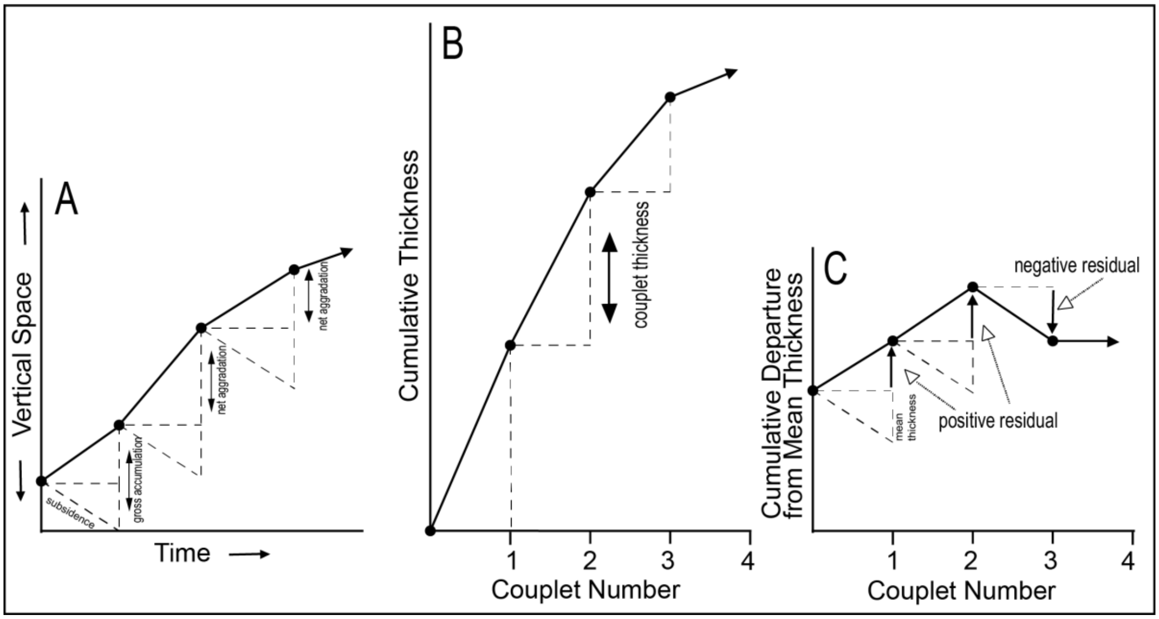


Figure 32 Fischer Plot Components

Components of modified Fischer plots showing successive cycle thickness relationship (modified from Sadler et al., 1993). (A) Visualization of the relationship between subsidence and net accumulation through time. (B) Cumulative thickness of strata as cycles stack. (C) Cumulative departure from mean thickness showing positive and negative residual relationship to mean thickness which indicate more or less accumulation (respectively) as a response to relative sea level rise and fall.

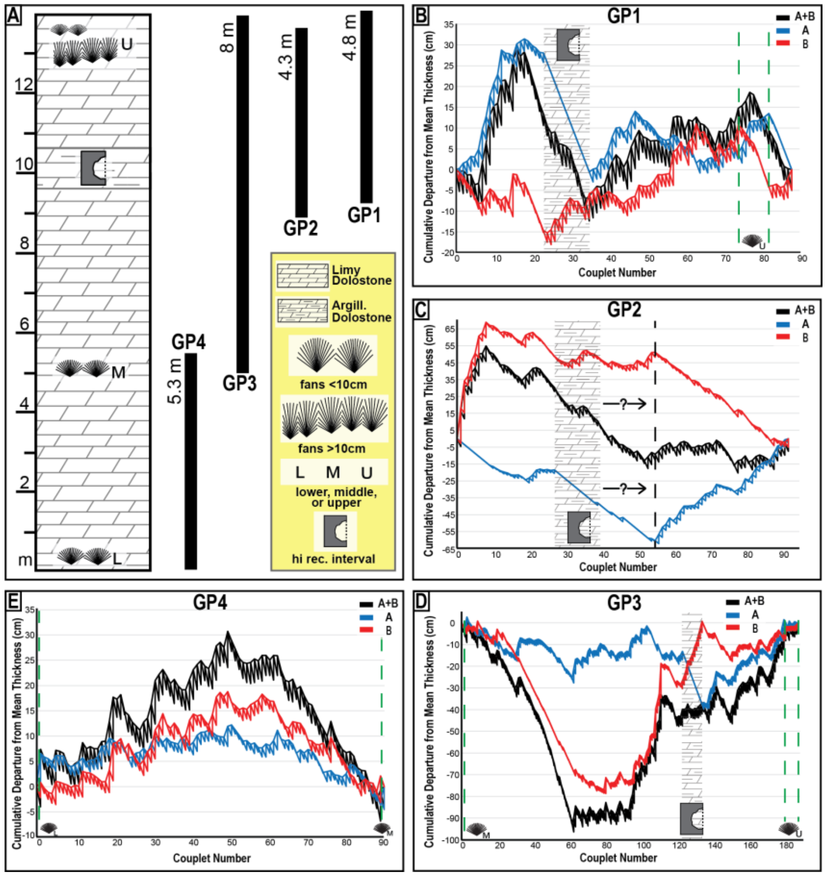


Figure 33 Ghaap Plateau Fischer Plots

Compilation of stratigraphic section and modified Fischer plots for four measured sections of the Reivilo Formation, Ghaap Plateau Facies, Transvaal Supergroup. (A) Composite stratigraphic column showing relative position of each measured section. (B) Fischer plot for GP1 composed of 88 couplets. A-type beds have a greater influence on total couplet (A+B) thickness except from couplets 22-34 (recessive interval). (C) Fischer plot for GP2 composed of 93 couplets. In contrast to the symmetric sequence (GP1), B-type beds control phases of changes in thickness. The discrepancy may be due to a 5 couplet set with thick B-type beds that is not exposed in GP1. The presence of a continuous trend of thinning A-type beds (couplets 39-55) after the recessive interval suggests prolonged environmental change. (D) Fischer plot for GP3 composed of 189 couplets. Overall, couplet thickness decreases from cumulative mean with a relative increase around couplet 90 that continues until end of sequence. Dramatic changes in thickness of B-type beds and symmetrical response of couplet thickness indicates B-type dominance of cycle thickness. When present, fans contribute to an increase in A-type prevalence, and temporarily control changes to couplet thickness. (E) Fischer plot for section GP4 composed of 91 couplets. Roughly symmetrical changes in A- and B-type bed thickness suggests a constant level of detrital carbonate input. A-type beds are thickest at the beginning of section, as a result of pseudomorph fans.

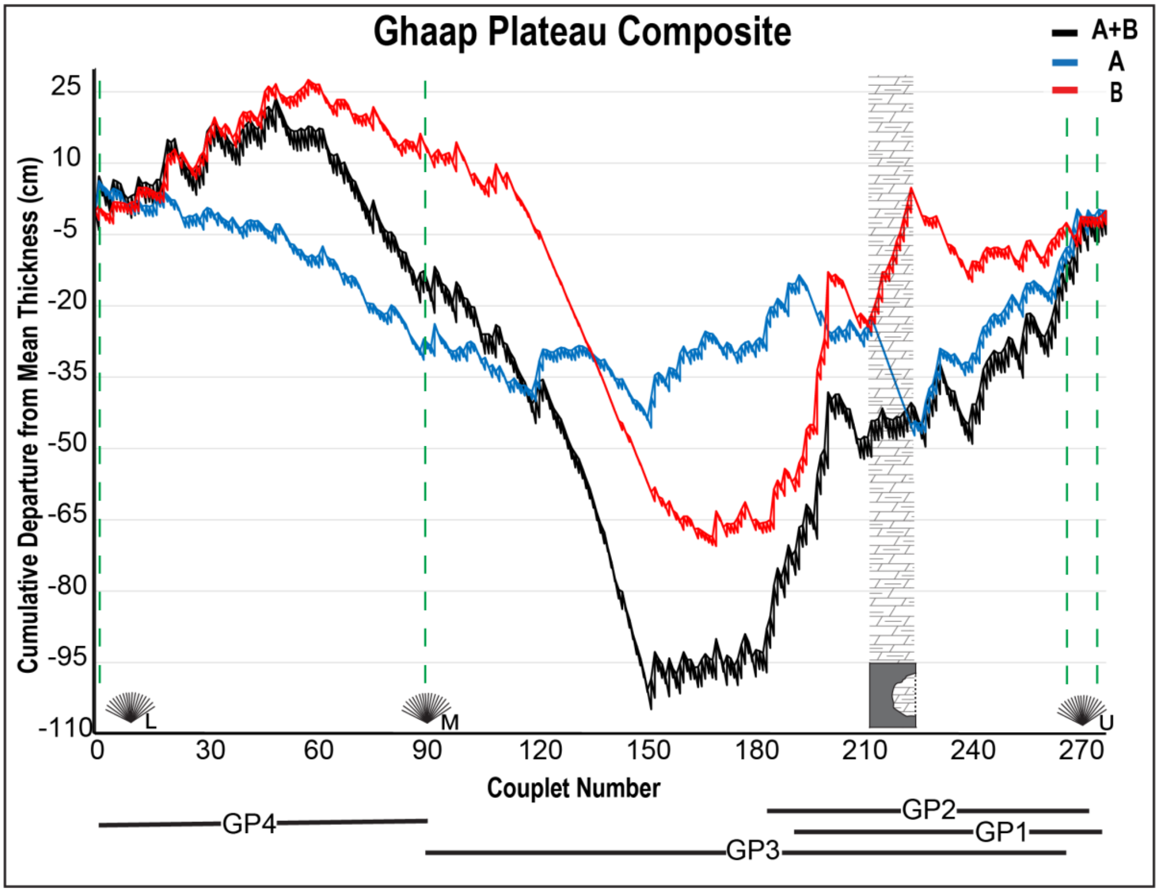


Figure 34 Ghaap Plateau Composite Fischer Plot

Modified Fischer plot composed of overlapping GP3 and GP4 sections (see Fig. 33) and containing 280 couplets. Lower (L) and middle (M) beds of pseudomorph fans have slight influence on cycle thickness, as B-type beds generally dominate couplet thickness throughout entire sequence. Couplets 118-150 indicate rapidly decreasing thickness of B-type beds while A-type beds remain relatively constant in thickness. Prior to and including the recessive interval, B-type beds control thickness and continue except for a minor contribution of A-type beds after couplet 226. In summary, this suggests that this environment of deposition in the Reivilo Formation was susceptible to changes in external sedimentary input (B-type beds).

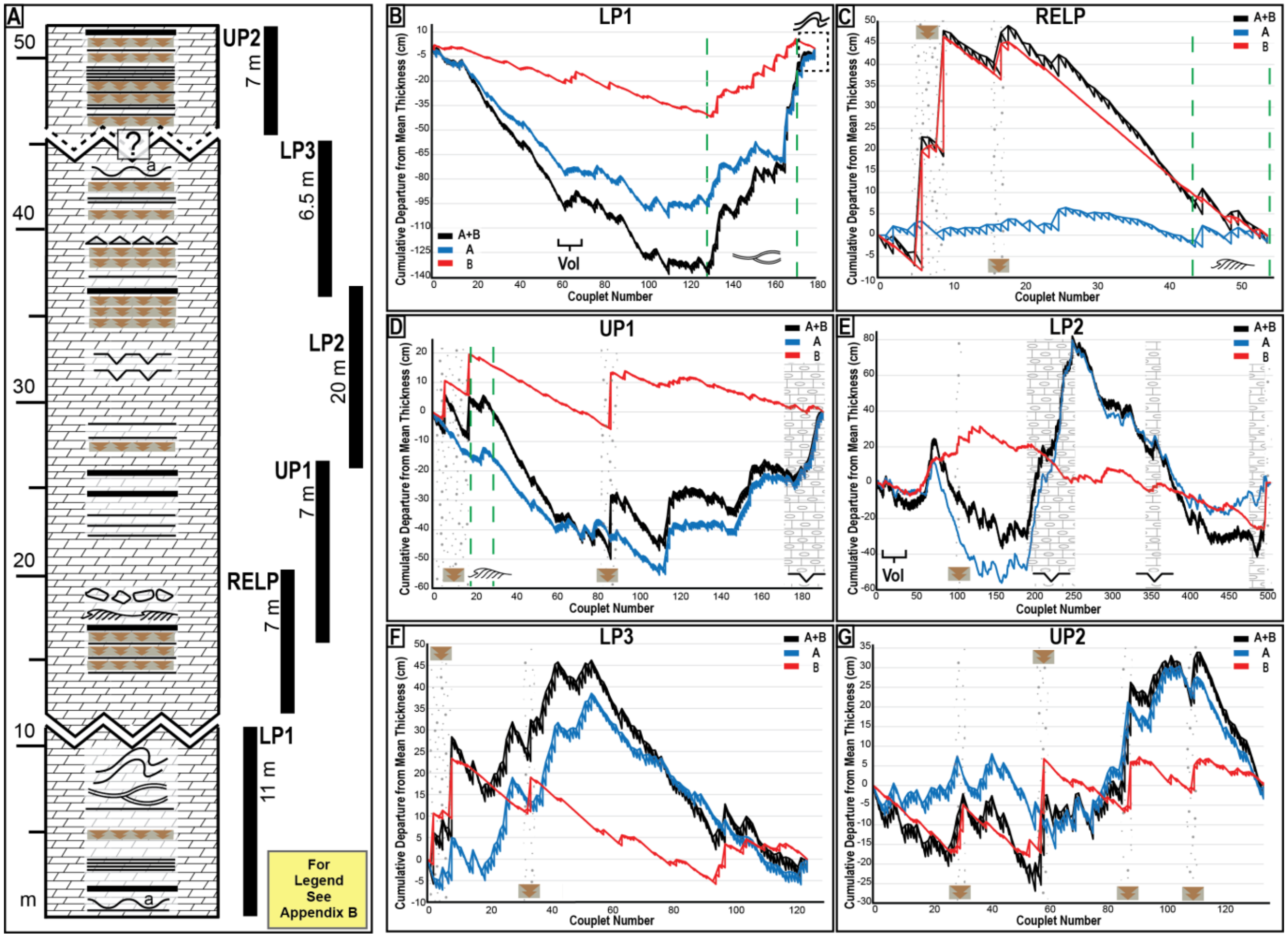

Figure 35 Prieska Fischer Plots

Compilation of stratigraphic sections and modified Fischer plots for six measured sections of the Upper Nauga Formation, Prieska Facies, Transvaal Supergroup. (A) Composite stratigraphic column showing relative position of each

Figure 35 Continued

measured section. (B) Fischer plot for LP1 composed of 181 couplets. A- and B-type beds symmetrically change in thickness, however A-type beds contribute more to overall cycle thickness, suggesting dominantly microbial carbonate precipitation. Carbonate beds that co-occur with tuff deposits (Vol) show relative increase in thickness of all components. A period of hummocky cross-stratification (couplets 127-175) in carbonate shows stable increases in thickness. Interpretation of convolute bedding at the end of sequence is obfuscated by termination of run. (C) Fischer plot for RELP composed of 54 couplets. Note that three beds of inverted conical structures result in dramatic positive residuals in mean “B-type” thickness, although A-type beds are stable throughout. (D) Fischer plot for UP1 composed of 193 couplets. Note that three beds of inverted conical structures result in dramatic positive residuals in mean “B-type” thickness. A-type beds, however, control overall changes in mean thickness. A dramatic increase in A-type beds coincides with the presence of highly-tufted, chert-rich facies that have polygonal bedding surfaces. (E) Fischer plot for LP2 composed of 507 couplets. Note that a thick inverted conical structures bed at the end of data. Overall, B-type beds have less significant contribution to overall cycle thickness. Near symmetrical curves for A-type and couplet thickness indicates an environment dominantly controlled by microbial processes. The three most significant positive residual trends in A-type beds coincide with strongly tufted microbial strata with thin, draping B-type beds and polygonal upper surfaces. (F) Fischer plot for LP3 composed of 125 couplets. Note the two occurrences of inverted conical structures result in increase in mean B-type thickness, which temporarily overrides dominantly A-type control on couplet thickness. (G) Fischer plot for UP2 composed of 136 couplets. Note the high frequency of thick inverted conical structure beds that buck the trend of symmetrical A-type and couplet curves.

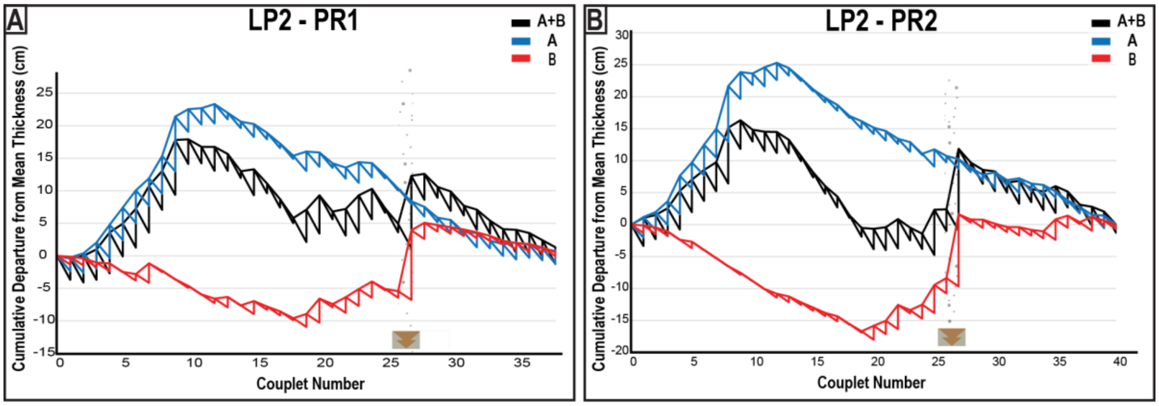


Figure 36 Comparison of LP2 Sections (1.5 m x2)

Comparison of two modified Fischer plots showing duplicate 1.5 m section (2 m laterally offset) of alternating grey- and brown-weathered carbonate strata from the LP2 section to evaluate lateral continuity of bed thickness. (A) Fischer plot of LP2-PR1 composed of 39 couplets. (B) Fischer plot for LP2-PR2 composed of 40 couplets. The equivalent magnitudes of change in both positive and negative residuals for A-type beds in both measured sections are nearly symmetrical. Comparatively, less than identical B-type curves in both sections suggests that B-type departures from mean thickness, and thus rate of accumulation of B-type beds, is more variable than A-type bed accumulation rates.

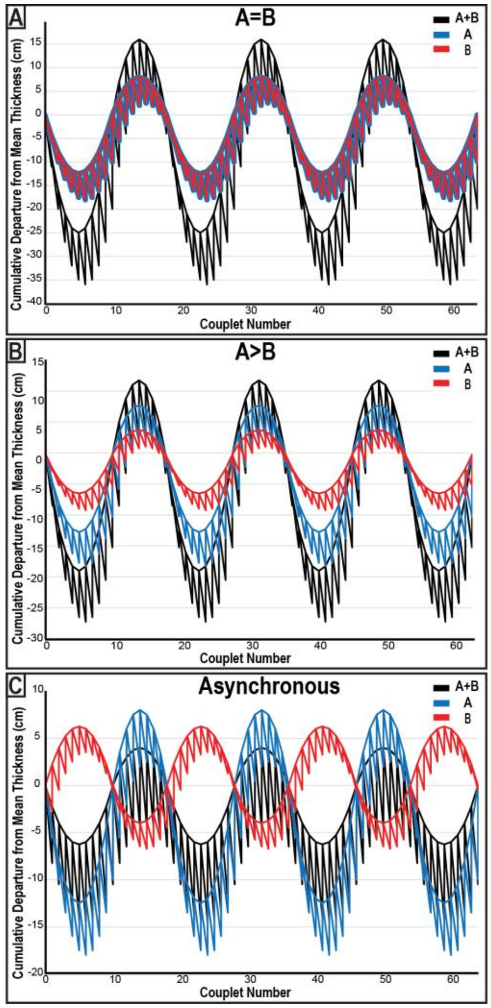


Figure 37 Hypothetical Fischer Plots

(A) Hypothetical modified Fischer plot of symmetrical and equal thickness A-type and B-type components (A=B) in 64 couplets. A and B have equal contribution to couplet thickness which is displayed qualitatively in symmetric curves. (B) Hypothetical modified Fischer plot of symmetrical and different thickness A-type and B-type components (A>B) in 64 couplets. A-type beds increase and decrease in thickness at a rate of 2x changes in B-type beds, which displays symmetrical, yet unequal curves. (C) Hypothetical modified Fischer plot of asynchronous and unequal thickness A-type and B-type components in 64 couplets. A-type beds change at a rate twice that of B-type beds, and if A increases, then B decreases (and vice-versa). This asynchronous relationship results in a couplet thickness that changes at a lower rate than either A- or B-type components, although couplet curve is symmetrical to dominant component (here: A-type).

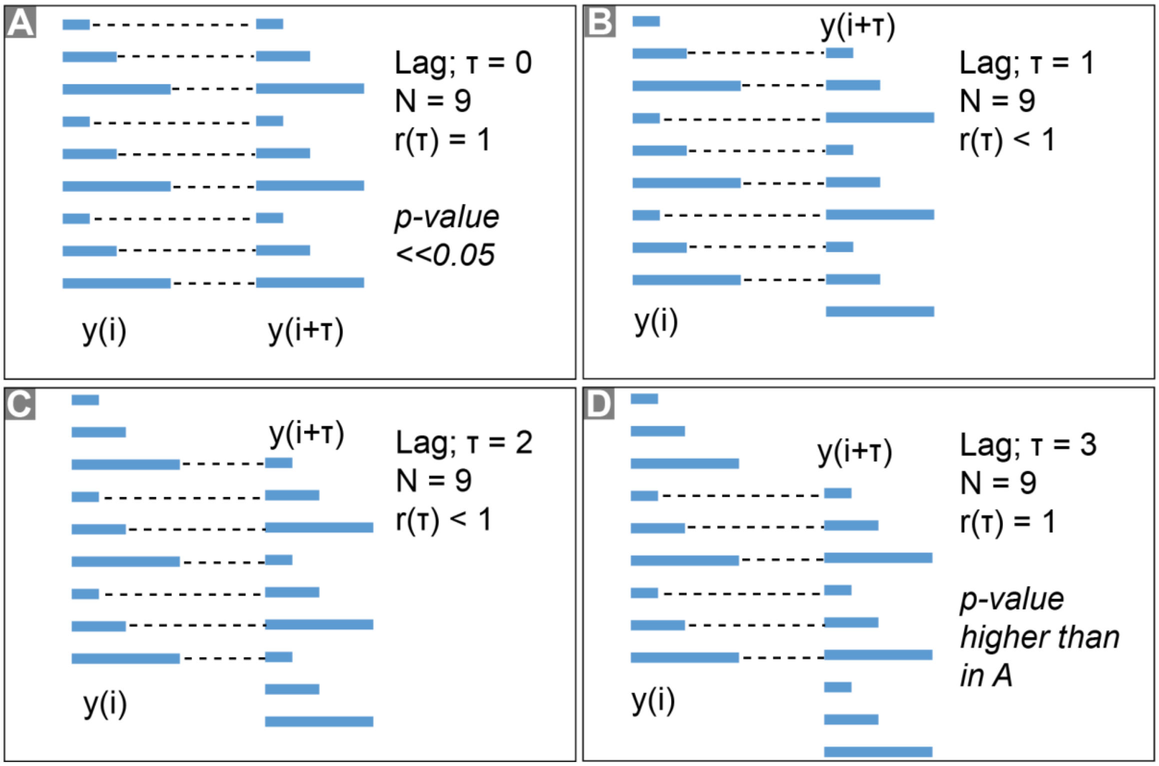


Figure 38 Illustration of Lag Number and Offset

Graphical illustration of two identical series composed of individual thicknesses (N); one is held stationary (yi) and the other (yi+t) is offset by increasing lag (T). (A) Perfect correlation coefficient r(T) is resultant from symmetrical, non-offset series with a p-value of 0. (B) and (C) Decreasing similarity of offset thickness at increasing lag. (D) Hypothetical correlation coefficient of r(T) = 1 at lag (T) = 3, with a p-value indicating less significance than in (A) due to decreasing pairs (N).

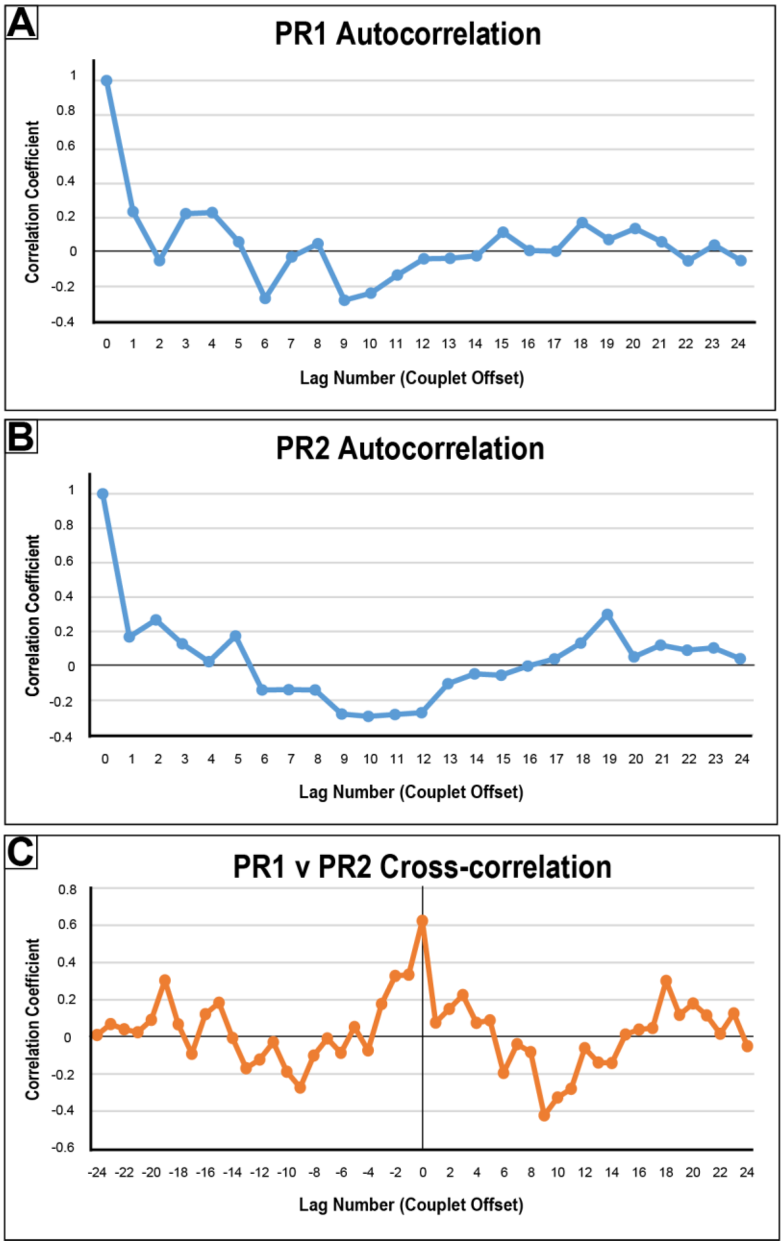


Figure 39 LP2 Duplicate Sections (1.5 m x2)

Autocorrelation and cross-correlation results for PR1 and PR2 (1.5 m, 39 couplets) that are offset by 2 m to analyze lateral continuity of couplet thickness. (A and B) Autocorrelation results for PR1 and for PR2 show a low degree of similarity and have no statistical significance (p-values >0.05). (C) Cross-correlation coefficient of 0.6 at lag = 0 confirms high degree of similarity, and negative and positive lags show high degree of “mirror” uniformity indicating similar degrees of variance.

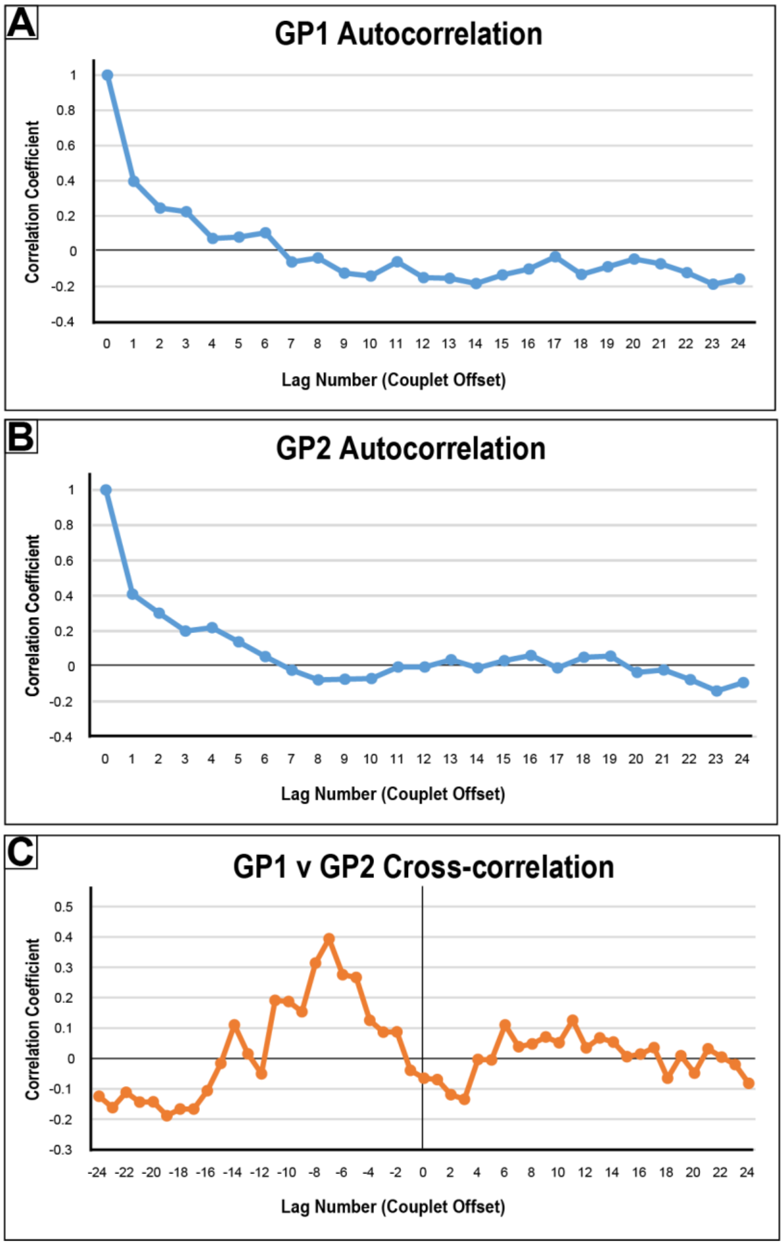


Figure 40 GP1 vs GP2 Auto- and Cross-correlation

Autocorrelation and cross-correlation results for GP1 and GP2 (4.8 m, 88 couplets; 4.3 m, 92 couplets) that are laterally offset by 23 m to analyze lateral continuity of couplet thickness. (A and B) Autocorrelation results for GP1 and GP2 indicate high degree of similarity with p-values <0.05 for lag = 1 to 4. (C) Cross-correlation results indicate a relatively high degree of similarity at lag = -7 couplets (p-value <0.05) which indicates the starting measurement bed is 7 couplets lower in GP2 than in GP1, which confirms field observations.

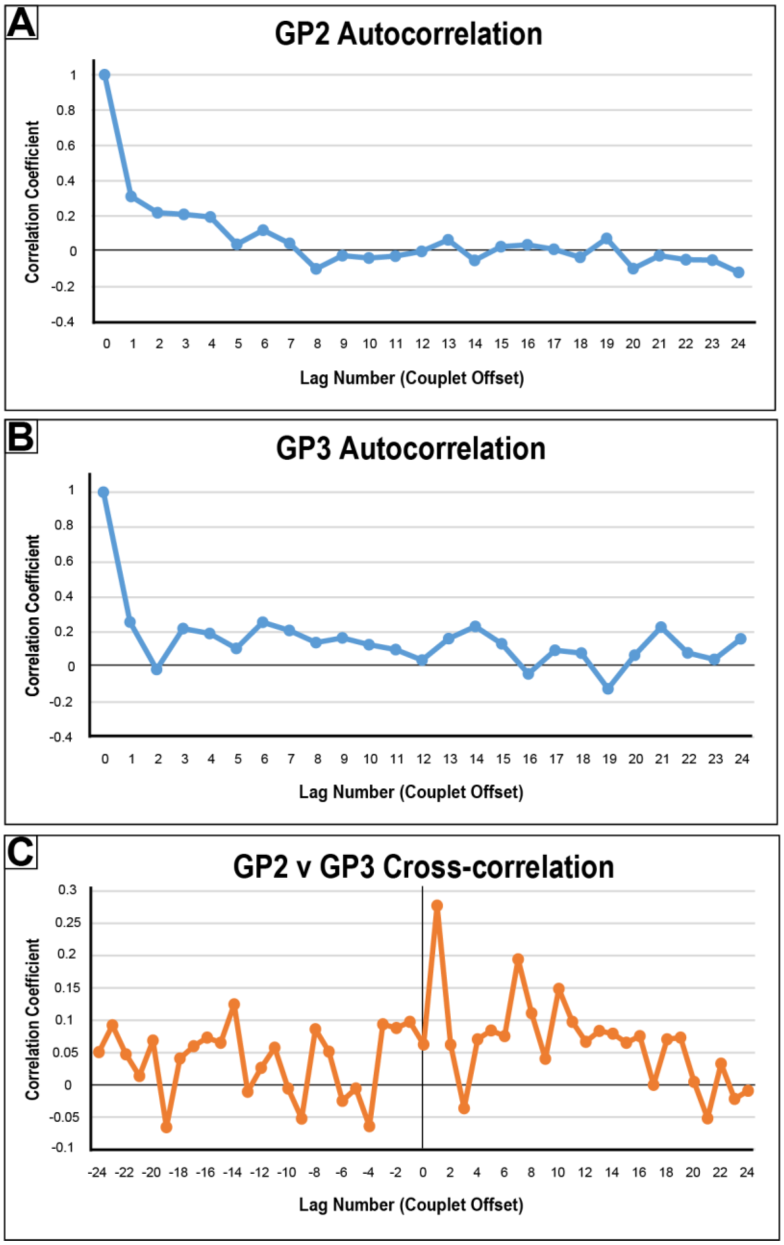


Figure 41 GP2 vs GP3 Auto- and Cross-correlation

Autocorrelation and cross-correlation results for B2 and B3 (4.3m, 93 couplets; 8 m, 190 couplets) to analyze similarity within two different section thicknesses. (A and B) Self-similarity is higher in B3 which suggests that higher couplet numbers (greater overall thickness) returns more statistically significant data. (C) Cross-correlation for B2 and B3 indicates a co-variance of ~0.27 for lag = 1 couplet offset, although data (Appendix D) shows high p-values indicating no statistical significance.

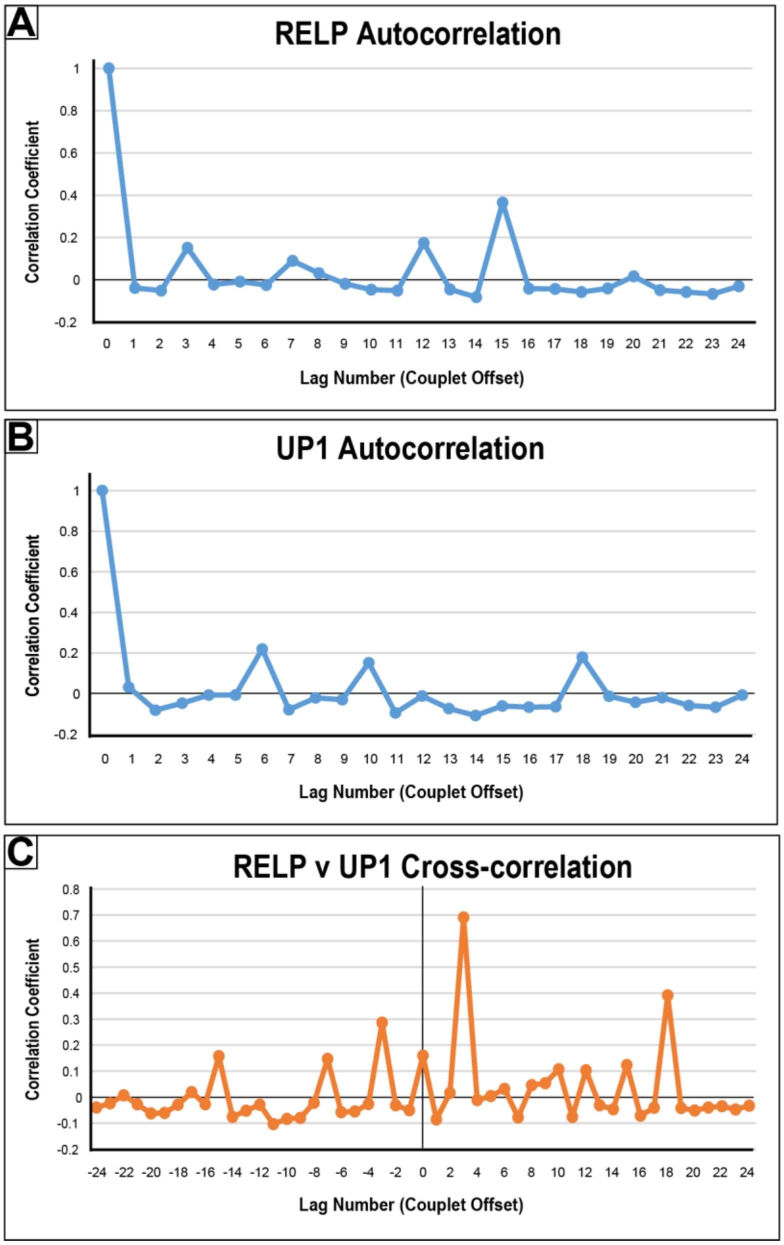


Figure 42 Comparison of RELP and UP1

Autocorrelation and cross-correlation results between Prieska Facies carbonate strata where tuffs and inverted conical structures show astoundingly physical similarity in section RELP (145 cm, 46 couplets) and section UP1 (177 cm, 46 couplets) that are ~2 km distant. (A) Autocorrelation for RELP shows high degree of similarity at lag = 15 couplets (p-value <0.05), although no similarity is detected in UP1 (B). (C) Cross-correlation indicates perfect correlation at lag = 3 couplets (p-value <<0.05).

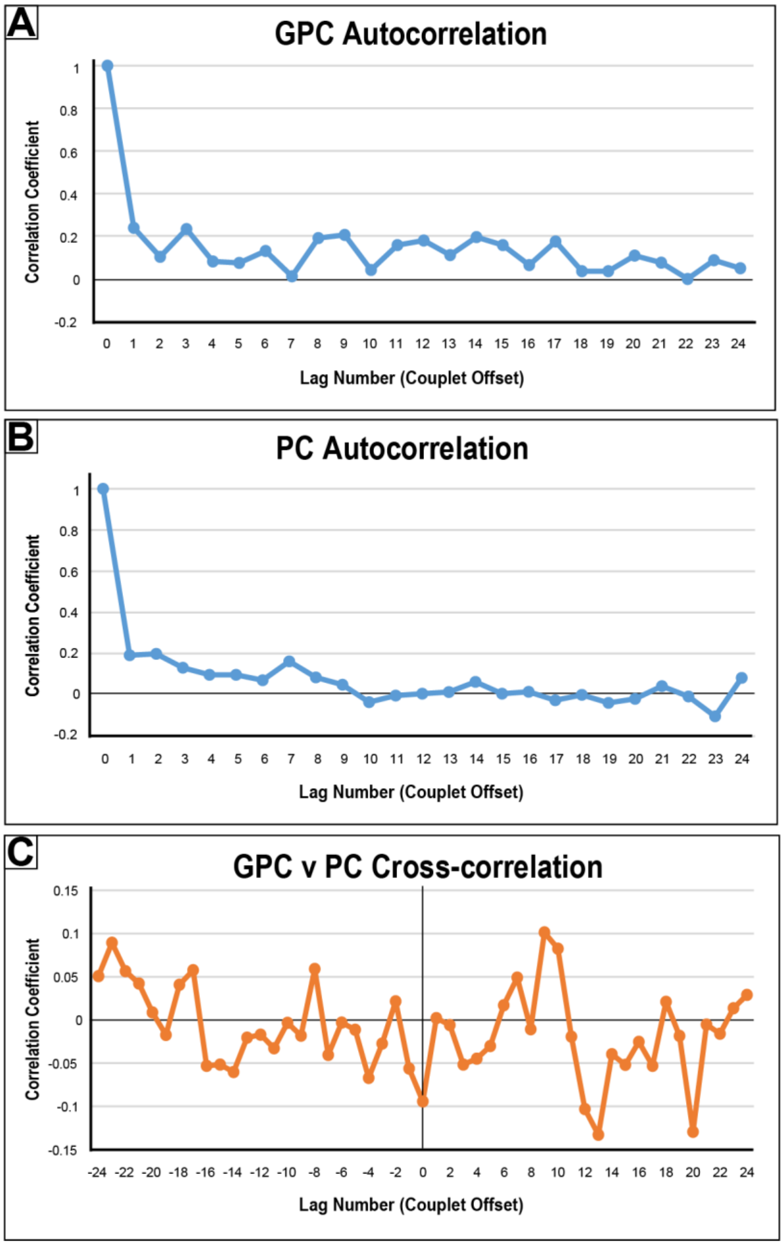


Figure 43 Comparison of GP and P Composite Sections

Autocorrelation and cross-correlation results between Ghaap Plateau Composite Section (11 m, 280 couplets) and Prieska Composite Strata from UP1 to LP2 (8 m, 280 couplets) that are ~250 km distant. (A and B) Autocorrelation for GPC and PC indicate a high degree of similarity over short lag intervals (1-3 couplet offset; p-values <0.05). However, cross-correlation is statistically significant at lags of 13 and 20 couplets (p-value <0.05) with a weak correlation coefficient of -0.13 which indicates opposing trend in thickness (i.e. when GP is thick, P is thin).

## Appendix B: Section Descriptions and Tuff Details

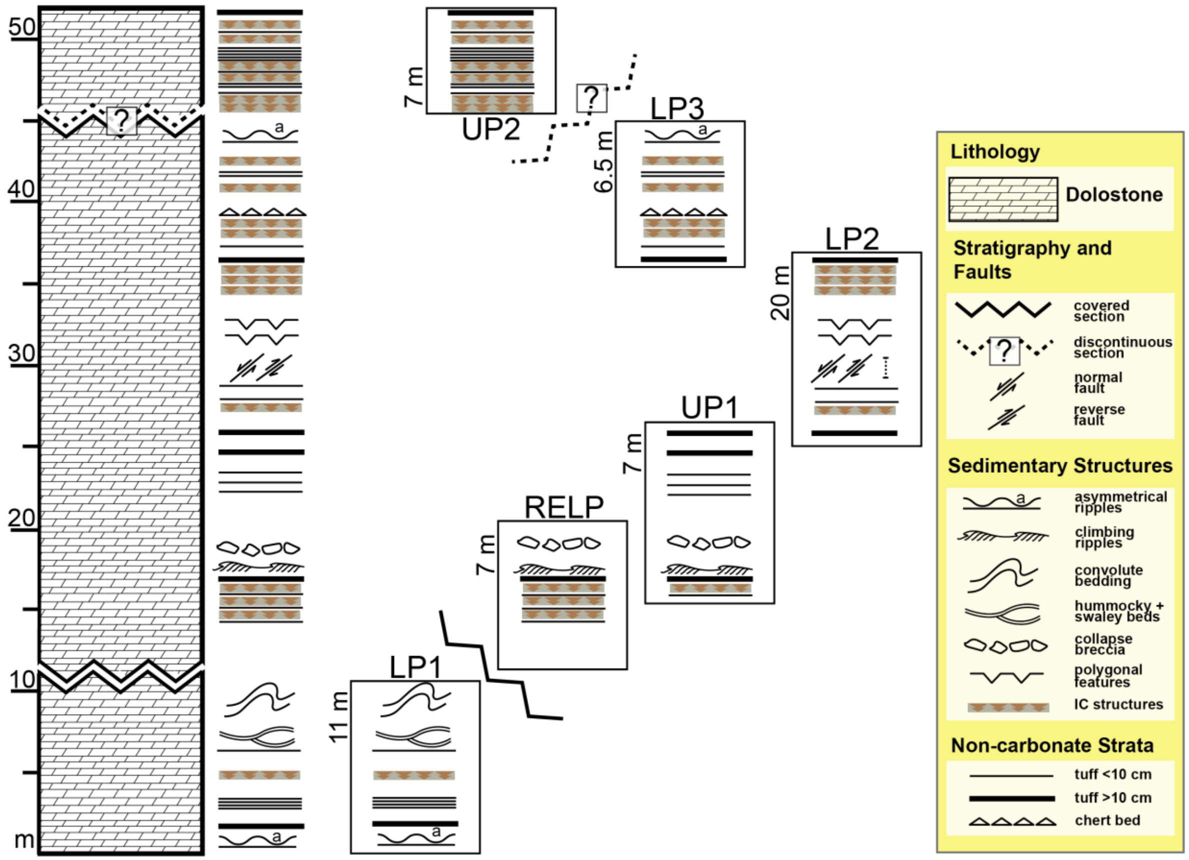


*Composite Prieska Section Stratigraphic Column*

*Lower Prieska 1* (-29.613319, 22.719388)

This section consists of 10.87 m of carbonate strata with thin, interbedded argillaceous limestone and minor coarse-grained carbonate sand intervals. Here, the alternation of the couplets contains lower beds of grey carbonate with a noticeable fining-upward grain size. Most contacts between A-type beds and B-type beds are stratiform, however some are rippled and/or tufted. The upper layers are brown-orange in color with the darker, more resistant laminae standing out in relief and having a dark-brown color. Many B-type beds are weathered and replaced with modern calcrete. This section contains two sedimentological features of note: a convolute bed 15 cm in thickness and hummocky and swaley cross-stratified beds.

*River's Edge Lower Prieska* (-29.614674, 22.720955)

This ~7 m section contains 3 m of finely laminated carbonate and argillaceous carbonate, 1.8 m of measured carbonate and tuffaceous strata, and approximately 2 m of inaccessible strata above. The carbonate strata here are thinly bedded, although fabric destructive features, including three prominent beds of inverted conical structures and a tuffaceous collapse breccia that obfuscate primary facies. Above the inverted conical structure beds there are tuff beds of 7.2 cm, 11.8 cm, and 40 cm, respectively. The oldest tuff shows evidence of rapid quenching with baking zones bounding the strata. The youngest tuff in this section is composed of at least 3 independent events, with the first event featuring accretionary lapilli and the final event featuring 4-5 sets of cross-stratified tuffaceous strata cemented with carbonate and climbing ripples orientation indicating a current direction from the NNE.

*Lower Prieska 2* (-29.614878, 22.721418)

LP2 represents the best continuous section of Upper Nauga Formation in the Prieska Facies, and in total measures 19.94 m of measured strata. The base of this section is composed of carbonate couplets, and strata is interrupted by a 25 cm tuffaceous bed that includes a rippled base with a 3 cm baked contact zone of underlying carbonate strata, a lower layer of lapilli, a minimum of three subsequent ash-fall events, and a 0.5 cm purple layer. Above this tuff, carbonate strata resumes totaling 5.6 m with a 5.2 cm inverted conical structure bed, a 12.5 cm tuff, and a 9.5 cm tuff.

The first tuff deposit in this section (25 cm) reappears as a result of a normal fault exposed at -29.614346, 22.721725. The strata then back folds and the 25 cm tuff becomes the lowest exposed bed. Above the 9.5 cm tuff in this repeated section, weathering of facies alternates between grey and brown at the m-scale with a minor appearance of highly-tufted facies with chert and calcite vugs. A conjugate reverse fault at -29.613650, 22.722918 exposes the 12.5 cm and 9.5 cm tuff again.

Above the 9.5 cm tuff, after the reverse fault, highly-tufted facies appear with regularity and alternate between grey and brown weathering. The tops of couplets are rippled, thin draping laminae, and when the upper planar surface is exposed, polygonal cracks are present. The top of this section has three beds of inverted conical structures and a 15.5 cm multi-horizon tuff.

*Lower Prieska 3* (-29.615382, 22.724091)

This section consists of 6.57 m of strata. The base of this section features a 15.5 cm tuff that appears identical in description to the top of LP2. Above the tuff lies another 7.6 cm tuff, a 12 cm inverted conical structure bed, and a 14 cm inverted conical structure bed. A minor chert bed of 5 cm is followed by highly-tufted A-type beds and rippled B-type beds. There also two (<10 cm) tuffaceous units and thin inverted conical structure beds with thicknesses of 8 cm and 2.5 cm.

*Upper Prieska 1* (-29.611301, 22.725865),

This section consists of 7.03 m of strata. The base of this section features a 9.3 cm tuff, a 14 cm inverted conical structure bed, and a multi-horizon tuff with the ultimate event featuring cross-bedded climbing ripples, followed by a breccia of tuffaceous debris in a brown carbonate matrix. Carbonate beds above have intercalated small (<10 cm) tuff beds, calcrete replacement of B-type beds, a 31 cm tuff, and a 26.3 cm tuff that features a baked zone, lapilli, and multiple stages. Infrequently, beds show tufted laminae with chert filled vugs.

*Upper Prieska 2* (-29.617819, 22.728299)

This section contains 6.94 m. Carbonate rocks here display extreme weathering, and include major incorporations of modern calcrete. Disruptive bedding is present with multiple inverted conical structure beds and multiple small (<10cm) tuffs.

*Volcaniclastic deposits in the Upper Nauga Formation*

The measurement of tuffaceous deposits also reinforces the stratigraphic reconstruction of continuous section from seemingly disjointed outcrops along the drainages to the Orange River, as tuffs were correlated with astoundingly similar internal bedding and external stratigraphic relationships, thicknesses <5% of correlative tuffs, and identical sequences of sedimentary structures within (see Fig. 22, Appendix A). Moreover, the cross-bedded climbing ripples in both the RELP section and the UP1 section provide details on both depositional environment and current direction as these clinoforms are oriented SSW, range from 0.5 to 2 cm in height, and have undulose surfaces in which antecedent tuffs are deposited. The presence of low amplitude cross-stratification and of graded tuff lapilli with baked zones on subjacent strata contradicts previous determination of exclusively deep slope to basinal environments of deposition (Beukes, 1987; Sumner and Beukes 2006). The following charts display measurements and descriptions of major tuff beds identified during field study.

**RELP**

| Location/Descrip. | Components | Measurements (cm) | | | | | | |
|---|---|---|---|---|---|---|---|---|
| **Tuff 1** | | **1** | **2** | **3** | **4** | **5** | **6** | **avg** |
| | Tuff | 7.2 | 7.5 | 7 | 7 | 7 | 7.2 | **7.15** |
| | | | | | | | | |
| **Tuff 2** | | | **1** | **2** | **3** | **4** | **5** | **avg** |
| | Tuff | | 11.1 | 10.9 | 10.4 | 11 | 10.9 | 10.86 |
| | BZ | | 1 | 0.9 | 1 | 1 | 0.8 | 0.94 |
| | Total | | 12.1 | 11.8 | 11.4 | 11 | 11.7 | **11.8** |
| | | | | | | | | |
| **Tuff 3** | | **1** | **2** | **3** | **4** | **5** | **6** | **avg** |
| X-beds present | Tuff | 40.8 | 39.5 | 40 | 40 | 39.9 | 39.4 | **39.93** |

**LP2**

| Location/Descrip. | Components | Measurements (cm) | | | | | | |
|---|---|---|---|---|---|---|---|---|
| **Tuff 1** | | | **1** | **2** | **3** | **4** | **5** | **avg** |
| **Lower** | Tuff | | 22.7 | 22 | 21 | 22 | 21.9 | 21.92 |
| Base of section | Baked Zone | | 3 | 3 | 3.1 | 3 | 3 | 3.02 |
| 29.6149047 S | Purp. Layer | | 2 | 2 | 1.9 | 1.8 | 2 | 1.94 |
| 22.7214703 E | Total | | 27.7 | 27 | 25.9 | 26.8 | 26.9 | **26.88** |
| | | | | | | | | |
| **Normal fault** | | | | | | | | |
| 29.6142778 S | | | | | | | | |
| 22.7219444 E | | | | | | | | |
| | | | | | | | | |
| **Tuff 1** | | | **1** | **2** | **3** | **4** | **5** | **avg** |
| **Middle** | Tuff | | 24 | 23.5 | 24 | 23.2 | 24 | 23.74 |
| | Baked Zone | | 3 | 2.9 | 3 | 3 | 3.1 | 3 |
| | Total | | 27 | 26.4 | 27 | 26.2 | 27.1 | **26.74** |
| **Reverse fault** | | | | | | | | |
| 29.6137324 S | | | | | | | | |
| 22.7230807 E | | | | | | | | |
| | | | **1** | **2** | **3** | **4** | **5** | **avg** |
| **Tuff 1** | Tuff | | 25.5 | 24 | 22 | 23.8 | 23.5 | 23.76 |
| **Upper** | Baked Zone | | 3.2 | 2.9 | 3 | 3.2 | 3.1 | 3.08 |
| | Total | | 28.7 | 26.9 | 25 | 27 | 26.6 | **26.84** |

**LP3**

| Location/Descrip. | Components | Measurements (cm) | | | | | | |
|---|---|---|---|---|---|---|---|---|
| **Tuff 1** | | | **1** | **2** | **3** | **4** | **5** | **avg** |
| | Baking Zone | | 1 | 1 | 1 | 1 | 1 | 1 |
| | Tuff | | 11.2 | 11.2 | 11.6 | 11.5 | 11.3 | 11.36 |
| | Upper grey | | 3 | 3 | 3 | 3 | 4 | 3.2 |
| | Total | | 15.2 | 15.2 | 15.6 | 15.5 | 16.3 | **15.56** |
| | | | | | | | | |
| **Small tuff 1** | | **1** | **2** | **3** | **4** | **5** | **6** | **avg** |
| | Tuff | 7.5 | 7.5 | 7.5 | 7.6 | 7.7 | 7.8 | **7.6** |
| | | | | | | | | |
| **Small tuff 2** | | **1** | **2** | **3** | **4** | **5** | **6** | **avg** |
| | Tuff | 5.7 | 5 | 5.6 | 5.5 | 5.2 | 5.3 | **5.38** |
| | | | | | | | | |
| **Small tuff 3** | | **1** | **2** | **3** | **4** | **5** | **6** | **avg** |
| | Tuff | 1.5 | 1.7 | 1.6 | 1.7 | 1.7 | 1.7 | **1.65** |

**UP1**

| Location/Descrip. | Components | Measurements (cm) | | | | | | |
|---|---|---|---|---|---|---|---|---|
| **Big tuff 1** | | **1** | **2** | **3** | **4** | **5** | **6** | **avg** |
| 29deg 36' 40.52" S | Tuff | 68.9 | 68.9 | 71 | 72 | 68 | 71 | **69.97** |
| 22deg 43' 33.20" E | | | | | | | | |
| | | | | | | | | |
| **Small tuff** | | **1** | **2** | **3** | **4** | **5** | | **avg** |
| | Tuff | 8.2 | 9.8 | 9.5 | 9.3 | 9.5 | | **9.26** |
| | | | | | | | | |
| **Big tuff w/ x-beds** | | **1** | **2** | **3** | **4** | **5** | | **avg** |
| (repeat of RELP Tuff 3) | Tuff | 32 | 32.5 | 32.3 | 33 | 32.5 | | **32.46** |
| | | | | | | | | |
| **Small tuff 2** | | **1** | **2** | **3** | **4** | **5** | **6** | **avg** |
| | Tuff | 1.7 | 1.2 | 1.2 | 1.5 | 1.7 | 1.5 | **1.47** |
| | | | | | | | | |
| **Small tuff 3** | | **1** | **2** | **3** | **4** | **5** | **6** | **avg** |
| | Tuff | 7.1 | 7.6 | 7.5 | 7.3 | 7.3 | 7.5 | **7.38** |
| | | | | | | | | |
| **small tuff 4** | | **1** | **2** | **3** | **4** | **5** | **6** | **avg** |
| | Tuff | 4.1 | 4.2 | 4.1 | 4 | 4 | 3.7 | **4.02** |
| | | | | | | | | |
| **Big tuff 3** | | **1** | **2** | **3** | **4** | **5** | | **avg** |
| | Tuff | 31.5 | 31 | 31.5 | 32 | 31.5 | | **31.5** |
| | | | | | | | | |
| **Big tuff 4** | | **1** | **2** | **3** | **4** | **5** | | **avg** |
| (repeat of LP2 Tuff 1) | Baked Zone | 3 | 3 | 3.1 | 3 | 3 | | 3.02 |
| | Tuff | 21.5 | 21.8 | 23 | 22.9 | 22 | | 22.24 |
| | Purp Layer | 1.1 | 1.3 | 1 | 1 | 0.7 | | 1.02 |
| | Total | 25.6 | 26.1 | 27.1 | 26.9 | 25.7 | | **26.28** |

**UP2**

| Location/Descrip. | Components | Measurements (cm) | | | | | | |
|---|---|---|---|---|---|---|---|---|
| **Small tuff 1** | | **1** | **2** | **3** | **4** | **5** | | **avg** |
| | Tuff | 4.7 | 4.6 | 4 | 4.1 | 4.5 | | **4.38** |
| | | | | | | | | |
| **Small tuff 2** | | **1** | **2** | **3** | **4** | **5** | | **avg** |
| | Tuff | 3 | 3.1 | 3.5 | 3.1 | 2.9 | | **3.12** |
| | | | | | | | | |
| **Big tuff 1** | | **1** | **2** | **3** | **4** | **5** | **6** | **avg** |
| | Baked Zone | 0.7 | 1 | 1 | 0.8 | 1 | 1 | 0.92 |
| | Tuff | 9.8 | 10 | 10.5 | 10 | 9.9 | 9.8 | 10 |
| | Grey top tuff | 3.8 | 3.1 | 3 | 3.5 | 2.2 | 2.7 | 3.05 |
| | Total | 14.3 | 14.1 | 14.5 | 14.3 | 13.1 | 13.5 | **13.97** |
| | | | | | | | | |
| **Small tuff 3** | | **1** | **2** | **3** | **4** | **5** | **6** | **avg** |
| | Tuff | 7.6 | 7.5 | 7.2 | 7.6 | 7 | 7 | **7.32** |
| | | | | | | | | |
| **Small tuff 4** | | **1** | **2** | **3** | **4** | **5** | **6** | **avg** |
| | Tuff | 11 | 10 | 11 | 11 | 11.2 | 10.2 | **10.73** |
| | | | | | | | | |
| **Big tuff 1 (?)** | | **1** | **2** | **3** | **4** | **5** | | **avg** |
| | Baked Zone | 1 | 1.2 | 1.2 | 1 | 1.2 | | 1.12 |
| | Tuff | 11.5 | 11 | 10 | 10 | 11 | | 10.7 |
| | Grey top tuff | 3.5 | 2 | 2.5 | 2.5 | 3.5 | | 2.8 |
| | Total | 16 | 14.2 | 13.7 | 13.5 | 15.7 | | **14.62** |
| | | | | | | | | |
| **Small tuff 3** (?) | | **1** | **2** | **3** | **4** | **5** | **6** | **avg** |
| | Tuff | 7.5 | 7.6 | 7.2 | 7.5 | 7.6 | 7.5 | **7.48** |
| | | | | | | | | |
| **Small tuff 5** | | **1** | **2** | **3** | **4** | **5** | **6** | **avg** |
| | Tuff | 5.2 | 5 | 5.2 | 5 | 5.4 | 5.3 | **5.18** |

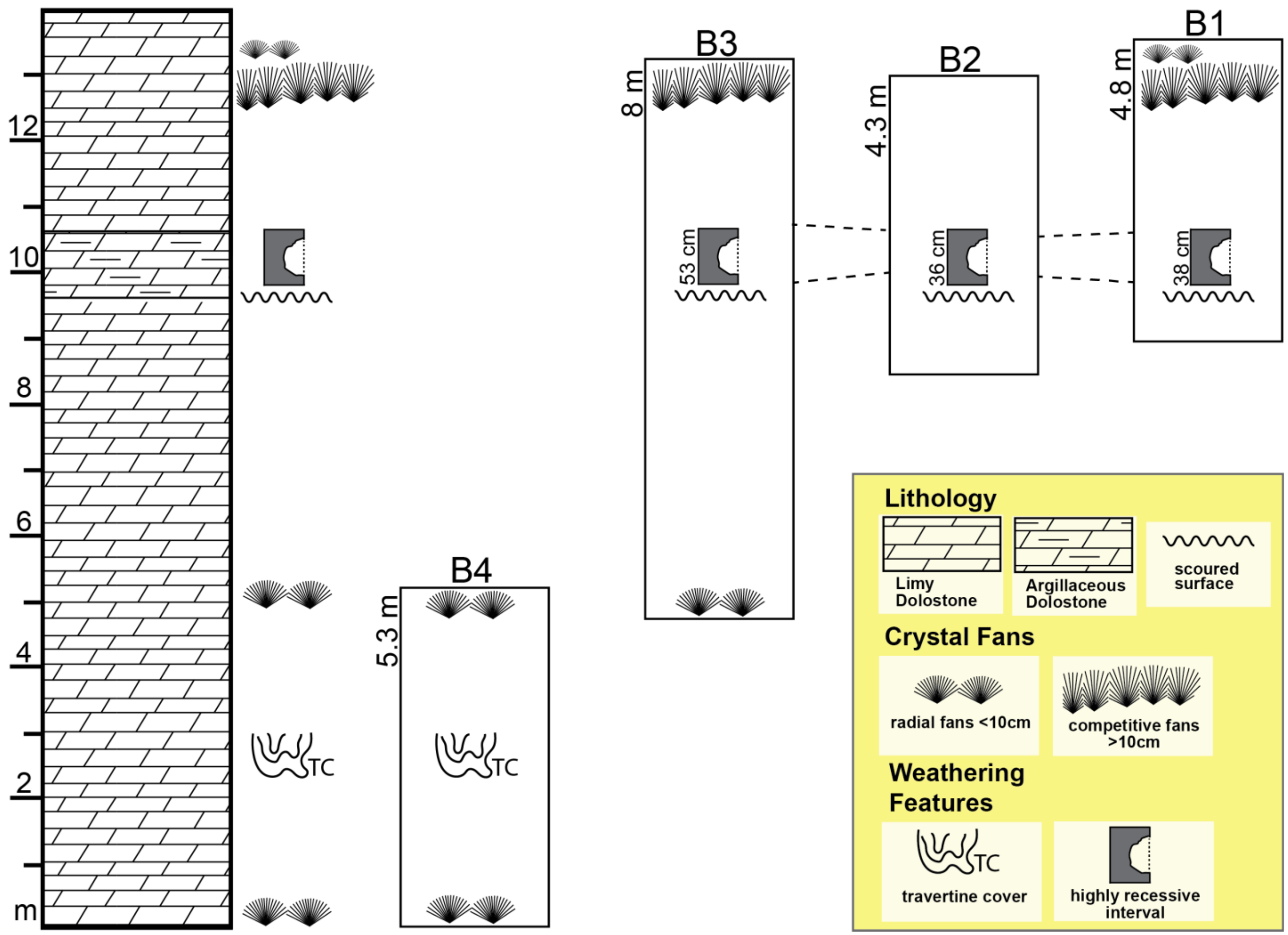


*Composite Ghaap Plateau Section Stratigraphic Column*

## Appendix C: Geochemical Data

| Sample | Type A/B | Color | $\delta^{13}C$ | $\delta^{18}O$ | Ca | Mg | Fe | Mn | Sr | Mg/Ca |
|---|---|---|---|---|---|---|---|---|---|---|
| | | | ‰ | | [ppm] | | | | | [ratio] |
| **J1** | A | Grey | -1.271 | -9.646 | 276307 | 56857 | 42742 | 6941 | 0 | 0.2058 |
| **J2** | A | Grey | -0.973 | -9.550 | 278096 | 63589 | 31473 | 7732 | 0 | 0.2287 |
| **J3** | B | Grey | -4.320 | -4.343 | 289579 | 22015 | 71705 | 10638 | 0 | 0.0760 |
| **J4** | A | Grey | -1.461 | -11.203 | 350925 | 11769 | 29872 | 5002 | 0 | 0.0335 |
| **J5** | A | Grey | -1.318 | -9.771 | 298714 | 48583 | 32166 | 7070 | 0 | 0.1626 |
| **J6** | B | Grey | -1.328 | -7.415 | 216519 | 82708 | 57152 | 11405 | 0 | 0.3820 |
| **J7** | A | Grey | -0.983 | -8.649 | 213114 | 93093 | 44112 | 12779 | 0 | 0.4368 |
| **J8** | B | Grey | -1.145 | -8.170 | 212701 | 83283 | 57761 | 13223 | 0 | 0.3915 |
| **J9** | A | Grey | -1.603 | -10.921 | 362400 | 7538 | 24259 | 4461 | 0 | 0.0208 |
| **J10** | A | Grey | -1.988 | -9.577 | 306353 | 39541 | 37514 | 5995 | 0 | 0.1291 |
| **J11** | B | Grey | -1.476 | -7.228 | 238330 | 74059 | 48492 | 12994 | 0 | 0.3107 |
| **J12** | A | Grey | -0.824 | -8.540 | 201045 | 92196 | 55828 | 12169 | 0 | 0.4586 |
| **J13** | B | Grey | -3.548 | -6.552 | 250368 | 79161 | 38530 | 5351 | 0 | 0.3162 |
| **J14** | B | Brown | -1.242 | -7.188 | 253503 | 60890 | 54249 | 11262 | 0 | 0.2402 |
| **J14b** | A | Brown | -1.059 | -8.836 | 229212 | 88720 | 40347 | 9071 | 0 | 0.3871 |
| **J15** | B | Brown | -1.411 | -7.374 | 253753 | 65283 | 48641 | 10768 | 0 | 0.2573 |
| **J16** | A | Brown | -1.732 | -8.575 | 254842 | 79994 | 30499 | 8269 | 0 | 0.3139 |
| **J17** | B | Brown | -1.417 | -7.497 | 240227 | 73744 | 48528 | 11697 | 0 | 0.3070 |
| **J18** | A | Brown | -2.207 | -6.839 | 198856 | 59852 | 109799 | 6201 | 0 | 0.3010 |
| **J19** | A | Brown | -1.285 | -9.254 | 253067 | 76427 | 37843 | 7284 | 0 | 0.3020 |
| **J20** | B | Brown | -0.898 | -7.787 | 238670 | 72248 | 51464 | 12180 | 0 | 0.3027 |
| **J21** | A | Brown | -0.790 | -8.730 | 225858 | 96025 | 33188 | 9024 | 0 | 0.4252 |
| **J22** | B | Brown | -0.933 | -7.290 | 243535 | 69939 | 49261 | 13154 | 0 | 0.2872 |
| **J23** | A | Brown | -0.993 | -9.299 | 247732 | 84513 | 30616 | 8414 | 0 | 0.3411 |
| **J24** | B | Brown | -0.745 | -6.328 | 266299 | 63403 | 37618 | 12765 | 0 | 0.2381 |
| **J25** | A | Brown | -1.407 | -9.608 | 266599 | 76649 | 26019 | 6594 | 0 | 0.2875 |

Appendix D: Statistical Data

AC Data GP1 v GP2

| Obs | _NAME_ | LAG | N | ACF | ACFSTD | ACFPROB |
|---|---|---|---|---|---|---|
| 1 | thickI | 0 | 90 | 1 | 0 | . |
| 2 | thickI | 1 | 89 | 0.39654 | 0.10541 | 0.00017 |
| 3 | thickI | 2 | 88 | 0.24473 | 0.12085 | 0.04286 |
| 4 | thickI | 3 | 87 | 0.22477 | 0.12624 | 0.075 |
| 5 | thickI | 4 | 86 | 0.07192 | 0.13061 | 0.58186 |
| 6 | thickI | 5 | 85 | 0.08075 | 0.13105 | 0.53779 |
| 7 | thickI | 6 | 84 | 0.10433 | 0.1316 | 0.42789 |
| 8 | thickI | 7 | 83 | -0.06104 | 0.13252 | 0.64509 |
| 9 | thickI | 8 | 82 | -0.03785 | 0.13283 | 0.77569 |
| 10 | thickI | 9 | 81 | -0.12468 | 0.13295 | 0.34834 |
| 11 | thickI | 10 | 80 | -0.14115 | 0.13424 | 0.29306 |
| 12 | thickI | 11 | 79 | -0.06051 | 0.13588 | 0.6561 |
| 13 | thickI | 12 | 78 | -0.15059 | 0.13618 | 0.2688 |
| 14 | thickI | 13 | 77 | -0.15339 | 0.13802 | 0.26639 |
| 15 | thickI | 14 | 76 | -0.18305 | 0.1399 | 0.19071 |
| 16 | thickI | 15 | 75 | -0.13513 | 0.14254 | 0.34309 |
| 17 | thickI | 16 | 74 | -0.10125 | 0.14395 | 0.48181 |
| 18 | thickI | 17 | 73 | -0.03222 | 0.14474 | 0.82382 |
| 19 | thickI | 18 | 72 | -0.13154 | 0.14482 | 0.36373 |
| 20 | thickI | 19 | 71 | -0.08775 | 0.14614 | 0.54823 |
| 21 | thickI | 20 | 70 | -0.04484 | 0.14673 | 0.75991 |
| 22 | thickI | 21 | 69 | -0.07111 | 0.14688 | 0.62829 |
| 23 | thickI | 22 | 68 | -0.12145 | 0.14726 | 0.40954 |
| 24 | thickI | 23 | 67 | -0.18765 | 0.14837 | 0.20597 |
| 25 | thickI | 24 | 66 | -0.15753 | 0.15098 | 0.2968 |
| 26 | thickII | 0 | 90 | 1 | 0 | . |
| 27 | thickII | 1 | 89 | 0.40899 | 0.10541 | 0.0001 |
| 28 | thickII | 2 | 88 | 0.30125 | 0.12177 | 0.01336 |
| 29 | thickII | 3 | 87 | 0.20004 | 0.12979 | 0.12324 |
| 30 | thickII | 4 | 86 | 0.21885 | 0.13317 | 0.1003 |
| 31 | thickII | 5 | 85 | 0.13762 | 0.13711 | 0.31552 |
| 32 | thickII | 6 | 84 | 0.05452 | 0.13863 | 0.69413 |
| 33 | thickII | 7 | 83 | -0.02232 | 0.13887 | 0.87229 |
| 34 | thickII | 8 | 82 | -0.07707 | 0.13891 | 0.57904 |
| 35 | thickII | 9 | 81 | -0.07349 | 0.13939 | 0.59803 |
| 36 | thickII | 10 | 80 | -0.07028 | 0.13982 | 0.6152 |
| 37 | thickII | 11 | 79 | -0.00492 | 0.14021 | 0.97202 |

| | | | | | | |
|---|---|---|---|---|---|---|
| 38 | thickII | 12 | 78 | -0.00466 | 0.14021 | 0.97346 |
| 39 | thickII | 13 | 77 | 0.03639 | 0.14021 | 0.79523 |
| 40 | thickII | 14 | 76 | -0.00913 | 0.14032 | 0.94813 |
| 41 | thickII | 15 | 75 | 0.03122 | 0.14032 | 0.82394 |
| 42 | thickII | 16 | 74 | 0.06071 | 0.1404 | 0.66543 |
| 43 | thickII | 17 | 73 | -0.00994 | 0.14069 | 0.94365 |
| 44 | thickII | 18 | 72 | 0.05081 | 0.1407 | 0.71799 |
| 45 | thickII | 19 | 71 | 0.05676 | 0.1409 | 0.6871 |
| 46 | thickII | 20 | 70 | -0.03476 | 0.14116 | 0.80549 |
| 47 | thickII | 21 | 69 | -0.02098 | 0.14125 | 0.8819 |
| 48 | thickII | 22 | 68 | -0.07586 | 0.14129 | 0.59133 |
| 49 | thickII | 23 | 67 | -0.14029 | 0.14174 | 0.32229 |
| 50 | thickII | 24 | 66 | -0.09313 | 0.14327 | 0.5157 |

CC Data GP1 v GP2

| Obs | _NAME_ | _CROSS_ | LAG | N | CCF | CCFSTD | CCFPROB |
|---|---|---|---|---|---|---|---|
| 1 | thickII | thickI | -24 | 66 | -0.12474 | 0.10541 | 0.23664 |
| 2 | thickII | thickI | -23 | 67 | -0.16162 | 0.10541 | 0.12522 |
| 3 | thickII | thickI | -22 | 68 | -0.11121 | 0.10541 | 0.29142 |
| 4 | thickII | thickI | -21 | 69 | -0.14326 | 0.10541 | 0.17411 |
| 5 | thickII | thickI | -20 | 70 | -0.14293 | 0.10541 | 0.17512 |
| 6 | thickII | thickI | -19 | 71 | -0.1883 | 0.10541 | 0.07404 |
| 7 | thickII | thickI | -18 | 72 | -0.16637 | 0.10541 | 0.1145 |
| 8 | thickII | thickI | -17 | 73 | -0.16679 | 0.10541 | 0.11358 |
| 9 | thickII | thickI | -16 | 74 | -0.10642 | 0.10541 | 0.31268 |
| 10 | thickII | thickI | -15 | 75 | -0.01656 | 0.10541 | 0.87517 |
| 11 | thickII | thickI | -14 | 76 | 0.11069 | 0.10541 | 0.29368 |
| 12 | thickII | thickI | -13 | 77 | 0.01505 | 0.10541 | 0.88643 |
| 13 | thickII | thickI | -12 | 78 | -0.05056 | 0.10541 | 0.63146 |
| 14 | thickII | thickI | -11 | 79 | 0.19086 | 0.10541 | 0.0702 |
| 15 | thickII | thickI | -10 | 80 | 0.18723 | 0.10541 | 0.0757 |
| 16 | thickII | thickI | -9 | 81 | 0.1541 | 0.10541 | 0.14375 |
| 17 | thickII | thickI | -8 | 82 | 0.31415 | 0.10541 | 0.00288 |
| 18 | thickII | thickI | -7 | 83 | 0.39386 | 0.10541 | 0.00019 |
| 19 | thickII | thickI | -6 | 84 | 0.27572 | 0.10541 | 0.0089 |
| 20 | thickII | thickI | -5 | 85 | 0.26675 | 0.10541 | 0.01139 |
| 21 | thickII | thickI | -4 | 86 | 0.12583 | 0.10541 | 0.23257 |
| 22 | thickII | thickI | -3 | 87 | 0.08702 | 0.10541 | 0.40908 |
| 23 | thickII | thickI | -2 | 88 | 0.08768 | 0.10541 | 0.40552 |
| 24 | thickII | thickI | -1 | 89 | -0.03893 | 0.10541 | 0.71187 |
| 25 | thickII | thickI | 0 | 90 | -0.06516 | 0.10541 | 0.53644 |
| 26 | thickII | thickI | 1 | 89 | -0.06992 | 0.10541 | 0.50713 |
| 27 | thickII | thickI | 2 | 88 | -0.11941 | 0.10541 | 0.25729 |
| 28 | thickII | thickI | 3 | 87 | -0.13479 | 0.10541 | 0.20098 |
| 29 | thickII | thickI | 4 | 86 | -0.00299 | 0.10541 | 0.97738 |
| 30 | thickII | thickI | 5 | 85 | -0.00487 | 0.10541 | 0.96312 |
| 31 | thickII | thickI | 6 | 84 | 0.11049 | 0.10541 | 0.29453 |
| 32 | thickII | thickI | 7 | 83 | 0.03893 | 0.10541 | 0.7119 |
| 33 | thickII | thickI | 8 | 82 | 0.04745 | 0.10541 | 0.65259 |
| 34 | thickII | thickI | 9 | 81 | 0.07097 | 0.10541 | 0.50075 |
| 35 | thickII | thickI | 10 | 80 | 0.05181 | 0.10541 | 0.62306 |
| 36 | thickII | thickI | 11 | 79 | 0.12545 | 0.10541 | 0.234 |
| 37 | thickII | thickI | 12 | 78 | 0.03456 | 0.10541 | 0.74305 |

| | | | | | | | |
|---|---|---|---|---|---|---|---|
| 38 | thickII | thickI | 13 | 77 | 0.06759 | 0.10541 | 0.5214 |
| 39 | thickII | thickI | 14 | 76 | 0.05392 | 0.10541 | 0.60899 |
| 40 | thickII | thickI | 15 | 75 | 0.00582 | 0.10541 | 0.956 |
| 41 | thickII | thickI | 16 | 74 | 0.01457 | 0.10541 | 0.89008 |
| 42 | thickII | thickI | 17 | 73 | 0.03588 | 0.10541 | 0.73355 |
| 43 | thickII | thickI | 18 | 72 | -0.06527 | 0.10541 | 0.53576 |
| 44 | thickII | thickI | 19 | 71 | 0.00911 | 0.10541 | 0.93112 |
| 45 | thickII | thickI | 20 | 70 | -0.04839 | 0.10541 | 0.64617 |
| 46 | thickII | thickI | 21 | 69 | 0.03143 | 0.10541 | 0.76555 |
| 47 | thickII | thickI | 22 | 68 | 0.00445 | 0.10541 | 0.96636 |
| 48 | thickII | thickI | 23 | 67 | -0.02 | 0.10541 | 0.8495 |
| 49 | thickII | thickI | 24 | 66 | -0.08191 | 0.10541 | 0.4371 |

AC Data GP2 v GP3

| Obs | _NAME_ | LAG | N | ACF | ACFSTD | ACFPROB |
|---|---|---|---|---|---|---|
| 1 | thickI | 0 | 140 | 1 | 0 | . |
| 2 | thickI | 1 | 139 | 0.31143 | 0.08452 | 0.00023 |
| 3 | thickI | 2 | 138 | 0.21886 | 0.09235 | 0.01779 |
| 4 | thickI | 3 | 137 | 0.21019 | 0.09598 | 0.02853 |
| 5 | thickI | 4 | 136 | 0.19536 | 0.09922 | 0.04895 |
| 6 | thickI | 5 | 135 | 0.04057 | 0.10193 | 0.69062 |
| 7 | thickI | 6 | 134 | 0.12096 | 0.10204 | 0.23585 |
| 8 | thickI | 7 | 133 | 0.04567 | 0.10306 | 0.65764 |
| 9 | thickI | 8 | 132 | -0.098 | 0.10321 | 0.34231 |
| 10 | thickI | 9 | 131 | -0.02399 | 0.10387 | 0.81731 |
| 11 | thickI | 10 | 130 | -0.03755 | 0.10391 | 0.71783 |
| 12 | thickI | 11 | 129 | -0.02604 | 0.104 | 0.80228 |
| 13 | thickI | 12 | 128 | -0.00005 | 0.10405 | 0.99961 |
| 14 | thickI | 13 | 127 | 0.06624 | 0.10405 | 0.52437 |
| 15 | thickI | 14 | 126 | -0.05028 | 0.10435 | 0.62995 |
| 16 | thickI | 15 | 125 | 0.02716 | 0.10452 | 0.79498 |
| 17 | thickI | 16 | 124 | 0.03769 | 0.10458 | 0.71856 |
| 18 | thickI | 17 | 123 | 0.01286 | 0.10467 | 0.90222 |
| 19 | thickI | 18 | 122 | -0.03342 | 0.10468 | 0.7495 |
| 20 | thickI | 19 | 121 | 0.07341 | 0.10476 | 0.48349 |
| 21 | thickI | 20 | 120 | -0.09693 | 0.10513 | 0.35653 |
| 22 | thickI | 21 | 119 | -0.02354 | 0.10576 | 0.82388 |
| 23 | thickI | 22 | 118 | -0.04674 | 0.1058 | 0.65863 |
| 24 | thickI | 23 | 117 | -0.04827 | 0.10595 | 0.64869 |
| 25 | thickI | 24 | 116 | -0.1186 | 0.1061 | 0.26366 |
| 26 | thickII | 0 | 140 | 1 | 0 | . |
| 27 | thickII | 1 | 139 | 0.25789 | 0.08452 | 0.00228 |
| 28 | thickII | 2 | 138 | -0.01282 | 0.08996 | 0.88664 |
| 29 | thickII | 3 | 137 | 0.22006 | 0.08997 | 0.01445 |
| 30 | thickII | 4 | 136 | 0.19322 | 0.09374 | 0.03928 |
| 31 | thickII | 5 | 135 | 0.10708 | 0.09654 | 0.26737 |
| 32 | thickII | 6 | 134 | 0.25716 | 0.09739 | 0.00828 |
| 33 | thickII | 7 | 133 | 0.21056 | 0.10212 | 0.03922 |
| 34 | thickII | 8 | 132 | 0.14098 | 0.10518 | 0.18011 |
| 35 | thickII | 9 | 131 | 0.16716 | 0.10652 | 0.11659 |
| 36 | thickII | 10 | 130 | 0.12903 | 0.10838 | 0.23383 |
| 37 | thickII | 11 | 129 | 0.10045 | 0.10947 | 0.35881 |

| | | | | | | |
|---|---|---|---|---|---|---|
| 38 | thickII | 12 | 128 | 0.04024 | 0.11012 | 0.71482 |
| 39 | thickII | 13 | 127 | 0.16313 | 0.11023 | 0.1389 |
| 40 | thickII | 14 | 126 | 0.23245 | 0.11194 | 0.03784 |
| 41 | thickII | 15 | 125 | 0.13398 | 0.11534 | 0.24538 |
| 42 | thickII | 16 | 124 | -0.03786 | 0.11644 | 0.74505 |
| 43 | thickII | 17 | 123 | 0.09615 | 0.11653 | 0.4093 |
| 44 | thickII | 18 | 122 | 0.07994 | 0.1171 | 0.49483 |
| 45 | thickII | 19 | 121 | -0.12302 | 0.11749 | 0.29506 |
| 46 | thickII | 20 | 120 | 0.06827 | 0.1184 | 0.56424 |
| 47 | thickII | 21 | 119 | 0.22861 | 0.11868 | 0.05408 |
| 48 | thickII | 22 | 118 | 0.08223 | 0.12179 | 0.49958 |
| 49 | thickII | 23 | 117 | 0.04508 | 0.12218 | 0.71218 |
| 50 | thickII | 24 | 116 | 0.16172 | 0.1223 | 0.18606 |

CC Data GP2 v GP3

| Obs | _NAME_ | _CROSS_ | LAG | N | CCF | CCFSTD | CCFPROB |
|---|---|---|---|---|---|---|---|
| 1 | thickII | thickI | -24 | 116 | 0.05057 | 0.084515 | 0.54962 |
| 2 | thickII | thickI | -23 | 117 | 0.09223 | 0.084515 | 0.27515 |
| 3 | thickII | thickI | -22 | 118 | 0.04709 | 0.084515 | 0.57744 |
| 4 | thickII | thickI | -21 | 119 | 0.01349 | 0.084515 | 0.87321 |
| 5 | thickII | thickI | -20 | 120 | 0.06857 | 0.084515 | 0.41715 |
| 6 | thickII | thickI | -19 | 121 | -0.06548 | 0.084515 | 0.4385 |
| 7 | thickII | thickI | -18 | 122 | 0.04091 | 0.084515 | 0.62834 |
| 8 | thickII | thickI | -17 | 123 | 0.05979 | 0.084515 | 0.47932 |
| 9 | thickII | thickI | -16 | 124 | 0.07312 | 0.084515 | 0.38694 |
| 10 | thickII | thickI | -15 | 125 | 0.06513 | 0.084515 | 0.44096 |
| 11 | thickII | thickI | -14 | 126 | 0.12453 | 0.084515 | 0.14064 |
| 12 | thickII | thickI | -13 | 127 | -0.0108 | 0.084515 | 0.89827 |
| 13 | thickII | thickI | -12 | 128 | 0.0261 | 0.084515 | 0.75745 |
| 14 | thickII | thickI | -11 | 129 | 0.05762 | 0.084515 | 0.49539 |
| 15 | thickII | thickI | -10 | 130 | -0.00563 | 0.084515 | 0.94686 |
| 16 | thickII | thickI | -9 | 131 | -0.05223 | 0.084515 | 0.53658 |
| 17 | thickII | thickI | -8 | 132 | 0.0862 | 0.084515 | 0.30775 |
| 18 | thickII | thickI | -7 | 133 | 0.05156 | 0.084515 | 0.54178 |
| 19 | thickII | thickI | -6 | 134 | -0.02494 | 0.084515 | 0.76796 |
| 20 | thickII | thickI | -5 | 135 | -0.00575 | 0.084515 | 0.94572 |
| 21 | thickII | thickI | -4 | 136 | -0.06414 | 0.084515 | 0.44794 |
| 22 | thickII | thickI | -3 | 137 | 0.09392 | 0.084515 | 0.26644 |
| 23 | thickII | thickI | -2 | 138 | 0.08794 | 0.084515 | 0.2981 |
| 24 | thickII | thickI | -1 | 139 | 0.09761 | 0.084515 | 0.2481 |
| 25 | thickII | thickI | 0 | 140 | 0.06258 | 0.084515 | 0.45902 |
| 26 | thickII | thickI | 1 | 139 | 0.27762 | 0.084515 | 0.00102 |
| 27 | thickII | thickI | 2 | 138 | 0.06218 | 0.084515 | 0.46187 |
| 28 | thickII | thickI | 3 | 137 | -0.03624 | 0.084515 | 0.6681 |
| 29 | thickII | thickI | 4 | 136 | 0.07033 | 0.084515 | 0.40532 |
| 30 | thickII | thickI | 5 | 135 | 0.08421 | 0.084515 | 0.31905 |
| 31 | thickII | thickI | 6 | 134 | 0.07539 | 0.084515 | 0.37235 |
| 32 | thickII | thickI | 7 | 133 | 0.1943 | 0.084515 | 0.02151 |
| 33 | thickII | thickI | 8 | 132 | 0.11088 | 0.084515 | 0.18954 |
| 34 | thickII | thickI | 9 | 131 | 0.04041 | 0.084515 | 0.63256 |
| 35 | thickII | thickI | 10 | 130 | 0.14849 | 0.084515 | 0.07893 |
| 36 | thickII | thickI | 11 | 129 | 0.0977 | 0.084515 | 0.24767 |
| 37 | thickII | thickI | 12 | 128 | 0.06659 | 0.084515 | 0.43078 |

| | | | | | | | |
|---|---|---|---|---|---|---|---|
| 38 | thickII | thickI | 13 | 127 | 0.08345 | 0.084515 | 0.32345 |
| 39 | thickII | thickI | 14 | 126 | 0.07925 | 0.084515 | 0.34839 |
| 40 | thickII | thickI | 15 | 125 | 0.06495 | 0.084515 | 0.44221 |
| 41 | thickII | thickI | 16 | 124 | 0.07529 | 0.084515 | 0.37301 |
| 42 | thickII | thickI | 17 | 123 | -0.00009 | 0.084515 | 0.99919 |
| 43 | thickII | thickI | 18 | 122 | 0.07039 | 0.084515 | 0.40491 |
| 44 | thickII | thickI | 19 | 121 | 0.07316 | 0.084515 | 0.38666 |
| 45 | thickII | thickI | 20 | 120 | 0.00468 | 0.084515 | 0.95584 |
| 46 | thickII | thickI | 21 | 119 | -0.05186 | 0.084515 | 0.53947 |
| 47 | thickII | thickI | 22 | 118 | 0.0327 | 0.084515 | 0.69884 |
| 48 | thickII | thickI | 23 | 117 | -0.02183 | 0.084515 | 0.79617 |
| 49 | thickII | thickI | 24 | 116 | -0.00931 | 0.084515 | 0.9123 |

AC Data PR1 v PR2

| Obs | _NAME_ | LAG | N | ACF | ACFSTD | ACFPROB |
|---|---|---|---|---|---|---|
| 1 | thickI | 0 | 39 | 1 | 0 | . |
| 2 | thickI | 1 | 38 | 0.23609 | 0.16013 | 0.14037 |
| 3 | thickI | 2 | 37 | -0.04879 | 0.16882 | 0.77257 |
| 4 | thickI | 3 | 36 | 0.22461 | 0.16918 | 0.18429 |
| 5 | thickI | 4 | 35 | 0.23167 | 0.17666 | 0.18972 |
| 6 | thickI | 5 | 34 | 0.06102 | 0.18429 | 0.74057 |
| 7 | thickI | 6 | 33 | -0.26964 | 0.1848 | 0.14455 |
| 8 | thickI | 7 | 32 | -0.02747 | 0.19463 | 0.88775 |
| 9 | thickI | 8 | 31 | 0.04951 | 0.19473 | 0.79929 |
| 10 | thickI | 9 | 30 | -0.27985 | 0.19505 | 0.15136 |
| 11 | thickI | 10 | 29 | -0.2378 | 0.20509 | 0.24625 |
| 12 | thickI | 11 | 28 | -0.1335 | 0.21204 | 0.52895 |
| 13 | thickI | 12 | 27 | -0.03873 | 0.21418 | 0.85651 |
| 14 | thickI | 13 | 26 | -0.03534 | 0.21436 | 0.86904 |
| 15 | thickI | 14 | 25 | -0.02065 | 0.21451 | 0.92331 |
| 16 | thickI | 15 | 24 | 0.11713 | 0.21456 | 0.58514 |
| 17 | thickI | 16 | 23 | 0.01013 | 0.2162 | 0.96264 |
| 18 | thickI | 17 | 22 | 0.00564 | 0.21621 | 0.97918 |
| 19 | thickI | 18 | 21 | 0.17289 | 0.21621 | 0.42394 |
| 20 | thickI | 19 | 20 | 0.07439 | 0.21973 | 0.73496 |
| 21 | thickI | 20 | 19 | 0.13836 | 0.22037 | 0.53012 |
| 22 | thickI | 21 | 18 | 0.06103 | 0.22259 | 0.78394 |
| 23 | thickI | 22 | 17 | -0.04996 | 0.22302 | 0.82275 |
| 24 | thickI | 23 | 16 | 0.04201 | 0.22331 | 0.85078 |
| 25 | thickI | 24 | 15 | -0.04893 | 0.22351 | 0.8267 |
| 26 | thickII | 0 | 39 | 1 | 0 | . |
| 27 | thickII | 1 | 38 | 0.16907 | 0.16013 | 0.29104 |
| 28 | thickII | 2 | 37 | 0.26781 | 0.16464 | 0.10382 |
| 29 | thickII | 3 | 36 | 0.12806 | 0.17546 | 0.46547 |
| 30 | thickII | 4 | 35 | 0.02439 | 0.17784 | 0.89092 |
| 31 | thickII | 5 | 34 | 0.17415 | 0.17792 | 0.32769 |
| 32 | thickII | 6 | 33 | -0.13908 | 0.18224 | 0.44535 |
| 33 | thickII | 7 | 32 | -0.13851 | 0.18494 | 0.45391 |
| 34 | thickII | 8 | 31 | -0.13964 | 0.18758 | 0.45664 |
| 35 | thickII | 9 | 30 | -0.28016 | 0.19023 | 0.14082 |
| 36 | thickII | 10 | 29 | -0.29328 | 0.20053 | 0.1436 |
| 37 | thickII | 11 | 28 | -0.28264 | 0.21124 | 0.18089 |

| | | | | | | |
|---|---|---|---|---|---|---|
| 38 | thickII | 12 | 27 | -0.27197 | 0.22073 | 0.21789 |
| 39 | thickII | 13 | 26 | -0.10387 | 0.22916 | 0.65037 |
| 40 | thickII | 14 | 25 | -0.04603 | 0.23036 | 0.84162 |
| 41 | thickII | 15 | 24 | -0.05459 | 0.2306 | 0.81285 |
| 42 | thickII | 16 | 23 | -0.00123 | 0.23093 | 0.99576 |
| 43 | thickII | 17 | 22 | 0.04087 | 0.23093 | 0.85952 |
| 44 | thickII | 18 | 21 | 0.13268 | 0.23111 | 0.56592 |
| 45 | thickII | 19 | 20 | 0.29963 | 0.23306 | 0.19857 |
| 46 | thickII | 20 | 19 | 0.05262 | 0.24274 | 0.82838 |
| 47 | thickII | 21 | 18 | 0.12112 | 0.24303 | 0.6182 |
| 48 | thickII | 22 | 17 | 0.0908 | 0.24457 | 0.71045 |
| 49 | thickII | 23 | 16 | 0.10418 | 0.24543 | 0.67123 |
| 50 | thickII | 24 | 15 | 0.04243 | 0.24657 | 0.86336 |

CC Data PR1 v PR2

| Obs | _NAME_ | _CROSS_ | LAG | N | CCF | CCFSTD | CCFPROB |
|---|---|---|---|---|---|---|---|
| 1 | thickII | thickI | -24 | 15 | 0.00967 | 0.16013 | 0.95186 |
| 2 | thickII | thickI | -23 | 16 | 0.06855 | 0.16013 | 0.66857 |
| 3 | thickII | thickI | -22 | 17 | 0.04127 | 0.16013 | 0.79661 |
| 4 | thickII | thickI | -21 | 18 | 0.02513 | 0.16013 | 0.87529 |
| 5 | thickII | thickI | -20 | 19 | 0.09195 | 0.16013 | 0.56581 |
| 6 | thickII | thickI | -19 | 20 | 0.30403 | 0.16013 | 0.05761 |
| 7 | thickII | thickI | -18 | 21 | 0.06729 | 0.16013 | 0.67433 |
| 8 | thickII | thickI | -17 | 22 | -0.09109 | 0.16013 | 0.56947 |
| 9 | thickII | thickI | -16 | 23 | 0.12157 | 0.16013 | 0.44771 |
| 10 | thickII | thickI | -15 | 24 | 0.18361 | 0.16013 | 0.25152 |
| 11 | thickII | thickI | -14 | 25 | -0.00635 | 0.16013 | 0.96835 |
| 12 | thickII | thickI | -13 | 26 | -0.16926 | 0.16013 | 0.2905 |
| 13 | thickII | thickI | -12 | 27 | -0.12184 | 0.16013 | 0.44673 |
| 14 | thickII | thickI | -11 | 28 | -0.02917 | 0.16013 | 0.85544 |
| 15 | thickII | thickI | -10 | 29 | -0.18691 | 0.16013 | 0.2431 |
| 16 | thickII | thickI | -9 | 30 | -0.27312 | 0.16013 | 0.08808 |
| 17 | thickII | thickI | -8 | 31 | -0.10079 | 0.16013 | 0.52906 |
| 18 | thickII | thickI | -7 | 32 | -0.00895 | 0.16013 | 0.95541 |
| 19 | thickII | thickI | -6 | 33 | -0.08632 | 0.16013 | 0.58984 |
| 20 | thickII | thickI | -5 | 34 | 0.05236 | 0.16013 | 0.74366 |
| 21 | thickII | thickI | -4 | 35 | -0.07325 | 0.16013 | 0.64736 |
| 22 | thickII | thickI | -3 | 36 | 0.17737 | 0.16013 | 0.268 |
| 23 | thickII | thickI | -2 | 37 | 0.328 | 0.16013 | 0.04053 |
| 24 | thickII | thickI | -1 | 38 | 0.33486 | 0.16013 | 0.03651 |
| 25 | thickII | thickI | 0 | 39 | 0.62453 | 0.16013 | 0.0001 |
| 26 | thickII | thickI | 1 | 38 | 0.0763 | 0.16013 | 0.63373 |
| 27 | thickII | thickI | 2 | 37 | 0.14981 | 0.16013 | 0.3495 |
| 28 | thickII | thickI | 3 | 36 | 0.22431 | 0.16013 | 0.16127 |
| 29 | thickII | thickI | 4 | 35 | 0.07489 | 0.16013 | 0.64001 |
| 30 | thickII | thickI | 5 | 34 | 0.0881 | 0.16013 | 0.58221 |
| 31 | thickII | thickI | 6 | 33 | -0.19386 | 0.16013 | 0.22602 |
| 32 | thickII | thickI | 7 | 32 | -0.03882 | 0.16013 | 0.80847 |
| 33 | thickII | thickI | 8 | 31 | -0.08241 | 0.16013 | 0.60679 |
| 34 | thickII | thickI | 9 | 30 | -0.42273 | 0.16013 | 0.00829 |
| 35 | thickII | thickI | 10 | 29 | -0.32666 | 0.16013 | 0.04135 |
| 36 | thickII | thickI | 11 | 28 | -0.27974 | 0.16013 | 0.08065 |
| 37 | thickII | thickI | 12 | 27 | -0.0609 | 0.16013 | 0.7037 |

| | | | | | | | |
|---|---|---|---|---|---|---|---|
| 38 | thickII | thickI | 13 | 26 | -0.13876 | 0.16013 | 0.38618 |
| 39 | thickII | thickI | 14 | 25 | -0.14063 | 0.16013 | 0.37981 |
| 40 | thickII | thickI | 15 | 24 | 0.01245 | 0.16013 | 0.93801 |
| 41 | thickII | thickI | 16 | 23 | 0.03901 | 0.16013 | 0.80752 |
| 42 | thickII | thickI | 17 | 22 | 0.04728 | 0.16013 | 0.76777 |
| 43 | thickII | thickI | 18 | 21 | 0.30037 | 0.16013 | 0.06068 |
| 44 | thickII | thickI | 19 | 20 | 0.11841 | 0.16013 | 0.45961 |
| 45 | thickII | thickI | 20 | 19 | 0.1793 | 0.16013 | 0.26283 |
| 46 | thickII | thickI | 21 | 18 | 0.11534 | 0.16013 | 0.47135 |
| 47 | thickII | thickI | 22 | 17 | 0.01648 | 0.16013 | 0.91805 |
| 48 | thickII | thickI | 23 | 16 | 0.12563 | 0.16013 | 0.43271 |
| 49 | thickII | thickI | 24 | 15 | -0.04964 | 0.16013 | 0.75656 |

AC Data RELP v UP1 Overlapped Area

| Obs | _NAME_ | LAG | N | ACF | ACFSTD | ACFPROB |
|---|---|---|---|---|---|---|
| 1 | thickI | 0 | 45 | 1 | 0 | . |
| 2 | thickI | 1 | 44 | -0.03858 | 0.14907 | 0.7958 |
| 3 | thickI | 2 | 43 | -0.05101 | 0.14929 | 0.73261 |
| 4 | thickI | 3 | 42 | 0.15082 | 0.14968 | 0.31364 |
| 5 | thickI | 4 | 41 | -0.02264 | 0.15302 | 0.88239 |
| 6 | thickI | 5 | 40 | -0.00883 | 0.15309 | 0.954 |
| 7 | thickI | 6 | 39 | -0.02443 | 0.15311 | 0.87322 |
| 8 | thickI | 7 | 38 | 0.08984 | 0.15319 | 0.55759 |
| 9 | thickI | 8 | 37 | 0.03091 | 0.15436 | 0.84127 |
| 10 | thickI | 9 | 36 | -0.01878 | 0.1545 | 0.90323 |
| 11 | thickI | 10 | 35 | -0.04666 | 0.15455 | 0.7627 |
| 12 | thickI | 11 | 34 | -0.05149 | 0.15486 | 0.73953 |
| 13 | thickI | 12 | 33 | 0.17359 | 0.15524 | 0.26348 |
| 14 | thickI | 13 | 32 | -0.0457 | 0.15949 | 0.77448 |
| 15 | thickI | 14 | 31 | -0.08195 | 0.15978 | 0.60805 |
| 16 | thickI | 15 | 30 | 0.36502 | 0.16072 | 0.02313 |
| 17 | thickI | 16 | 29 | -0.04196 | 0.17819 | 0.81384 |
| 18 | thickI | 17 | 28 | -0.04337 | 0.17841 | 0.80795 |
| 19 | thickI | 18 | 27 | -0.05863 | 0.17864 | 0.74275 |
| 20 | thickI | 19 | 26 | -0.04077 | 0.17907 | 0.81992 |
| 21 | thickI | 20 | 25 | 0.01588 | 0.17928 | 0.92943 |
| 22 | thickI | 21 | 24 | -0.04937 | 0.17931 | 0.78304 |
| 23 | thickI | 22 | 23 | -0.05762 | 0.17961 | 0.74837 |
| 24 | thickI | 23 | 22 | -0.06723 | 0.18002 | 0.70881 |
| 25 | thickI | 24 | 21 | -0.03072 | 0.18058 | 0.8649 |
| 26 | thickII | 0 | 45 | 1 | 0 | . |
| 27 | thickII | 1 | 44 | 0.03198 | 0.14907 | 0.83012 |
| 28 | thickII | 2 | 43 | -0.08096 | 0.14922 | 0.58743 |
| 29 | thickII | 3 | 42 | -0.04645 | 0.1502 | 0.7571 |
| 30 | thickII | 4 | 41 | -0.00644 | 0.15052 | 0.96589 |
| 31 | thickII | 5 | 40 | -0.00684 | 0.15052 | 0.96378 |
| 32 | thickII | 6 | 39 | 0.22014 | 0.15053 | 0.14363 |
| 33 | thickII | 7 | 38 | -0.07868 | 0.15752 | 0.61744 |
| 34 | thickII | 8 | 37 | -0.01993 | 0.15839 | 0.89988 |
| 35 | thickII | 9 | 36 | -0.03003 | 0.15845 | 0.8497 |
| 36 | thickII | 10 | 35 | 0.15292 | 0.15857 | 0.33488 |
| 37 | thickII | 11 | 34 | -0.09485 | 0.16182 | 0.55778 |

| | | | | | | |
|---|---|---|---|---|---|---|
| 38 | thickII | 12 | 33 | -0.01136 | 0.16305 | 0.94447 |
| 39 | thickII | 13 | 32 | -0.07247 | 0.16307 | 0.65673 |
| 40 | thickII | 14 | 31 | -0.10748 | 0.16378 | 0.51167 |
| 41 | thickII | 15 | 30 | -0.06 | 0.16534 | 0.71668 |
| 42 | thickII | 16 | 29 | -0.06662 | 0.16582 | 0.68788 |
| 43 | thickII | 17 | 28 | -0.06416 | 0.16642 | 0.69983 |
| 44 | thickII | 18 | 27 | 0.17998 | 0.16697 | 0.28106 |
| 45 | thickII | 19 | 26 | -0.01251 | 0.17122 | 0.94178 |
| 46 | thickII | 20 | 25 | -0.04215 | 0.17124 | 0.80555 |
| 47 | thickII | 21 | 24 | -0.01964 | 0.17147 | 0.90881 |
| 48 | thickII | 22 | 23 | -0.05822 | 0.17152 | 0.73429 |
| 49 | thickII | 23 | 22 | -0.06649 | 0.17196 | 0.69901 |
| 50 | thickII | 24 | 21 | -0.00626 | 0.17253 | 0.97104 |

CC Data RELP v UP1 Overlapped area

| Obs | _NAME_ | _CROSS_ | LAG | N | CCF | CCFSTD | CCFPROB |
|---|---|---|---|---|---|---|---|
| 1 | thickII | thickI | -24 | 21 | -0.04016 | 0.14907 | 0.78761 |
| 2 | thickII | thickI | -23 | 22 | -0.02328 | 0.14907 | 0.8759 |
| 3 | thickII | thickI | -22 | 23 | 0.00717 | 0.14907 | 0.96165 |
| 4 | thickII | thickI | -21 | 24 | -0.02712 | 0.14907 | 0.85562 |
| 5 | thickII | thickI | -20 | 25 | -0.0625 | 0.14907 | 0.67504 |
| 6 | thickII | thickI | -19 | 26 | -0.06106 | 0.14907 | 0.68209 |
| 7 | thickII | thickI | -18 | 27 | -0.02976 | 0.14907 | 0.84176 |
| 8 | thickII | thickI | -17 | 28 | 0.01975 | 0.14907 | 0.8946 |
| 9 | thickII | thickI | -16 | 29 | -0.02701 | 0.14907 | 0.8562 |
| 10 | thickII | thickI | -15 | 30 | 0.15795 | 0.14907 | 0.28935 |
| 11 | thickII | thickI | -14 | 31 | -0.07624 | 0.14907 | 0.60903 |
| 12 | thickII | thickI | -13 | 32 | -0.05208 | 0.14907 | 0.72683 |
| 13 | thickII | thickI | -12 | 33 | -0.02903 | 0.14907 | 0.84561 |
| 14 | thickII | thickI | -11 | 34 | -0.10332 | 0.14907 | 0.48826 |
| 15 | thickII | thickI | -10 | 35 | -0.08329 | 0.14907 | 0.57635 |
| 16 | thickII | thickI | -9 | 36 | -0.07954 | 0.14907 | 0.59362 |
| 17 | thickII | thickI | -8 | 37 | -0.02215 | 0.14907 | 0.88187 |
| 18 | thickII | thickI | -7 | 38 | 0.14717 | 0.14907 | 0.32353 |
| 19 | thickII | thickI | -6 | 39 | -0.05837 | 0.14907 | 0.69537 |
| 20 | thickII | thickI | -5 | 40 | -0.05485 | 0.14907 | 0.71291 |
| 21 | thickII | thickI | -4 | 41 | -0.02659 | 0.14907 | 0.85843 |
| 22 | thickII | thickI | -3 | 42 | 0.28671 | 0.14907 | 0.05444 |
| 23 | thickII | thickI | -2 | 43 | -0.03126 | 0.14907 | 0.8339 |
| 24 | thickII | thickI | -1 | 44 | -0.05004 | 0.14907 | 0.73712 |
| 25 | thickII | thickI | 0 | 45 | 0.15907 | 0.14907 | 0.28595 |
| 26 | thickII | thickI | 1 | 44 | -0.08512 | 0.14907 | 0.568 |
| 27 | thickII | thickI | 2 | 43 | 0.01602 | 0.14907 | 0.9144 |
| 28 | thickII | thickI | 3 | 42 | 0.69009 | 0.14907 | 0 |
| 29 | thickII | thickI | 4 | 41 | -0.01139 | 0.14907 | 0.93911 |
| 30 | thickII | thickI | 5 | 40 | 0.00401 | 0.14907 | 0.97852 |
| 31 | thickII | thickI | 6 | 39 | 0.03183 | 0.14907 | 0.83093 |
| 32 | thickII | thickI | 7 | 38 | -0.07788 | 0.14907 | 0.60137 |
| 33 | thickII | thickI | 8 | 37 | 0.04568 | 0.14907 | 0.75929 |
| 34 | thickII | thickI | 9 | 36 | 0.0535 | 0.14907 | 0.71969 |
| 35 | thickII | thickI | 10 | 35 | 0.10718 | 0.14907 | 0.47216 |
| 36 | thickII | thickI | 11 | 34 | -0.07605 | 0.14907 | 0.60995 |
| 37 | thickII | thickI | 12 | 33 | 0.10355 | 0.14907 | 0.48727 |

| | | | | | | | |
|---|---|---|---|---|---|---|---|
| 38 | thickII | thickI | 13 | 32 | -0.03095 | 0.14907 | 0.8355 |
| 39 | thickII | thickI | 14 | 31 | -0.04666 | 0.14907 | 0.75427 |
| 40 | thickII | thickI | 15 | 30 | 0.12293 | 0.14907 | 0.40958 |
| 41 | thickII | thickI | 16 | 29 | -0.07107 | 0.14907 | 0.63353 |
| 42 | thickII | thickI | 17 | 28 | -0.04096 | 0.14907 | 0.78352 |
| 43 | thickII | thickI | 18 | 27 | 0.39126 | 0.14907 | 0.00867 |
| 44 | thickII | thickI | 19 | 26 | -0.04203 | 0.14907 | 0.77798 |
| 45 | thickII | thickI | 20 | 25 | -0.051 | 0.14907 | 0.73227 |
| 46 | thickII | thickI | 21 | 24 | -0.04012 | 0.14907 | 0.78783 |
| 47 | thickII | thickI | 22 | 23 | -0.03509 | 0.14907 | 0.81392 |
| 48 | thickII | thickI | 23 | 22 | -0.04695 | 0.14907 | 0.75282 |
| 49 | thickII | thickI | 24 | 21 | -0.03287 | 0.14907 | 0.82546 |

AC Data GPC V PC

| Obs | _NAME_ | LAG | N | ACF | ACFSTD | ACFPROB |
|---|---|---|---|---|---|---|
| 1 | thickI | 0 | 280 | 1 | 0 | . |
| 2 | thickI | 1 | 279 | 0.23785 | 0.059761 | 0.00007 |
| 3 | thickI | 2 | 278 | 0.10258 | 0.063052 | 0.10376 |
| 4 | thickI | 3 | 277 | 0.23253 | 0.063645 | 0.00026 |
| 5 | thickI | 4 | 276 | 0.08009 | 0.06661 | 0.22923 |
| 6 | thickI | 5 | 275 | 0.07393 | 0.066953 | 0.26947 |
| 7 | thickI | 6 | 274 | 0.13002 | 0.067244 | 0.05317 |
| 8 | thickI | 7 | 273 | 0.01008 | 0.068136 | 0.88245 |
| 9 | thickI | 8 | 272 | 0.19014 | 0.068141 | 0.00527 |
| 10 | thickI | 9 | 271 | 0.20504 | 0.07001 | 0.0034 |
| 11 | thickI | 10 | 270 | 0.04018 | 0.072123 | 0.57747 |
| 12 | thickI | 11 | 269 | 0.15732 | 0.072203 | 0.02934 |
| 13 | thickI | 12 | 268 | 0.17863 | 0.073417 | 0.01497 |
| 14 | thickI | 13 | 267 | 0.1103 | 0.074953 | 0.14115 |
| 15 | thickI | 14 | 266 | 0.19501 | 0.07553 | 0.00983 |
| 16 | thickI | 15 | 265 | 0.15693 | 0.077308 | 0.04237 |
| 17 | thickI | 16 | 264 | 0.06321 | 0.078437 | 0.42029 |
| 18 | thickI | 17 | 263 | 0.17358 | 0.078619 | 0.02725 |
| 19 | thickI | 18 | 262 | 0.03514 | 0.079976 | 0.66039 |
| 20 | thickI | 19 | 261 | 0.0351 | 0.080031 | 0.66095 |
| 21 | thickI | 20 | 260 | 0.10744 | 0.080086 | 0.17976 |
| 22 | thickI | 21 | 259 | 0.07454 | 0.080599 | 0.35506 |
| 23 | thickI | 22 | 258 | -0.00153 | 0.080845 | 0.98491 |
| 24 | thickI | 23 | 257 | 0.08556 | 0.080845 | 0.28991 |
| 25 | thickI | 24 | 256 | 0.04842 | 0.081168 | 0.55081 |
| 26 | thickII | 0 | 280 | 1 | 0 | . |
| 27 | thickII | 1 | 279 | 0.1924 | 0.059761 | 0.00128 |
| 28 | thickII | 2 | 278 | 0.19947 | 0.061934 | 0.00128 |
| 29 | thickII | 3 | 277 | 0.13166 | 0.064187 | 0.04024 |
| 30 | thickII | 4 | 276 | 0.09723 | 0.065145 | 0.13556 |
| 31 | thickII | 5 | 275 | 0.09705 | 0.065661 | 0.13941 |
| 32 | thickII | 6 | 274 | 0.07145 | 0.066171 | 0.28024 |
| 33 | thickII | 7 | 273 | 0.16297 | 0.066446 | 0.01418 |
| 34 | thickII | 8 | 272 | 0.08454 | 0.067859 | 0.21281 |
| 35 | thickII | 9 | 271 | 0.04969 | 0.068234 | 0.46645 |
| 36 | thickII | 10 | 270 | -0.03569 | 0.068363 | 0.60159 |
| 37 | thickII | 11 | 269 | -0.00341 | 0.06843 | 0.9603 |

| | | | | | | |
|---|---|---|---|---|---|---|
| 38 | thickII | 12 | 268 | 0.00584 | 0.06843 | 0.93196 |
| 39 | thickII | 13 | 267 | 0.01424 | 0.068432 | 0.83512 |
| 40 | thickII | 14 | 266 | 0.06268 | 0.068443 | 0.3598 |
| 41 | thickII | 15 | 265 | 0.00583 | 0.068647 | 0.93233 |
| 42 | thickII | 16 | 264 | 0.01547 | 0.068649 | 0.82174 |
| 43 | thickII | 17 | 263 | -0.0265 | 0.068662 | 0.69957 |
| 44 | thickII | 18 | 262 | 0.00079 | 0.068698 | 0.99088 |
| 45 | thickII | 19 | 261 | -0.03888 | 0.068698 | 0.57144 |
| 46 | thickII | 20 | 260 | -0.01888 | 0.068777 | 0.78375 |
| 47 | thickII | 21 | 259 | 0.04208 | 0.068795 | 0.5408 |
| 48 | thickII | 22 | 258 | -0.00771 | 0.068887 | 0.91086 |
| 49 | thickII | 23 | 257 | -0.10413 | 0.06889 | 0.13064 |
| 50 | thickII | 24 | 256 | 0.08267 | 0.06945 | 0.2339 |

CC Data GPC V PC

| Obs | _NAME_ | _CROSS_ | LAG | N | CCF | CCFSTD | CCFPROB |
|---|---|---|---|---|---|---|---|
| 1 | thickII | thickI | -24 | 256 | 0.05065 | 0.059761 | 0.39669 |
| 2 | thickII | thickI | -23 | 257 | 0.08938 | 0.059761 | 0.13476 |
| 3 | thickII | thickI | -22 | 258 | 0.05651 | 0.059761 | 0.34432 |
| 4 | thickII | thickI | -21 | 259 | 0.04229 | 0.059761 | 0.47918 |
| 5 | thickII | thickI | -20 | 260 | 0.0088 | 0.059761 | 0.88293 |
| 6 | thickII | thickI | -19 | 261 | -0.01739 | 0.059761 | 0.77101 |
| 7 | thickII | thickI | -18 | 262 | 0.04066 | 0.059761 | 0.49624 |
| 8 | thickII | thickI | -17 | 263 | 0.05775 | 0.059761 | 0.33385 |
| 9 | thickII | thickI | -16 | 264 | -0.05293 | 0.059761 | 0.3758 |
| 10 | thickII | thickI | -15 | 265 | -0.05156 | 0.059761 | 0.38828 |
| 11 | thickII | thickI | -14 | 266 | -0.06028 | 0.059761 | 0.31316 |
| 12 | thickII | thickI | -13 | 267 | -0.02045 | 0.059761 | 0.7322 |
| 13 | thickII | thickI | -12 | 268 | -0.01703 | 0.059761 | 0.77572 |
| 14 | thickII | thickI | -11 | 269 | -0.03275 | 0.059761 | 0.58372 |
| 15 | thickII | thickI | -10 | 270 | -0.00326 | 0.059761 | 0.95654 |
| 16 | thickII | thickI | -9 | 271 | -0.01804 | 0.059761 | 0.76276 |
| 17 | thickII | thickI | -8 | 272 | 0.05911 | 0.059761 | 0.32265 |
| 18 | thickII | thickI | -7 | 273 | -0.04033 | 0.059761 | 0.49973 |
| 19 | thickII | thickI | -6 | 274 | -0.00295 | 0.059761 | 0.96062 |
| 20 | thickII | thickI | -5 | 275 | -0.01129 | 0.059761 | 0.85017 |
| 21 | thickII | thickI | -4 | 276 | -0.06695 | 0.059761 | 0.26256 |
| 22 | thickII | thickI | -3 | 277 | -0.0272 | 0.059761 | 0.64898 |
| 23 | thickII | thickI | -2 | 278 | 0.02159 | 0.059761 | 0.7179 |
| 24 | thickII | thickI | -1 | 279 | -0.05608 | 0.059761 | 0.34802 |
| 25 | thickII | thickI | 0 | 280 | -0.09411 | 0.059761 | 0.1153 |
| 26 | thickII | thickI | 1 | 279 | 0.00226 | 0.059761 | 0.96989 |
| 27 | thickII | thickI | 2 | 278 | -0.00587 | 0.059761 | 0.92179 |
| 28 | thickII | thickI | 3 | 277 | -0.05147 | 0.059761 | 0.38914 |
| 29 | thickII | thickI | 4 | 276 | -0.04487 | 0.059761 | 0.45277 |
| 30 | thickII | thickI | 5 | 275 | -0.03008 | 0.059761 | 0.61469 |
| 31 | thickII | thickI | 6 | 274 | 0.01713 | 0.059761 | 0.77437 |
| 32 | thickII | thickI | 7 | 273 | 0.04895 | 0.059761 | 0.41275 |
| 33 | thickII | thickI | 8 | 272 | -0.0106 | 0.059761 | 0.85921 |
| 34 | thickII | thickI | 9 | 271 | 0.10131 | 0.059761 | 0.09002 |
| 35 | thickII | thickI | 10 | 270 | 0.08252 | 0.059761 | 0.16732 |
| 36 | thickII | thickI | 11 | 269 | -0.01927 | 0.059761 | 0.74708 |
| 37 | thickII | thickI | 12 | 268 | -0.10301 | 0.059761 | 0.08475 |

| | | | | | | | |
|---|---|---|---|---|---|---|---|
| 38 | thickII | thickI | 13 | 267 | -0.13289 | 0.059761 | 0.02617 |
| 39 | thickII | thickI | 14 | 266 | -0.03965 | 0.059761 | 0.50701 |
| 40 | thickII | thickI | 15 | 265 | -0.0519 | 0.059761 | 0.38517 |
| 41 | thickII | thickI | 16 | 264 | -0.02516 | 0.059761 | 0.67381 |
| 42 | thickII | thickI | 17 | 263 | -0.05304 | 0.059761 | 0.37476 |
| 43 | thickII | thickI | 18 | 262 | 0.02105 | 0.059761 | 0.72468 |
| 44 | thickII | thickI | 19 | 261 | -0.01837 | 0.059761 | 0.75853 |
| 45 | thickII | thickI | 20 | 260 | -0.1295 | 0.059761 | 0.03024 |
| 46 | thickII | thickI | 21 | 259 | -0.00526 | 0.059761 | 0.92985 |
| 47 | thickII | thickI | 22 | 258 | -0.01593 | 0.059761 | 0.78975 |
| 48 | thickII | thickI | 23 | 257 | 0.01357 | 0.059761 | 0.82035 |
| 49 | thickII | thickI | 24 | 256 | 0.02916 | 0.059761 | 0.62562 |

## Appendix E: Data for Measured Sections

Ghaap Plateau 1

| Number | cm | Designation | Note |
|---|---|---|---|
| 1 | 2.7 | a | |
| 2 | 2.1 | b | |
| 3 | 3.7 | a | |
| 4 | 1.8 | b | |
| 5 | 2.9 | a | |
| 6 | 1.4 | b | |
| 7 | 3.6 | a | |
| 8 | 1.7 | b | |
| 9 | 2.3 | a | |
| 10 | 0.6 | b | |
| 11 | 4.3 | a | |
| 12 | 1.3 | b | |
| 13 | 7.2 | a | |
| 14 | 3.1 | b | |
| 15 | 5.6 | a | |
| 16 | 4.4 | b | |
| 17 | 7.4 | a | |
| 18 | 4.6 | b | |
| 19 | 5.4 | a | |
| 20 | 2.1 | b | |
| 21 | 4.6 | a | |
| 22 | 1.3 | b | |
| 23 | 8.3 | a | |
| 24 | 2.4 | b | |
| 25 | 1.7 | a | |
| 26 | 3.8 | b | |
| 27 | 2.3 | a | |
| 28 | 0.8 | b | |
| 29 | 1.8 | a | |
| 30 | 10.3 | b | |
| 31 | 5.4 | a | |
| 32 | 2.7 | b | |
| 33 | 3.1 | a | |
| 34 | 0.5 | b | |
| 35 | 3 | a | |
| 36 | 3.3 | b | |
| 37 | 1.9 | a | |

| Number | cm | Designation | Note |
|---|---|---|---|
| 38 | 0.7 | b | |
| 39 | 1.4 | a | |
| 40 | 0.5 | b | |
| 41 | 1.8 | a | |
| 42 | 0.5 | b | |
| 43 | 1.4 | a | |
| 44 | 0.5 | b | |
| 45 | 2.3 | a | |
| 46 | 0.5 | b | erosion surface |
| 47 | 0.05 | a | argillaceous |
| 48 | 2.3 | b | argillaceous |
| 49 | 0.05 | a | argillaceous |
| 50 | 3.6 | b | argillaceous |
| 51 | 0.05 | a | argillaceous |
| 52 | 5.5 | b | argillaceous |
| 53 | 0.05 | a | argillaceous |
| 54 | 2.4 | b | argillaceous |
| 55 | 0.05 | a | argillaceous |
| 56 | 5 | b | argillaceous |
| 57 | 0.05 | a | argillaceous |
| 58 | 4.8 | b | argillaceous |
| 59 | 0.05 | a | argillaceous |
| 60 | 4.2 | b | argillaceous |
| 61 | 0.05 | a | argillaceous |
| 62 | 2 | b | argillaceous |
| 63 | 0.05 | a | argillaceous |
| 64 | 2.9 | b | argillaceous |
| 65 | 0.05 | a | argillaceous |
| 66 | 1.3 | b | argillaceous |
| 67 | 0.05 | a | argillaceous |
| 68 | 3.1 | b | argillaceous |
| 69 | 0.05 | a | argillaceous |
| 70 | 6 | b | |
| 71 | 3.1 | a | |
| 72 | 3.4 | b | |
| 73 | 2.7 | a | |
| 74 | 3.7 | b | |
| 75 | 4.6 | a | |
| 76 | 0.5 | b | |

| Number | cm | Designation | Note |
|---|---|---|---|
| 77 | 2.4 | a | |
| 78 | 3.5 | b | |
| 79 | 4.6 | a | |
| 80 | 3.7 | b | |
| 81 | 5.6 | a | |
| 82 | 2.2 | b | |
| 83 | 4.6 | a | |
| 84 | 2.3 | b | |
| 85 | 2.6 | a | |
| 86 | 1.7 | b | |
| 87 | 1.1 | a | |
| 88 | 2.2 | b | |
| 89 | 3.3 | a | |
| 90 | 3.8 | b | |
| 91 | 5 | a | |
| 92 | 3.4 | b | |
| 93 | 4.2 | a | |
| 94 | 3.2 | b | |
| 95 | 1.6 | a | |
| 96 | 5.5 | b | |
| 97 | 1.2 | a | |
| 98 | 2.6 | b | |
| 99 | 2.1 | a | |
| 100 | 2.8 | b | |
| 101 | 1.5 | a | |
| 102 | 3.1 | b | |
| 103 | 1.4 | a | |
| 104 | 4 | b | |
| 105 | 1 | a | |
| 106 | 4.3 | b | |
| 107 | 1.7 | a | |
| 108 | 2.8 | b | |
| 109 | 2 | a | |
| 110 | 3 | b | |
| 111 | 2.7 | a | |
| 112 | 3 | b | |
| 113 | 3.5 | a | |
| 114 | 8 | b | |
| 115 | 1.9 | a | |

| Number | cm | Designation | Note |
|---|---|---|---|
| 116 | 3.7 | b | |
| 117 | 0.6 | a | |
| 118 | 4.5 | b | |
| 119 | 1.8 | a | |
| 120 | 0.05 | b | |
| 121 | 2.5 | a | |
| 122 | 5.5 | b | |
| 123 | 1 | a | |
| 124 | 4 | b | |
| 125 | 15 | weathered | chg to a-crack |
| 126 | 6.2 | b | |
| 127 | 3.2 | a | |
| 128 | 0.6 | b | |
| 129 | 1.7 | a | |
| 130 | 3.2 | b | |
| 131 | 3.4 | a | |
| 132 | 0.9 | b | |
| 133 | 2.7 | a | |
| 134 | 0.6 | b | |
| 135 | 1.4 | a | |
| 136 | 1.8 | b | |
| 137 | 3.6 | a | |
| 138 | 5.2 | b | |
| 139 | 3.8 | a | |
| 140 | 1.2 | b | |
| 141 | 2.8 | a | |
| 142 | 3.2 | b | |
| 143 | 2.9 | a | |
| 144 | 5.1 | b | |
| 145 | 2.2 | a | |
| 146 | 1.8 | b | |
| 147 | 1.5 | a | |
| 148 | 7.5 | b | |
| 149 | 4 | a | FANS small |
| 150 | 1.9 | b | |
| 151 | 4.9 | a | FANS small |
| 152 | 1.6 | b | |
| 153 | 5.8 | a | |
| 154 | 1.5 | b | |

| Number | cm | Designation | Note |
|---|---|---|---|
| 155 | 2.8 | a | |
| 156 | 1.9 | b | |
| 157 | 2.4 | a | |
| 158 | 0.6 | b | |
| 159 | 2.8 | a | |
| 160 | 0.05 | b | |
| 161 | 3.1 | a | |
| 162 | 0.2 | b | |
| 163 | 3.2 | a | |
| 164 | 0.3 | b | |
| 165 | 0.6 | a | |
| 166 | 3 | b | |
| 167 | 0.3 | a | |
| 168 | 3.2 | b | |
| 169 | 0.05 | a | |
| 170 | 2 | b | |
| 171 | 0.05 | a | |
| 172 | 3.2 | b | |
| 173 | 0.05 | a | |
| 174 | 4.7 | b | |
| 175 | 0.05 | a | |
| 176 | 5 | b | |
| TOTAL | 480.2 | | |

**Notes:**

Argillaceous beds indicated by high degree of weathering and calcrete with b-type still present and measurable. Weathered sections changed to crack .05 to maintain pattern for analysis. Crack top indicates separation of bedding plane and calcrete in-fill.

Ghaap Plateau 2

| Number | cm | Designation | Note |
|---|---|---|---|
| 1 | 21 | b | |
| 2 | 0.05 | a | |
| 3 | 18.9 | b | |
| 4 | 0.05 | a | |
| 5 | 5.7 | b | |
| 6 | 0.05 | a | |
| 7 | 11.8 | b | |
| 8 | 0.05 | a | |
| 9 | 7.5 | b | |
| 10 | 0.05 | a | |
| 11 | 13 | b | |
| 12 | 0.05 | a | |
| 13 | 4.8 | b | |
| 14 | 0.05 | a | |
| 15 | 9.2 | b | |
| 16 | 0.05 | a | |
| 17 | 1 | b | |
| 18 | 0.05 | a | |
| 19 | 2.5 | b | |
| 20 | 1 | a | |
| 21 | 1.3 | b | |
| 22 | 0.5 | a | |
| 23 | 0.5 | b | |
| 24 | 0.6 | a | |
| 25 | 3.4 | b | |
| 26 | 1.1 | a | |
| 27 | 2.4 | b | crack top |
| 28 | 1.2 | a | |
| 29 | 2 | b | |
| 30 | 0.7 | a | crack top |
| 31 | 0.5 | b | |
| 32 | 1.6 | a | |
| 33 | 1.4 | b | |
| 34 | 2 | a | crack top |
| 35 | 1.8 | b | |
| 36 | 0.6 | a | |
| 37 | 7.1 | b | |

| Number | cm | Designation | Note |
|---|---|---|---|
| 38 | 0.05 | a | |
| 39 | 3.9 | b | |
| 40 | 2.9 | a | |
| 41 | 3.5 | b | |
| 42 | 3.7 | a | |
| 43 | 0.7 | b | |
| 44 | 4.5 | a | |
| 45 | 1.2 | b | |
| 46 | 2.4 | a | |
| 47 | 0.4 | b | |
| 48 | 1.3 | a | |
| 49 | 0.05 | b | |
| 50 | 2.1 | a | |
| 51 | 0.5 | b | |
| 52 | 1.3 | a | |
| 53 | 0.3 | b | |
| 54 | 2.1 | a | |
| 55 | 1 | b | erosion surface |
| 56 | 0.05 | a | argillaceous |
| 57 | 1.8 | b | argillaceous |
| 58 | 0.05 | a | argillaceous |
| 59 | 2 | b | argillaceous |
| 60 | 0.05 | a | argillaceous |
| 61 | 2.5 | b | argillaceous |
| 62 | 0.05 | a | argillaceous |
| 63 | 5.3 | b | argillaceous |
| 64 | 0.05 | a | argillaceous |
| 65 | 1.7 | b | argillaceous |
| 66 | 0.05 | a | argillaceous |
| 67 | 6 | b | argillaceous |
| 68 | 0.05 | a | argillaceous |
| 69 | 5.7 | b | argillaceous |
| 70 | 0.05 | a | argillaceous |
| 71 | 3.2 | b | argillaceous |
| 72 | 0.05 | a | argillaceous |
| 73 | 1.3 | b | argillaceous |
| 74 | 0.05 | a | argillaceous |
| 75 | 2.3 | b | argillaceous |
| 76 | 0.05 | a | argillaceous |

| Number | cm | Designation | Note |
|---|---|---|---|
| 77 | 1.4 | b | argillaceous |
| 78 | 1.5 | a | argillaceous |
| 79 | 1 | b | argillaceous |
| 80 | 0.05 | a | |
| 81 | 1.5 | b | |
| 82 | 0.05 | a | |
| 83 | 1.5 | b | |
| 84 | 0.05 | a | |
| 85 | 4.6 | b | |
| 86 | 1.2 | a | crack top |
| 87 | 2 | b | |
| 88 | 0.05 | a | |
| 89 | 2 | b | |
| 90 | 0.05 | a | |
| 91 | 1.9 | b | |
| 92 | 2.5 | a | |
| 93 | 3 | b | |
| 94 | 0.05 | a | |
| 95 | 3.5 | b | |
| 96 | 0.05 | a | |
| 97 | 2.5 | b | |
| 98 | 0.05 | a | |
| 99 | 5.8 | b | |
| 100 | 0.05 | a | |
| 101 | 1.9 | b | |
| 102 | 0.05 | a | |
| 103 | 1.6 | b | |
| 104 | 0.05 | a | |
| 105 | 7 | b | |
| 106 | 0.05 | a | |
| 107 | 5.7 | b | |
| 108 | 1.5 | a | |
| 109 | 3 | b | |
| 110 | 0.6 | a | crack top |
| 111 | 1.2 | b | |
| 112 | 5.5 | a | |
| 113 | 1.2 | b | |
| 114 | 6 | a | |
| 115 | 2 | b | crack top |

| Number | cm | Designation | Note |
|---|---|---|---|
| 116 | 3.6 | a | |
| 117 | 0.5 | b | |
| 118 | 5.5 | a | |
| 119 | 1.5 | b | |
| 120 | 0.05 | a | |
| 121 | 1.3 | b | crack top |
| 122 | 4 | a | crack top |
| 123 | 1.6 | b | |
| 124 | 5.6 | a | |
| 125 | 0.8 | b | |
| 126 | 4.6 | a | |
| 127 | 1.9 | b | crack top |
| 128 | 1.8 | a | |
| 129 | 0.05 | b | |
| 130 | 2 | a | crack top |
| 131 | 2.7 | b | |
| 132 | 2 | a | crack top |
| 133 | 1.8 | b | |
| 134 | 4 | a | |
| 135 | 0.05 | b | |
| 136 | 4.1 | a | |
| 137 | 2.1 | b | |
| 138 | 4 | a | |
| 139 | 2.7 | b | |
| 140 | 2.5 | a | |
| 141 | 0.05 | b | |
| 142 | 2.9 | a | |
| 143 | 2.4 | b | |
| 144 | 5.7 | a | |
| 145 | 1.9 | b | |
| 146 | 1.3 | a | |
| 147 | 0.8 | b | |
| 148 | 1 | a | |
| 149 | 0.5 | b | |
| 150 | 1.3 | a | |
| 151 | 0.2 | b | |
| 152 | 1 | a | |
| 153 | 0.5 | b | |
| 154 | 0.05 | a | |

| Number | cm | Designation | Note |
|---|---|---|---|
| 155 | 4.3 | b | |
| 156 | 3.1 | a | |
| 157 | 2 | b | |
| 158 | 3.2 | a | |
| 159 | 0.2 | b | |
| 160 | 6.7 | a | |
| 161 | 0.05 | b | |
| 162 | 1 | a | |
| 163 | 0.5 | b | |
| 164 | 5.2 | a | |
| 165 | 1.5 | b | |
| 166 | 5.4 | a | |
| 167 | 2.1 | b | |
| 168 | 3.5 | a | |
| 169 | 0.05 | b | |
| 170 | 3.7 | a | |
| 171 | 1 | b | |
| 172 | 2.4 | a | |
| 173 | 0.05 | b | |
| 174 | 2.9 | a | |
| 175 | 4.3 | b | |
| 176 | 5.5 | a | |
| 177 | 1.5 | b | |
| 178 | 6 | a | |
| 179 | 2.3 | b | |
| 180 | 2.8 | a | |
| 181 | 2.5 | b | |
| 182 | 4.5 | a | |
| 183 | 5 | b | |
| 184 | 2.5 | a | |
| TOTAL | 429.85 | | |

**Notes:**

Argillaceous beds indicated by high degree of weathering and calcrete with b-type still present and measurable.

Weathered sections changed to crack .05 to maintain pattern for analysis.

Crack top indicates separation of bedding plane and calcrete in-fill.

Ghaap Plateau 3

| Number | cm | Designation | Note |
|---|---|---|---|
| 1 | 1.2 | a | 4.5 fans below |
| 2 | 0.8 | b | |
| 3 | 1.5 | a | |
| 4 | 0.05 | b | |
| 5 | 6.8 | a | |
| 6 | 3 | b | |
| 7 | 0.05 | a | |
| 8 | 2.8 | b | |
| 9 | 1.2 | a | |
| 10 | 0.7 | b | |
| 11 | 1.2 | a | |
| 12 | 2.4 | b | crack top |
| 13 | 0.7 | a | |
| 14 | 2.3 | b | |
| 15 | 1.7 | a | |
| 16 | 0.05 | b | |
| 17 | 2.3 | a | |
| 18 | 6.2 | b | crack top |
| 19 | 2.9 | a | |
| 20 | 0.2 | b | |
| 21 | 1.2 | a | lateral pinch-out |
| 22 | 0.7 | b | |
| 23 | 3.8 | a | |
| 24 | 0.05 | b | |
| 25 | 2.5 | a | |
| 26 | 0.05 | b | |
| 27 | 1.5 | a | |
| 28 | 2.5 | b | |
| 29 | 0.3 | a | |
| 30 | 0.7 | b | |
| 31 | 0.7 | a | |
| 32 | 0.9 | b | |
| 33 | 2.6 | a | crack top |
| 34 | 1.6 | b | |
| 35 | 0.05 | a | |
| 36 | 4.1 | b | undulose top |
| 37 | 2.7 | a | |

| Number | cm | Designation | Note |
|---|---|---|---|
| 38 | 0.6 | b | |
| 39 | 0.7 | a | |
| 40 | 6.2 | b | tufted mat surface |
| 41 | 3.3 | a | |
| 42 | 0.3 | b | |
| 43 | 0.5 | a | |
| 44 | 0.5 | b | |
| 45 | 0.3 | a | |
| 46 | 3.4 | b | |
| 47 | 2.2 | a | |
| 48 | 0.2 | b | |
| 49 | 2.9 | a | |
| 50 | 0.05 | b | |
| 51 | 1.1 | a | |
| 52 | 0.9 | b | |
| 53 | 1.6 | a | |
| 54 | 1 | b | |
| 55 | 2.2 | a | |
| 56 | 0.6 | b | |
| 57 | 1.3 | a | |
| 58 | 0.7 | b | |
| 59 | 1.7 | a | |
| 60 | 0.05 | b | |
| 61 | 4.7 | a | |
| 62 | 0.7 | b | |
| 63 | 6 | a | |
| 64 | 1.6 | b | |
| 65 | 4.5 | a | |
| 66 | 0.05 | b | |
| 67 | 2 | a | |
| 68 | 0.05 | b | |
| 69 | 1.7 | a | |
| 70 | 0.3 | b | |
| 71 | 2.1 | a | |
| 72 | 0.2 | b | |
| 73 | 2.7 | a | |
| 74 | 0.3 | b | |
| 75 | 2.5 | a | |
| 76 | 0.5 | b | |

| Number | cm | Designation | Note |
|---|---|---|---|
| 77 | 2 | a | |
| 78 | 0.05 | b | |
| 79 | 1.7 | a | |
| 80 | 0.3 | b | |
| 81 | 2.1 | a | |
| 82 | 0.2 | b | |
| 83 | 2.7 | a | |
| 84 | 0.3 | b | |
| 85 | 2.5 | a | |
| 86 | 0.5 | b | |
| 87 | 2 | a | |
| 88 | 0.05 | b | |
| 89 | 1.7 | a | |
| 90 | 0.3 | b | |
| 91 | 1.5 | a | |
| 92 | 0.7 | b | |
| 93 | 1.4 | a | |
| 94 | 0.1 | b | |
| 95 | 1.4 | a | |
| 96 | 0.1 | b | |
| 97 | 1.6 | a | |
| 98 | 0.3 | b | |
| 99 | 2.4 | a | |
| 100 | 0.05 | b | |
| 101 | 0.7 | a | |
| 102 | 0.05 | b | |
| 103 | 1.2 | a | |
| 104 | 0.05 | b | |
| 105 | 0.5 | a | |
| 106 | 0.05 | b | |
| 107 | 1.9 | a | |
| 108 | 0.05 | b | |
| 109 | 2.2 | a | |
| 110 | 1.5 | b | |
| 111 | 0.6 | a | crack top |
| 112 | 0.05 | b | |
| 113 | 0.6 | a | |
| 114 | 1.1 | b | |
| 115 | 0.9 | a | |

| Number | cm | Designation | Note |
|---|---|---|---|
| 116 | 0.05 | b | |
| 117 | 1.8 | a | |
| 118 | 0.05 | b | |
| 119 | 1.3 | a | |
| 120 | 0.3 | b | |
| 121 | 1 | a | |
| 122 | 0.05 | b | |
| 123 | 0.5 | a | |
| 124 | 0.05 | b | |
| 125 | 6.5 | a | |
| 126 | 0.05 | b | |
| 127 | 6.7 | a | |
| 128 | 3 | b | |
| 129 | 2.7 | a | |
| 130 | 0.05 | b | |
| 131 | 1.4 | a | |
| 132 | 1.6 | b | |
| 133 | 1 | a | |
| 134 | 0.4 | b | |
| 135 | 5 | a | |
| 136 | 3.1 | b | |
| 137 | 1.9 | a | |
| 138 | 0.05 | b | |
| 139 | 1.6 | a | |
| 140 | 1.4 | b | |
| 141 | 5.9 | a | |
| 142 | 0.5 | b | |
| 143 | 3.6 | a | |
| 144 | 2.9 | b | |
| 145 | 0.5 | a | |
| 146 | 2 | b | |
| 147 | 2.9 | a | |
| 148 | 1.3 | b | |
| 149 | 2.4 | a | |
| 150 | 0.05 | b | |
| 151 | 2.1 | a | |
| 152 | 2.2 | b | |
| 153 | 4.2 | a | |
| 154 | 1.5 | b | |

| Number | cm | Designation | Note |
|---|---|---|---|
| 155 | 3.8 | a | |
| 156 | 1.5 | b | |
| 157 | 1.7 | a | |
| 158 | 1.5 | b | |
| 159 | 2 | a | |
| 160 | 1.8 | b | crack top |
| 161 | 1.2 | a | |
| 162 | 7.4 | b | crack top |
| 163 | 0.7 | a | |
| 164 | 0.6 | b | |
| 165 | 1.3 | a | |
| 166 | 0.05 | b | |
| 167 | 3.5 | a | |
| 168 | 2.8 | b | |
| 169 | 1.6 | a | |
| 170 | 1.9 | b | crack top |
| 171 | 0.4 | a | |
| 172 | 2.2 | b | |
| 173 | 2.4 | a | |
| 174 | 3.2 | b | crack top |
| 175 | 3.4 | a | |
| 176 | 3.7 | b | crack top |
| 177 | 2.8 | a | |
| 178 | 3.6 | b | |
| 179 | 2.4 | a | |
| 180 | 0.05 | b | |
| 181 | 0.9 | a | |
| 182 | 0.05 | b | |
| 183 | 3.4 | a | |
| 184 | 2.3 | b | crack top |
| 185 | 2.8 | a | |
| 186 | 1.1 | b | |
| 187 | 1.5 | a | |
| 188 | 2.2 | b | crack top |
| 189 | 7.1 | a | |
| 190 | 2.2 | b | crack top |
| 191 | 4.2 | a | |
| 192 | 2.5 | b | crack top |
| 193 | 2.2 | a | |

| Number | cm | Designation | Note |
|---|---|---|---|
| 194 | 8.4 | b | crack top |
| 195 | 3.9 | a | |
| 196 | 3.9 | b | crack top |
| 197 | 1.4 | a | |
| 198 | 0.7 | b | |
| 199 | 1.2 | a | |
| 200 | 5.8 | b | |
| 201 | 7 | a | |
| 202 | 1.2 | b | crack top |
| 203 | 1.9 | a | |
| 204 | 0.05 | b | |
| 205 | 2.3 | a | |
| 206 | 3 | b | |
| 207 | 3.9 | a | |
| 208 | 5 | b | |
| 209 | 1 | a | |
| 210 | 3.6 | b | crack top |
| 211 | 1 | a | |
| 212 | 7.5 | b | |
| 213 | 0.05 | a | |
| 214 | 3 | b | |
| 215 | 0.05 | a | |
| 216 | 2 | b | |
| 217 | 0.05 | a | |
| 218 | 13.5 | b | |
| 219 | 3 | a | |
| 220 | 5.2 | b | |
| 221 | 0.05 | a | |
| 222 | 5.5 | b | |
| 223 | 0.05 | a | |
| 224 | 16 | b | argillaceous |
| 225 | 1.6 | a | |
| 226 | 1 | b | |
| 227 | 2.7 | a | |
| 228 | 2.5 | b | |
| 229 | 3 | a | |
| 230 | 1.2 | b | |
| 231 | 1 | a | |
| 232 | 1.5 | b | |

| Number | cm | Designation | Note |
|---|---|---|---|
| 233 | 2.7 | a | |
| 234 | 0.05 | b | |
| 235 | 4 | a | |
| 236 | 0.05 | b | |
| 237 | 1 | a | |
| 238 | 0.05 | b | |
| 239 | 1 | a | |
| 240 | 0.05 | b | |
| 241 | 0.9 | a | |
| 242 | 3 | b | |
| 243 | 3.6 | a | |
| 244 | 1.2 | b | |
| 245 | 2.9 | a | |
| 246 | 1 | b | |
| 247 | 4 | a | |
| 248 | 3.7 | b | argillaceous |
| 249 | .05 | a | argillaceous |
| 250 | 4.1 | b | argillaceous |
| 251 | .05 | a | argillaceous |
| 252 | 4.5 | b | argillaceous |
| 253 | .05 | a | argillaceous |
| 254 | 6.3 | b | argillaceous |
| 255 | .05 | a | argillaceous |
| 256 | 2.1 | b | argillaceous |
| 257 | .05 | a | argillaceous |
| 258 | 3.8 | b | argillaceous |
| 259 | .05 | a | argillaceous |
| 260 | 3.9 | b | argillaceous |
| 261 | .05 | a | argillaceous |
| 262 | 4.8 | b | argillaceous |
| 263 | .05 | a | argillaceous |
| 264 | 3.9 | b | argillaceous |
| 265 | .05 | a | argillaceous |
| 266 | 5.2 | b | argillaceous |
| 267 | .05 | a | argillaceous |
| 268 | 4.9 | b | argillaceous |
| 269 | .05 | a | argillaceous |
| 270 | 5.3 | b | argillaceous |
| 271 | 3.1 | a | |

| Number | cm | Designation | Note |
|---|---|---|---|
| 272 | 0.05 | b | |
| 273 | 1.6 | a | |
| 274 | 0.05 | b | |
| 275 | 2.4 | a | |
| 276 | 0.05 | b | |
| 277 | 6.2 | a | |
| 278 | 1.9 | b | |
| 279 | 5.1 | a | |
| 280 | 1.5 | b | |
| 281 | 3.1 | a | |
| 282 | 2.2 | b | |
| 283 | 5.2 | a | |
| 284 | 2.4 | b | |
| 285 | 6.5 | a | |
| 286 | 0.05 | b | |
| 287 | 1.7 | a | |
| 288 | 0.05 | b | |
| 289 | 1.7 | a | |
| 290 | 0.05 | b | |
| 291 | 1.4 | a | |
| 292 | 1.8 | b | |
| 293 | 2.6 | a | |
| 294 | 1.4 | b | |
| 295 | 1 | a | |
| 296 | 0.05 | b | |
| 297 | 0.8 | a | |
| 298 | 1.4 | b | |
| 299 | 2.8 | a | |
| 300 | 0.05 | b | |
| 301 | 2.1 | a | |
| 302 | 1.4 | b | |
| 303 | 4 | a | |
| 304 | 4.4 | b | |
| 305 | 2.1 | a | |
| 306 | 2 | b | |
| 307 | 5.4 | a | |
| 308 | 1.7 | b | crack top |
| 309 | 4.4 | a | |
| 310 | 4.1 | b | |

| Number | cm | Designation | Note |
|---|---|---|---|
| 311 | 2.6 | a | |
| 312 | 3.2 | b | |
| 313 | 3.7 | a | crack top |
| 314 | 1.6 | b | |
| 315 | 2.9 | a | |
| 316 | 2.4 | b | |
| 317 | 1.6 | a | |
| 318 | 2 | b | |
| 319 | 2.6 | a | |
| 320 | 1.6 | b | |
| 321 | 3.2 | a | |
| 322 | 2.1 | b | |
| 323 | 3.6 | a | |
| 324 | 2.7 | b | crack top |
| 325 | 3.6 | a | |
| 326 | 0.05 | b | |
| 327 | 1 | a | |
| 328 | 1 | b | |
| 329 | 0.7 | a | |
| 330 | 1.6 | b | |
| 331 | 5.1 | a | |
| 332 | 4.2 | b | crack top |
| 333 | 4.1 | a | crack top |
| 334 | 4.2 | b | crack top |
| 335 | 2.1 | a | |
| 336 | 2.2 | b | |
| 337 | 2.7 | a | |
| 338 | 0.6 | b | |
| 339 | 1.4 | a | |
| 340 | 0.7 | b | |
| 341 | 1.6 | a | |
| 342 | 1 | b | |
| 343 | 1.2 | a | |
| 344 | 2.4 | b | |
| 345 | 1.6 | a | |
| 346 | 4.2 | b | crack top |
| 347 | 3.1 | a | |
| 348 | 3.3 | b | crack top |
| 349 | 4.8 | a | |

| Number | cm | Designation | Note |
|---|---|---|---|
| 350 | 2.6 | b | |
| 351 | 5.1 | a | |
| 352 | 3.6 | b | |
| 353 | 3.7 | a | |
| 354 | 2.4 | b | |
| 355 | 3.6 | a | |
| 356 | 3.1 | b | |
| 357 | 2.4 | a | |
| 358 | 0.7 | b | |
| 359 | 6.4 | a | |
| 360 | 0.3 | b | |
| 361 | 5.7 | a | |
| 362 | 2.6 | b | |
| 363 | 0.9 | a | |
| 364 | 5.7 | b | |
| 365 | 0.05 | a | |
| 366 | 2 | b | FANS present |
| 367 | 5.2 | a | FANS present |
| 368 | 1.9 | b | FANS present |
| 369 | 1 | a | FANS present |
| 370 | 2.1 | b | FANS present |
| 371 | 2.2 | a | FANS present |
| 372 | 1.8 | b | FANS present |
| 373 | 3.3 | a | FANS present |
| 374 | 2.1 | b | FANS present |
| 375 | 1.9 | a | FANS present |
| 376 | 2.6 | b | FANS present |
| 377 | 2.1 | a | FANS present |
| 378 | 2.9 | b | FANS present |
| TOTAL | 795.35 | | |

**Notes:**
Argillaceous beds indicated by high degree of weathering and calcrete with b-type still present and measurable.

Weathered beds changed to crack .05 to maintain pattern for analysis.

Crack top indicates separation of bedding plane and calcrete in-fill.

FANS present in adjacent bedding planes, not where measured.

Ghaap Plateau 4

| Number | cm | Designation | Note |
|---|---|---|---|
| 1 | 8.4 | a | FANS |
| 2 | 3 | b | |
| 3 | 1.1 | a | |
| 4 | 1 | b | |
| 5 | 1.5 | a | |
| 6 | 1.4 | b | |
| 7 | 1.2 | a | |
| 8 | 1.9 | b | |
| 9 | 3.1 | a | |
| 10 | 4.6 | b | |
| 11 | 1.8 | a | crack top |
| 12 | 2 | b | |
| 13 | 1.7 | a | |
| 14 | 1.9 | b | |
| 15 | 0.04 | a | |
| 16 | 1.9 | b | |
| 17 | 1.6 | a | |
| 18 | 1.7 | b | |
| 19 | 2.1 | a | |
| 20 | 2.6 | b | |
| 21 | 2.5 | a | |
| 22 | 2 | b | |
| 23 | 2.6 | a | |
| 24 | 5.1 | b | |
| 25 | 0.9 | a | |
| 26 | 1.9 | b | |
| 27 | 2.3 | a | crack top |
| 28 | 2.1 | b | |
| 29 | 1.9 | a | |
| 30 | 1.7 | b | |
| 31 | 2.4 | a | crack top |
| 32 | 1.6 | b | |
| 33 | 3.9 | a | |
| 34 | 1.5 | b | |
| 35 | 1.9 | a | |
| 36 | 2.2 | b | |
| 37 | 3.4 | a | |

| Number | cm | Designation | Note |
|---|---|---|---|
| 38 | 4.5 | b | |
| 39 | 1.4 | a | |
| 40 | 7.4 | b | |
| 41 | 1.2 | a | |
| 42 | 2.4 | b | |
| 43 | 2 | a | |
| 44 | 2.9 | b | crack top |
| 45 | 0.6 | a | |
| 46 | 0.05 | b | crack top |
| 47 | 0.04 | a | |
| 48 | 3.3 | b | crack top |
| 49 | 2 | a | |
| 50 | 0.6 | b | |
| 51 | 2.6 | a | |
| 52 | 2 | a | |
| 53 | 0.6 | b | |
| 54 | 2.6 | a | |
| 55 | 1.2 | b | |
| 56 | 0.9 | a | |
| 57 | 3 | b | |
| 58 | 3.9 | a | |
| 59 | 3.9 | b | |
| 60 | 2.9 | a | |
| 61 | 2.9 | b | crack top |
| 62 | 1.8 | a | |
| 63 | 5.7 | b | crack top |
| 64 | 0.8 | a | |
| 65 | 3.4 | b | |
| 66 | 2.7 | a | |
| 67 | 4.2 | b | crack top |
| 68 | 1.1 | a | |
| 69 | 0.05 | b | crack top |
| 70 | 1.6 | a | |
| 71 | 1.4 | b | |
| 72 | 1.6 | a | |
| 73 | 3.2 | b | crack top |
| 74 | 3.2 | a | |
| 75 | 1.1 | b | |
| 76 | 0.9 | a | |

| Number | cm | Designation | Note |
|---|---|---|---|
| 77 | 0.05 | b | crack top |
| 78 | 1.1 | a | |
| 79 | 3.1 | b | |
| 80 | 2.5 | a | crack top |
| 81 | 5 | b | crack top |
| 82 | 3.2 | a | |
| 83 | 3.4 | b | |
| 84 | 2.4 | a | |
| 85 | 1.8 | b | |
| 86 | 1.9 | a | crack top |
| 87 | 2.4 | b | |
| 88 | 2.2 | a | crack top |
| 89 | 1 | b | |
| 90 | 1.4 | a | |
| 91 | 1.3 | b | |
| 92 | 1.2 | a | |
| 93 | 4.3 | b | crack top |
| 94 | 1.6 | a | |
| 95 | 5.6 | b | crack top |
| 96 | 1.7 | a | |
| 97 | 3.1 | b | |
| 98 | 4 | a | crack top |
| 99 | 1.3 | b | |
| 100 | 2.1 | a | |
| 101 | 3.2 | b | |
| 102 | 0.8 | a | crack top |
| 103 | 0.05 | b | crack top |
| 104 | 0.8 | a | |
| 105 | 1.5 | b | |
| 106 | 0.7 | a | |
| 107 | 1.4 | b | crack top |
| 108 | 1.9 | a | |
| 109 | 2.5 | b | |
| 110 | 1.1 | a | |
| 111 | 1.9 | b | |
| 112 | 2.1 | a | |
| 113 | 3.1 | b | |
| 114 | 0.9 | a | |
| 115 | 2.6 | b | |

| Number | cm | Designation | Note |
|---|---|---|---|
| 116 | 1.8 | a | crack top |
| 117 | 2.7 | b | |
| 118 | 2.6 | a | |
| 119 | 3.3 | b | |
| 120 | 1.5 | a | crack top |
| 121 | 1.4 | b | |
| 122 | 2.8 | a | crack top |
| 123 | 1.6 | b | |
| 124 | 3.9 | a | |
| 125 | 2.1 | b | |
| 126 | 148 | traver. cover | chg to a-crack |
| 127 | 11 | traver. cover | chg to b-crack |
| 128 | 1 | b | |
| 129 | 1.5 | a | |
| 130 | 0.6 | b | |
| 131 | 2 | a | |
| 132 | 1.7 | b | |
| 133 | 1 | a | |
| 134 | 3.5 | b | |
| 135 | 8 | weathered | chg to a-crack |
| 136 | 2 | b | crack top |
| 137 | 2.5 | a | |
| 138 | 2 | b | |
| 139 | 1.2 | a | |
| 140 | 1 | b | |
| 141 | 2.5 | a | |
| 142 | 0.05 | b | crack top |
| 143 | 1.6 | a | |
| 144 | 2 | b | |
| 145 | 0.7 | a | |
| 146 | 1.5 | b | |
| 147 | 0.3 | a | |
| 148 | 2.1 | b | |
| 149 | 0.2 | a | |
| 150 | 2.5 | b | |
| 151 | 2 | a | |
| 152 | 0.5 | b | |
| 153 | 2 | a | |
| 154 | 5 | b | crack top |

| Number | cm | Designation | Note |
|---|---|---|---|
| 155 | 1 | a | |
| 156 | 0.5 | b | |
| 157 | 1.7 | a | |
| 158 | 0.5 | b | |
| 159 | 1.5 | a | |
| 160 | 1.2 | b | |
| 161 | 2.5 | a | |
| 162 | 0.9 | b | |
| 163 | 3.7 | a | |
| 164 | 0.5 | b | |
| 165 | 1.6 | a | |
| 166 | 1.5 | b | |
| 167 | 1 | a | |
| 168 | 0.7 | b | |
| 169 | 0.9 | a | |
| 170 | 2.6 | b | crack top |
| 171 | 1 | a | |
| 172 | 2.9 | b | |
| 173 | 0.05 | a | |
| 174 | 1.5 | b | |
| 175 | 1 | a | |
| 176 | 2 | b | |
| 177 | 1 | a | |
| 178 | 0.5 | b | |
| 179 | 1 | a | |
| 180 | 5.3 | b | |
| 181 | 4.5 | a | FANS small |
| 182 | .05 | b | |
| TOTAL | 531.03 | | |

**Notes:**

Argillaceous beds indicated by high degree of weathering and calcrete with b-type still present and measurable.

Weathered/ traver. cover beds changed to crack .05 to maintain pattern for analysis.

Crack top indicates separation of bedding plane and calcrete in-fill.

Lower Prieska 1

| Number | cm | Designation | Note |
|---|---|---|---|
| 1 | 56 | tuff | chg to a-crack |
| 2 | 3 | b | |
| 3 | 4.5 | a | |
| 4 | 0.05 | b | crack |
| 5 | 2 | a | |
| 6 | 0.6 | b | |
| 7 | 1 | a | |
| 8 | 0.05 | b | crack |
| 9 | 1.4 | a | |
| 10 | 0.3 | b | |
| 11 | 1.2 | a | |
| 12 | 1.2 | b | |
| 13 | 2.5 | a | |
| 14 | 0.9 | b | |
| 15 | 1.9 | a | |
| 16 | 1 | b | |
| 17 | 1.5 | a | |
| 18 | 1.5 | b | |
| 19 | 3.5 | a | |
| 20 | 0.4 | b | |
| 21 | 2.2 | a | |
| 22 | 0.5 | b | |
| 23 | 1.2 | a | |
| 24 | 0.9 | b | |
| 25 | 4.5 | a | |
| 26 | 0.9 | b | |
| 27 | 3.5 | a | |
| 28 | 0.9 | b | |
| 29 | 0.9 | a | |
| 30 | 0.05 | b | crack |
| 31 | 0.9 | a | |
| 32 | 0.3 | b | |
| 33 | 0.5 | a | |
| 34 | 0.3 | b | |
| 35 | 0.6 | a | |
| 36 | 0.5 | b | |
| 37 | 2.8 | a | |

| Number | cm | Designation | Note |
|---|---|---|---|
| 38 | 0.05 | b | |
| 39 | 1.1 | a | |
| 40 | 0.5 | b | |
| 41 | 1 | a | |
| 42 | 0.2 | b | |
| 43 | 1.2 | a | |
| 44 | 0.3 | b | |
| 45 | 0.5 | a | |
| 46 | 0.3 | b | |
| 47 | 0.5 | a | |
| 48 | 0.2 | b | |
| 49 | 0.6 | a | |
| 50 | 0.5 | b | |
| 51 | 3 | a | |
| 52 | 0.8 | b | |
| 53 | 0.5 | a | |
| 54 | 0.6 | b | |
| 55 | 2.6 | a | |
| 56 | 0.05 | b | crack |
| 57 | 1.1 | a | |
| 58 | 0.3 | b | |
| 59 | 1 | a | |
| 60 | 0.4 | b | |
| 61 | 0.9 | a | |
| 62 | 0.4 | b | |
| 63 | 1.4 | a | |
| 64 | 0.5 | b | |
| 65 | 1.2 | a | |
| 66 | 0.5 | b | |
| 67 | 1.9 | a | |
| 68 | 1.4 | b | |
| 69 | 1.5 | a | |
| 70 | 0.9 | b | |
| 71 | 1.9 | a | |
| 72 | 7.5 | weathered | chg to b-crack |
| 73 | 2.2 | a | |
| 74 | 2.1 | weathered | chg to b-crack |
| 75 | 2.2 | a | |
| 76 | 2 | weathered | chg to b-crack |

| Number | cm | Designation | Note |
|---|---|---|---|
| 77 | 1.3 | purple | excluded |
| 78 | 12 | weathered | excluded |
| 79 | 1 | a | |
| 80 | 1 | weathered | chg to b-crack |
| 81 | 1.7 | a | |
| 82 | 2 | weathered | chg to b-crack |
| 83 | 2.6 | a | |
| 84 | 0.05 | b | crack |
| 85 | 1 | a | |
| 86 | 1.1 | b | |
| 87 | 4.4 | a | |
| 88 | 1.1 | b | |
| 89 | 1 | a | |
| 90 | 1.1 | b | |
| 91 | 1 | a | |
| 92 | 0.9 | b | |
| 93 | 1.8 | a | |
| 94 | 0.6 | b | |
| 95 | 0.7 | a | |
| 96 | 0.6 | b | |
| 97 | 0.5 | a | |
| 98 | 0.05 | b | crack |
| 99 | 1.1 | a | |
| 100 | 0.05 | b | crack |
| 101 | 0.9 | a | |
| 102 | 0.7 | b | |
| 103 | 2.2 | a | |
| 104 | 0.05 | b | crack |
| 105 | 2.2 | a | |
| 106 | 8.6 | weathered | chg to b-crack |
| 107 | 0.5 | purple layer | excluded |
| 108 | 1 | a | |
| 109 | 0.05 | b | crack |
| 110 | 2.2 | a | |
| 111 | 0.5 | b | |
| 112 | 0.7 | a | |
| 113 | 1 | b | |
| 114 | 0.9 | a | |
| 115 | 0.05 | b | crack |

| Number | cm | Designation | Note |
|---|---|---|---|
| 116 | 1 | a | |
| 117 | 0.05 | b | crack |
| 118 | 1.1 | a | |
| 119 | 0.05 | b | crack |
| 120 | 0.5 | a | |
| 121 | 0.05 | b | crack |
| 122 | 2.1 | a | |
| 123 | 0.5 | b | |
| 124 | 0.9 | a | |
| 125 | 7 | weathered | chg to b-crack |
| 126 | 5.2 | tuff | chg to a-crack |
| 127 | 3.5 | tuff pt2 | excluded, MLT |
| 128 | 8 | tuff pt3 | excluded, MLT |
| 129 | 5.9 | tuff pt4 | excluded, MLT |
| 130 | 26.4 | weathered | excluded |
| 131 | 0.5 | b | |
| 132 | 3 | a | |
| 133 | 2.8 | b | undulose |
| 134 | 4.2 | a | |
| 135 | 3 | weathered | chg to b-crack |
| 136 | 2.9 | a | |
| 137 | 0.05 | b | crack |
| 138 | 3 | a | |
| 139 | 4 | b | |
| 140 | 3.2 | a | |
| 141 | 4.9 | weathered | chg to b-crack |
| 142 | 2.5 | a | |
| 143 | 4.6 | b | |
| 144 | 2.8 | a | |
| 145 | 0.05 | b | crack |
| 146 | 0.9 | a | |
| 147 | 0.05 | b | crack |
| 148 | 1.9 | a | |
| 149 | 1 | b | |
| 150 | 3.6 | a | |
| 151 | 0.05 | b | crack |
| 152 | 2.2 | a | |
| 153 | 0.05 | b | crack |
| 154 | 3 | a | |

| Number | cm | Designation | Note |
|---|---|---|---|
| 155 | 0.05 | b | crack |
| 156 | 2.2 | a | |
| 157 | 0.05 | b | crack |
| 158 | 0.9 | a | |
| 159 | 0.05 | b | crack |
| 160 | 6 | a | |
| 161 | 0.05 | b | crack |
| 162 | 5.3 | a | |
| 163 | 0.5 | b | crack |
| 164 | 0.8 | a | |
| 165 | 0.05 | b | crack |
| 166 | 2.8 | a | |
| 167 | 0.05 | b | crack |
| 168 | 1 | a | |
| 169 | 0.05 | b | crack |
| 170 | 0.9 | a | |
| 171 | 0.2 | b | |
| 172 | 2.8 | a | |
| 173 | 0.05 | b | crack |
| 174 | 9.6 | weathered | chg to a-crack |
| 175 | 4.4 | xmas | chg to b |
| 176 | 3.1 | weathered | excluded |
| 177 | 2.9 | a | |
| 178 | 4.2 | weathered | chg to b-crack |
| 179 | 1.7 | a | |
| 180 | 1.2 | weathered | chg to b-crack |
| 181 | 2.5 | a | |
| 182 | 1.4 | weathered | chg to b-crack |
| 183 | 4.3 | a | |
| 184 | 0.7 | b | |
| 185 | 4.2 | a | |
| 186 | 0.2 | b | |
| 187 | 1.5 | a | |
| 188 | 0.4 | b | |
| 189 | 0.8 | a | |
| 190 | 0.3 | b | |
| 191 | 0.7 | a | |
| 192 | 0.3 | b | |
| 193 | 0.5 | a | |

| Number | cm | Designation | Note |
|---|---|---|---|
| 194 | 0.2 | b | |
| 195 | 2.2 | a | |
| 196 | 0.05 | b | crack |
| 197 | 0.6 | a | |
| 198 | 0.1 | b | |
| 199 | 0.7 | a | |
| 200 | 0.1 | b | |
| 201 | 1.9 | a | |
| 202 | 0.8 | b | |
| 203 | 0.9 | a | |
| 204 | 0.05 | b | crack |
| 205 | 1.2 | a | |
| 206 | 0.05 | b | crack |
| 207 | 0.7 | a | |
| 208 | 1.5 | b | |
| 209 | 4 | a | |
| 210 | 0.3 | b | |
| 211 | 1.3 | a | |
| 212 | 1.4 | b | |
| 213 | 2.9 | a | |
| 214 | 0.3 | b | |
| 215 | 5.1 | a | |
| 216 | 0.05 | b | crack |
| 217 | 5 | a | |
| 218 | 0.2 | b | |
| 219 | 3.9 | a | |
| 220 | 0.05 | b | crack |
| 221 | 0.7 | a | |
| 222 | 0.1 | b | |
| 223 | 0.9 | a | |
| 224 | 0.05 | b | crack |
| 225 | 0.4 | a | |
| 226 | 1 | b | |
| 227 | 1.2 | a | |
| 228 | 0.4 | b | |
| 229 | 0.4 | a | |
| 230 | 0.7 | b | |
| 231 | 9.4 | a | |
| 232 | 0.3 | b | |

| Number | cm | Designation | Note |
|---|---|---|---|
| 233 | 2.4 | a | |
| 234 | 0.05 | b | crack |
| 235 | 3.8 | a | |
| 236 | 0.4 | b | |
| 237 | 2.7 | a | |
| 238 | 0.4 | b | |
| 239 | 1.6 | a | |
| 240 | 0.6 | b | |
| 241 | 3.9 | a | |
| 242 | 0.5 | b | |
| 243 | 2.1 | a | |
| 244 | 1.6 | b | |
| 245 | 1.2 | a | |
| 246 | 0.9 | b | |
| 247 | 3.9 | a | |
| 248 | 0.8 | b | |
| 249 | 2.5 | a | |
| 250 | 0.05 | b | crack |
| 251 | 1.1 | a | |
| 252 | 0.05 | b | crack |
| 253 | 5.3 | a | |
| 254 | 0.05 | b | crack |
| 255 | 4.3 | a | |
| 256 | 0.6 | b | |
| 257 | 2.7 | a | |
| 258 | 1 | b | |
| 259 | 5.8 | a | |
| 260 | 0.7 | b | |
| 261 | 2.1 | a | |
| 262 | 0.4 | b | |
| 263 | 0.9 | a | |
| 264 | 0.4 | b | |
| 265 | 1.1 | a | |
| 266 | 0.1 | b | |
| 267 | 2.4 | a | |
| 268 | 0.05 | b | crack |
| 269 | 7.2 | a | |
| 270 | 12.3 | weathered | chg to b-crack |
| 271 | 4.4 | a | |

| Number | cm | Designation | Note |
|---|---|---|---|
| 272 | 1 | b | |
| 273 | 8.7 | a | |
| 274 | 3.4 | b | |
| 275 | 4.5 | a | |
| 276 | 0.5 | b | |
| 277 | 4.2 | a | |
| 278 | 10.4 | b | |
| 279 | 10.5 | a | |
| 280 | 0.9 | b | |
| 281 | 3.6 | a | |
| 282 | 2 | b | |
| 283 | 3.1 | a | |
| 284 | 3.4 | b | |
| 285 | 2.1 | a | |
| 286 | 1.3 | b | |
| 287 | 1.9 | a | |
| 288 | 0.1 | b | |
| 289 | 2.4 | a | |
| 290 | 0.1 | b | |
| 291 | 0.7 | a | |
| 292 | 0.5 | b | |
| 293 | 3.5 | a | |
| 294 | 1 | b | |
| 295 | 4.3 | a | |
| 296 | 1.5 | b | |
| 297 | 5.3 | a | |
| 298 | 3.6 | b | |
| 299 | 5.6 | a | |
| 300 | 0.05 | b | crack |
| 301 | 1.1 | a | |
| 302 | 1.5 | b | |
| 303 | 2.7 | a | |
| 304 | 0.05 | b | crack |
| 305 | 4.2 | a | |
| 306 | 2 | b | |
| 307 | 6.2 | a | |
| 308 | 0.05 | b | crack |
| 309 | 4.8 | a | |
| 310 | 1.2 | b | |

| Number | cm | Designation | Note |
|---|---|---|---|
| 311 | 2.3 | a | |
| 312 | 8.2 | b | |
| 313 | 7.2 | a | |
| 314 | 1.4 | b | |
| 315 | 1.9 | tuff | chg to a-crack |
| 316 | 0.2 | purple | excluded |
| 317 | 1.4 | b | |
| 318 | 1.4 | a | |
| 319 | 0.05 | b | crack |
| 320 | 1.9 | a | |
| 321 | 0.05 | b | crack |
| 322 | 2 | a | |
| 323 | 6.8 | b | |
| 324 | 1.7 | a | |
| 325 | 0.05 | b | crack |
| 326 | 4.5 | a | |
| 327 | 0.1 | b | |
| 328 | 0.8 | a | |
| 329 | 0.3 | b | |
| 330 | 1 | a | |
| 331 | 0.1 | b | |
| 332 | 2.4 | a | |
| 333 | 6.8 | b | |
| 334 | 3.2 | a | |
| 335 | 4.1 | b | |
| 336 | 1.2 | a | |
| 337 | 0.9 | b | |
| 338 | 3.2 | a | |
| 339 | 0.05 | b | crack |
| 340 | 2.3 | a | |
| 341 | 0.05 | b | crack |
| 342 | 22.1 | a | |
| 343 | 1.6 | b | |
| 344 | 13.4 | a | |
| 345 | 6.7 | b | |
| 346 | 2.2 | a | |
| 347 | 1.2 | b | |
| 348 | 5.2 | a | |
| 349 | 1.8 | b | |

| Number | cm | Designation | Note |
|---|---|---|---|
| 350 | 12.2 | a | |
| 351 | 1.7 | b | |
| 352 | 2.9 | a | |
| 353 | 3.2 | b | |
| 354 | 65.2 | a | |
| 355 | 0.05 | b | crack |
| 356 | 14.8 | a | |
| 357 | 0.05 | b | crack |
| 358 | 1.4 | a | |
| 359 | 0.05 | b | crack |
| 360 | 9.6 | a | |
| 361 | 0.05 | b | crack |
| 362 | 5.9 | a | |
| 363 | 0.2 | b | |
| 364 | 2.8 | a | |
| 365 | 0.4 | b | |
| 366 | 3.7 | a | |
| 367 | 0.6 | b | |
| 368 | 2.8 | a | |
| 369 | 0.2 | b | |
| 370 | 2.7 | a | |
| 371 | 13.8 | weathered | chg to b-crack |
| 372 | 6.9 | a | |
| 373 | 6 | weathered | chg to b-crack |
| 374 | 2.2 | a | excluded, odd A |
| 375 | 0.1 | tuff | excluded |
| 376 | 130 | weathered | excluded |
| 377 | 31.6 | hummocky | excluded |
| Total | 1087.4 | | |

RELP

| Number | cm | Designation | Note |
|---|---|---|---|
| 1 | 1.5 | a | |
| 2 | 0.3 | b | |
| 3 | 3.7 | a | |
| 4 | 0.5 | b | |
| 5 | 1.1 | a | |
| 6 | 0.1 | b | |
| 7 | 1 | a | |
| 8 | 0.05 | b | crack |
| 9 | 3.2 | a | |
| 10 | 0.05 | b | crack |
| 11 | 2 | a | |
| 12 | 28 | CTS | chg to b |
| 13 | 7.2 | tuff | chg to a-crack |
| 14 | 2.9 | b | |
| 15 | 0.1 | a | |
| 16 | 1.6 | b | |
| 17 | 2.5 | a | |
| 18 | 27 | CTS | chg to b |
| 19 | 2 | a | |
| 20 | 0.5 | b | |
| 21 | 1 | a | |
| 22 | 0.3 | b | |
| 23 | 2 | a | |
| 24 | 11.8 | tuff | chg to b-crack |
| 25 | 1.5 | a | |
| 26 | 0.5 | b | |
| 27 | 1.5 | a | |
| 28 | 0.5 | b | |
| 29 | 2.3 | a | |
| 30 | 0.2 | b | |
| 31 | 1.5 | a | |
| 32 | 0.2 | b | |
| 33 | 1.7 | a | |
| 34 | 8.5 | CTS | chg to b |
| 35 | 2.7 | a | |
| 36 | 2 | b | |
| 37 | 1.5 | a | |

| Number | cm | Designation | Note |
|---|---|---|---|
| 38 | 0.4 | b | |
| 39 | 0.2 | a | |
| 40 | 0.1 | b | |
| 41 | 2.6 | a | |
| 42 | 0.1 | b | |
| 43 | 7.5 | weathered | chg to a-crack |
| 44 | 0.6 | b | |
| 45 | 2.3 | a | |
| 46 | 0.5 | b | |
| 47 | 1.3 | a | |
| 48 | 39.9 | tuff xbeds | chg to b-crack |
| 49 | 5 | a | |
| 50 | 0.1 | b | |
| 51 | 2 | a | |
| 52 | 0.1 | b | |
| 53 | 1 | a | |
| 54 | 0.1 | b | |
| 55 | 1.3 | a | |
| 56 | 0.1 | b | |
| 57 | 0.8 | a | |
| 58 | 0.1 | b | |
| 59 | 1.9 | a | |
| 60 | 0.1 | b | |
| 61 | 1.3 | a | |
| 62 | 0.1 | b | |
| 63 | 1.6 | a | |
| 64 | 0.2 | b | |
| 65 | 0.8 | a | |
| 66 | 0.1 | b | |
| 67 | 1.2 | a | |
| 68 | 0.1 | b | |
| 69 | 1.3 | a | |
| 70 | 0.1 | b | |
| 71 | 1.3 | a | |
| 72 | 0.1 | b | |
| 73 | 0.8 | a | |
| 74 | 0.1 | b | |
| 75 | 0.9 | a | |
| 76 | 0.1 | b | |

| Number | cm | Designation | Note |
|---|---|---|---|
| 77 | 0.4 | a | |
| 78 | 0.1 | b | |
| 79 | 1.1 | a | |
| 80 | 0.1 | b | |
| 81 | 0.9 | a | |
| 82 | 0.1 | b | |
| 83 | 1.3 | a | |
| 84 | 0.1 | b | |
| 85 | 0.4 | a | |
| 86 | 0.5 | b | |
| 87 | 1.5 | a | |
| 88 | 0.1 | b | |
| 89 | 5.1 | a | |
| 90 | 1 | b | |
| 91 | 0.8 | a | |
| 92 | 0.1 | b | |
| 93 | 0.7 | a | |
| 94 | 0.1 | b | |
| 95 | 0.3 | a | |
| 96 | 0.1 | b | |
| 97 | 3 | a | |
| 98 | 1.7 | b | |
| 99 | 2.4 | a | |
| 100 | 1 | b | undulose |
| 101 | 0.5 | a | |
| 102 | 0.2 | b | undulose |
| 103 | 1.9 | a | |
| 104 | 0.1 | b | |
| 105 | 0.3 | a | |
| 106 | 1.8 | b | undulose |
| 107 | 1.6 | a | |
| 108 | 0.2 | b | |
| Total | 232.7 | | |

Lower Prieska 2

| Number | cm | Designation | Note |
|---|---|---|---|
| 1 | 2 | a | |
| 2 | 0.9 | b | |
| 3 | 4 | a | |
| 4 | 0.5 | b | |
| 5 | 0.4 | a | |
| 6 | 0.5 | b | |
| 7 | 1.5 | a | |
| 8 | 0.6 | b | |
| 9 | 3 | a | |
| 10 | 0.5 | b | |
| 11 | 0.9 | a | |
| 12 | 0.05 | b | crack |
| 13 | 1.6 | a | |
| 14 | 0.05 | b | crack |
| 15 | 4.3 | a | |
| 16 | 0.05 | b | crack |
| 17 | 5 | a | |
| 18 | 3 | b | |
| 19 | 2.4 | a | |
| 20 | 0.8 | b | |
| 21 | 2.8 | a | |
| 22 | 1.8 | b | |
| 23 | 3.9 | a | |
| 24 | 0.6 | b | |
| 25 | 1.5 | a | |
| 26 | 0.05 | b | crack |
| 27 | 1.4 | a | |
| 28 | 0.05 | b | crack |
| 29 | 0.8 | a | |
| 30 | 0.4 | b | |
| 31 | 2.2 | a | |
| 32 | 1 | b | |
| 33 | 5.4 | a | |
| 34 | 0.5 | b | |
| 35 | 0.7 | a | |
| 36 | 0.05 | b | crack |
| 37 | 2.5 | a | |

| Number | cm | Designation | Note |
|---|---|---|---|
| 38 | 0.5 | b | |
| 39 | 0.6 | a | |
| 40 | 2.5 | weathered | chg to b-crack |
| 41 | 1 | a | |
| 42 | 0.5 | b | |
| 43 | 0.3 | a | |
| 44 | 0.5 | b | |
| 45 | 0.5 | a | |
| 46 | 0.6 | b | |
| 47 | 2 | a | |
| 48 | 0.9 | b | |
| 49 | 2 | a | |
| 50 | 0.6 | b | |
| 51 | 5.2 | a | |
| 52 | 1 | b | |
| 53 | 3.2 | a | |
| 54 | 0.3 | b | |
| 55 | 3.5 | a | |
| 56 | 0.5 | b | |
| 57 | 2.3 | a | |
| 58 | 0.05 | b | crack |
| 59 | 2.5 | a | |
| 60 | 0.2 | b | |
| 61 | 0.8 | a | |
| 62 | 0.3 | b | |
| 63 | 3.1 | a | |
| 64 | 0.4 | b | |
| 65 | 3 | a | |
| 66 | 0.5 | b | |
| 67 | 21 | tuff | chg to a-crack |
| 68 | 0.05 | purple | excluded |
| 69 | 5 | weathered | chg to b-crack |
| 70 | 3 | a | |
| 71 | 0.05 | b | crack |
| 72 | 4 | a | |
| 73 | 1 | b | |
| 74 | 0.6 | a | |
| 75 | 2.4 | b | |
| 76 | 4 | a | |

| Number | cm | Designation | Note |
|---|---|---|---|
| 77 | 0.1 | b | |
| 78 | 0.5 | a | |
| 79 | 0.05 | b | crack |
| 80 | 2.3 | a | |
| 81 | 0.3 | b | |
| 82 | 4.2 | a | |
| 83 | 0.05 | b | crack |
| 84 | 1.6 | a | |
| 85 | 0.05 | b | crack |
| 86 | 3.2 | a | |
| 87 | 1.3 | b | |
| 88 | 1.9 | a | |
| 89 | 0.7 | b | |
| 90 | 3.8 | a | |
| 91 | 1 | b | |
| 92 | 0.6 | a | |
| 93 | 0.7 | b | |
| 94 | 4.3 | a | |
| 95 | 1 | b | |
| 96 | 1 | a | |
| 97 | 0.5 | b | |
| 98 | 4 | a | |
| 99 | 1 | b | |
| 100 | 1.5 | a | |
| 101 | 1 | b | |
| 102 | 1 | a | |
| 103 | 1.2 | b | |
| 104 | 3 | a | |
| 105 | 1.5 | b | |
| 106 | 3.5 | a | |
| 107 | 0.9 | b | |
| 108 | 2.7 | a | |
| 109 | 0.5 | b | |
| 110 | 2.2 | a | |
| 111 | 0.05 | b | crack |
| 112 | 2.7 | a | |
| 113 | 1.8 | b | |
| 114 | 1 | a | |
| 115 | 3 | b | |

| Number | cm | Designation | Note |
|---|---|---|---|
| 116 | 2 | a | |
| 117 | 0.6 | b | |
| 118 | 2.7 | a | |
| 119 | 0.6 | b | |
| 120 | 2 | a | |
| 121 | 2.2 | b | |
| 122 | 2.6 | a | |
| 123 | 1.1 | b | |
| 124 | 2 | a | |
| 125 | 1.3 | b | |
| 126 | 2 | a | |
| 127 | 2.4 | b | |
| 128 | 3.7 | a | |
| 129 | 1.2 | b | |
| 130 | 5.6 | a | |
| 131 | 2 | b | |
| 132 | 4.5 | a | |
| 133 | 2.5 | b | |
| 134 | 5.5 | a | |
| 135 | 1.5 | b | |
| 136 | 2.8 | a | |
| 137 | 2.6 | b | |
| 138 | 1.5 | a | |
| 139 | 0.6 | b | |
| 140 | 5 | a | |
| 141 | 3 | b | |
| 142 | 7.5 | a | |
| 143 | 1.4 | b | |
| 144 | 4 | a | |
| 145 | 1 | b | |
| 146 | 2.3 | a | |
| 147 | 1.3 | b | |
| 148 | 3 | a | |
| 149 | 0.6 | b | |
| 150 | 1.5 | a | |
| 151 | 1 | b | |
| 152 | 1.8 | a | |
| 153 | 1.5 | b | |
| 154 | 0.6 | a | |

| Number | cm | Designation | Note |
|---|---|---|---|
| 155 | 0.7 | b | |
| 156 | 0.6 | a | |
| 157 | 0.3 | b | |
| 158 | 0.5 | a | |
| 159 | 0.4 | b | |
| 160 | 0.6 | a | |
| 161 | 0.5 | b | |
| 162 | 0.6 | a | |
| 163 | 0.3 | b | |
| 164 | 0.5 | a | |
| 165 | 1.2 | b | |
| 166 | 0.5 | a | |
| 167 | 0.1 | b | |
| 168 | 0.9 | a | |
| 169 | 2.2 | b | |
| 170 | 2.5 | a | |
| 171 | 0.05 | b | crack |
| 172 | 3 | a | |
| 173 | 3.2 | b | |
| 174 | 0.7 | a | |
| 175 | 0.4 | b | |
| 176 | 2 | a | |
| 177 | 1.7 | b | |
| 178 | 0.3 | a | |
| 179 | 0.3 | b | |
| 180 | 0.9 | a | |
| 181 | 0.3 | b | |
| 182 | 0.2 | a | |
| 183 | 32 | weathered | chg to b-crack |
| 184 | 0.7 | a | |
| 185 | 0.3 | b | |
| 186 | 1.6 | a | |
| 187 | 1 | b | |
| 188 | 0.7 | a | |
| 189 | 1 | b | |
| 190 | 2.2 | a | |
| 191 | 1 | b | |
| 192 | 1.1 | a | |
| 193 | 0.9 | b | |

| Number | cm | Designation | Note |
|---|---|---|---|
| 194 | 1.5 | a | |
| 195 | 1 | b | |
| 196 | 2.3 | a | |
| 197 | 0.4 | b | |
| 198 | 0.3 | a | |
| 199 | 1 | b | |
| 200 | 2.2 | a | |
| 201 | 0.5 | b | |
| 202 | 0.4 | a | |
| 203 | 1 | b | |
| 204 | 1.7 | a | |
| 205 | 1 | b | |
| 206 | 0.3 | a | |
| 207 | 1 | b | |
| 208 | 1.4 | a | |
| 209 | 30 | weathered | excluded |
| 210 | 5.2 | CTS | chg to b |
| 211 | 0.8 | a | |
| 212 | 0.6 | b | |
| 213 | 0.7 | a | |
| 214 | 5 | b | |
| 215 | 0.8 | a | |
| 216 | 0.5 | b | |
| 217 | 1.2 | a | |
| 218 | 0.5 | b | |
| 219 | 1.5 | a | |
| 220 | 0.7 | b | |
| 221 | 2.5 | a | |
| 222 | 0.2 | b | |
| 223 | 1.3 | a | |
| 224 | 0.2 | b | |
| 225 | 3.0 | a | |
| 226 | 0.5 | b | |
| 227 | 1.2 | a | |
| 228 | 1 | b | |
| 229 | 1.3 | a | |
| 230 | 0.2 | b | |
| 231 | 1.2 | a | |
| 232 | 0.7 | b | |

| Number | cm | Designation | Note |
|---|---|---|---|
| 233 | 1.3 | a | |
| 234 | 0.4 | b | |
| 235 | 2.2 | a | |
| 236 | 0.3 | b | |
| 237 | 12.5 | tuff | chg to a-crack |
| 238 | 0.3 | b | |
| 239 | 3 | a | |
| 240 | 6.2 | b | |
| 241 | 0.8 | a | |
| 242 | 0.5 | b | |
| 243 | 3 | a | |
| 244 | 0.5 | b | |
| 245 | 3.8 | a | |
| 246 | 0.5 | b | |
| 247 | 1 | a | |
| 248 | 4 | b | |
| 249 | 2.8 | a | |
| 250 | 0.3 | b | crack top |
| 251 | 4 | a | |
| 252 | 0.05 | b | crack |
| 253 | 0.9 | a | |
| 254 | 0.5 | b | |
| 255 | 1 | a | |
| 256 | 0.3 | b | |
| 257 | 1.2 | a | |
| 258 | 0.3 | b | |
| 259 | 0.6 | a | |
| 260 | 0.5 | b | |
| 261 | 0.9 | a | |
| 262 | 0.5 | b | |
| 263 | 1 | a | |
| 264 | 0.4 | b | |
| 265 | 1 | a | |
| 266 | 0.5 | b | |
| 267 | 2 | a | |
| 268 | 3.8 | b | |
| 269 | 3 | a | |
| 270 | 0.4 | b | |
| 271 | 2.7 | a | |

| Number | cm | Designation | Note |
|---|---|---|---|
| 272 | 0.4 | b | |
| 273 | 0.7 | a | |
| 274 | 0.2 | b | crack top |
| 275 | 11 | a | |
| 276 | 0.05 | b | crack |
| 277 | 1.9 | a | |
| 278 | 0.3 | b | |
| 279 | 1.2 | a | |
| 280 | 0.5 | b | |
| 281 | 13.5 | weathered | excluded |
| 282 | 9.5 | tuff | chg to a-crack |
| 283 | 17 | weathered | chg to b-crack |
| 284 | 1 | a | |
| 285 | 0.5 | b | |
| 286 | 2.2 | a | |
| 287 | 0.05 | b | crack |
| 288 | 1 | a | |
| 289 | 0.5 | b | |
| 290 | 4.5 | a | |
| 291 | 0.6 | b | |
| 292 | 3.5 | a | |
| 293 | 0.2 | b | |
| 294 | 2 | a | |
| 295 | 0.05 | b | crack |
| 296 | 2.7 | a | |
| 297 | 0.6 | b | |
| 298 | 6 | a | |
| 299 | 0.05 | b | crack |
| 300 | 3 | a | |
| 301 | 0.7 | b | |
| 302 | 2.5 | a | |
| 303 | 1.7 | b | |
| 304 | 1.4 | a | |
| 305 | 0.05 | b | crack |
| 306 | 2.2 | a | |
| 307 | 0.3 | b | |
| 308 | 1.5 | a | |
| 309 | 0.2 | b | |
| 310 | 0.9 | a | |

| Number | cm | Designation | Note |
|---|---|---|---|
| 311 | 0.4 | b | |
| 312 | 0.8 | a | |
| 313 | 0.4 | b | |
| 314 | 0.7 | a | |
| 315 | 0.5 | b | |
| 316 | 1 | a | |
| 317 | 0.05 | b | crack |
| 318 | 1.2 | a | |
| 319 | 0.2 | b | |
| 320 | 1 | a | |
| 321 | 0.6 | b | |
| 322 | 2.9 | a | |
| 323 | 0.2 | b | |
| 324 | 1.2 | a | |
| 325 | 0.5 | b | |
| 326 | 3.5 | a | |
| 327 | 1.3 | b | |
| 328 | 4.9 | a | |
| 329 | 1.2 | b | |
| 330 | 3.6 | a | |
| 331 | 0.3 | b | |
| 332 | 2 | a | |
| 333 | 0.5 | b | |
| 334 | 1.1 | a | undulose |
| 335 | 0.5 | b | |
| 336 | 3 | a | |
| 337 | 0.05 | b | crack |
| 338 | 4 | a | |
| 339 | 0.05 | b | crack |
| 340 | 7.3 | a | |
| 341 | 0.2 | b | |
| 342 | 1.9 | a | |
| 343 | 0.3 | b | |
| 344 | 5.7 | a | |
| 345 | 0.5 | b | |
| 346 | 2.7 | a | |
| 347 | 0.6 | b | |
| 348 | 2.4 | a | |
| 349 | 0.5 | b | |

| Number | cm | Designation | Note |
|---|---|---|---|
| 350 | 1.2 | a | |
| 351 | 0.6 | b | |
| 352 | 0.5 | a | |
| 353 | 0.5 | b | |
| 354 | 1.6 | a | |
| 355 | 0.5 | b | |
| 356 | 1.5 | a | |
| 357 | 0.05 | b | crack |
| 358 | 10.9 | a | |
| 359 | 8.6 | weathered | chg to b-crack |
| 360 | 1.4 | a | |
| 361 | 0.7 | b | |
| 362 | 2.2 | a | |
| 363 | 0.9 | b | |
| 364 | 0.5 | a | |
| 365 | 2 | b | |
| 366 | 1.4 | a | |
| 367 | 0.6 | b | |
| 368 | 0.7 | a | |
| 369 | 1.1 | b | |
| 370 | 2 | a | |
| 371 | 0.6 | b | |
| 372 | 1.7 | a | |
| 373 | 0.7 | b | |
| 374 | 2 | a | |
| 375 | 0.7 | b | |
| 376 | 1.9 | a | crack top |
| 377 | 1.2 | b | |
| 378 | 3.1 | a | |
| 379 | 0.7 | b | |
| 380 | 4 | a | |
| 381 | 0.3 | b | |
| 382 | 2 | a | |
| 383 | 1.2 | b | |
| 384 | 1.2 | a | |
| 385 | 0.2 | b | |
| 386 | 1.2 | a | |
| 387 | 1 | b | |
| 388 | 1.9 | a | |

| Number | cm | Designation | Note |
|---|---|---|---|
| 389 | 0.6 | b | |
| 390 | 5.7 | a | vug chert |
| 391 | 0.6 | b | |
| 392 | 5.4 | a | vug chert |
| 393 | 2 | b | crack top |
| 394 | 3.5 | a | |
| 395 | 0.2 | b | |
| 396 | 4.9 | a | vug chert |
| 397 | 0.5 | b | |
| 398 | 5.5 | a | vug chert |
| 399 | 0.05 | b | crack |
| 400 | 5.5 | a | vug chert |
| 401 | 2 | b | |
| 402 | 7.5 | a | vug chert |
| 403 | 8 | weathered | chg to b-crack |
| 404 | 5.5 | a | vug chert |
| 405 | 0.2 | b | |
| 406 | 3.2 | a | vug chert |
| 407 | 0.5 | b | |
| 408 | 4.6 | a | vug chert |
| 409 | 3 | weathered | chg to b-crack |
| 410 | 8.5 | a | vug chert |
| 411 | 2 | weathered | chg to b-crack |
| 412 | 5 | a | vug chert |
| 413 | 0.5 | b | |
| 414 | 2 | a | vug chert |
| 415 | 0.9 | b | |
| 416 | 3.5 | a | vug chert |
| 417 | 2.5 | weathered | chg to b-crack |
| 418 | 4 | a | vug chert |
| 419 | 3.9 | weathered | chg to b-crack |
| 420 | 9.5 | a | vug chert |
| 421 | 0.9 | b | |
| 422 | 2.5 | a | |
| 423 | 0.5 | b | |
| 424 | 1.1 | a | |
| 425 | 0.05 | b | crack |
| 426 | 5 | a | |
| 427 | 0.5 | b | |

| Number | cm | Designation | Note |
|---|---|---|---|
| 428 | 8.2 | a | |
| 429 | 0.05 | b | crack |
| 430 | 4.3 | a | |
| 431 | 0.5 | b | |
| 432 | 1.4 | a | |
| 433 | 0.5 | b | |
| 434 | 1.8 | a | |
| 435 | 0.6 | b | |
| 436 | 1 | a | |
| 437 | 0.5 | b | |
| 438 | 1 | a | |
| 439 | 0.05 | b | crack |
| 440 | 3.1 | a | |
| 441 | 0.05 | b | crack |
| 442 | 6 | a | vug chert |
| 443 | 0.05 | b | crack |
| 444 | 3.3 | a | vug chert |
| 445 | 0.6 | b | |
| 446 | 3 | a | vug chert |
| 447 | 0.05 | b | crack |
| 448 | 2.1 | a | vug chert |
| 449 | 0.6 | b | |
| 450 | 4 | a | vug chert |
| 451 | 0.5 | b | |
| 452 | 1.5 | a | vug chert |
| 453 | 0.05 | b | crack |
| 454 | 9 | a | |
| 455 | 0.05 | b | crack |
| 456 | 1 | a | vug chert |
| 457 | 0.3 | b | |
| 458 | 2 | a | vug chert |
| 459 | 0.3 | b | |
| 460 | 4.4 | a | vug chert |
| 461 | 0.8 | b | |
| 462 | 4.2 | a | vug chert |
| 463 | 0.05 | b | |
| 464 | 10 | a | vug chert |
| 465 | 0.05 | b | crack |
| 466 | 3 | a | vug chert |

| Number | cm | Designation | Note |
|---|---|---|---|
| 467 | 0.05 | b | crack |
| 468 | 4.5 | a | vug chert |
| 469 | 0.05 | b | crack |
| 470 | 5.2 | a | vug chert |
| 471 | 0.05 | b | crack |
| 472 | 2.2 | a | vug chert |
| 473 | 0.05 | b | crack |
| 474 | 4.8 | a | vug chert |
| 475 | 0.05 | b | crack |
| 476 | 14 | a | vug chert |
| 477 | 0.3 | b | |
| 478 | 4.5 | a | vug chert |
| 479 | 0.05 | b | crack |
| 480 | 8.6 | a | vug chert |
| 481 | 0.05 | b | crack |
| 482 | 5.5 | a | vug chert |
| 483 | 0.05 | b | crack |
| 484 | 10 | a | vug chert |
| 485 | 0.05 | b | crack |
| 486 | 2 | a | vug chert |
| 487 | 0.7 | b | |
| 488 | 5.2 | a | vug chert |
| 489 | 0.4 | b | |
| 490 | 1 | a | |
| 491 | 0.9 | b | |
| 492 | 2.5 | a | vug chert |
| 493 | 0.8 | b | |
| 494 | 6 | a | vug chert |
| 495 | 0.5 | b | |
| 496 | 1 | a | |
| 497 | 0.05 | b | crack |
| 498 | 4 | a | vug chert |
| 499 | 0.05 | b | crack |
| 500 | 5.3 | a | vug chert |
| 501 | 0.05 | b | crack |
| 502 | 3.5 | a | vug chert |
| 503 | 0.05 | b | crack |
| 504 | 5.2 | a | vug chert |
| 505 | 1.4 | b | |

| Number | cm | Designation | Note |
|---|---|---|---|
| 506 | 10.5 | a | vug chert |
| 507 | 11 | weathered | excluded |
| 508 | 2 | b | |
| 509 | 1 | a | |
| 510 | 1 | b | |
| 511 | 1.5 | a | |
| 512 | 0.5 | b | |
| 513 | 0.6 | a | |
| 514 | 1 | b | |
| 515 | 2 | a | |
| 516 | 0.5 | b | |
| 517 | 1 | a | |
| 518 | 0.6 | b | |
| 519 | 1.5 | a | |
| 520 | 0.05 | b | crack |
| 521 | 2.7 | a | |
| 522 | 0.05 | b | crack |
| 523 | 4.3 | a | |
| 524 | 4.5 | weathered | excluded |
| 525 | 2.5 | b | |
| 526 | 1.8 | a | |
| 527 | 1.8 | b | |
| 528 | 1.1 | a | |
| 529 | 0.7 | b | |
| 530 | 1 | a | |
| 531 | 0.5 | b | |
| 532 | 1 | a | |
| 533 | 0.05 | b | crack |
| 534 | 4.5 | a | |
| 535 | 3.5 | weathered | excluded |
| 536 | 0.7 | b | |
| 537 | 2.5 | a | |
| 538 | 0.05 | b | crack |
| 539 | 1.6 | a | |
| 540 | 0.5 | b | |
| 541 | 1 | a | |
| 542 | 2.5 | b | |
| 543 | 1 | a | |
| 544 | 0.5 | b | |

| Number | cm | Designation | Note |
|---|---|---|---|
| 545 | 1.2 | a | |
| 546 | 0.6 | b | |
| 547 | 1.5 | a | |
| 548 | 0.6 | b | |
| 549 | 0.6 | a | |
| 550 | 0.4 | b | |
| 551 | 1.2 | a | |
| 552 | 0.4 | b | |
| 553 | 1.8 | a | |
| 554 | 0.5 | b | |
| 555 | 1.7 | a | |
| 556 | 0.6 | b | |
| 557 | 3 | a | |
| 558 | 0.05 | b | crack |
| 559 | 1.5 | a | |
| 560 | 0.3 | b | |
| 561 | 0.6 | a | |
| 562 | 0.05 | b | crack |
| 563 | 0.9 | a | |
| 564 | 0.5 | b | |
| 565 | 1.5 | a | |
| 566 | 0.05 | b | crack |
| 567 | 0.8 | a | |
| 568 | 0.5 | b | |
| 569 | 1 | a | |
| 570 | 2 | b | |
| 571 | 0.8 | a | |
| 572 | 0.5 | b | |
| 573 | 0.5 | a | |
| 574 | 0.7 | b | |
| 575 | 2 | a | |
| 576 | 0.5 | b | |
| 577 | 0.6 | a | |
| 578 | 0.5 | b | |
| 579 | 2 | a | |
| 580 | 0.6 | b | |
| 581 | 2 | a | |
| 582 | 0.6 | b | |
| 583 | 0.9 | a | GWP Begins |

| Number | cm | Designation | Note |
|---|---|---|---|
| 584 | 0.6 | b | |
| 585 | 1 | a | |
| 586 | 3.2 | b | |
| 587 | 1 | a | |
| 588 | 1.2 | b | |
| 589 | 2 | a | |
| 590 | 1.2 | b | |
| 591 | 0.6 | a | |
| 592 | 1.7 | b | |
| 593 | 2 | a | |
| 594 | 2 | b | |
| 595 | 0.7 | a | |
| 596 | 5 | weathered | chg to b-crack |
| 597 | 1.7 | a | |
| 598 | 2.2 | b | |
| 599 | 0.7 | a | |
| 600 | 1.6 | b | |
| 601 | 2.5 | a | |
| 602 | 30 | weathered | chg to b-crack |
| 603 | 4.5 | a | |
| 604 | 1.2 | b | |
| 605 | 2 | a | |
| 606 | 0.2 | b | |
| 607 | 40 | unknown | excluded |
| 608 | 1.5 | a | |
| 609 | 0.4 | b | |
| 610 | 4.2 | a | |
| 611 | 1 | b | undulose |
| 612 | 2.1 | a | |
| 613 | 0.4 | b | |
| 614 | 2.7 | a | |
| 615 | 0.7 | b | |
| 616 | 2.9 | a | |
| 617 | 0.5 | b | |
| 618 | 1 | a | |
| 619 | 24 | weathered | excluded |
| 620 | 0.7 | b | |
| 621 | 1 | a | |
| 622 | 0.5 | b | |

| Number | cm | Designation | Note |
|---|---|---|---|
| 623 | 3.5 | a | |
| 624 | 0.7 | b | |
| 625 | 3 | a | |
| 626 | 0.4 | b | |
| 627 | 2.2 | a | |
| 628 | 0.6 | b | |
| 629 | 3.2 | a | |
| 630 | 0.7 | b | |
| 631 | 1.5 | a | |
| 632 | 0.4 | b | |
| 633 | 1 | a | |
| 634 | 1.6 | b | |
| 635 | 0.5 | a | |
| 636 | 0.5 | b | |
| 637 | 0.6 | a | |
| 638 | 0.5 | b | |
| 639 | 3 | a | |
| 640 | 0.5 | b | |
| 641 | 1.5 | a | |
| 642 | 1 | b | |
| 643 | 5.3 | a | |
| 644 | 0.05 | b | crack |
| 645 | 3.7 | a | |
| 646 | 0.05 | b | crack |
| 647 | 2.5 | a | |
| 648 | 0.5 | b | |
| 649 | 4.2 | a | |
| 650 | 0.6 | b | |
| 651 | 3.1 | a | |
| 652 | 0.3 | b | |
| 653 | 1.5 | a | |
| 654 | 0.2 | b | |
| 655 | 1.5 | a | |
| 656 | 0.5 | b | |
| 657 | 4.8 | a | BWP Begins |
| 658 | 0.5 | b | |
| 659 | 2.5 | a | |
| 660 | 2 | weathered | excluded |
| 661 | 1 | b | |

| Number | cm | Designation | Note |
|---|---|---|---|
| 662 | 2 | a | |
| 663 | 0.2 | b | |
| 664 | 1.2 | a | |
| 665 | 0.2 | b | |
| 666 | 1 | a | |
| 667 | 0.1 | b | |
| 668 | 1.6 | a | |
| 669 | 0.05 | b | crack |
| 670 | 0.5 | a | |
| 671 | 0.2 | b | |
| 672 | 1.5 | a | |
| 673 | 0.3 | b | |
| 674 | 1.2 | a | |
| 675 | 0.3 | b | |
| 676 | 2.4 | a | |
| 677 | 0.4 | b | |
| 678 | 1 | a | |
| 679 | 0.5 | b | |
| 680 | 1.2 | a | crack top |
| 681 | 1 | b | |
| 682 | 3.7 | a | |
| 683 | 0.3 | b | |
| 684 | 0.7 | a | |
| 685 | 0.2 | b | |
| 686 | 2.7 | a | |
| 687 | 0.5 | b | |
| 688 | 2.7 | a | |
| 689 | 0.3 | b | |
| 690 | 2 | a | vug chert |
| 691 | 3.1 | weathered | chg to b-crack |
| 692 | 2.2 | a | vug chert |
| 693 | 0.2 | b | |
| 694 | 3.7 | a | vug chert |
| 695 | 0.05 | b | crack |
| 696 | 1.1 | a | |
| 697 | 0.5 | b | |
| 698 | 0.4 | a | |
| 699 | 0.3 | b | |
| 700 | 0.2 | a | |

| Number | cm | Designation | Note |
|---|---|---|---|
| 701 | 0.5 | b | crack top |
| 702 | 3.4 | a | BWP Ends |
| 703 | 0.2 | b | |
| 704 | 2.7 | a | |
| 705 | 0.6 | b | |
| 706 | 1.8 | a | |
| 707 | 0.5 | b | |
| 708 | 2.1 | a | |
| 709 | 0.3 | b | |
| 710 | 1.7 | a | crack top |
| 711 | 1 | b | |
| 712 | 1.6 | a | |
| 713 | 0.9 | b | crack top |
| 714 | 3.2 | a | |
| 715 | 0.7 | b | |
| 716 | 0.4 | a | crack top |
| 717 | 0.7 | b | |
| 718 | 1.7 | a | undulose |
| 719 | 0.4 | b | |
| 720 | 5.2 | a | undulose |
| 721 | 3 | b | |
| 722 | 4 | a | |
| 723 | 0.6 | b | |
| 724 | 4.2 | a | undulose |
| 725 | 1 | b | |
| 726 | 2 | a | |
| 727 | 0.3 | b | |
| 728 | 1 | a | |
| 729 | 0.6 | b | |
| 730 | 1.7 | a | |
| 731 | 2.5 | b | |
| 732 | 0.6 | a | |
| 733 | 0.7 | b | |
| 734 | 1 | a | |
| 735 | 0.5 | b | |
| 736 | 1.4 | a | crack top |
| 737 | 1 | b | |
| 738 | 1 | a | |
| 739 | 0.3 | b | |

| Number | cm | Designation | Note |
|---|---|---|---|
| 740 | 0.6 | a | |
| 741 | 1.1 | b | |
| 742 | 1.4 | a | |
| 743 | 0.2 | b | |
| 744 | 1.2 | a | |
| 745 | 0.05 | b | crack |
| 746 | 1.6 | a | |
| 747 | 1.1 | b | |
| 748 | 4 | a | |
| 749 | 0.5 | b | |
| 750 | 2.6 | a | undulose |
| 751 | 0.7 | b | |
| 752 | 3.6 | a | vug chert |
| 753 | 0.2 | b | |
| 754 | 1.2 | a | |
| 755 | 0.05 | b | crack |
| 756 | 1.2 | a | |
| 757 | 0.2 | b | |
| 758 | 1.1 | a | |
| 759 | 0.5 | b | |
| 760 | 1 | a | |
| 761 | 0.2 | b | |
| 762 | 0.5 | a | |
| 763 | 0.2 | b | |
| 764 | 1.6 | a | |
| 765 | 1.15 | b | silicified/black |
| 766 | 1.1 | a | |
| 767 | 1 | b | |
| 768 | 0.9 | a | |
| 769 | 0.05 | b | crack |
| 770 | 2 | a | |
| 771 | 0.3 | b | |
| 772 | 1.5 | a | |
| 773 | 0.5 | b | |
| 774 | 0.5 | a | |
| 775 | 1 | b | |
| 776 | 3 | a | |
| 777 | 0.05 | b | crack |
| 778 | 2.2 | a | |

| Number | cm | Designation | Note |
|---|---|---|---|
| 779 | 0.6 | b | |
| 780 | 0.7 | a | |
| 781 | 1 | b | |
| 782 | 1.1 | a | |
| 783 | 0.6 | b | |
| 784 | 1.5 | a | undulose |
| 785 | 0.5 | b | |
| 786 | 4 | a | undulose |
| 787 | 0.5 | b | |
| 788 | 2.1 | a | |
| 789 | 0.3 | b | |
| 790 | 1.1 | a | |
| 791 | 0.7 | b | |
| 792 | 2 | a | |
| 793 | 0.9 | b | |
| 794 | 2.4 | a | |
| 795 | 0.5 | b | |
| 796 | 0.7 | a | |
| 797 | 0.5 | b | |
| 798 | 2.2 | a | |
| 799 | 0.05 | b | |
| 800 | 1 | a | |
| 801 | 0.6 | b | |
| 802 | 1.2 | a | |
| 803 | 0.3 | b | |
| 804 | 1 | a | |
| 805 | 0.3 | b | |
| 806 | 1.9 | a | |
| 807 | 0.3 | b | |
| 808 | 1 | a | |
| 809 | 0.5 | b | |
| 810 | 1.6 | a | |
| 811 | 0.5 | b | |
| 812 | 1.5 | a | |
| 813 | 0.5 | b | |
| 814 | 0.7 | a | |
| 815 | 2.5 | b | |
| 816 | 2.7 | a | |
| 817 | 0.3 | b | |

| Number | cm | Designation | Note |
|---|---|---|---|
| 818 | 5 | a | |
| 819 | 0.05 | b | crack |
| 820 | 5.5 | a | |
| 821 | 1 | b | |
| 822 | 1.2 | a | |
| 823 | 0.2 | b | |
| 824 | 3 | a | |
| 825 | 0.4 | b | |
| 826 | 0.2 | silicified | excluded |
| 827 | 1 | weathered | excluded |
| 828 | 0.3 | silicified | excluded |
| 829 | 1.8 | a | |
| 830 | 0.2 | b | |
| 831 | 2.5 | a | |
| 832 | 0.2 | b | |
| 833 | 0.5 | a | |
| 834 | 0.2 | b | |
| 835 | 0.5 | a | |
| 836 | 0.2 | b | |
| 837 | 0.7 | a | |
| 838 | 0.05 | b | crack |
| 839 | 5.5 | a | vug chert |
| 840 | 1 | b | |
| 841 | 5.6 | a | vug chert |
| 842 | 1 | b | poly. Surface |
| 843 | 1.5 | weathered | excluded |
| 844 | 4.5 | a | |
| 845 | 0.7 | b | |
| 846 | 1 | a | |
| 847 | 0.2 | b | |
| 848 | 0.9 | a | |
| 849 | 0.3 | b | |
| 850 | 2.6 | a | |
| 851 | 0.5 | b | |
| 852 | 1 | a | |
| 853 | 2 | b | |
| 854 | 1.5 | a | |
| 855 | 0.05 | b | crack |
| 856 | 2.2 | a | |

| Number | cm | Designation | Note |
|---|---|---|---|
| 857 | 0.05 | b | crack |
| 858 | 1 | a | |
| 859 | 0.2 | b | |
| 860 | 3 | a | |
| 861 | 0.3 | b | |
| 862 | 0.9 | a | |
| 863 | 0.2 | b | |
| 864 | 1 | a | |
| 865 | 0.6 | b | |
| 866 | 3 | a | |
| 867 | 0.1 | b | |
| 868 | 1.5 | a | |
| 869 | 1 | tuff | excluded |
| 870 | 0.5 | b | |
| 871 | 1.6 | a | |
| 872 | 0.7 | b | |
| 873 | 1.6 | a | |
| 874 | 0.4 | b | |
| 875 | 5.7 | a | |
| 876 | 0.5 | b | |
| 877 | 1.2 | a | |
| 878 | 0.5 | b | |
| 879 | 1.9 | a | |
| 880 | 0.4 | b | |
| 881 | 4 | a | |
| 882 | 0.7 | b | |
| 883 | 4.1 | a | |
| 884 | 0.5 | b | |
| 885 | 2.4 | a | |
| 886 | 0.4 | b | |
| 887 | 1.2 | a | |
| 888 | 0.3 | b | |
| 889 | 1 | a | |
| 890 | 0.8 | b | |
| 891 | 3 | a | |
| 892 | 0.5 | b | |
| 893 | 3 | weathered | excluded |
| 894 | 3.8 | a | |
| 895 | 1 | b | |

| Number | cm | Designation | Note |
|---|---|---|---|
| 896 | 2.5 | a | |
| 897 | 0.8 | b | |
| 898 | 1 | a | |
| 899 | 1 | b | |
| 900 | 1.2 | a | |
| 901 | 1 | b | |
| 902 | 2.2 | a | |
| 903 | 0.05 | b | crack |
| 904 | 4 | a | |
| 905 | 0.5 | b | |
| 906 | 2 | a | |
| 907 | 0.9 | b | |
| 908 | 1.1 | a | |
| 909 | 3 | b | |
| 910 | 1.5 | a | |
| 911 | 1 | b | |
| 912 | 4.1 | a | |
| 913 | 0.05 | b | crack |
| 914 | 1.6 | a | |
| 915 | 2 | b | |
| 916 | 2.2 | a | |
| 917 | 0.9 | b | |
| 918 | 2.1 | a | undulose |
| 919 | 0.05 | b | crack |
| 920 | 2.1 | a | |
| 921 | 0.05 | b | crack |
| 922 | 5 | a | |
| 923 | 0.5 | b | |
| 924 | 2 | a | |
| 925 | 0.05 | b | crack |
| 926 | 4 | a | |
| 927 | 0.05 | b | crack |
| 928 | 1.4 | a | |
| 929 | 1.7 | b | |
| 930 | 4 | weathered | excluded |
| 931 | 3 | a | |
| 932 | 0.3 | b | |
| 933 | 2.5 | a | |
| 934 | 0.05 | b | crack |

| Number | cm | Designation | Note |
|---|---|---|---|
| 935 | 4 | a | strongly tufted |
| 936 | 0.4 | b | |
| 937 | 3.9 | a | |
| 938 | 0.5 | b | |
| 939 | 1 | a | |
| 940 | 0.3 | b | |
| 941 | 15.5 | weathered | excluded |
| 942 | 3.2 | a | strongly tufted |
| 943 | 0.4 | b | |
| 944 | 4 | a | |
| 945 | 0.5 | b | |
| 946 | 4.4 | a | |
| 947 | 0.6 | b | |
| 948 | 1.2 | a | |
| 949 | 0.2 | b | |
| 950 | 0.9 | a | |
| 951 | 0.3 | b | |
| 952 | 1 | a | |
| 953 | 0.3 | b | |
| 954 | 3.8 | a | ST Begins |
| 955 | 0.4 | b | |
| 956 | 3.5 | a | |
| 957 | 0.5 | b | |
| 958 | 3 | a | |
| 959 | 14 | weathered | chg to b-crack |
| 960 | 4.1 | a | |
| 961 | 0.2 | b | |
| 962 | 2.3 | a | |
| 963 | 0.2 | b | |
| 964 | 2 | a | |
| 965 | 0.6 | b | |
| 966 | 3.6 | a | |
| 967 | 0.05 | b | crack |
| 968 | 1.9 | a | |
| 969 | 0.2 | b | |
| 970 | 2.3 | a | |
| 971 | 0.3 | b | |
| 972 | 5 | a | |
| 973 | 0.05 | b | crack |

| Number | cm | Designation | Note |
|---|---|---|---|
| 974 | 3.5 | a | |
| 975 | 3 | weathered | chg to b-crack |
| 976 | 1.9 | a | |
| 977 | 0.05 | b | crack |
| 978 | 2.6 | a | |
| 979 | 0.05 | b | crack |
| 980 | 1.5 | a | |
| 981 | 0.5 | b | |
| 982 | 2.8 | a | |
| 983 | 0.3 | b | |
| 984 | 1.2 | a | |
| 985 | 0.5 | b | |
| 986 | 0.5 | a | |
| 987 | 0.5 | b | |
| 988 | 1 | a | vug chert |
| 989 | 0.1 | b | |
| 990 | 1 | a | vug chert |
| 991 | 1.2 | b | |
| 992 | 1.6 | a | vug chert |
| 993 | 0.05 | b | crack |
| 994 | 2 | a | |
| 995 | 7.5 | weathered | chg to b-crack |
| 996 | 3.1 | a | |
| 997 | 1 | b | |
| 998 | 5.4 | a | |
| 999 | 0.5 | b | |
| 1000 | 2.2 | a | |
| 1001 | 1.5 | b | |
| 1002 | 4.5 | a | |
| 1003 | 0.05 | b | crack |
| 1004 | 5.3 | a | |
| 1005 | 1.2 | b | |
| 1006 | 5.2 | a | |
| 1007 | 1 | b | |
| 1008 | 1.4 | a | |
| 1009 | 0.2 | b | |
| 1010 | 1.2 | a | |
| 1011 | 0.05 | b | crack |
| 1012 | 1.5 | a | |

| Number | cm | Designation | Note |
|---|---|---|---|
| 1013 | 1 | b | |
| 1014 | 11 | a | |
| 1015 | 10.5 | weathered | chg to b-crack |
| 1016 | 3.1 | tuff | chg to a-crack |
| 1017 | 4.5 | CTS | chg to B |
| 1018 | 5 | a | |
| 1019 | 3.6 | weathered | excluded |
| 1020 | 12.6 | CTS | chg to B |
| 1021 | 0.6 | weathered | chg to a-crack |
| 1022 | 11 | CTS | chg to b |
| 1023 | 5 | weathered | chg to a-crack |
| 1024 | 0.5 | b | |
| 1025 | 1.5 | a | |
| 1026 | 0.7 | b | |
| 1027 | 4.3 | a | |
| 1028 | 0.6 | b | |
| 1029 | 1.5 | a | |
| 1030 | 1 | b | |
| 1031 | 3.5 | a | |
| 1032 | 0.5 | b | |
| 1033 | 15.5 | tuff | excluded |
| Total | 1994.55 | | |

Lower Prieska 3

| Number | cm | Designation | Note |
|---|---|---|---|
| 1 | 15.5 | tuff | chg to a-crack |
| 2 | 12 | weathered | chg to b-crack |
| 3 | 7.6 | tuff | chg to a-crack |
| 4 | 14 | weathered | excluded |
| 5 | 12 | CTS | chg to b |
| 6 | 31 | weathered | excluded |
| 7 | 2 | a | |
| 8 | 0.2 | b | |
| 9 | 2 | a | |
| 10 | 0.5 | b | |
| 11 | 5.3 | a | |
| 12 | 2 | b | |
| 13 | 0.7 | a | |
| 14 | 0.1 | b | |
| 15 | 3 | a | |
| 16 | 63 | weathered | chg to b-crack |
| 17 | 10 | a | |
| 18 | 14 | CTS | chg to b |
| 19 | 4.5 | weathered | excluded |
| 20 | 2 | a | |
| 21 | 0.1 | b | |
| 22 | 0.5 | a | |
| 23 | 0.6 | b | |
| 24 | 2 | a | |
| 25 | 0.5 | b | |
| 26 | 0.5 | a | |
| 27 | 0.2 | b | |
| 28 | 0.5 | a | |
| 29 | 0.6 | b | |
| 30 | 2 | a | |
| 31 | 0.05 | b | crack |
| 32 | 5.5 | a | |
| 33 | 0.05 | b | crack |
| 34 | 0.5 | a | |
| 35 | 0.2 | b | |
| 36 | 0.4 | a | |
| 37 | 0.1 | b | |

| Number | cm | Designation | Note |
|---|---|---|---|
| 38 | 1 | a | |
| 39 | 0.1 | b | |
| 40 | 4 | a | |
| 41 | 0.05 | b | crack |
| 42 | 3 | a | |
| 43 | 1.5 | weathered | chg to b-crack |
| 44 | 1 | chert | excluded |
| 45 | 5.1 | chert | excluded |
| 46 | 3.1 | a | |
| 47 | 0.05 | b | crack |
| 48 | 5 | a | |
| 49 | 0.05 | b | crack |
| 50 | 3 | a | |
| 51 | 0.05 | b | crack |
| 52 | 5 | a | |
| 53 | 0.2 | b | |
| 54 | 3.5 | a | |
| 55 | 0.05 | b | crack |
| 56 | 8 | a | |
| 57 | 0.05 | b | crack |
| 58 | 5 | a | |
| 59 | 0.05 | b | crack |
| 60 | 4.7 | a | |
| 61 | 0.2 | b | |
| 62 | 0.9 | a | |
| 63 | 0.1 | b | |
| 64 | 1.9 | a | |
| 65 | 0.5 | b | |
| 66 | 1 | a | |
| 67 | 0.2 | b | |
| 68 | 1 | a | |
| 69 | 0.2 | b | |
| 70 | 1.5 | a | |
| 71 | 1.2 | b | |
| 72 | 1.7 | a | |
| 73 | 6.5 | weathered | excluded |
| 74 | 8 | CTS | chg to b |
| 75 | 2.2 | a | |
| 76 | 0.05 | b | crack |

| Number | cm | Designation | Note |
|---|---|---|---|
| 77 | 3.8 | a | |
| 78 | 0.5 | b | |
| 79 | 2 | a | |
| 80 | 0.05 | b | crack |
| 81 | 7 | a | |
| 82 | 0.05 | b | crack |
| 83 | 5.5 | a | |
| 84 | 0.05 | b | crack |
| 85 | 4.5 | a | |
| 86 | 17.5 | weathered | chg to b-crack |
| 87 | 4.5 | a | |
| 88 | 0.05 | b | crack |
| 89 | 6.1 | a | |
| 90 | 0.05 | b | crack |
| 91 | 3.1 | a | |
| 92 | 0.4 | b | |
| 93 | 1.1 | a | |
| 94 | 0.7 | b | |
| 95 | 2 | a | |
| 96 | 0.05 | b | crack |
| 97 | 1.5 | a | |
| 98 | 0.05 | b | crack |
| 99 | 3 | a | |
| 100 | 0.05 | b | crack |
| 101 | 2.5 | a | |
| 102 | 0.05 | b | crack |
| 103 | 2 | a | |
| 104 | 0.05 | b | crack |
| 105 | 4.5 | a | |
| 106 | 21.5 | weathered | chg to b-crack |
| 107 | 5.4 | tuff | excluded |
| 108 | 4 | a | |
| 109 | 0.05 | b | crack |
| 110 | 4.6 | a | |
| 111 | 8 | weathered | chg to b-crack |
| 112 | 2.5 | a | |
| 113 | 0.05 | b | crack |
| 114 | 4 | a | |
| 115 | 6 | weathered | excluded |

| Number | cm | Designation | Note |
|---|---|---|---|
| 116 | 0.05 | b | crack |
| 117 | 1.5 | a | |
| 118 | 0.05 | b | crack |
| 119 | 1 | a | |
| 120 | 0.6 | b | |
| 121 | 1.2 | a | |
| 122 | 0.05 | b | crack |
| 123 | 1.1 | a | |
| 124 | 1.2 | b | |
| 125 | 1.5 | a | |
| 126 | 1 | weathered | chg to b-crack |
| 127 | 1 | a | |
| 128 | 1.7 | tuff | chg to b-crack |
| 129 | 1.5 | a | |
| 130 | 0.05 | b | crack |
| 131 | 2 | a | |
| 132 | 6.5 | weathered | chg to b-crack |
| 133 | 0.5 | a | |
| 134 | 0.2 | b | |
| 135 | 2.2 | a | |
| 136 | 2.5 | CTS | chg to b |
| 137 | 2.8 | weathered | excluded |
| 138 | 1.2 | a | |
| 139 | 0.5 | b | |
| 140 | 1.5 | a | |
| 141 | 0.4 | b | |
| 142 | 0.7 | a | |
| 143 | 0.6 | b | |
| 144 | 2 | a | |
| 145 | 0.8 | b | |
| 146 | 1.8 | a | |
| 147 | 0.1 | b | |
| 148 | 2.7 | a | |
| 149 | 0.3 | b | |
| 150 | 0.6 | a | |
| 151 | 5.5 | weathered | chg to b-crack |
| 152 | 2.5 | a | |
| 153 | 0.05 | b | crack |
| 154 | 2.3 | a | |

| Number | cm | Designation | Note |
|---|---|---|---|
| 155 | 0.05 | b | crack |
| 156 | 1.6 | a | |
| 157 | 6.5 | weathered | chg to b-crack |
| 158 | 2.5 | a | |
| 159 | 0.5 | b | |
| 160 | 1 | a | |
| 161 | 1.6 | weathered | chg to b-crack |
| 162 | 3.1 | a | |
| 163 | 0.3 | b | |
| 164 | 1 | a | |
| 165 | 0.1 | b | |
| 166 | 1.1 | a | |
| 167 | 0.05 | b | crack |
| 168 | 0.7 | a | |
| 169 | 1 | b | |
| 170 | 1.9 | a | |
| 171 | 0.3 | b | |
| 172 | 1.2 | a | |
| 173 | 1.5 | b | |
| 174 | 2 | a | |
| 175 | 0.5 | b | |
| 176 | 1.5 | a | |
| 177 | 0.5 | b | |
| 178 | 12 | weathered | excluded |
| 179 | 1.7 | a | |
| 180 | 0.5 | b | |
| 181 | 1.8 | a | |
| 182 | 0.05 | b | crack |
| 183 | 0.9 | a | |
| 184 | 28 | weathered | chg to b-crack |
| 185 | 3.3 | a | |
| 186 | 0.3 | b | |
| 187 | 1.3 | a | |
| 188 | 0.1 | b | |
| 189 | 2.7 | a | |
| 190 | 0.2 | b | |
| 191 | 1 | a | |
| 192 | 0.3 | b | |
| 193 | 1.2 | a | |

| Number | cm | Designation | Note |
|---|---|---|---|
| 194 | 0.5 | b | |
| 195 | 1 | a | |
| 196 | 0.1 | b | |
| 197 | 1 | a | |
| 198 | 0.1 | b | |
| 199 | 1.4 | a | |
| 200 | 2.4 | b | |
| 201 | 1.7 | a | |
| 202 | 2.7 | b | |
| 203 | 1.2 | a | |
| 204 | 0.8 | b | |
| 205 | 3.7 | a | |
| 206 | 5.6 | b | |
| 207 | 0.9 | a | |
| 208 | 0.2 | b | |
| 209 | 1.1 | a | |
| 210 | 0.7 | b | |
| 211 | 1.4 | a | |
| 212 | 0.2 | b | |
| 213 | 1.8 | a | |
| 214 | 0.3 | b | |
| 215 | 2.1 | a | |
| 216 | 0.3 | b | |
| 217 | 2.2 | a | |
| 218 | 2.2 | b | |
| 219 | 2.4 | a | |
| 220 | 2 | b | |
| 221 | 1.9 | a | |
| 222 | 0.3 | b | |
| 223 | 1.7 | a | |
| 224 | 0.3 | b | |
| 225 | 1 | a | |
| 226 | 0.2 | b | |
| 227 | 0.7 | a | |
| 228 | 0.3 | b | |
| 229 | 1.7 | a | |
| 230 | 0.3 | b | |
| 231 | 0.9 | a | |
| 232 | 1.6 | b | |

| Number | cm | Designation | Note |
|---|---|---|---|
| 233 | 1.8 | a | |
| 234 | 0.2 | b | |
| 235 | 2.3 | a | |
| 236 | 0.3 | b | |
| 237 | 1.7 | a | |
| 238 | 0.5 | b | |
| 239 | 2.4 | a | |
| 240 | 0.7 | b | |
| 241 | 1.6 | a | |
| 242 | 1.8 | b | |
| 243 | 1.3 | a | |
| 244 | 0.3 | b | |
| 245 | 2 | a | |
| 246 | 1.1 | b | |
| 247 | 2.5 | a | |
| 248 | 0.2 | b | |
| 249 | 2.2 | a | |
| 250 | 0.3 | b | |
| 251 | 2 | a | |
| 252 | 0.05 | b | crack |
| 253 | 1.8 | a | |
| 254 | 0.5 | b | |
| 255 | 5 | a | |
| 256 | 0.05 | b | crack |
| 257 | 2.5 | a | |
| 258 | 0.05 | b | crack |
| 259 | 3 | a | |
| 260 | 0.05 | b | crack |
| 261 | 3.5 | a | excluded, Odd A |
| Total | 657.4 | | |

Lower Prieska 2 - Subset 1

| Number | cm | Designation | Note |
|---|---|---|---|
| 1 | 2.1 | a | BWP Begins |
| 2 | 1.2 | b | |
| 3 | 3 | a | undulose |
| 4 | 1.1 | b | |
| 5 | 4 | a | vug chert |
| 6 | 0.7 | b | |
| 7 | 5.1 | a | vug chert |
| 8 | 1.2 | b | |
| 9 | 5 | a | vug chert |
| 10 | 0.05 | b | crack |
| 11 | 5 | a | vug chert |
| 12 | 1 | b | |
| 13 | 4.2 | a | vug chert |
| 14 | 3 | b | |
| 15 | 5.8 | a | vug chert |
| 16 | 0.2 | b | |
| 17 | 8.4 | a | vug chert |
| 18 | 0.05 | b | crack |
| 19 | 3.5 | a | vug chert |
| 20 | 0.3 | b | |
| 21 | 2.5 | a | |
| 22 | 0.05 | b | crack |
| 23 | 3 | a | GWP Begins |
| 24 | 0.7 | b | |
| 25 | 1 | a | |
| 26 | 1.6 | b | |
| 27 | 1 | a | |
| 28 | 0.05 | b | crack |
| 29 | 2 | a | |
| 30 | 2 | b | |
| 31 | 1 | a | |
| 32 | 0.5 | b | |
| 33 | 0.7 | a | |
| 34 | 0.6 | b | |
| 35 | 0.5 | a | |
| 36 | 0.3 | b | |
| 37 | 0.5 | weathered | excluded |

| Number | cm | Designation | Note |
|---|---|---|---|
| 38 | 3 | a | |
| 39 | 2 | b | |
| 40 | 2.2 | a | |
| 41 | 3.7 | b | |
| 42 | 0.7 | a | |
| 43 | 0.5 | b | |
| 44 | 1.7 | a | |
| 45 | 2.4 | b | |
| 46 | 3.2 | a | |
| 47 | 2.6 | b | |
| 48 | 2.2 | a | |
| 49 | 2.5 | b | |
| 50 | 0.5 | a | |
| 51 | 0.2 | b | |
| 52 | 0.3 | a | |
| 53 | 1 | b | |
| 54 | 0.4 | a | |
| 55 | 7.2 | weathered | excluded |
| 56 | 10.7 | CTS | chg to b |
| 57 | 1.5 | a | BWP Begins |
| 58 | 2.5 | b | |
| 59 | 0.7 | a | |
| 60 | 1 | b | |
| 61 | 2 | a | |
| 62 | 1 | b | |
| 63 | 0.5 | a | |
| 64 | 1 | b | |
| 65 | 2.2 | a | |
| 66 | 0.9 | b | |
| 67 | 1.2 | a | |
| 68 | 0.8 | b | |
| 69 | 1.8 | a | |
| 70 | 0.6 | b | |
| 71 | 2.6 | a | |
| 72 | 1 | b | |
| 73 | 2 | a | |
| 74 | 1.2 | b | |
| 75 | 1.8 | a | |
| 76 | 0.8 | b | |

| Number | cm | Designation | Note |
|---|---|---|---|
| 77 | 2 | a | |
| 78 | 0.6 | b | |
| 79 | 1.6 | a | |
| 80 | 0.8 | b | BWP Ends |
| Total | 152 | | |

Lower Prieska 2 - Subset 2

| Number | cm | Designation | Note |
|---|---|---|---|
| 1 | 3.2 | a | BWP Begins |
| 2 | 1.2 | b | |
| 3 | 2.8 | a | undulose |
| 4 | 1 | b | crack top |
| 5 | 3.7 | a | vug chert |
| 6 | 0.7 | b | |
| 7 | 6 | a | vug chert |
| 8 | 0.05 | b | crack |
| 9 | 4.1 | a | vug chert |
| 10 | 1 | b | |
| 11 | 4.8 | a | vug chert |
| 12 | 0.05 | b | crack |
| 13 | 4.5 | a | vug chert |
| 14 | 0.05 | b | crack |
| 15 | 8.7 | a | vug chert |
| 16 | 0.05 | b | crack |
| 17 | 4.2 | a | |
| 18 | 0.3 | b | |
| 19 | 1.8 | a | |
| 20 | 0.05 | b | crack |
| 21 | 3 | a | GWP Begins |
| 22 | 0.05 | b | crack |
| 23 | 2.7 | a | |
| 24 | 0.6 | b | |
| 25 | 6 | weathered | excluded |
| 26 | 1.2 | a | |
| 27 | 0.9 | b | |
| 28 | 0.4 | a | |
| 29 | 0.4 | b | |
| 30 | 0.3 | a | |
| 31 | 0.5 | b | |
| 32 | 0.7 | a | |
| 33 | 0.5 | b | |
| 34 | 0.9 | a | |
| 35 | 0.8 | b | |
| 36 | 0.1 | b | |
| 37 | 0.3 | a | |

| Number | cm | Designation | Note |
|---|---|---|---|
| 38 | 0.2 | b | |
| 39 | 1.2 | a | crack top |
| 40 | 2.2 | b | |
| 41 | 1 | a | |
| 42 | 2.1 | b | |
| 43 | 1.5 | a | crack top |
| 44 | 3.8 | b | |
| 45 | 0.8 | a | |
| 46 | 0.5 | b | |
| 47 | 1.5 | a | |
| 48 | 2.2 | b | |
| 49 | 0.2 | a | |
| 50 | 0.6 | purple layer | excluded |
| 51 | 4.4 | b | |
| 52 | 2.7 | a | |
| 53 | 2.4 | b | |
| 54 | 1 | a | |
| 55 | 9.6 | weathered | excluded |
| 56 | 11.3 | CTS | chg to b |
| 57 | 1.5 | a | BWP Begins |
| 58 | 0.5 | b | |
| 59 | 0.7 | a | |
| 60 | 1.3 | b | |
| 61 | 0.9 | a | |
| 62 | 0.7 | b | |
| 63 | 2.4 | a | |
| 64 | 0.8 | b | |
| 65 | 0.8 | a | vug chert |
| 66 | 1.3 | b | |
| 67 | 2.3 | a | |
| 68 | 0.9 | b | |
| 69 | 1.2 | a | |
| 70 | 1.1 | b | |
| 71 | 1.8 | a | |
| 72 | 3.2 | b | |
| 73 | 1 | a | |
| 74 | 1.9 | b | |
| 75 | 0.6 | a | |
| 76 | 0.3 | b | |

| Number | cm | Designation | Note |
|---|---|---|---|
| 77 | 1 | a | |
| 78 | 2.2 | b | |
| 79 | 0.8 | a | |
| 80 | 1.9 | a | |
| 81 | 0.7 | b | |
| 82 | 0.6 | a | |
| 83 | 0.7 | b | |
| 84 | 4 | a | excluded, odd A |
| Total | 153.9 | | |

Upper Prieska 1

| Number | cm | Designation | Note |
|---|---|---|---|
| 1 | 0.6 | a | GWP Begins |
| 2 | 0.1 | b | |
| 3 | 2.4 | a | |
| 4 | 0.2 | b | |
| 5 | 1 | a | |
| 6 | 0.2 | b | |
| 7 | 1.1 | a | |
| 8 | 0.05 | b | crack |
| 9 | 1.1 | a | |
| 10 | 1.5 | b | |
| 11 | 1.1 | a | |
| 12 | 12.3 | CTS | chg to b |
| 13 | 1 | a | |
| 14 | 0.3 | b | |
| 15 | 0.7 | a | |
| 16 | 0.1 | b | |
| 17 | 2.1 | a | |
| 18 | 0.4 | b | |
| 19 | 1.5 | a | |
| 20 | 0.1 | b | |
| 21 | 0.4 | a | |
| 22 | 0.1 | b | |
| 23 | 1 | a | |
| 24 | 0.1 | b | |
| 25 | 0.6 | a | |
| 26 | 0.3 | b | |
| 27 | 0.7 | a | |
| 28 | 9.9 | TUFF | chg to b-crack |
| 29 | 2 | a | |
| 30 | 0.1 | b | |
| 31 | 1.8 | a | |
| 32 | 0.3 | b | |
| 33 | 1.5 | a | |
| 34 | 0.5 | b | |
| 35 | 1.1 | a | |
| 36 | 14 | CTS | chg to b |
| 37 | 0.9 | a | |

| Number | cm | Designation | Note |
|---|---|---|---|
| 38 | 0.5 | b | |
| 39 | 2.5 | a | |
| 40 | 0.2 | b | |
| 41 | 1.7 | a | |
| 42 | 0.05 | b | crack |
| 43 | 1.7 | a | |
| 44 | 0.2 | b | |
| 45 | 1 | a | |
| 46 | 1.2 | b | |
| 47 | 4 | a | |
| 48 | 32.6 | tuff xbeds | chg to b-crack |
| 49 | 4.1 | a | |
| 50 | 0.3 | b | |
| 51 | 1.8 | a | |
| 52 | 0.1 | b | |
| 53 | 1 | a | |
| 54 | 0.2 | b | |
| 55 | 1.9 | a | |
| 56 | 0.1 | b | |
| 57 | 0.5 | a | |
| 58 | 0.2 | b | |
| 59 | 1.4 | a | |
| 60 | 0.3 | b | |
| 61 | 1.3 | a | |
| 62 | 0.3 | b | |
| 63 | 1.5 | a | |
| 64 | 0.3 | b | |
| 65 | 0.8 | a | |
| 66 | 0.3 | b | |
| 67 | 1.3 | a | |
| 68 | 0.3 | b | |
| 69 | 1 | a | |
| 70 | 0.2 | b | |
| 71 | 1.1 | a | |
| 72 | 0.1 | b | |
| 73 | 0.9 | a | |
| 74 | 0.2 | b | |
| 75 | 0.9 | a | |
| 76 | 0.2 | b | |

| Number | cm | Designation | Note |
|---|---|---|---|
| 77 | 0.8 | a | |
| 78 | 0.3 | b | |
| 79 | 1.1 | a | |
| 80 | 0.2 | b | |
| 81 | 1 | a | |
| 82 | 0.1 | b | |
| 83 | 1.2 | a | |
| 84 | 0.1 | b | |
| 85 | 1.1 | a | |
| 86 | 0.6 | b | |
| 87 | 1.9 | a | |
| 88 | 0.6 | b | |
| 89 | 1 | a | |
| 90 | 1.2 | tuff | chg to b-crack |
| 91 | 1.1 | a | |
| 92 | 0.1 | b | |
| 93 | 1 | a | |
| 94 | 0.2 | b | |
| 95 | 0.5 | a | |
| 96 | 0.4 | b | |
| 97 | 3 | a | |
| 98 | 1.5 | tuff | chg to b-crack |
| 99 | 2.9 | a | |
| 100 | 0.1 | b | |
| 101 | 0.2 | a | |
| 102 | 0.3 | b | silicified |
| 103 | 1.4 | a | |
| 104 | 0.2 | b | |
| 105 | 1.5 | a | |
| 106 | 0.1 | b | |
| 107 | 1.3 | a | |
| 108 | 0.1 | b | |
| 109 | 0.8 | a | |
| 110 | 0.5 | b | |
| 111 | 1.6 | a | |
| 112 | 0.7 | b | |
| 113 | 1 | a | |
| 114 | 0.3 | b | |
| 115 | 1.4 | a | |

| Number | cm | Designation | Note |
|---|---|---|---|
| 116 | 0.1 | b | |
| 117 | 0.8 | a | |
| 118 | 0.1 | b | |
| 119 | 0.5 | a | |
| 120 | 0.1 | b | |
| 121 | 2.3 | a | |
| 122 | 0.5 | b | |
| 123 | 2.5 | a | |
| 124 | 7.4 | tuff | chg to b-crack |
| 125 | 2.1 | a | |
| 126 | 0.2 | b | |
| 127 | 2.9 | a | |
| 128 | 0.5 | b | |
| 129 | 0.6 | a | |
| 130 | 0.3 | b | |
| 131 | 3.2 | a | |
| 132 | 0.5 | b | |
| 133 | 3.2 | a | |
| 134 | 2.2 | weathered | chg to b-crack |
| 135 | 1.2 | a | |
| 136 | 0.1 | b | |
| 137 | 1.1 | a | |
| 138 | 0.1 | b | |
| 139 | 1.5 | a | |
| 140 | 0.6 | b | |
| 141 | 0.8 | a | |
| 142 | 0.2 | b | |
| 143 | 0.8 | a | |
| 144 | 0.2 | b | |
| 145 | 1 | a | |
| 146 | 0.4 | b | |
| 147 | 3 | a | |
| 148 | 1 | b | |
| 149 | 4.4 | a | |
| 150 | 0.2 | b | |
| 151 | 1 | a | |
| 152 | 0.5 | b | |
| 153 | 1.1 | a | |
| 154 | 0.2 | b | |

| Number | cm | Designation | Note |
|---|---|---|---|
| 155 | 0.7 | a | |
| 156 | 4 | tuff | chg to b-crack |
| 157 | 2.5 | a | |
| 158 | 0.3 | b | |
| 159 | 5.3 | a | |
| 160 | 31.5 | tuff | chg to b-crack |
| 161 | 3 | a | |
| 162 | 0.05 | b | crack |
| 163 | 2.1 | a | |
| 164 | 0.05 | b | crack |
| 165 | 1.5 | a | |
| 166 | 0.05 | b | crack |
| 167 | 1.3 | a | |
| 168 | 0.3 | b | |
| 169 | 1 | a | |
| 170 | 0.3 | b | |
| 171 | 0.5 | a | |
| 172 | 0.3 | b | |
| 173 | 1.5 | weathered | excluded |
| 174 | 13 | tuff | chg to a-crack |
| 175 | 0.2 | b | |
| 176 | 2.5 | a | |
| 177 | 60 | weathered | excluded |
| 178 | 19.2 | CTS | chg to b |
| 179 | 2.1 | a | |
| 180 | 0.8 | b | |
| 181 | 1.8 | a | |
| 182 | 0.3 | b | |
| 183 | 3.7 | a | |
| 184 | 0.2 | b | |
| 185 | 0.5 | a | |
| 186 | 0.1 | b | |
| 187 | 1 | a | |
| 188 | 0.2 | b | |
| 189 | 1.3 | a | |
| 190 | 0.4 | b | |
| 191 | 2.5 | a | |
| 192 | 3 | b | |
| 193 | 1 | a | |

| Number | cm | Designation | Note |
|---|---|---|---|
| 194 | 0.3 | b | |
| 195 | 1 | a | |
| 196 | 0.2 | b | |
| 197 | 1.1 | a | |
| 198 | 0.2 | b | |
| 199 | 0.5 | a | BWP Begins |
| 200 | 0.3 | b | |
| 201 | 2.4 | a | |
| 202 | 0.3 | b | |
| 203 | 1.2 | a | |
| 204 | 0.2 | b | |
| 205 | 1.2 | a | |
| 206 | 0.3 | b | |
| 207 | 1.1 | a | |
| 208 | 0.5 | b | |
| 209 | 2.2 | a | |
| 210 | 0.5 | b | |
| 211 | 1.7 | a | |
| 212 | 0.2 | b | |
| 213 | 1.3 | a | |
| 214 | 0.2 | b | |
| 215 | 0.9 | a | |
| 216 | 0.5 | b | |
| 217 | 1.1 | a | |
| 218 | 0.05 | b | crack |
| 219 | 2.1 | a | |
| 220 | 0.5 | b | |
| 221 | 1.4 | a | |
| 222 | 0.2 | b | |
| 223 | 0.8 | a | |
| 224 | 0.4 | b | |
| 225 | 3.9 | a | |
| 226 | 1.5 | b | |
| 227 | 1 | a | |
| 228 | 0.6 | b | |
| 229 | 1.3 | a | |
| 230 | 0.3 | b | |
| 231 | 6.3 | a | |
| 232 | 0.5 | b | |

| Number | cm | Designation | Note |
|---|---|---|---|
| 233 | 6.4 | a | |
| 234 | 0.3 | b | |
| 235 | 7 | a | |
| 236 | 2 | b | |
| 237 | 1.5 | a | |
| 238 | 0.05 | b | crack |
| 239 | 4.2 | a | |
| 240 | 1.6 | b | undulose |
| 241 | 2 | a | |
| 242 | 0.05 | b | crack |
| 243 | 1.7 | a | |
| 244 | 0.7 | b | |
| 245 | 1.6 | a | |
| 246 | 2 | b | |
| 247 | 1.7 | a | |
| 248 | 0.5 | b | |
| 249 | 2.5 | a | |
| 250 | 0.8 | b | |
| 251 | 3.7 | a | |
| 252 | 0.05 | b | crack |
| 253 | 0.6 | a | |
| 254 | 0.9 | b | |
| 255 | 1.7 | a | |
| 256 | 1 | b | |
| 257 | 2.6 | a | |
| 258 | 0.5 | b | |
| 259 | 2 | a | |
| 260 | 0.5 | b | |
| 261 | 1.7 | a | |
| 262 | 0.5 | b | |
| 263 | 2.1 | a | |
| 264 | 0.2 | b | undulose |
| 265 | 2.6 | a | |
| 266 | 0.4 | b | |
| 267 | 2 | a | |
| 268 | 0.2 | b | |
| 269 | 1.5 | a | |
| 270 | 0.05 | b | crack |
| 271 | 1 | a | |

| Number | cm | Designation | Note |
|---|---|---|---|
| 272 | 7.8 | weathered | chg to b-crack |
| 273 | 3.1 | a | |
| 274 | 0.4 | b | |
| 275 | 1.5 | a | |
| 276 | 0.6 | b | |
| 277 | 2.7 | a | |
| 278 | 0.3 | b | |
| 279 | 2.4 | a | |
| 280 | 1.4 | b | |
| 281 | 1.6 | a | |
| 282 | 0.05 | b | crack |
| 283 | 1.7 | a | |
| 284 | 0.5 | b | |
| 285 | 1 | a | |
| 286 | 0.3 | b | |
| 287 | 3.4 | a | |
| 288 | 0.3 | b | |
| 289 | 0.5 | a | |
| 290 | 0.4 | b | |
| 291 | 0.7 | a | |
| 292 | 0.05 | b | crack |
| 293 | 2 | a | |
| 294 | 0.7 | b | |
| 295 | 2 | a | |
| 296 | 0.5 | b | |
| 297 | 2 | a | |
| 298 | 0.3 | b | |
| 299 | 1.7 | a | |
| 300 | 0.7 | b | |
| 301 | 4 | a | |
| 302 | 0.05 | b | crack |
| 303 | 3.4 | a | |
| 304 | 0.6 | b | |
| 305 | 4 | a | |
| 306 | 0.5 | b | |
| 307 | 3.1 | a | |
| 308 | 0.6 | b | |
| 309 | 3.3 | a | |
| 310 | 0.05 | b | |

| Number | cm | Designation | Note |
|---|---|---|---|
| 311 | 3.2 | a | |
| 312 | 0.05 | b | crack |
| 313 | 3 | a | |
| 314 | 26.3 | tuff | chg to b-crack |
| 315 | 6.3 | a | |
| 316 | 1.2 | b | |
| 317 | 3.4 | a | |
| 318 | 1.3 | b | |
| 319 | 2.3 | a | |
| 320 | 0.5 | b | |
| 321 | 2.5 | a | |
| 322 | 0.05 | b | crack |
| 323 | 1.5 | a | |
| 324 | 0.05 | b | crack |
| 325 | 3 | a | |
| 326 | 0.4 | b | |
| 327 | 3 | a | undulose |
| 328 | 0.4 | b | |
| 329 | 3 | a | undulose |
| 330 | 1 | b | crack top |
| 331 | 1.5 | a | |
| 332 | 0.05 | b | crack |
| 333 | 2.4 | a | |
| 334 | 0.5 | b | |
| 335 | 0.5 | a | |
| 336 | 0.5 | b | |
| 337 | 3 | a | |
| 338 | 0.05 | b | crack |
| 339 | 1.1 | a | |
| 340 | 0.7 | b | |
| 341 | 3.2 | a | vug chert |
| 342 | 0.7 | b | |
| 343 | 1.7 | a | |
| 344 | 0.5 | b | |
| 345 | 1.7 | a | |
| 346 | 0.05 | b | crack |
| 347 | 1.6 | a | |
| 348 | 0.5 | b | |
| 349 | 1 | a | |

| Number | cm | Designation | Note |
|---|---|---|---|
| 350 | 0.05 | b | crack |
| 351 | 3.5 | a | |
| 352 | 0.5 | b | |
| 353 | 1.6 | a | |
| 354 | 0.3 | b | |
| 355 | 0.8 | a | |
| 356 | 1 | b | |
| 357 | 0.7 | a | |
| 358 | 0.7 | b | |
| 359 | 2.5 | a | |
| 360 | 1 | b | |
| 361 | 3 | a | |
| 362 | 0.05 | b | crack |
| 363 | 3.5 | a | |
| 364 | 0.05 | b | crack |
| 365 | 4 | a | |
| 366 | 0.05 | b | crack |
| 367 | 0.7 | a | |
| 368 | 0.5 | b | |
| 369 | 5 | a | |
| 370 | 0.05 | b | crack |
| 371 | 2 | a | |
| 372 | 1.2 | b | |
| 373 | 2.5 | a | |
| 374 | 1.7 | b | |
| 375 | 4.8 | a | vug chert |
| 376 | 0.7 | b | |
| 377 | 5 | a | vug chert |
| 378 | 1 | b | |
| 379 | 5.5 | a | vug chert |
| 380 | 0.05 | b | crack |
| 381 | 6.2 | a | vug chert |
| 382 | 0.7 | b | |
| 383 | 4 | a | vug chert |
| 384 | 0.05 | b | crack |
| 385 | 3 | a | |
| 386 | 0.05 | b | crack |
| 387 | 2.5 | a | |
| 388 | 0.05 | b | crack |

| Number | cm | Designation | Note |
|---|---|---|---|
| 389 | 6.5 | a | excluded, odd A |
| Total | 706.8 | | |

Upper Prieska 2

| Number | cm | Designation | Note |
|---|---|---|---|
| 1 | 0.5 | a | |
| 2 | 0.3 | b | |
| 3 | 0.8 | a | |
| 4 | 0.2 | b | |
| 5 | 1.4 | a | |
| 6 | 0.1 | b | |
| 7 | 3 | a | |
| 8 | 0.3 | b | |
| 9 | 4 | a | |
| 10 | 0.8 | b | |
| 11 | 4.2 | a | |
| 12 | 0.1 | b | |
| 13 | 4.7 | a | |
| 14 | 0.1 | b | |
| 15 | 1 | a | |
| 16 | 0.7 | b | |
| 17 | 0.05 | b | crack |
| 18 | 0.3 | a | |
| 19 | 0.2 | b | |
| 20 | 0.9 | a | |
| 21 | 0.1 | b | |
| 22 | 4.4 | a | |
| 23 | 0.05 | b | crack |
| 24 | 3.7 | a | |
| 25 | 0.3 | b | |
| 26 | 3 | a | |
| 27 | 0.6 | b | |
| 28 | 1.9 | a | |
| 29 | 1 | b | |
| 30 | 3.7 | a | |
| 31 | 0.3 | b | |
| 32 | 0.6 | a | |
| 33 | 0.05 | b | crack |
| 34 | 1.1 | a | |
| 35 | 0.1 | b | |
| 36 | 3.5 | a | |
| 37 | 3.5 | weathered | chg to b-crack |

| Number | cm | Designation | Note |
|---|---|---|---|
| 38 | 4 | a | |
| 39 | 1 | b | |
| 40 | 4.2 | a | |
| 41 | 0.1 | b | |
| 42 | 2.4 | a | |
| 43 | 0.2 | b | |
| 44 | 2 | a | |
| 45 | 0.1 | b | |
| 46 | 4 | a | |
| 47 | 1.5 | weathered | chg to b-crack |
| 48 | 1.6 | a | |
| 49 | 0.1 | b | |
| 50 | 2 | a | |
| 51 | 0.2 | b | |
| 52 | 4.5 | a | |
| 53 | 1 | b | |
| 54 | 3.9 | a | |
| 55 | 0.9 | b | |
| 56 | 5.5 | a | |
| 57 | 2 | b | |
| 58 | 5.3 | a | |
| 59 | 5.2 | CTS | chg to b |
| 60 | 0.3 | a | |
| 61 | 7 | CTS | chg to b |
| 62 | 7.5 | weathered | chg to a-crack |
| 63 | 4.4 | tuff | chg to b-crack |
| 64 | 1 | a | |
| 65 | 0.1 | b | |
| 66 | 1.2 | a | |
| 67 | 0.2 | b | |
| 68 | 0.3 | weathered | excluded |
| 69 | 2.2 | a | |
| 70 | 0.1 | b | |
| 71 | 2.4 | a | |
| 72 | 0.3 | b | |
| 73 | 2 | a | |
| 74 | 0.2 | b | |
| 75 | 5.5 | a | |
| 76 | 0.2 | b | |

| Number | cm | Designation | Note |
|---|---|---|---|
| 77 | 2.7 | a | |
| 78 | 1.7 | b | |
| 79 | 6.1 | a | |
| 80 | 0.3 | b | |
| 81 | 2.8 | a | |
| 82 | 0.05 | b | crack |
| 83 | 5.2 | a | |
| 84 | 0.2 | b | |
| 85 | 0.6 | a | |
| 86 | 0.2 | b | |
| 87 | 0.9 | a | |
| 88 | 0.5 | b | |
| 89 | 2.1 | a | |
| 90 | 0.6 | b | |
| 91 | 4.4 | a | |
| 92 | 0.1 | b | |
| 93 | 1.3 | a | |
| 94 | 0.05 | b | crack |
| 95 | 1.3 | a | |
| 96 | 0.05 | b | crack |
| 97 | 0.8 | a | |
| 98 | 0.05 | b | crack |
| 99 | 1.2 | a | crack top |
| 100 | 1 | b | |
| 101 | 1.3 | a | |
| 102 | 0.2 | b | |
| 103 | 3.1 | a | |
| 104 | 0.8 | b | |
| 105 | 1.2 | a | |
| 106 | 0.5 | b | |
| 107 | 0.5 | a | |
| 108 | 4.4 | b | |
| 109 | 0.4 | a | |
| 110 | 7 | weathered | chg to b-crack |
| 111 | 3.1 | tuff | chg to a-crack |
| 112 | 4 | weathered | chg to b-crack |
| 113 | 7.2 | a | |
| 114 | 1.3 | tuff | chg to b-crack |
| 115 | 1.2 | a | |

| Number | cm | Designation | Note |
|---|---|---|---|
| 116 | 11 | CTS | chg to b |
| 117 | 2.5 | tuff | chg to a-crack |
| 118 | 14 | CTS | chg to b |
| 119 | 7 | weathered | excluded |
| 120 | 1.1 | a | |
| 121 | 0.2 | b | |
| 122 | 3.6 | a | |
| 123 | 0.1 | b | |
| 124 | 14 | tuff | chg to a-crack |
| 125 | 11.5 | weathered | chg to b-crack |
| 126 | 7.3 | tuff | chg to a-crack |
| 127 | 2.5 | weathered | chg to b-crack |
| 128 | 7.6 | a | |
| 129 | 0.2 | b | |
| 130 | 1.6 | a | |
| 131 | 0.1 | b | |
| 132 | 3.2 | a | |
| 133 | 0.7 | b | |
| 134 | 3.8 | a | |
| 135 | 0.4 | b | |
| 136 | 4 | a | |
| 137 | 21 | weathered | chg to b-crack |
| 138 | 10.7 | tuff | chg to a-crack |
| 139 | 2 | b | |
| 140 | 2.2 | a | |
| 141 | 0.7 | b | |
| 142 | 8 | a | |
| 143 | 0.5 | b | |
| 144 | 3.3 | a | |
| 145 | 0.8 | b | |
| 146 | 14.6 | tuff | chg to a-crack |
| 147 | 11 | weathered | chg to b-crack |
| 148 | 1.5 | a | |
| 149 | 0.2 | b | |
| 150 | 2 | a | |
| 151 | 1 | b | |
| 152 | 7.5 | tuff | chg to a-crack |
| 153 | 1.1 | b | |
| 154 | 8.5 | a | |

| Number | cm | Designation | Note |
|---|---|---|---|
| 155 | 0.05 | b | crack |
| 156 | 2 | a | |
| 157 | 0.3 | b | |
| 158 | 4 | a | |
| 159 | 0.05 | b | crack |
| 160 | 4.2 | a | |
| 161 | 0.05 | b | crack |
| 162 | 4.5 | a | |
| 163 | 1.6 | b | |
| 164 | 5 | a | |
| 165 | 0.05 | b | crack |
| 166 | 4 | a | |
| 167 | 1 | b | |
| 168 | 2.7 | a | |
| 169 | 0.05 | b | crack |
| 170 | 2 | a | |
| 171 | 0.2 | b | |
| 172 | 2.4 | a | |
| 173 | 0.1 | b | |
| 174 | 6.5 | a | |
| 175 | 1.2 | b | |
| 176 | 9.3 | a | |
| 177 | 1.5 | b | |
| 178 | 9.2 | a | undulose |
| 179 | 12 | CTS | chg to b |
| 180 | 1.6 | a | |
| 181 | 1 | b | |
| 182 | 1.5 | a | |
| 183 | 1 | b | |
| 184 | 1 | a | |
| 185 | 2 | b | |
| 186 | 1.3 | a | |
| 187 | 0.05 | b | crack |
| 188 | 4 | a | |
| 189 | 0.9 | b | |
| 190 | 1.9 | a | |
| 191 | 0.5 | b | |
| 192 | 1.6 | a | |
| 193 | 0.9 | b | |

| Number | cm | Designation | Note |
|---|---|---|---|
| 194 | 6 | a | strong tufts |
| 195 | 55 | weathered | chg to b-crack |
| 196 | 6 | a | |
| 197 | 0.05 | b | crack |
| 198 | 3.5 | a | |
| 199 | 0.05 | b | crack |
| 200 | 4.8 | a | |
| 201 | 0.05 | b | crack |
| 202 | 5 | a | |
| 203 | 0.05 | b | crack |
| 204 | 4 | a | |
| 205 | 0.3 | b | |
| 206 | 2 | a | crack top |
| 207 | 2.5 | b | |
| 208 | 3.5 | a | |
| 209 | 0.05 | b | crack |
| 210 | 1.8 | a | |
| 211 | 0.7 | b | |
| 212 | 3 | a | |
| 213 | 0.05 | b | crack |
| 214 | 3 | a | |
| 215 | 0.3 | b | |
| 216 | 0.5 | a | |
| 217 | 0.5 | b | |
| 218 | 1.5 | a | |
| 219 | 9.5 | weathered | chg to b-crack |
| 220 | 5.1 | tuff | chg to a-crack |
| 221 | 2.5 | a | |
| 222 | 1.6 | b | |
| 223 | 5 | a | |
| 224 | 6.4 | CTS | chg to b |
| 225 | 3.1 | a | |
| 226 | 2 | b | |
| 227 | 2 | a | |
| 228 | 1.5 | b | |
| 229 | 1.6 | a | |
| 230 | 0.2 | b | |
| 231 | 0.5 | a | |
| 232 | 1.5 | b | |

| Number | cm | Designation | Note |
|---|---|---|---|
| 233 | 0.5 | a | |
| 234 | 1 | b | |
| 235 | 1.7 | a | |
| 236 | 0.3 | b | |
| 237 | 1 | a | |
| 238 | 0.2 | b | |
| 239 | 1.2 | a | |
| 240 | 0.6 | b | |
| 241 | 0.8 | a | |
| 242 | 0.7 | b | |
| 243 | 0.6 | a | |
| 244 | 1 | b | |
| 245 | 3 | a | |
| 246 | 0.1 | b | |
| 247 | 1 | a | |
| 248 | 9 | weathered | chg to b-crack |
| 249 | 1.7 | a | |
| 250 | 1 | b | |
| 251 | 2 | a | |
| 252 | 1 | b | |
| 253 | 0.1 | a | |
| 254 | 1.7 | b | |
| 255 | 1.9 | a | |
| 256 | 0.2 | b | |
| 257 | 2.5 | a | |
| 258 | 0.5 | b | |
| 259 | 2 | a | strong tufts |
| 260 | 1 | b | |
| 261 | 0.5 | a | strong tufts |
| 262 | 1 | b | |
| 263 | 0.7 | a | |
| 264 | 0.5 | b | |
| 265 | 0.8 | a | |
| 266 | 0.3 | b | |
| 267 | 0.5 | a | |
| 268 | 0.3 | b | |
| 269 | 1.5 | a | |
| 270 | 0.05 | b | crack |
| 271 | 3 | a | |

| Number | cm | Designation | Note |
|---|---|---|---|
| 272 | 0.5 | b | |
| 273 | 3 | a | |
| 274 | 0.3 | b | |
| Total | 692.7 | | |

# VITA

Jake (J.H.) Alexander was raised on a barrier island in Corpus Christi, TX. He completed his AS Geology with scholastic excellence at Austin Community College in May 2015, and earned his BS Geology *summa cum laude* from Texas A&M University – Corpus Christi in December 2017. He performed undergraduate research under the supervision of Dr. Jim Silliman to geochemically diagnose provenance of sediments in southern Corpus Christi Bay. He began his studies at the University of Tennessee in August 2018, and he completed an integrated analysis of Ordovician hardgrounds which he presented at the 2019 SEGSA sectional meeting in Charleston, SC. In the summer of 2019, he interned at ExxonMobil in Spring, TX where he worked on Pennsylvanian mixed carbonate and clastic successions of the western Central Basin Platform, Permian Basin. He completed his Master's degree in June 2020, and will intern with LithiumAmericas as a Field Geologist in Nevada during the summer of 2020.